Conducting pyrolysed carbon scaffolds for cell replacement therapy and energy applications

Bunea, Ada-Ioana

Publication date:
2017

Document Version
Publisher's PDF, also known as Version of record

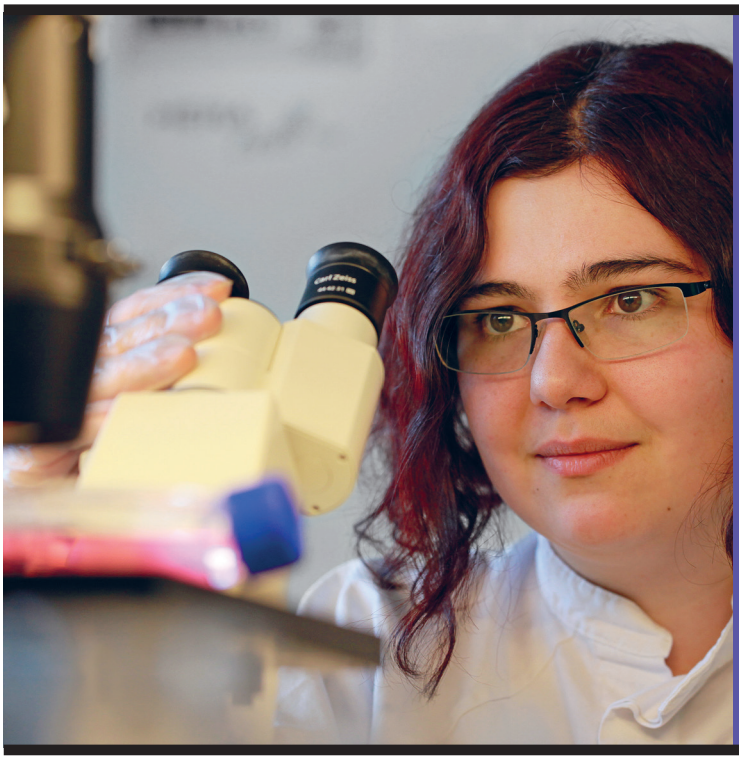

Conducting pyrolysed carbon scaffolds for cell replacement therapy and energy applications

Ada-Ioana Bunea
PhD Thesis December 2017

DTU Nanotech
Department of Micro- and Nanotechnology

Technical University of Denmark

Conducting pyrolysed carbon scaffolds for cell replacement therapy and energy applications

Ph.D. Thesis

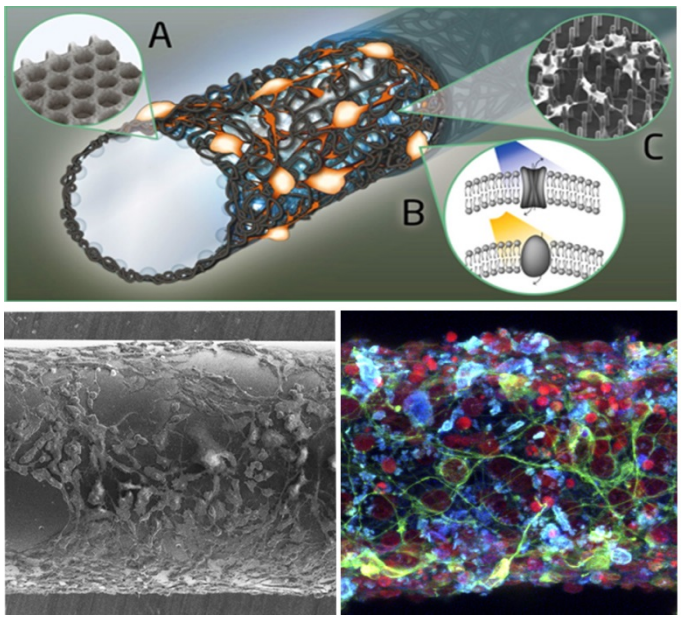

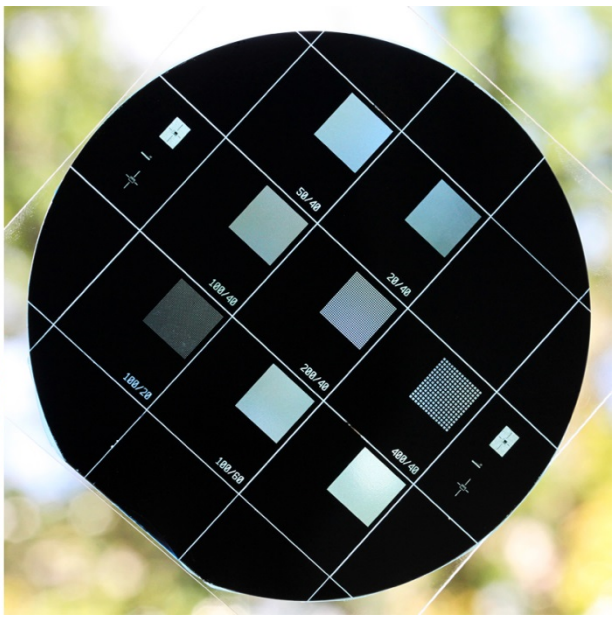

Ada-Ioana Bunea

Main supervisor: **Prof. Jenny Emnéus**

Co-supervisor: Assoc. Prof. Stephan Sylvest Keller

Co-supervisor: Prof. Niels Bent Larsen

DTU Nanotech
Department of Micro- and Nanotechnology

Preface

What is a scientist after all? It is a curious man looking through a keyhole, the keyhole of nature, trying to know what's going on.
Jacques Yves Cousteau

This written thesis is a documentation of my past three years in research. I would like to introduce you to it by first explaining where it all began…

The first question I ask myself when I start a new research project is "Why: what is this work trying to bring to the world?". That does not mean I am only interested in "a final product". On the contrary, I believe theoretical knowledge can help advance just as much (or maybe even more) as applied research. In the beginning, my project was meant to be more inclined towards fundamental science, trying to make sense of previous results gathered in the group – that was very interesting to me, because I always want to be able to answer the question "Why?". Along the way, I found myself looking into possible applications of carbon in stem cell research. One particular idea shaped up so nicely (and I have Jenny to thank for that) that I ended up getting sidetracked and started working on developing a new "product" instead of doing the fundamental work. On the one hand, this made me sad, because there are so many unanswered questions, and I was hoping to be able to help with that. On the other hand, though, I enjoyed so much working on a potential cure for Parkinson's disease – even if just in the very early stages of developing it. I am not an entrepreneur at heart, so the idea of "product" for me is not in terms of commercialising, or money, but more in terms of "this is finished work". In times of an "experimental crisis", it was a great help to me to have a clear goal in mind and know why I am struggling to find a solution. I believe that stem cell research will help shape our future, and, as any human being, I wanted to be part of something great. And this is how the work behind this thesis came to be…

Another important issue when doing research is "How do we investigate this?". For the project described here, various techniques and methods were necessary. Cleanroom fabrication, numerous characterisation techniques and stem cell culture were essential. I am very happy that my PhD project gave me the great opportunity of learning how to operate many machines I was previously unfamiliar with, taught me a great deal more about the synergies between different research fields and expanded my overall knowledge a great deal.

A quick guide to how this thesis is structured: I will first provide the background for my work by talking about our idea and the fields it can be applied in. I will then talk about fabrication issues and characterisation techniques. In every chapter, after providing the theoretical background for the work, I will discuss my experiments and results.

Table of contents

Abstract

Combining a conductive material with a transparent material allows creating a device with integrated functions that takes advantage of both properties. Such an optoelectrical device can function as substrate for the attachment of biological samples, as actuator for specific functions of the biological samples and as sensor to monitor the triggered responses.

Carbon is a widely used electrode material due to its numerous advantages (electrochemical properties, price, stability, biocompatibility and versatility for fabrication). Additionally, glass-like carbon fabricated through the pyrolysis of SU-8 has been shown to enhance stem cell differentiation into dopaminergic neurons. Due to these properties, carbon was chosen as the conductive material for the development of optoelectrical devices.

Quartz is transparent in the UV and visible range. It is thermally resistant up to 1600°C, chemically inert, hard, durable and non-porous. These properties make it ideal as the transparent component in the development of optoelectrical devices.

The aim of this work is to contribute to the development of optoelectrical devices for applications in two different fields: 1) the treatment of Parkinson's disease and 2) energy harvesting from photosynthetic organisms. During the duration of this PhD project, the optoelectrical devices designed in the group have moved from an idea to the proof-of-concept stage.

The experimental work performed as part of this thesis combined cleanroom fabrication, pyrolysis, characterisation of the fabricated structures, and biological applications. The work aimed at Parkinson's disease has focused on the differentiation of stem cells into dopaminergic neurons and analysing the ability to release dopamine of the neurons generated by culturing on carbon electrodes. The work aimed at applications in biophotovoltaics has explored energy harvesting from thylakoid membranes as photosynthetic systems residing on patterned carbon electrodes for generating electrical power.

Resumé

Ved at kombinere ledende og gennemsigtige materialer opnås mulighed for at skabe en enhed med integrerede funktioner der udnytter begge egenskaber. En sådan optoelektrisk enhed kan anvendes som substrat til vedhæftning af biologiske prøver, til at aktivere specifikke funktioner i de biologiske prøver, og som sensor til at overvåge de aktiverede funktioner.

Kulstof er et almindeligt anvendt elektrodemateriale baseret på dets mange fordele, herunder elektrokemiske egenskaber, pris, stabilitet, biokompatibilitet og alsidige fremstillingsmuligheder. Envidere har glaslignende kulstof fremstillet gennem pyrolyse af SU-8 vist sig at forbedre differentiering af stamceller til dopaminerge neuroner. Med baggrund i disse egenskaber har vi valgt kulstof som ledende materiale til udvikling af optoelektriske enheder.

Kvarts absorberer hverken ultraviolet eller synligt lys og fremstår derved gennemsigtigt. Det er termisk resistent op til 1600 °C, kemisk inert, hårdt, holdbart og ikke-porøst, hvilket gør kvarts ideelt som transparent materiale til udvikling af optoelektriske enheder.

Formålet med dette arbejde er at bidrage til udviklingen af optoelektriske apparater til applikationer inden for to områder: 1) behandling af Parkinsons sygdom og 2) elektrisk energihøstning fra fotosyntetiske organismer. I løbet af dette ph.d.-projekt er de optoelektriske enheder designet i gruppen blevet udviklet fra idé til proof-of-concept.

Det eksperimentelle arbejde, som er udført i denne afhandling, har kombineret rentrums-fabrikation, pyrolyse, strukturel karakterisering af de fremstillede materialer, og biologiske anvendelser af de strukturerede materialer. Arbejdet rettet mod Parkinsons sygdom har fokuseret på differentiering af stamceller til dopaminerge neuroner og analyse af de resulterende neuroners evne til at frigive dopamin ved dyrkning på kulstof-elektroder. Aktiviteterne indenfor energihøstning har udforsket brugen af thylakoidmembraner som fotosyntetiske systemer på mønstrede kulstof-elektroder til at generere elektrisk strøm.

List of publications

– including pending publications –

Paper I (appendix I):

Single step fabrication of optical fiber-based carbon electrodes for dopamine detection from cells
Ada-Ioana Bunea, Ramona Valentina Mateiu, Alberto Martinez Serrano, Arto Heiskanen, Stephan Sylvest Keller, Niels Bent Larsen and Jenny Emnéus
Manuscript in preparation for Electrochemistry Communications (communication).

Paper II (appendix II):

Transparent, carbon-based electrode chips for enhanced photocurrent generation from thylakoid membranes
Ada-Ioana Bunea, Arto Heiskanen, Galina Pankratova, Giulio Tesei, Mikael Lund, Hans-Erik Åkerlund, Dónal Leech, Niels Bent Larsen, Stephan Sylvest Keller, Lo Gorton and Jenny Emnéus
Manuscript awaiting submission in Advanced Energy Materials (full paper).

Patent (appendix III):

Pyrolysed optical waveguides as optoelectrical scaffolds for cell replacement therapy and energy applications
Jenny Emnéus, Ada-Ioana Bunea, Stephan Sylvest Keller, Anders Kristensen and Arto Heiskanen
PCT application filed on 29.06.2017; will be published on 29.12.2017.

Conferences:

I participated to 6 international conferences and 2 local conferences, where I presented a total of 2 posters and 6 oral presentations. A list of the attended conferences and my scientific contributions can be found in appendix VI.

Contribution to the publications

Paper I:

I had a major contribution in designing the experiments. I planned and performed the experiments and data analysis. I wrote the manuscript and updated it after input from the co-authors.

Paper II:

I designed, planned and performed the experiments and data analysis with the exception of calculations. I discussed the theoretical approach with collaborators that then performed the calculations. I had a major contribution in interpreting the results from calculations. I wrote the manuscript and updated it after input from the co-authors.

Patent:

I performed proof of concept experiments to support the claims for the patent application. I performed a literature search to evaluate the possibility of patenting the invention. I filed the Invention Notification and presented the idea to the DTU Patent Office. I was involved in reviewing the text written for the PCT application by the patent agent.

List of abbreviations

– in alphabetical order –

AAAD	Aromatic amino acid decarboxylase
AES	Auger electron spectroscopy
ALS	Amyotrophic lateral sclerosis
ASC	Adult stem cells
BBB	Blood-brain barrier
Bcl-X_L	Basal cell lymphoma extra-large
CA	Chronoamperometry
CE	Counter electrode
ChR	Channelrhodopsin
CNS	Central nervous system
CNT	Carbon nanotube
COMT	Catechol-O-methyltransferase
CRT	Cell replacement therapy
CRT	Cell replacement therapy
CV	Cyclic voltammetry
DA	Dopamine
db-cAMP	N^6,2′-O-Dibutyryladenosine 3′,5′-cyclic monophosphate sodium salt
DD	Differentiation day
DMEM	Dulbecco's Modified Eagle Medium
DPV	Differential pulse voltammetry
ECM	Extracellular matrix
ECM	Extracellular matrix
EDL	Electrical double layer
EGF	Epidermal growth factor
ESC	Embryonic stem cells
ESCA	Electron spectroscopy for chemical analysis
GBL	Gamma-butyrolactone
GCE	Glassy carbon electrode
GDNF	Glial derived neutrophic factor
GF	Growth factor
HAR	High aspect ratio
hESC	Human embryonic stem cells
HOMO	Highest occupied molecular orbital
HOPG	Highly oriented pyrolytic graphite
hrEGF	Human recombinant epidermal growth factor
hrFGF	Human recombinant fibroblast growth factor
IHP	Inner Helmholtz plane

iPSC	Induced pluripotent stem cells
IR	Infrared
IUPAC	International Union of Pure and Applied Chemistry
LUMO	Lowest unoccupied molecular orbital
MAO	Monoamine oxidase
MSC	Mesenchymal stem cells
MWCNT	Multi walled carbon nanotube
NADH	Nicotinamide adenine dinucleotide
NGF	Nerve growth factor
NSC	Neural stem cells
OF	Optical fiber
OFE	Optical fiber electrode
OHP	Outer Helmholtz plane
PBEC	Photo-bioelectrochemical cell
PD	Parkinson's disease
PGE	Pyrolytic graphite electrode
PGMEA	Propylene glycol methyl ether acetate
PI	Polyimide
PLL	Poly-L-lysine
PNS	Peripheral nervous system
PRC	Photosynthetic reaction center
PS I	Photosystem I
PS II	Photosystem II
PT	Plasma treatment
RE	Reference electrode
RES	Renewable energy source
RT	Room temperature
SCE	Saturated calomel electrode
SEM	Scanning electron microscopy
SHE	Standard hydrogen electrode
SN	Substantia nigra
SWCNT	Single walled carbon nanotube
TCPS	Tissue culture polystyrene
TGA	Thermogravimetric analysis
TH	Tyrosine hydroxylase
TH^+	TH-positive
UHV	Ultra-high vacuum
UPDRS	Unified Parkinson disease rating scale
UV	Ultraviolet
WE	Working electrode
XPS	X-ray photoelectron spectroscopy

Chapter 1: Introduction

When one tugs at a single thing in nature, he finds it attached to the rest of the world.
John Muir

This chapter provides the reader with a brief background of the work and the main motivation behind it. The optoelectrical devices developed as part of my thesis are described and the two target applications are detailed. The main objectives of the work are stated and several milestones are listed as intermediary steps in reaching the end-goal for both envisioned applications. The structure of the thesis is described at the end of the introduction.

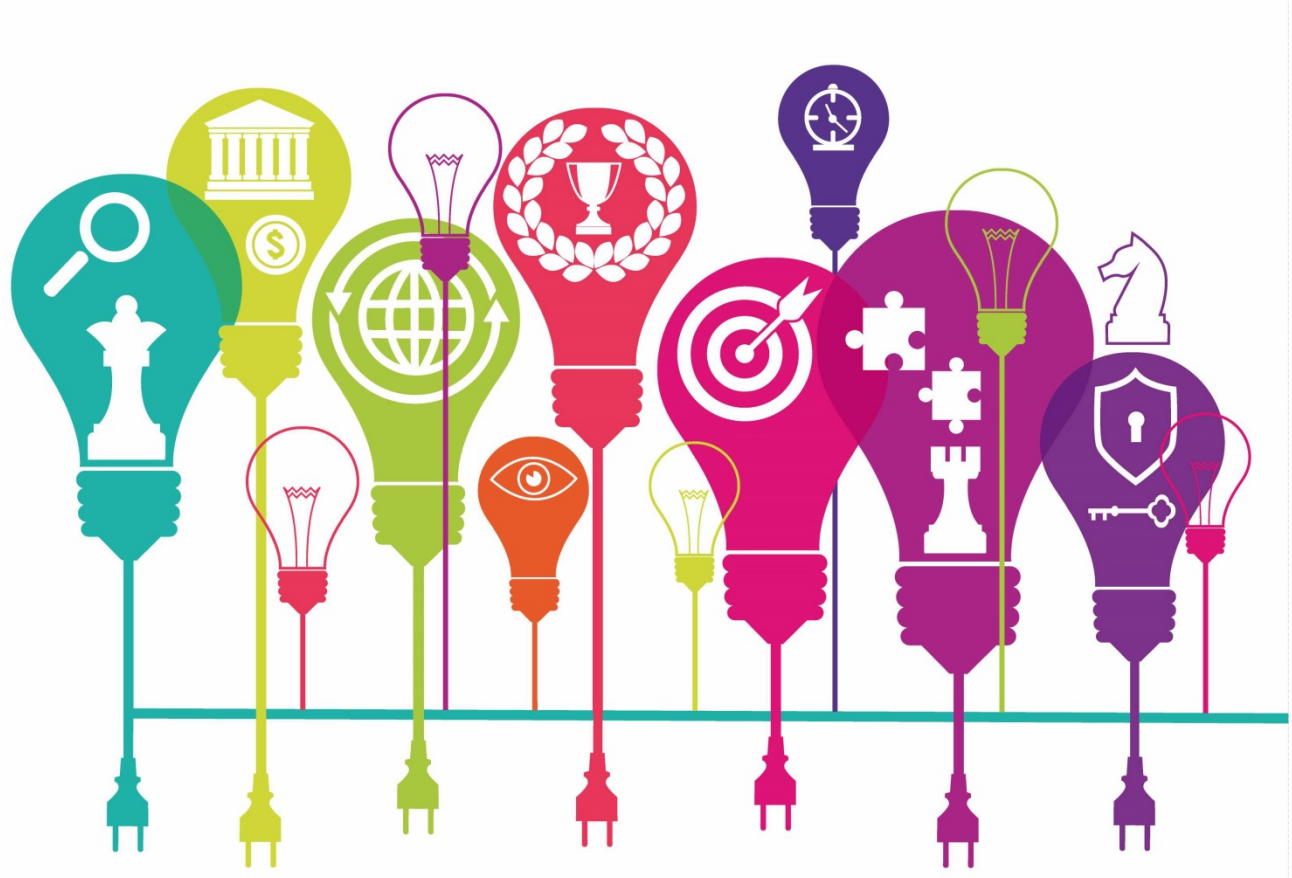

1.1. Motivation

Anyone who has never made a mistake has never tried anything new.
Albert Einstein

The main motivation behind my PhD project is to contribute to the development of personalised treatment for Parkinson's disease (PD). As the average life span of the population increases, PD incidence is constantly increasing, and there is no available cure yet [1]. PD is characterised by a loss of nigrostriatal dopaminergic nerve cells, which leads to insufficient quantities of dopamine in the brain [2]. Cell replacement therapy (CRT) has recently developed into a promising approach for the treatment of neurodegenerative disorders, PD included [3,4].

Carbon is a widely used electrode material and it can be employed for monitoring electrochemically active species (such as dopamine) released from cell populations. Our group has previously reported that pyrolytic carbon surfaces lead to spontaneous differentiation of a human neural stem cell line into dopaminergic neurons, and that the obtained neurons are able to repeatedly release dopamine upon K^+-induced stimulation [5].

From understanding stem cell differentiation, my project moved to a different idea, that of developing an optoelectrical integrated device which is able to function as carrier, sensor and to deliver stimuli to local biological systems. One can envision that such a device could be used in the treatment of PD to replace the dysfunctional neurons by new, mature dopaminergic neurons which are able to release dopamine when it is needed and help bring balance to the patient's brain chemistry. However, the device can be adapted for much more than just PD treatment. Replacing the type of cells can allow using it for other neurodegenerative diseases. A modified version of the device could be applied in the field of energy conversion.

1.1.1. The optoelectrical device

Combining a conductive material (carbon) with a transparent material (quartz) allows creating a device with integrated functions that takes advantage of both properties. **Figure 1.1** shows the conceptual design of the optoelectrical device designed for the treatment of PD.

The device consists in a transparent quartz core covered with a patterned carbon layer that allows light to leak out in the region where cells are attached. The carbon has a dual function: electrode material and substrate for cell attachment. By using the carbon surface as electrode, the local environment can be monitored using electrochemical detection methods. The core allows light to be transmitted until the "leaky" region, where it can reach the surface – this is where the cells are residing. On the surface, light-responsive cells can release dopamine when stimulated at an appropriate wavelength. The system would be controlled by a user-friendly software – for example from a phone or a tablet. Thus, the device would be able to monitor local dopamine concentrations and stimulate dopamine release when the local concentration drops below a critical point – making it suitable for personalised treatment in PD.

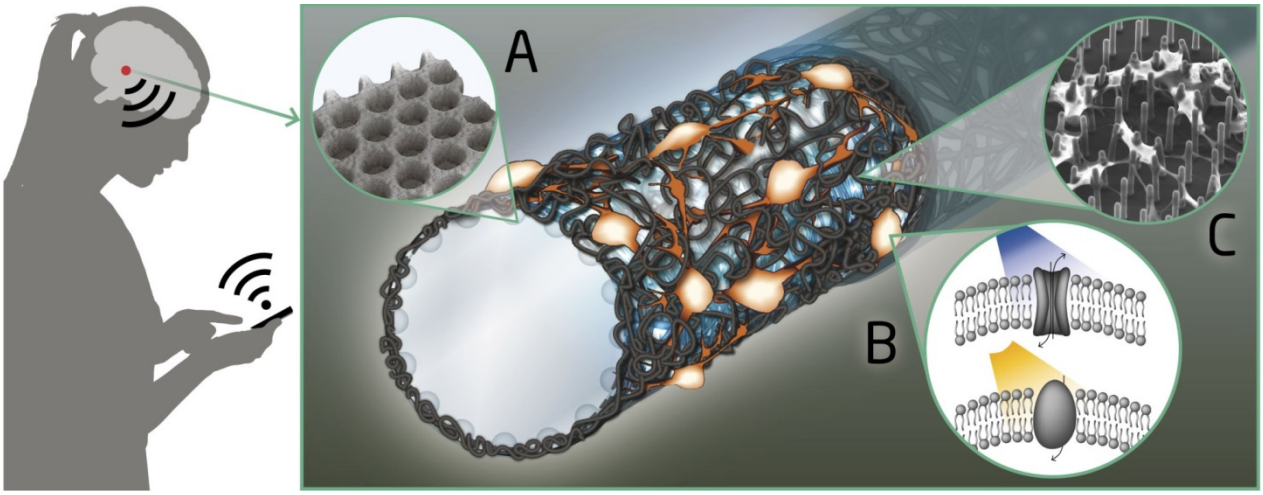

Figure 1.1: Schematic representation of the implantable device concept: A: Carbon scaffold – substrate for cell culture and electrode; B: Optogenetically modified cells that respond to specific wavelengths; C: Cell population attached to the carbon scaffold. The detection and dopamine release functions would be remotely controlled using custom-made software (left).

Alternatively, the system can be used as basis for biofuel cells. In this case, the carbon would still work both as electrode and substrate for the attachment of the biological components of interest. Instead of having stem cells on the carbon, photosynthetic organisms (such as cyanobacteria or algae) can be used. The photosynthetic organisms would then be stimulated by light coming from the sun and the device would function as bioanode in a photo-bioelectrochemical cell (PBEC) and help harvest energy (**figure 1.2**).

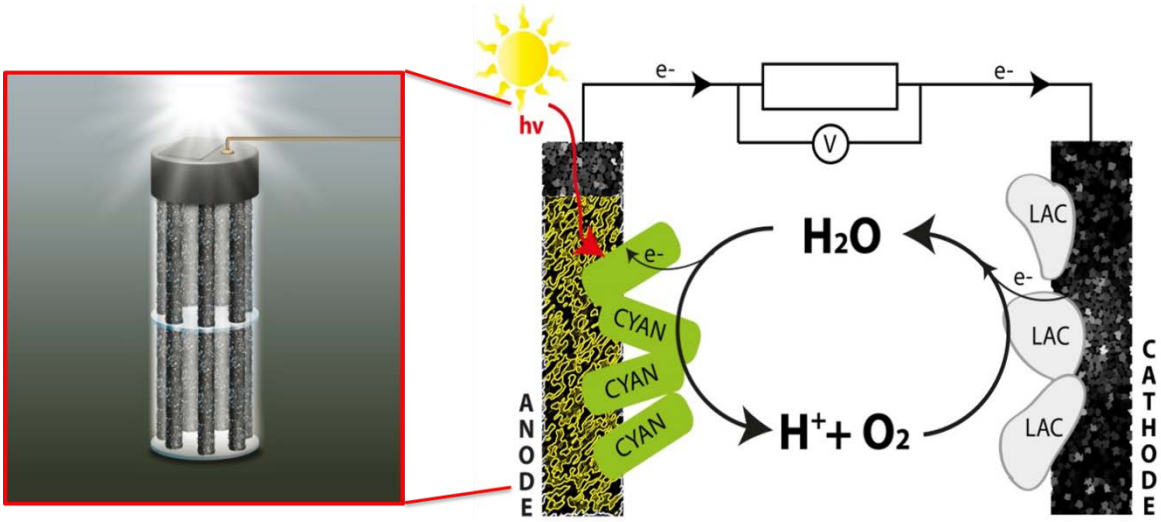

Figure 1.2: Schematic representation of the photo-bioelectrochemical cell (right). The bioanode can consist of a bundle of optical fibres with "leaky" segments (left) or in a large patterned carbon-on-quartz area. Either way, the device allows light to reach the photosynthetic organisms and harvests the generated electrons.

1.2. Objectives of the thesis

You are never too old to set another goal or to dream a new dream.
C. S. Lewis

The main objective of the thesis is to design and fabricate devices that combine electrochemical detection and optical stimulation for biological samples. In the beginning of my project, the idea for the devices existed, but I was the first to be involved in developing and testing the different aspects. The work performed for this thesis can be divided into two main parts, according to the envisioned applications. Two long-term objectives of the work can be highlighted:

I. Development of an optoelectrical device for the treatment of Parkinson's disease

The purpose is to have an implantable device that can monitor local dopamine concentrations in target areas of the brain and to replenish the neurotransmitter when its level becomes too low. Several different aspects require testing and optimisation and they can be considered as separate milestones in the development of the device:

1st milestone: Turn an optical fibre into an optical fibre electrode (OFE).
2nd milestone: Employ OFE as substrate for cell culture and differentiation and as sensor for dopamine exocytosis.
3rd milestone: Modify OFE to have a "leaky" section.
4th milestone: Have an optogenetically-modified cell line and employ light to stimulate dopamine release from such cells grown on the OFE.
5th milestone: Integrate the light source and incorporate all described functions into an implantable device.
6th milestone: Develop a system that allows remote control of the functions.

II. Development of an optoelectrical bioanode for photo-bioelectrochemical cells

The goal is to fabricate a device that can harvest the energy generated by photosynthetic organisms upon exposure to sunlight. Different milestones can also be highlighted in this case:

1st milestone: Design and fabricate a carbon-on-quartz electrode chip that shows good electrochemistry and is transparent.
2nd milestone: Employ the electrode chip for harvesting energy from photosynthetic organisms and optimise current generation.
3rd milestone: Build a photo-bioelectrochemical cell using the electrode chip as bioanode and optimise its efficiency.
4th milestone: Upscale production and use developed system for mass-producing cheap and efficient biophotovoltaic systems.

This PhD project has allowed me to work on the development of devices for the aforementioned directions. However, due to the existing timeframe, both devices are at an early development stage. The first two milestones from each direction have been accomplished during this PhD. The perspectives of the work will be taken up in chapter 5.

1.3. Structure of the thesis

Science is concerned with what is possible, while engineering is concerned with choosing, from among the many possible ways, one that meets a number of often poorly stated economic and practical objectives.
Richard Hamming

I want my thesis to tell the story of what I have been doing during the past three years in research in a way that is logical and understandable to the reader. For this purpose, I identified three defining questions that I want to answer and structured the thesis accordingly:

1) What am I investigating, and why?

Chapter 2 talks about the real-world challenges that my work is addressing and about the biological systems of interest when addressing these challenges. Parkinson's disease and cell-replacement therapy are described, as they represent the motivation for developing a cell-based brain implant. The need for renewable energy and how energy harvesting from photosynthetic organisms can help supply green energy is explained, using thylakoid membranes as model system.

2) What devices do I use in the investigation?

Chapter 3 is about carbon electrodes, from the properties of carbon to fabrication techniques employed for my project. The two different types of electrodes developed for the two goals of the thesis are described.

3) What do I need to know about the systems?

Chapter 4 encompasses different characterisation methods and how they are employed to investigate the developed devices at different stages.

Each one of these chapters starts with a wide theoretical introduction to the topic, which then narrows down towards the specifics of my work, with two different sections for the two different applications. In the end of each chapter, a brief description of the main results is given. Additional details can be found in the attached journal article manuscripts (appendices 1 and 2).

The fifth chapter then summarises the conclusions of my work and its future perspectives.

Each chapter has a cover page containing a short summary and an artistic image.

Experimental protocols employed throughout my project and additional experimental details can be found attached in appendices 4 and 5.

Appendix VI provides a list of attended conferences. The scope of each conference and my personal contributions are described.

Chapter 2: Biological systems of interest

Biochemistry is the science of life. All our life processes – walking, talking, moving, feeding – are essentially chemical reactions. So biochemistry is actually the chemistry of life, and it's supremely interesting.
Aaron Ciechanover

Two different biological systems were investigated as part of this work, in agreement with the two applications envisioned.

The first part of this chapter will explain more about Parkinson's disease, cell replacement therapy and optogenetics to provide the framework for understanding the necessity of improving the treatment options for the disease. Signalling factors and regulatory mechanisms involved in cell proliferation and differentiation are briefly described, since these play a crucial role in the generation of dopaminergic neurons *in vitro*. Details about the stem cell line used in this project are also provided.

The second part of this chapter will talk about the need for renewable energy and the potential of biophotovoltaics. Thylakoid membranes are described, as they are the sites for photosynthesis, without going deeply into the biological mechanisms involved, since they are outside the scope of the thesis. Thylakoid membranes were used as model systems to explore the possibility of applying our device for energy conversion applications.

2.1. Stem cell therapy for Parkinson's disease

I think science has begun to demonstrate that aging is a disease. If it is, it can be cured.
Tom Robbins

2.1.1. Brief history of Parkinson's disease

The disease was first described in detail by James Parkinson in his 1817 monograph, "An Essay on the Shaking Palsy" [6]. Towards the end of the nineteenth century, Jean Martin Charcot identified the critical clinical features of the disease [7], and named it after James Parkinson, as a way to recognise his leading contribution in the field. Paul Blocq and Georges Marinesco published in 1893 the case study of a patient suffering from unilateral parkinsonian tremor, whose brain revealed upon autopsy an encapsulated tumour in the *substantia nigra* (SN). This led Édouard Brissaud to formulate his hypothesis, according to which the SN is the major site in PD, which he published in 1895. 24 years later, Constantin Trétiakof published a thesis supporting Brissaud's findings, noting neural degeneration in the SN of all PD patients that he had examined. Although not well received initially by other scientists, the hypothesis was later supported by more and more studies, leading to our current understanding of the disease [7].

2.1.2. Incidence of Parkinson's disease

Two systematic reviews were chosen as indicators for the incidence of PD. One of them [8] refers to PD case studies conducted between 1935 and 2001, and the other [9] refers to newer case studies, published between 2001 and 2014. Both review incidence based on age and gender groups. **Table 1.1** shows results from the most recent study [9]. The incidence is presented as number of people affected per 100000 person-years[1].

Both reviews [8,9] show that the usual onset of the disease is after the age of 40, and that the prevalence increases in the population up to the age of 80. The male population is more affected by the disease, possibly due to higher dopamine levels in the striatum of the female brain linked to higher oestrogen activity [9].

The numbers presented show that PD is indeed a modern day problem, and it is forecast that the incidence will increase even more, as the average life span of the population increases [1].

Table 1.1: Meta-analysis of gender and age specific PD incidence, adapted from [9]

Age group	Incidence in women[1]	Incidence in men[1]
40-49	2.94	3.59
50-59	13.40	19.68
60-69	58.53	55.10
70-79	104.99	132.72
80+	66.02	110.48
Total	37.16	44.21

[1] Person-years are an estimate of the years at risk of all people that contributed to a study [237]

2.1.3. Diagnosis of Parkinson's disease

The diagnosis of PD is usually made based on physical examination and patient history. However, the disease is misdiagnosed in 10-25% of the cases [6]. There are four cardinal features of PD:

i) tremor at rest – most common feature, exhibited by 80% of the patients, usually starting in the hands;
ii) bradykinesia – slowness of motion, reduced frequency and amplitude of repetitive movements;
iii) cogwheel rigidity – when muscles respond with cogwheel-like jerks to the use of constant force in bending the limb;
iv) postural instability – usually developed in later stages of the disease [6].

When at least one of these four cardinal features is present, PD must be taken into consideration, but several other factors should be evaluated before making a final diagnosis.

Associated features that can support the diagnosis of PD are: unilateral symptom onset, constantly elevated levodopa effect, reduced armswing, problems with rising from a chair, impaired olfactory sense, hypophonia (soft speech), hunched posture, sleep disturbances, difficulties turning in bed, uncontrolled drooling, constipation, micrographia (small, decreasing handwriting), seborrhoea, abnormal pattern of movement, depression or anxiety [6].

In cases where the response to dopaminergic treatment is minimal, alternate diagnoses should be considered. Several diseases can present several symptoms similar to PD: dementia with Lewy bodies, multiple system atrophy, vascular parkinsonism, drug-induced parkinsonism, cortical-basal ganglionic degeneration, progressive supranuclear palsy, essential tremor or normal pressure hydrocephalus. A correct diagnosis is essential in ensuring patient care and selecting the best treatment approach.

There are multiple rating scales for evaluating the progress of PD, with the Unified Parkinson Disease Rating Scale (UPDRS) being the most comprehensive and widely-used [10]. It has also been applied (in its entirety, or using only subscale 3, related to motor examination) for mass screening for parkinsonism. However, there are limitations, some coming from the examiner's skill, some from the patient's own assessment, and some from variations due to medication or other factors, so the use of UPRDS must be done with caution [10].

Despite the long term interest in the disease, and the numerous studies involving medical doctors and scientists, there is no definitive test that can identify PD with certainty in the early stages [2].

2.1.4. Pharmacological treatment of Parkinson's disease

Usually, the treatment of PD is pharmacological. Since the main characteristic of the disease is lack of dopamine in the brain, the goal is to increase the neurotransmitter concentration in the target areas. However, dopamine cannot be administered as a drug in PD because it cannot pass the blood brain barrier (BBB) [11], so other approaches are required for therapy.

The most common treatment is levodopa (L-Dopa), a dopamine precursor that can pass through the BBB via the L1 facilitative transporter [12]. Levodopa is converted to dopamine inside the brain by L-amino-acid decarboxylase [13] and can thus help supplement the insufficient dopamine quantities in Parkinson's disease patients. However, L-dopa is metabolised excessively in the periphery (before passing through the BBB), with only 1% of the active substance reaching the target site when administered alone [14]. Two enzymes are responsible for this, aromatic amino acid decarboxylase (AAAD) and catechol-O-methyltransferase (COMT). In order to avoid peripheral metabolisation, L-dopa is often administered in formulations that include AAAD inhibitors (the most common being carbidopa). This leads to improved bioavailability, but still only 10% of the administered drug reaches the brain. More recent formulations include also a COMT inhibitor (entacapone) in order to enhance the bioavailability of L-dopa even further [15]. Despite the therapeutic benefits, chronic usage of L-dopa in PD leads to several motor complications, especially dyskinesias (involuntary muscle movements) [16,17]. Other side effects are behavioural changes and neurological symptoms such as delusions, hallucinations, anxiety, euphoria and depression [18]. The entirety of the negative pharmacological action is hard to evaluate, because most of the side effects are also characteristic to the disease and might be either independent, or potentiated by the treatment.

Dopamine agonists are also a good option for PD treatment [19,20]. Instead of increasing dopamine levels in the brain, they mimic the action of dopamine and stimulate the same receptors. Dopamine agonists can be administered either as monotherapy or together with L-dopa-based drugs. The most used dopamine agonists are pramipexole and ropinirole. Both of these drugs not only help with managing the symptoms, but also lead to a reduced rate of nigrostriatal innervation loss [20]. Unlike L-dopa-based drugs, dopamine agonists are not associated with motor complications, but still exhibit neurological symptoms as side effects [16,18].

One other approach is the usage of monoamine oxidase (MAO) inhibitors [16,21]. The two most common MAO-inhibitors presently used are selegiline and rasagiline, used either as monotherapy or combined with L-dopa [21]. MAO is an enzyme responsible for the oxidative deamination of biogenic amine neurotransmitters. MAO inhibition leads to increased dopamine concentration in the synaptic cleft and at postsynaptic receptor sites [21]. This also helps alleviate depression and anxiety, two possible symptoms of PD and side-effects of PD treatments. Also, the oxidation reaction catalysed by MAO has reactive oxygen species (ROS) such as hydrogen peroxide as by-products, so its inhibition has neuroprotective effects [22]. As monotherapy, MAO-inhibitors are not as effective as L-dopa or dopamine agonists, but they can be used in the early stages of the disease to avoid some of the side effects from chronic levodopa treatments.

2.1.5. Surgical treatment of Parkinson's disease

For patients non-responsive to medication, or in late stages of the disease, deep brain stimulation (DBS) can offer the means to control the symptoms [23–25]. DBS involves a surgical procedure in which an electrode is implanted in a target area of the brain and used to transmit electrical impulses to modulate brain activity [23]. It is employed for different neurological diseases, including PD, and

8000-10000 new patients receive an implant each year [24]. Different stimulation sites can be used, depending on the symptoms that need to be controlled the most. The *thalamic nucleus ventralis intermedius* is the preferred site for controlling tremors. The *globus pallidus internus* can be selected as target site when the goal is to control L-dopa-induced dyskinesia. In order to reduce the need for medication, the *subthalamic nucleus* can be chosen as target site [23]. The DBS system has three components: the electrodes, an implantable pulse generator and an extension cable (**Figure 2.1**). Insertion of the DBS electrode is done via stereotactic surgery while the patient is awake (using only local anaesthesia) [23,24]. After successful insertion of the electrode, a second surgery is needed, where the implantable pulse generator is placed in the anterior chest or abdomen, and the extension cable is placed subcutaneously to connect the electrode and the pulse generator. Although DBS is a good treatment option for severe cases, it is still an invasive procedure that requires multiple surgeries, and the complication rate is between 4 and 9.7% [23].

Figure 2.1: DBS system: X-ray image after DBS surgery. 1: Electrodes; 2: Pulse generator; 3: Extension cable. (reproduced from [23]*)*

Both the medication available and the surgical procedure offer only alleviation of the symptoms, or, in the best-case scenario, can also slow down the progress of the disease by offering neuroprotection. Although different drugs can help the patients tremendously, especially in the early stages of the disease, chronic treatment comes with side effects, and the neurodegeneration keeps progressing anyway. Currently, there is no treatment option for PD that offers a cure, and this is where CRT might come into play in the near future.

2.1.6. Optogenetics for neural systems

Optogenetics involves combining genetic and optical methods to achieve gain or loss of function of well-defined events in specific living cells [26,27].

Different light-sensitive transmembrane proteins have been investigated as optogenetic tools (**figure 2.2**):

i) Channelrhodopsins (ChRs) passively transport cations and depolarise neurons upon illumination [28,29]. Originally, ChRs responded to blue light (470 nm) [30], but different mutants respond to wavelengths between 450 and 545 nm [31].

ii) Halorhodopsins (HR) actively pump Cl^- into the cell to hyperpolarise neurons when illuminated. The first identified halorhodopsin responds to yellow light (~590 nm) [29]. Mutants that can respond to other wavelengths have been developed since [31,32].

iii) Archaeorhodopsins actively pump H^+ out of the cell to hyperpolarise neurons when illuminated. Different mutants can be activated by green-blue to green-yellow light (wavelengths between 480 and 570 nm) [29,33].

Additionally, type II fusion proteins that allow optical control of intracellular signaling have been developed [31,34]. These optogenetic tools are called OptoXRs. They have shown high spatial and temporal resolution and have been employed for modulating behaviour *in vivo* in mice [34].

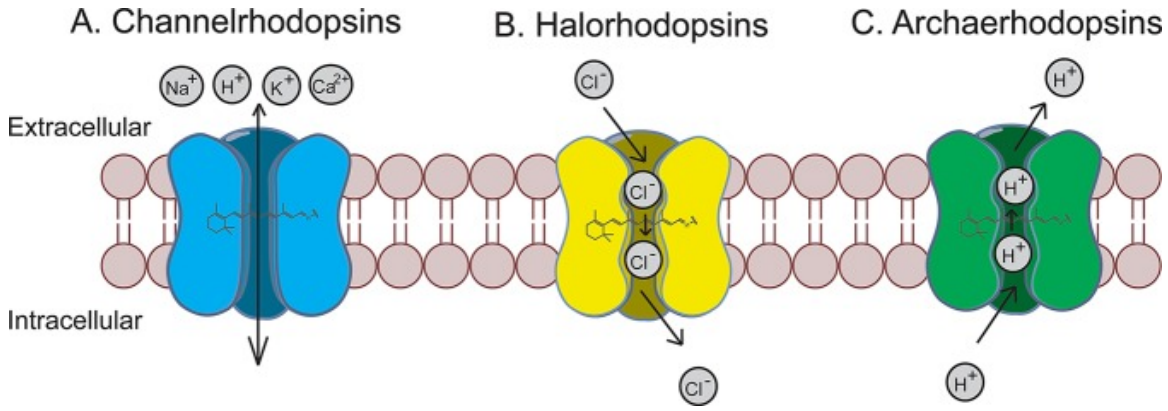

Figure 2.2: Light-responsive transmembrane proteins: channelrhodopsins, halorhodopsins and archaeorhodopsins and corresponding schematic transport mechanisms.
Figure reproduced from [29].

Miniaturised and implantable optoelectronics are another important component in optogenetic systems [26,35,36]. These allow external control and deliver the light to the light-responsive systems, triggering the desired response in the genetically-modified cells. The development of such optoelectronics is beyond the scope of this thesis, so it will not be further detailed.

Optogenetics shows promise for the treatment of neurodegenerative disorders, since it offers the ability to investigate, stimulate or inhibit neurons *in vivo* [28–30,36–38], for example for trigerring dopamine exocytosis.

Since current regulations do not allow direct implantation of genetically modified cells, one viable alternative is encapsulation. A suitable device has already been developed and applied in the treatment of Alzheimer disease [39]. The device could be easily adapted to deliver light-responsive cells attached to on an optical fibre (**figure 2.3**).

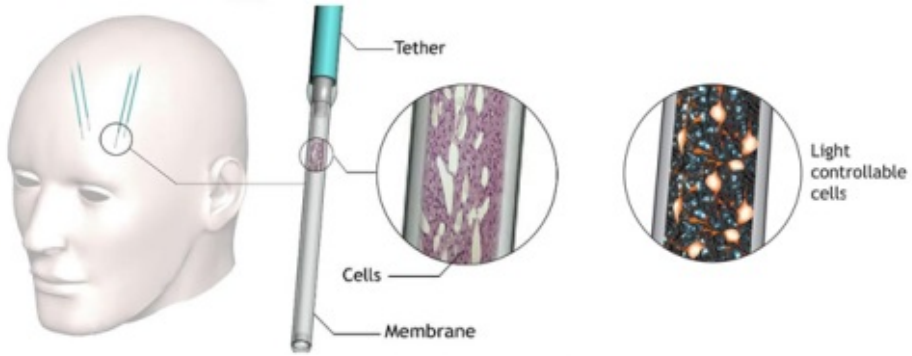

Figure 2.3: Encapsulated cell delivery device for neurological disorders (left) and envisioned system with light-responsive cells grown on carbon on the outside of an optical fibre (right).
The device (left) is reproduced from [39]

2.1.7. Stem cells

Stem cells have several properties that make them unique and interesting. They are undifferentiated cells capable of proliferation, unlimited self-renewal and differentiation [40,41]. Depending on their ability to differentiate, cells can be totipotent, pluripotent, multipotent or unipotent. Totipotent cells are only found in zygotes and blastomeres and are the only cells capable of generating both embryonic and extraembryonic tissues [42]. Pluripotent stem cells are capable to differentiate into cell types from all three germ layers (ectoderm, mesoderm and endoderm). Adult stem cells (ASCs) can only differentiate into one type of cell (unipotent cells) or into a few cell types from the same lineage (multipotent cells) [43].

The two main sources of pluripotent stem cells are: harvesting of embryonic stem cells (ESCs) and reprogramming of somatic cells (usually fibroblasts) to induced pluripotent stem cells (iPSCs) [40].

ESCs can be obtained from early stage embryos, most commonly from the inner cell mass of blastocysts or even from blastomeres (cleavage-stage embryos) [40]. Stable ESC lines can be established, expanded and used for further research. As early as 1977, stem cell transplants were already attempted in mice "for analysing mammalian differentiation and disease" [44]. Before the development of iPSCs in 2006, ESCs were the only pluripotent cell source [45].

Somatic cell nuclear transfer is an experimental procedure developed already almost 60 years ago. By transplanting endoderm nuclei to unfertilised eggs in frogs, Gurdon *et al*. obtained healthy adult specimens. Gurdon *et al*. concluded that either the nuclei remain undifferentiated and totipotent, or they are able to revert to a totipotent state under specific circumstances [46]. These experiments formed the ideological basis for the development of iPSCs in 2006, by Yamanaka *et al.* [47]. Sir John Gurdon and Shinya Yamanaka were awarded the Nobel Prize in Physiology or Medicine in 2012 [48] for "the discovery that mature cells can be reprogrammed to become pluripotent". One of the advantages of iPSCs is that they can be obtained in the laboratory by reprogramming cells harvested directly from the patient who is to benefit from CRT, thus reducing the risk of immune response from the implantation. Also, the reprogramming of fibroblasts into iPSC circumvents some of the ethical concerns of using ESCs [48].

Neural stem cells (NSCs) are a subtype of stem cells that can be found in the central nervous system (CNS) or peripheral nervous system (PNS). They can differentiate into neurons and glial cells [45,49,50]. Controlled differentiation has been a topic of tremendous interest in the field of stem cell research [49,51–54]. Using NSCs as progenitors for dopaminergic neurons is one of the key factors in the attempt of using CRT as treatment for Parkinson's disease [45].

2.1.8. Cell replacement therapy for Parkinson's disease

CRT has recently become a promising and highly researched area of biomedicine. As the name suggests, CRT aims at transplanting functional cells to replace dead ones, restoring functionality of the tissue [55]. One of the fields where CRT is particularly interesting is neurodegenerative disorders, such as PD, Huntington's disease, amyotrophic lateral sclerosis (ALS), Alzheimer's

disease and multiple sclerosis [3,4,40,55–58]. Since the pathology of PD is neuronal loss in the SN, CRT is an interesting treatment option.

Pioneering research in the field was done already in the late 1970s, when intrastriatal grafts of foetal mesencephalic tissue rich in dopaminergic neurons were introduced in rat brains with lesions of the nigrostriatal system and lead to functional recovery [59]. Since then, rodent and primate models have been used to test CRT benefits, and some cell therapies for PD proved promising enough that they reached the point of clinical trials [57,58,60] (ongoing at the moment).

There are multiple possible cell sources for cell replacement therapy (**figure 2.4**). The "proof of concept" approach for CRT in PD involved human foetal ventral midbrain tissue [16,56]. However, there are issues with ethics, tissue availability and graft-to-graft variations. Stem cells seem to be a better alternative for the future of CRT.

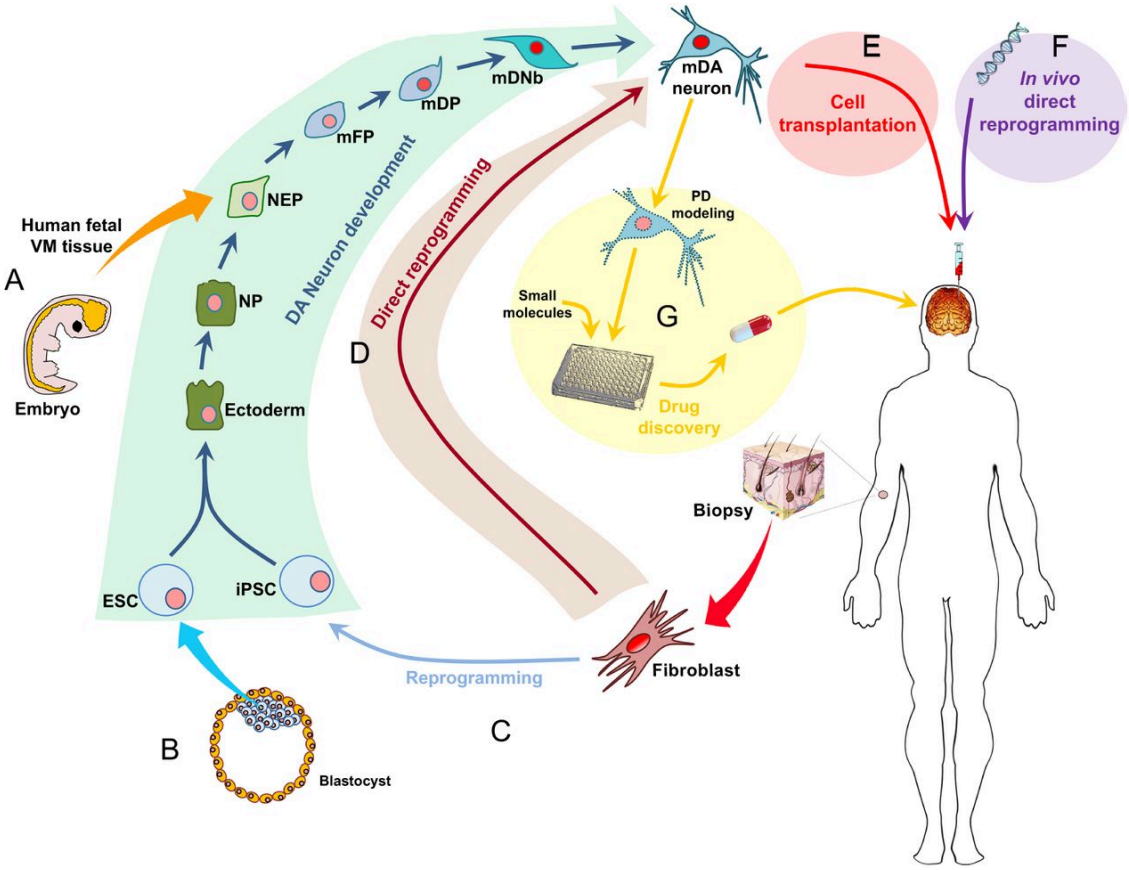

Figure 2.4: Schematic representation of possible cell sources and pathways that lead to the formation of midbrain dopaminergic neurons (mDA) that can be used for CRT in PD and for drug screening. Figure reproduced from [16].

2.1.9. Signalling compounds

Cell-to-cell communication is enabled by signalling compounds in multicellular organisms. Unlike unicellular organisms, such as bacteria, where the growth rate depends primarily on the availability of nutrients in the environment, cells in multicellular organisms respond to various chemical signals from their environment and other nearby cells.

Growth factors (GFs) are usually extracellular signalling proteins involved in the communication between cells over short distances [61,62]. They act by binding to specific plasma membrane receptors, which activates a response mechanism within the cell. Sometimes, the term "growth factors" has been used interchangeably with that of "cytokine". Extracellular signalling proteins interacting with cells of the hematopoietic or immune system are called cytokines (immunocytokines or immunokines) [61].

The nerve growth factor (NGF) was the first GF to be isolated and studied by Stanley Cohen and Rita Levi-Montalcini [63]. It took almost ten years before the epidermal growth factor (EGF) was discovered by Stanley Cohen [64]. Stanley Cohen and Rita Levi-Montalcini were jointly awarded the Nobel Prize in Physiology or Medicine in 1986 "for their discoveries of growth factors". Presently, over 200 GFs are known and their receptors have been investigated in order to elucidate growth regulation [61,65].

GFs can be involved in signalling via different pathways [61,62] (**figure 2.5**). The "standard" idea of GF comes from paracrine cell signalling, where a specific GF is released from a cell and can then bind to high affinity receptors on a neighbouring cell. GFs are supposed to be local mediators of cell communication, so they can quickly bind on the target receptors. If they are not bound, GFs can be destroyed by extracellular enzymes or immobilised by the extracellular matrix (ECM). If the cell expressing a specific GF also has high affinity receptors for that GF, auto-stimulation of the cell occurs, either via autocrine signalling (when the GF is first released from the cell before binding on the receptor) or via intracrine signalling (when the receptors are inside the cell, and the GF is not released into the ECM). Juxtacrine communication occurs when the GFs are anchored in the membrane of the signalling cell, and can only signal a directly adjacent cell.

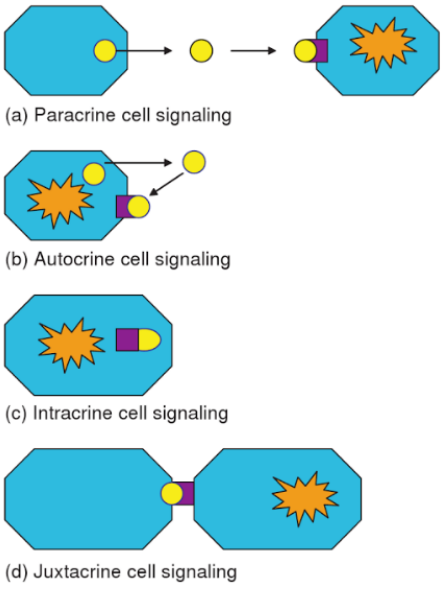

Figure 2.5: Mechanisms for signalling between cells. Figure reproduced from [61]

2.1.10. Factors regulating stem cell fate

The natural microenvironment that surrounds stem cells in the body is called the stem cell niche [66–68]. The stem cell niche is important in tissue homeostasis and it influences the wound healing

process. An array of biochemical and biophysical signals determines cell fate by guiding the cell to either proliferation or differentiation in different possible stages of the process. Stem cells have the potential to generate any one of the adult cell types upon differentiation, and this is an extremely interesting ability for regenerative medicine. The difficulty lies in controlling stem cell fate by selecting appropriate conditions to direct differentiation into a specific type of cell. Differentiation depends on both the intrinsic behaviour of the stem cell and on external controls (chemical and physical properties of the environment) [66,67]. Usually, when discussing about directing stem cell differentiation, the term refers to enhancing the relative proportion of a specific cell type obtained after differentiation. It is still necessary to elucidate the effect of combinations of different control cues for truly being able to control the process, and this might make it possible to obtain pure populations after differentiation.

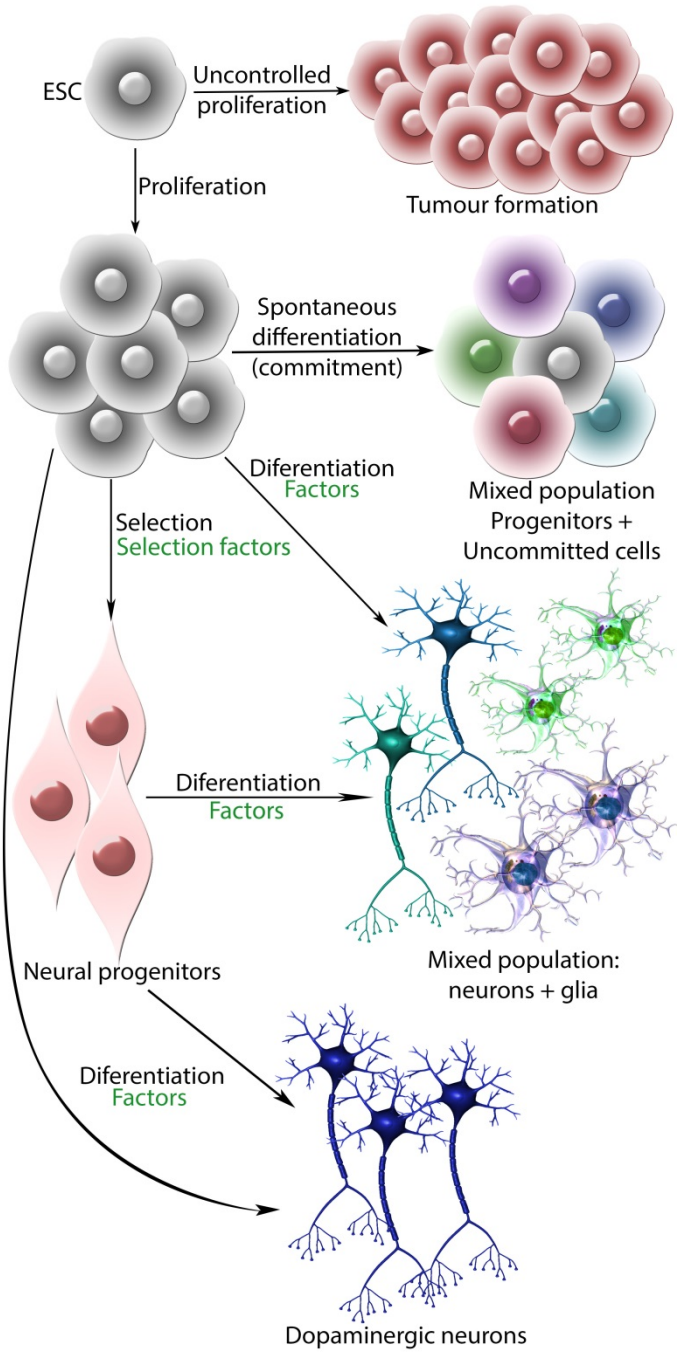

Figure 2.6: From embryonic stem cells (ESCs) to dopaminergic neurons: cell fate and where different factors can influence the outcome of differentiation.

Figure 2.6 shows the possible pathways to obtain a population of dopaminergic neurons from ESCs. ESCs can commit to a certain lineage, becoming progenitor cells. By using appropriate selection factors, a population of neural progenitors can be obtained. These can differentiate into neurons and glial cells (astrocytes, oligodendrocytes and microglia).

Differentiation can be directed towards a certain cell type, for example dopaminergic neurons, from either the neural progenitors or directly from the ESC population with the right combination of factors.

One challenge regarding stem cells is that uncontrolled proliferation can lead to tumour formation.

2.1.9.1. Biochemical factors influencing differentiation

Soluble factors play an important role in differentiation [66–72]. Different chemical compounds are included in this category, such as GFs, morphogenetic factors, cytokines, enzymes and certain small molecules [68]. Soluble factors can activate cellular signalling pathways that alter gene expression and thus influence cell fate.

Shouldiner *et al.* [69] investigated the effect of 8 different GFs on the differentiation of human ESCs (hESCs). Their study found that none of the GFs directed differentiation of the cells into only one type of cells. However, there were clear differences in gene expression after the differentiation. They concluded that the tested GFs had rather an inhibitory effect on certain differentiation pathways, leading to enhanced differentiation into other cell types. Hwang *et al.* [70] screened 41 inhibitors of protein kinases on rat mesenchymal stem cells (MSCs) and on mouse ESCs. Only 14 of the tested inhibitors had an effect on directing differentiation, and only in certain concentrations. For example, H-1152 (an adenosine triphosphate (ATP) competitive inhibitor of G protein ROCK) enhanced differentiation of mouse ESCs from 25% to 55% when added in a concentration of 0.1-2 µM, but had cytotoxic effect above 5µM. This shows that the choice of soluble factors and concentration needs to be optimised for a specific pathway. Kirkeby *et al.* [71] used a concentration gradient of GSK3 inhibitor to chemically activate WNT signalling on a population of hESCs. The GSK3 gradient led to regional differentiation into cell types specific to the ventral forebrain, midbrain or hindbrain. These are just a few examples that show how soluble factors can influence differentiation.

2.1.9.2. Mechanical factors influencing differentiation

The ECM can influence cell fate through its physical properties as well as through its chemical properties [73]. The biomaterial used as substrate for cell culture and its physical properties (such as stiffness, topography, porosity and geometry) also play a role in the commitment of stem cells [74] (**figure 2.7**). In the body, tissue development happens under mechanical stimulation. Mechanical signals are converted into biochemical responses through mechano-transduction [72]. The matrix stiffness and the dynamics of the ECM are sensed by the cells through integrin-ECM interactions. Focal adhesion kinases mediate integrin signalling. This means that cell adhesion, focal adhesion points and cell spreading on the surface influence differentiation [75].

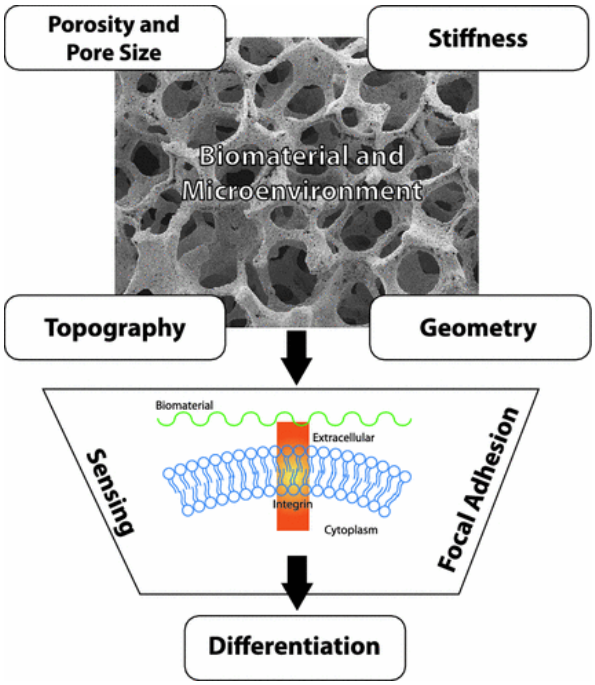

Figure 2.7: Substrate factors that influence stem cell differentiation.
Figure reproduced from [74]

By mimicking the *in vivo* environment of adult cells, differentiation can be enhanced into a certain direction. Matrix stiffness and elasticity play an important role in this [51,76,77]. The brain (elasticity of ~1 kPa) is considerably softer than muscles (~10 kPa), which are much softer than bones (~100 kPa) [51]. Engler *et al.* [51] described the matrix effect on naïve MSCs. They showed that matrixes with a stiffness of 0.1-1 kPa are neurogenic, 8-17 kPa are myogenic and 25-40 kPa are osteogenic for populations of MSCs. When adding soluble factors promoting differentiation into myocytes to cells grown on a neurogenic matrix, mixed populations were obtained. This is an indication that different factors can have either synergetic or discordant effects on cell fate.

2.1.11. hVM1 Bcl-X_L neurogenic cell line

The hVM1 Bcl-X_L cell line used in this PhD project was developed in the group of professor Alberto Martínez-Serrano at Universidad Autonóma de Madrid [78,79]. Cells from foetal human mesencephalon were first isolated and immortalised as the multipotent cell line hVM1 [78] in 2009. Upon differentiation, hVM1 cells generate neurons and glial cells (astrocytes, oligodendrocytes) expressing genes specific to the midbrain. Neuronal subtypes derived from hVM1 Bcl-X_L cells include dopaminergic, GABA and glutamatergic neurons, but not serotonergic or noradrenergic neurons.

Tyrosine hydroxylase (TH) is a rate-limiting enzyme involved in the synthesis of neurotransmitters. In the case of differentiated hVM1 cells, the presence of the TH gene indicates dopaminergic phenotype (since serotonergic or noradrenergic neurons cannot be generated from hVM1 cells).

Bcl-X_L (basal cell lymphoma extra-large) is a transmembrane protein with anti-apoptotic role in mammals and with a role in neuronal differentiation. Incorporation of the Bcl-X_L gene into the hVM1 cell line was shown to lead to increased survival rates during differentiation, to protect from cytotoxic compounds and to enhance the generation of dopaminergic (TH positive, TH^+) neurons [79]. This is why the hVM1 Bcl-X_L cell subline became in use in 2009. Since then, several research articles have described the differentiation of hVM1 Bcl-X_L cells and the potential of these cells for CRT [5,80,81].

In my work, I have used hVM1 Bcl-X_L cells for generating dopaminergic neurons and investigating dopamine exocytosis as part of developing an implantable device for the treatment of PD. This is described in more details in chapter 4 and appendix I.

The experimental protocols related to the culture and differentiation of hVM1 Bcl-X_L cells are attached as appendix IV.

2.2. Harvesting solar energy in biophotovoltaics

Food is simply sunlight in cold storage.
John Harvey Kellogg

2.2.1. Renewable energy sources

"Energy is the convertible currency of technology" [82]. In a world where the population keeps increasing, so does the need for sustainable development. One important step towards sustainable development is represented by replacing conventional energy sources with clean, renewable energy sources (RESs) [82–86].
Currently, several different RESs are in use: hydropower, biomass, geothermal, solar, wind, wave and tidal energy. In 2010, RESs accounted for 16.6% of the total energy consumed, but there is a projected increase to 47.7% in 2040 [86]. Replacing oil and coal with RESs is one of the goals of well-developed countries, as a measure of reducing pollution and the impact of population growth and technological needs on the environment [84,87–89].

2.2.2. Harvesting solar energy using photosynthetic organisms

Solar thermal energy is the most abundant RES. Out of the sun's emission of $2.8 \cdot 10^{23}$ kWh, approximately $1.8 \cdot 10^{14}$ kWh are intercepted by Earth. Converting solar energy into electric energy with high efficiency has been one of humanity's goals in the last decades [90–93].
Research in photovoltaics (PV) started in the 1950s, with the first applications emerging in the 1970s [91]. Between 2000 and 2012, solar PV was the fastest growing renewable power technology in the world [91]. After years of research, which lead to improved efficiency and lower fabrication costs, solar panels have become a common sight in developed countries.
One emerging technology alternative to conventional solar cells is that of biophotovoltaic (BPV) devices [94–97]. BPV devices are solar cells that generate electricity using the photosynthetic abilities of biological components.
Photosynthesis takes place in thylakoid membranes (TMs), which for plants are found inside chloroplasts. The light reactions of photosynthesis make use of solar energy to split water and synthesise ATP and nicotinamide adenine dinucleotide phosphate (NADPH) [98]. The dark reactions use the ATP and NADPH to fix CO_2 and synthesise organic molecules such as amino acids, fatty acids, sucrose and starch [98]. **Figure 2.8** shows a schematic of the light and dark reactions involved in photosynthesis.

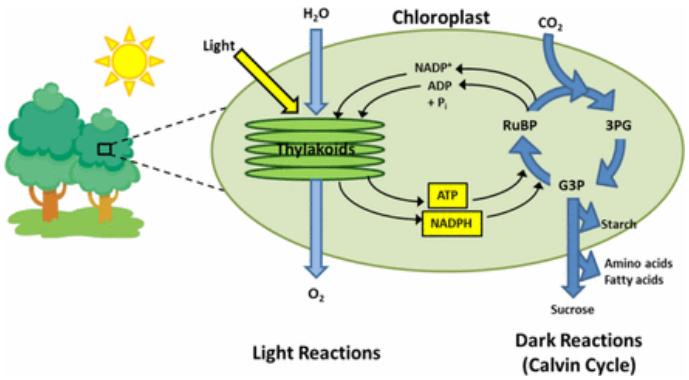

Figure 2.8: The light reactions of photosynthesis convert light energy into ATP and NADPH. The dark reactions use the ATP and NADPH to convert CO_2 into organic molecules. RuBP = ribulose-1,5-biphosphate; 3PG = 3-phosphoglycerate; G3P = glyceraldehyde 3-phosphate. Figure reproduced from [98]

PBECs can be constructed using an enzyme-modified cathode and a bioanode where the light reactions of photosynthesis take place (**figure 2.9**).

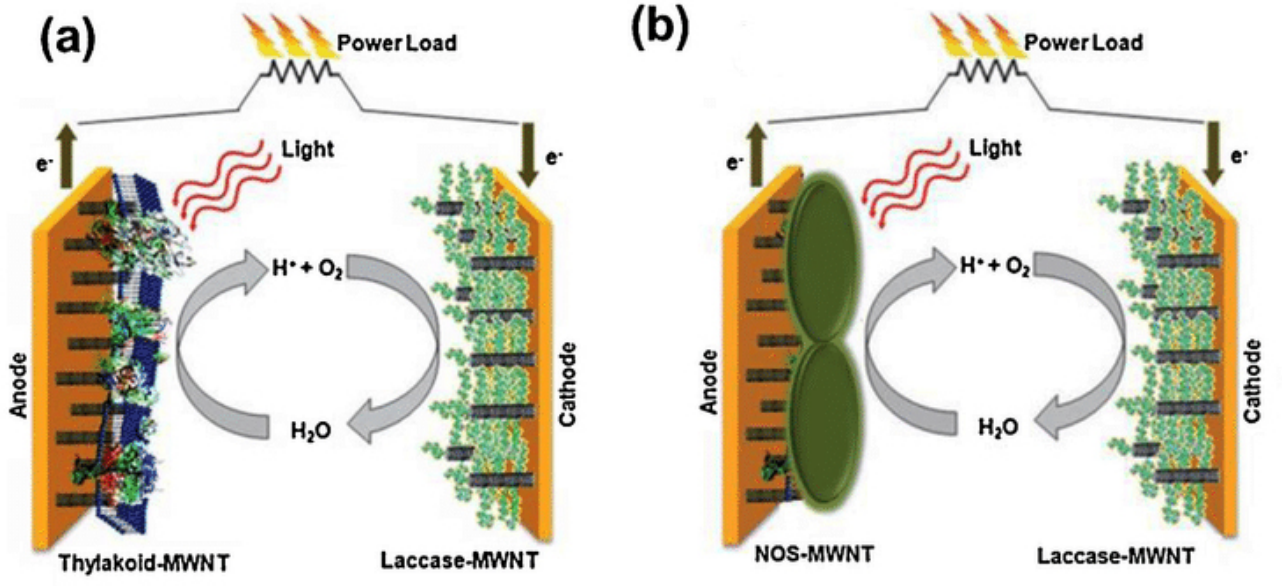

Figure 2.9: Schematic diagram of a photo-bioelectrochemical cell with a thylakoid-based bioanode (a); Nostoc cyanobacteria (NOS)-based bioanode (b).
Figure reproduced from [100]

Different biological components can be employed as photosynthetic systems in a PBEC:

i) Photosynthetic microorganisms, such as cyanobacteria [99,100] or algae [101].
ii) TM extracts [102].
iii) Photosystems I and II (PS I and PS II) [103–105].

2.2.3. Structure and function of thylakoid membranes

Thylakoids are photosynthetically active structural components found in chloroplasts and cyanobacteria [106]. They are the sites where cyanobacteria, algae and plants convert solar energy into chemical energy with high efficiency in the process of photosynthesis. Disc-shaped lamellae stack and form grana, which are connected by stroma lamellae (**figure 2.10**). These interconnected lamellae form the TM or thylakoid network [106–108]. The thylakoid network forms a separate compartment in chloroplasts and cyanobacteria, unlike similar entities

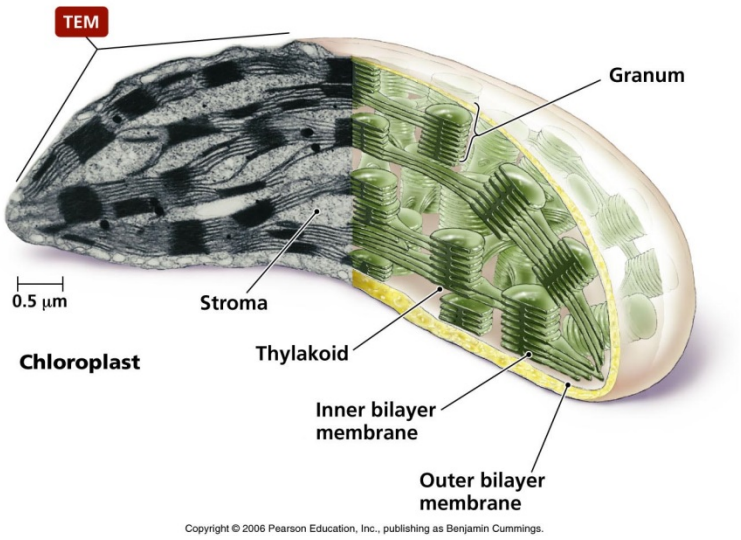

Figure 2.10: TEM image of a chloroplast from a plant cell (left) and schematic representation of chloroplast components (right) showing thylakoids, stroma, grana and bilayer membranes.
Figure reproduced from [108].

that perform anoxygenic photosynthesis in other bacteria [106,109].

Thylakoids are lipid bilayers. Two membrane protein complexes are involved in photosynthesis, PS I and PS II. The energy is harvested with the aid of the cytochrome b_6f complex and ATP synthase [106,110].

TMs can be used as photosynthetic reaction centres (PRCs) for studies dedicated to the development of PBECs [98,111,112]. For this purpose, the mechanism of electron transfer in TMs [113] and communication between TMs and electrodes has been investigated using soluble mediators [111,114] and redox polymers [111].

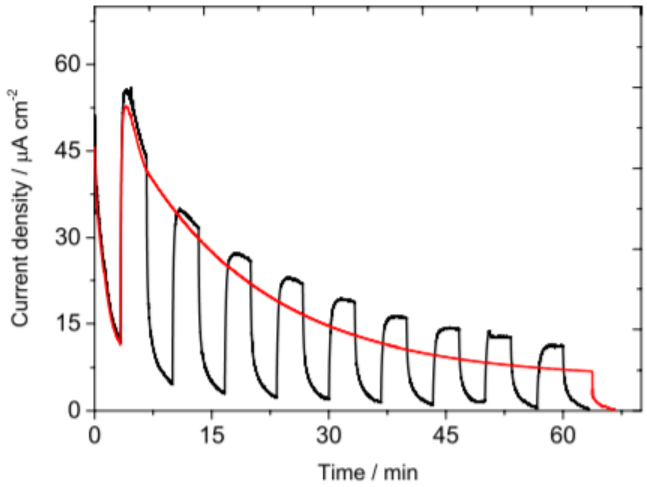

Figure 2.11: Chronoamperograms showing photocurrent decay from thylakoid membranes upon cyclic 'ON-OFF' illumination (black) and continuous illumination (red).
Figure reproduced from [111] *– supporting information.*

One of the inconveniences of using TM extracts instead of live organisms as PRCs is the decrease in photosynthetic activity when exposed to light [111,112] (**figure 2.11**). This is due to photo-induced damage in the PS II complex [115,116]. However, TMs are valuable as model systems for developing PBECs, since they are easier to manipulate than photosynthetic organisms such as cyanobacteria or algae, but more relevant than isolated PS I and PS II systems [102].
In this work, I have used TMs as model system for testing photocurrent generation from photosynthetic components using custom-made electrode chips. This is described in more details in chapter 4 and Appendix II.

Chapter 3: Carbon electrodes

Life exists in the universe only because the carbon atom possesses certain exceptional properties.
James Jeans

This chapter starts by describing carbon allotropes and why carbon materials are interesting for use in electrochemical and biological applications. The structure of glass-like carbons and the use of glassy carbon as electrode material are described. Afterwards, photolithography and pyrolysis are explained, since these were essential for fabrication of the electrodes used for my PhD project. After introducing the theoretical notions important for the experimental part, I provide a detailed description of the fabrication procedures that I used to obtain optical fibre electrodes and carbon-based electrode chips.

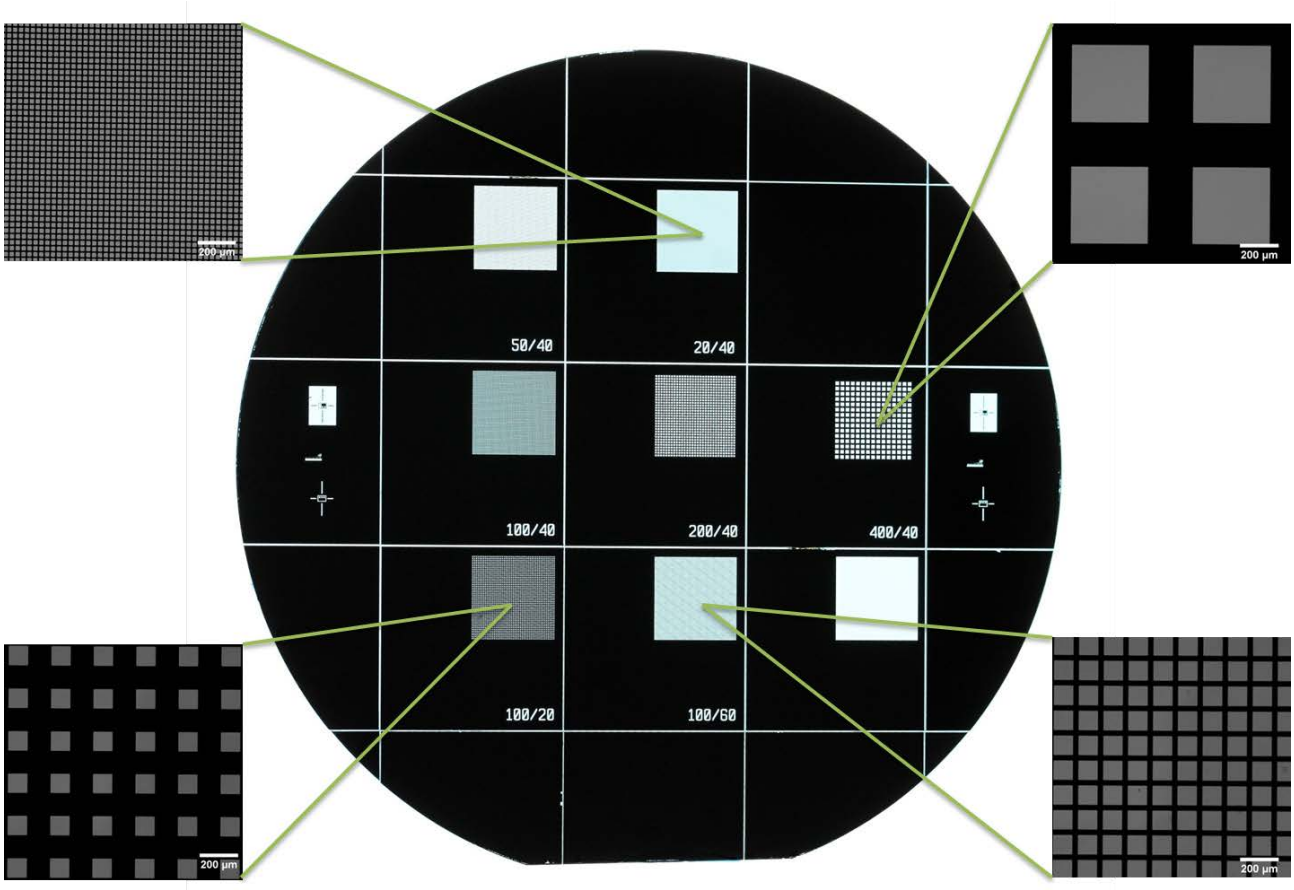

3.1. Carbon as electrode material

What we normally think of as 'life' is based on chains of carbon atoms, with a few other atoms, such as nitrogen or phosphorous. One can speculate that one might have life with some other chemical basis, such as silicon, but carbon seems the most favourable case, because it has the richest chemistry
Stephen Hawking

Carbon is an extremely interesting element, with special properties that set it apart from other atoms. It is the element with the richest chemistry, the basis for all organic molecules and for life on Earth as we know it. Over 95% of known chemical compounds contain carbon [117].
From an electrochemical point of view, it has been a material of interest for the past two centuries, since Sir Humphry Davy used his graphite electrodes to produce alkali metals [118] and thus initiated the development of electrochemistry. Since then, carbon electrodes have been widely used because of their advantageous properties: low fabrication costs, wide potential window, relatively inert electrochemistry and good electrocatalytic activity [119]. Although carbon has been investigated as electrode material for a long time now, new carbon-based materials (such as graphene and carbon nanotubes) have recently been developed and applied for electrode fabrication with good results.

3.1.1. Carbon allotropes: structure and properties

Carbon has numerous allotropes (**figure 3.1**), which can be classified after different criteria, such as valence orbital hybridisation (sp^3, sp^2, sp) [120], origin (naturally-occurring or synthetic) [121], dimensionality (0D, 1D, 2D or 3D) [122] etc. The most well-known carbon allotropes are diamond, graphite, amorphous carbon, fullerenes, graphene and carbon nanotubes. Other allotropes include carbynes, graphdiyne, londsaleite and C540 (fullerite) [117,120–125]. The Nobel Prize in Chemistry in 1996 was awarded to Robert Curl Jr., Sir Harold Kroto and Richard Smalley "for their discovery of fullerenes", clusters of carbon atoms with high symmetry arranged in the shape of closed shells.

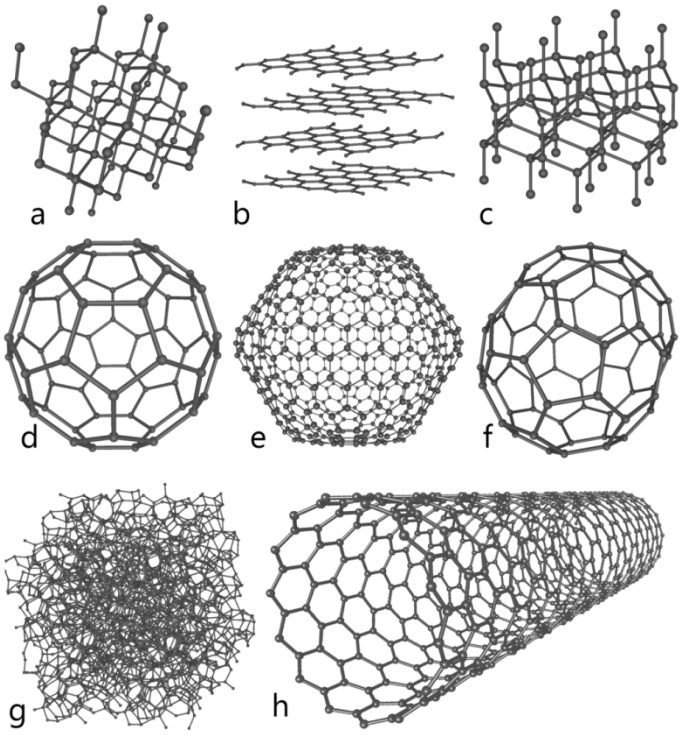

Figure 3.1: The structure of some carbon allotropes: diamond (a), graphite (b), lonsdaleite (c), C_{60} buckminsterfullerene (d), C_{540} fullerene (e), C_{70} fullerene (f), amorphous carbon (g) and single walled carbon nanotube (h). Figure reproduced from [125].

For a material to be used as electrode material, conductivity is an essential property. Different carbon allotropes have very different conductivities, so not all of them are suitable for the development of

electrodes.

Diamond is a crystalline allotrope of carbon with sp^3 hybridisation (tetrahedral) and a C-C bond with a length of 1.54 Å [126,127]. It has very low electrical conductivity, meaning that it is not suitable as electrode material. Its conductivity can be improved by doping with elements such as boron or nitrogen, leading to materials with conductivity suitable for electrochemical applications [119]. For example, boron-doped diamond has a resistivity between 0.05 and 0.5 Ω·cm, depending on the doping level [119].

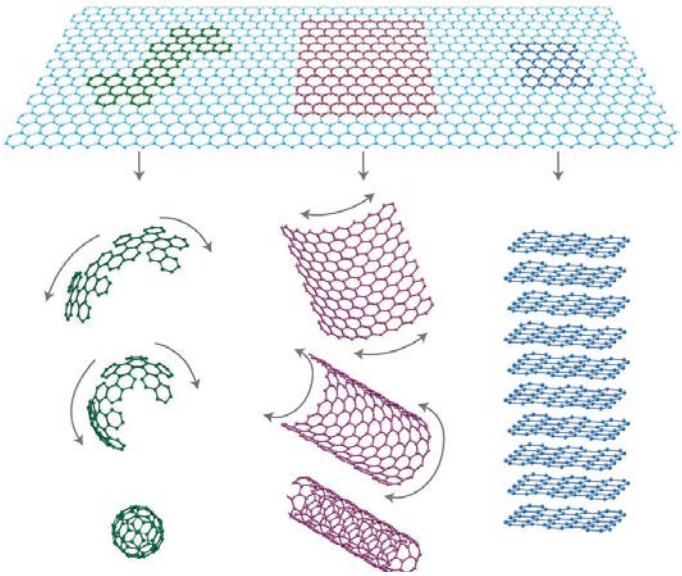

Figure 3.2: Graphene as building material for other carbon materials: wrapped up as fullerene (left), rolled into carbon nanotubes (middle) or stacked into graphite (right) Figure reproduced from [132]

Graphite is another crystalline allotrope of carbon. The atoms are arranged in a honeycomb lattice made of ideally infinite graphene sheets stacked and held together by weak Van der Waals forces (**figure 3.2**). The carbon atoms have sp^2 hybridisation, with a bond length of 1.42 Å and a distance of 3.41 Å between planes [126,127]. Graphite is a good conducting material and it has been used for a long time as electrode material. Randomly oriented graphite has a resistivity of 1×10^{-3} Ω·cm [119]. Highly oriented pyrolytic graphite (HOPG) has a resistivity of 4×10^{-5} in the a-axis (basal plane) and of 0.17 in the c-axis (edge plane) [119]. This explains the recent interest in graphene, since it is a material with very good electronic conduction [122,128–132].

Carbon nanotubes (CNTs) have also attracted a lot of interest among researchers and have been used for electrode modification [122,125,131,133]. They consist of rolled up graphene. Single-walled carbon nanotubes (SWCNTs) are derived from a single layer of graphene, while multi-walled carbon nanotubes (MWCNTs) are derived from multiple graphene layers [125].

3.1.2. Glass-like carbon: history and structure

According to the International Union of Pure and Applied Chemistry (IUPAC) definition, glass-like carbon is “an agranular non-graphitizable carbon with a very high isotropy of its structural and physical properties and with a very low permeability for liquids and gases. The original surfaces and the fracture surfaces have a pseudo-glassy appearance” [134]. Glassy carbon and vitreous carbon are trademarks for glass-like carbon [134].

“Cellulose-carbon” was the first gas-impermeable carbon (or glass-like carbon), developed by Davidson in 1957 and patented in 1961 [135]. Glassy carbon was first reported by Yamada and Sato

in 1962 [136]. Already in the 1960s, glass-like carbon materials became very popular among researchers, although their structure was not yet well understood [137]. This interest was due to the fact that it was found early that glass-like carbons exhibit several interesting properties, such as: good thermal and chemical resistance, surface stability and good behaviour as electrode materials [137].

Glass-like carbons are made by the carbonisation of thermosetting resins (such as polyacrylonitrile, furfuryl alcohol and phenol/formaldehyde resins). The carbonisation can be done either by pyrolysis in inert atmosphere at temperatures between 1000-3000°C, or under a pressure of 140-700 bar [137]. Glass-like carbon has an electrical resistivity between 3.5-5 x 10^{-3} Ω·cm [138].

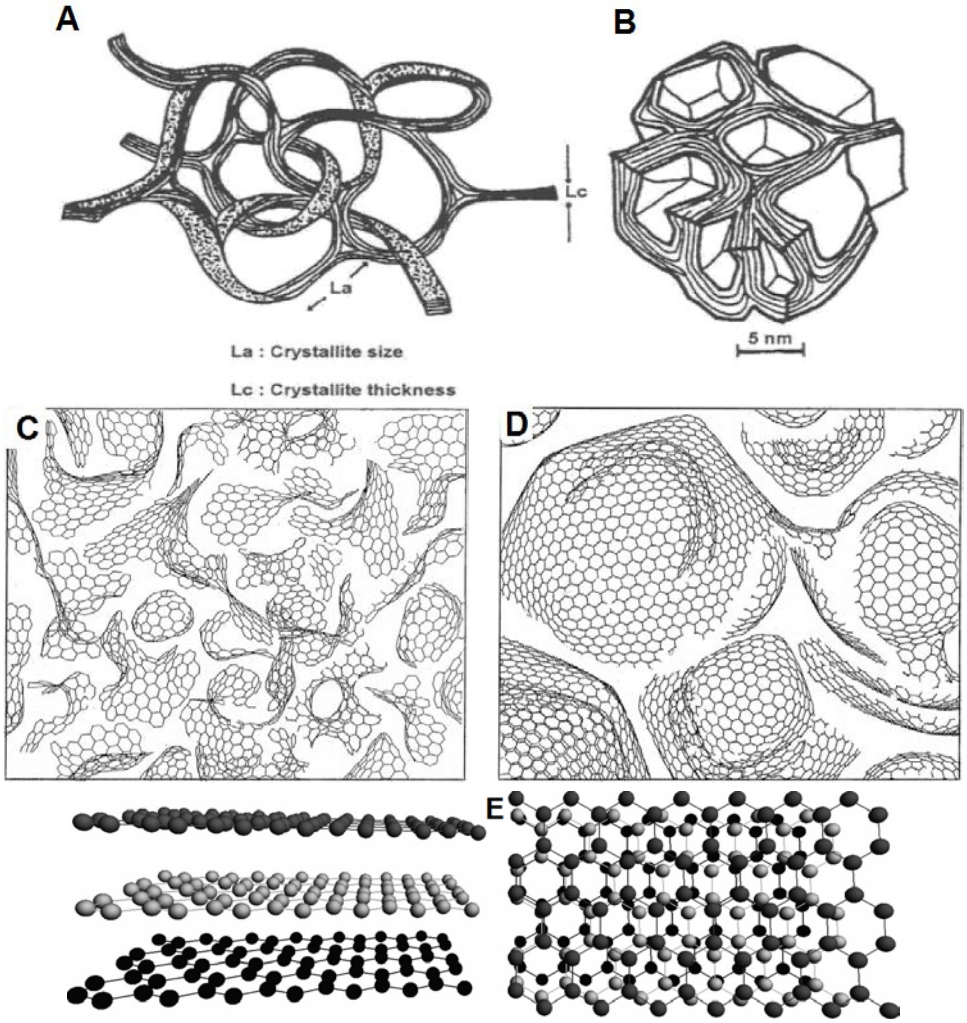

Figure 3.3: Top: structural models for glassy carbon proposed by Jenkins and Kawamura in 1971 (a) and by Shiraishi in 1984 (b). Middle: simulated models for the structure of glass-like carbon obtained at low temperature (c) and high temperature (d). Bottom: geometry example of paracrystalline glass-like carbon structure consisting in three carbon layers, based on glassy carbon pyrolysed at 600°C (e).
Figure reproduced from [135] *(a, b);* [139] *(c, d) and* [140] *(e).*

Several possible structures for glass-like carbon have been proposed and discussed throughout time [124,135,137,141,142]. **Figure 3.3** shows some of the proposed and simulated structures. The

current view is that glass-like carbon is a form of disordered carbon which consists in alternating amorphous and crystalline regions and with a level of microstructural disorder in between amorphous carbon and graphite [143]. The degree of disorder depends on the parameters of the pyrolysis process [139].

3.1.3. Glassy carbon as working electrode

Zittel and Miller were the first to employ a glassy carbon electrode (GCE) in electroanalytical chemistry, in 1965 [144]. They performed a systematic investigation of the electrochemical properties of GCEs using a three electrode system, with the GCE as working electrode, a pyrolytic graphite electrode (PGE) as counter electrode and a saturated calomel electrode (SCE) as reference. They determined that the whole surface area of the GCE was active, that the electrode was relatively insensitive to pH changes and its widest usable potential span was between -0.8 and +1.3 V (E vs SCE). The differential capacitance of GCE in 1M H_2SO_4 was determined to be of 200 $\mu F \cdot cm^{-2}$, leading to a relatively high background current, but without making the electrode unusable. Compared to other stationary electrodes, GCEs proved to be surprisingly resistant to surface contamination. Overall, the first assessment of glassy carbon as electrode material proved very positive and promising. Since then, GCE proved to be an incredibly useful tool in electroanalytical chemistry, and became one of the standard electrodes for electrochemical measurements [138,145].

3.1.4. Sensing with carbon electrodes

One of the applications of carbon electrodes is the quantification of small electroactive molecules of biological relevance, such as dopamine (DA), uric acid, ascorbic acid, NADPH or H_2O_2 [146]. They can also be used for detection and quantification of pharmaceutical compounds, either for preparation purposes, or from biological samples [147]. Different types of carbon electrodes can be used for this purpose, such as GCE, carbon paste, fullerene, graphite, diamond or even screen printed carbon electrodes [147]. There are numerous examples of biosensors developed by modification of carbon electrodes: enzymatic sensors, immunosensors, DNA sensors and aptasensors [129,146,148–150]. Glucose sensing, a highly researched topic, makes use of carbon-based biosensors and recent developments focus especially on disposable screen-printed or inkjet-printed carbon electrodes [146,151–153]. A different field in which carbon electrodes are useful tools is environmental detection [146,154,155].

Water treatment (desalinisation) can also be done using carbon electrodes [156].

3.1.5. Cells and carbon

Glass-like carbon is biocompatible and has been employed as substrate for cell culture [5,157,158] and as implantable material [159]. Additionally, hVM1 Bcl-xL cells have been shown to spontaneously differentiate into dopaminergic neurons on glass-like carbon [5]. Combined with its electrochemical properties, biocompatibility makes carbon an extremely interesting material for developing an integrated optoelectrical device as potential implant.

3.2. UV photolithography

We live in a society exquisitely dependent on science and technology,
in which hardly anyone knows anything about science and technology.
Carl Sagan

Lithography is a process used in microfabrication in which a pattern is transferred into a reactive polymer layer (commonly called a resist) supported on a substrate [160]. UV photolithography (sometimes called optical lithography) uses near-ultraviolet (near-UV) radiation (360 – 410 nm [160]) to transfer the pattern from a photomask to a light-sensitive resist (photoresist).
Photolithography is widely used for the fabrication of microelectromechanical systems (MEMS) in electronic applications [160–164]. Microstructures fabricated using photolithography can be employed for a variety of purposes, including cell culture applications [5,165].

3.2.1. Photoresists

The principal components of a photoresist are: the polymer (base resin), the photoinitiator (sensitiser) and the solvent [166]. The polymer reacts differently in specific conditions, and is the building block of the structures fabricated using the photolithography process. The photoinitiator controls the photochemical reaction through chemical amplification in the case of some photoresists (such as SU-8) [166,167]. The solvent ensures that the photoresist is a homogenous mixture and allows the spin-coating of uniform layers.

Depending on the response to light, photoresists can be either positive tone or negative tone. In the case of a positive tone resist, the areas exposed to light become soluble in the developer and will be removed after processing. For negative photoresists, the areas exposed to light become insoluble in the developer and constitute the pattern for the obtained structure, while the unexposed areas will be solubilised by the developer.

Several properties are important for a good photoresist: adhesion, sensitivity, contrast, etching resistance, resolution, purity, shelf life, solvent content, glass transition temperature (T_g), cost and how easy it is to manufacture and process [166].

3.2.2. SU-8

SU-8 is a negative tone, epoxy-based photoresist developed and patented by IBM. Commercial formulations became available in 1996, from MicroChem (USA). Polymerisation of SU-8 results in a thermoset polymer [168].
SU-8 contains bisphenol A novolac epoxy (EPON® resin SU-8, trademark of Shell Chemical Company, **figure 3.4**) dissolved in an organic

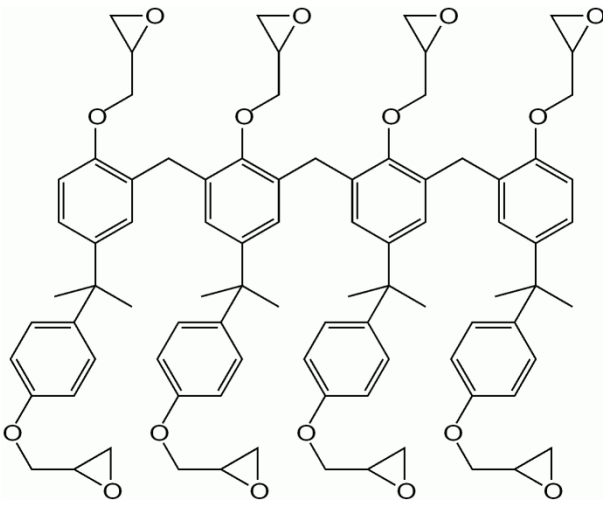

Figure 3.4: Chemical structure of Bisphenol A novolac epoxy, the resin in SU-8 photoresist. Figure reproduced from [166]

solvent – gammabutyrolactone (GBL), propylene glycol methyl ether acetate (PGMEA) or cyclopentanone – with up to 10% triarylsulfonium hexafluoroantimonate salt as photoacid generator [166]. It is a resist with good mechanical properties and high resistance to both chemicals and temperature. The main advantage of SU-8, and the reason why it became so popular, is its low absorption at 365 nm (up to thicknesses of 2 mm). This makes it ideal for patterning structures with high aspect ratio (HAR). Different densities and viscosities of SU-8 are available, allowing the fabrication of films with thicknesses between 0.5 and 500 µm in one single coating step [166,169].

3.2.3. Process steps in UV photolithography

The main steps in UV photolithography are spin-coating, exposure, post-exposure bake and development. Different surface pretreatments and baking steps can be employed, depending on the resist, desired application etc. Drying and post-treatment of fabricated structures are also sometimes necessary. The photolithography steps will be described in the following paragraphs, with focus on SU-8 processing. **Figure 3.5** shows a schematic view of the process.

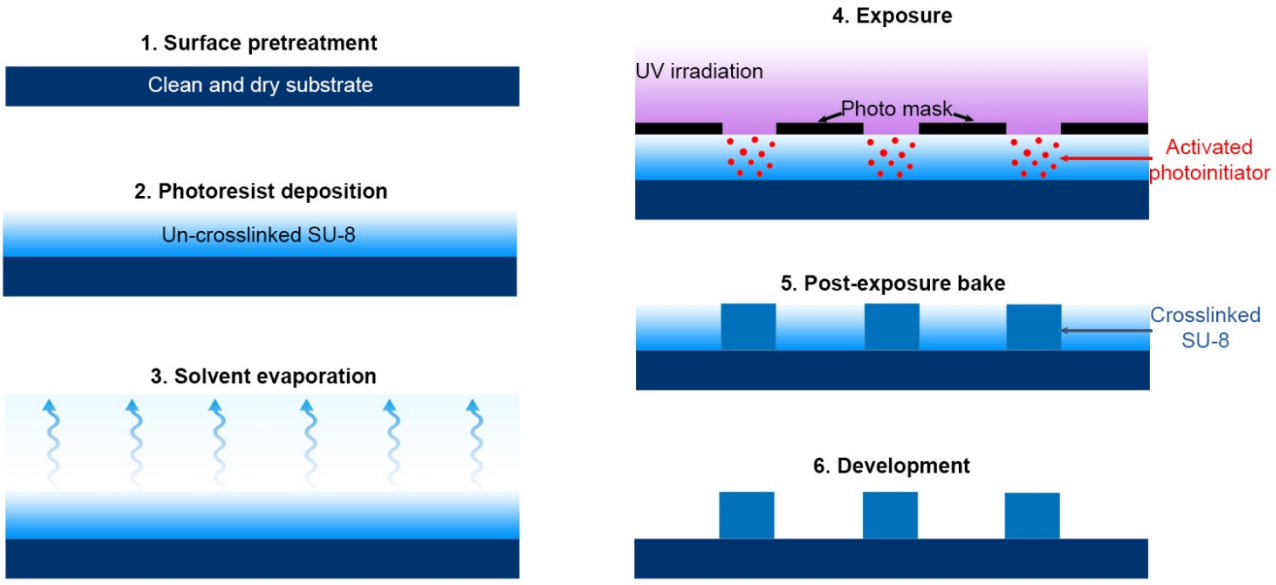

Figure 3.5: Steps involved in SU-8 photolithography.

3.2.3.1. Surface pretreatment

In order to achieve good adhesion of the photoresist, the substrate needs to be clean and perfectly dry. Commercial substrates with almost no surface impurities are available for cleanroom fabrication. Alternatively, substrates can be cleaned using diluted hydrofluoric acid, piranha mixture or RCA cleaning (a two-step cleaning procedure which removes organic residues and metal ions) [166]. To ensure reduced surface hydration, the substrates can be baked at temperatures above the boiling point of water prior to spin-coating.

3.2.3.2. Spin-coating (photoresist deposition)

Deposition of resist on the substrate is normally done by using spin-coating, to ensure uniformity of the resist layer [170]. The thickness of the obtained layer depends mainly on the resist properties (density, viscosity), spinning parameters (acceleration, speed, duration) and substrate.

3.2.3.3. Pre-exposure bake (solvent evaporation)

After spin-coating, a soft bake step can be employed to allow evaporation of the solvent prior to exposure [170]. The duration, temperature and conditions for this pre-exposure bake need to be optimised for a specific process. Different resists and different layer thicknesses will require different parameters. If baking at temperatures higher than room temperature (RT), ramping is needed to avoid flowing of the resist on the wafer [170]. An edge bead removal step can be employed before hard contact exposure to improve lithographic resolution.

3.2.3.4. Exposure

Exposure parameters also need process-specific optimisation. The exposure usually requires a mask that will define the pattern to be removed (for positive photoresists) or the pattern desired on the substrate (for negative photoresists). The exposure can be done in hard contact, soft contact or proximity. The contact mode and the exposure dose will influence development time and structure definition. SU-8 is a negative photoresist, so the pattern on the mask is a negative of the patterned layer to be fabricated. Exposure of SU-8 is done in the long-wavelength ultraviolet (UV-A) domain, at 365 nm.

3.2.3.5. Post-exposure bake

In the case of SU-8, a post-exposure bake is necessary to ensure crosslinking of the polymer [166]. The crosslinking process is activated by the UV exposure, but requires further heating to obtain a polymerised resist layer [166].

3.2.3.6. Development

The development is normally done by immersing the substrate in developer for a certain amount of time, under stirring. For thicker resist layers, longer development times will be needed. In the case of SU-8, PGMEA is usually used as developer.

3.2.3.7. Drying

After development, the structures need to be dried properly to avoid structure collapse. This is done by first rinsing with a liquid with lower surface tension than the developer [166]. For SU-8, the structures can be rinsed with isopropyl alcohol and then blow-dried with nitrogen. Depending on the size of the structures, freeze-drying or supercritical drying might be needed (for example, for HAR structures with spacing of several µm).

3.2.3.8. Descumming

Removal of unwanted residual resist can be done where necessary. For SU-8, this can be done either by using a mild oxygen plasma treatment (PT), or by short immersion in acetone [166]. If acetone is used, an additional drying step is required.

3.2.3.9. Hard bake

For certain applications, a hard bake of the developed structures can be employed as well. This step ensures removal of solvent residues from the matrix and layer annealing. For SU-8, hard baking improves the hardness of the polymer layer and its resistance to etching [166]. After this step, the SU-8 structures are better crosslinked, with a T_g higher than 200°C [166] and high thermal and chemical resistance.

3.2.3.10. Removal (stripping)

When the photoresist is used as sacrificial layer, or when the substrate needs to be reused, the last step of the photolithography process is polymer removal. This needs to be done in a way that does not affect the rest of the device. For SU-8 removal, plasma ashing can be employed [166].

3.3. Pyrolysis

The science of today is the technology of tomorrow.
Edward Teller

The process of pyrolysis involves heating at high temperatures in the absence of oxygen. It can be employed to obtained glass-like carbon from certain precursors. Not all polymers are suitable candidates as carbon precursors for pyrolysis. Pure hydrocarbon polymers degrade into volatile products during pyrolysis [142]. Other polymers (such as polyvinylidene chloride) develop graphitic regions when heated at very high temperatures, up to 3000°C, and are considered graphitising carbons [171]. In the case of thermosetting polymers, such as polyfurfuryl alcohol or phenolic polymers, the energy required to break the C-C bonds is too high, so they behave as non-graphitising carbons [171]. Instead, thermosetting polymers release heteroatoms and hydrogen, resulting in mass loss and shrinkage. Eventually, glass-like carbons are formed, which preserve the initial shape of the polymer [172]. Recently, proteins (such as silk fibroin or spider webs) have also been used for obtaining carbonaceous materials through pyrolysis [173–175].

Both SU-8 and polyimide (PI), the carbon precursors tested in this work, are thermosetting polymers, so they generate glass-like carbon when pyrolysed [168,176,177].

3.3.1. Step-by-step pyrolysis of thermosetting resins

The steps involved in the pyrolysis of thermosetting resins were described by Jenkins and Kawamura [141,142]. As mass-loss progresses, the polymeric material undergoes a series of chemical changes, including dehydrogenation, hydrogen transfer, condensation, cyclisation and isomerisation.

The first step is called the pre-carboniz sation phase and takes place at temperatures below 300°C. Solvent molecules and residual monomers are removed from the polymer layer. Between 300°C and 500°C, halogens and other heteroatoms are removed, leading to the formation of a network of conjugated carbon systems. This is referred to as carbonisation phase I. Around 450°C, dehydrogenation begins. At higher temperatures, up to 1200°C, in the carbonisation phase II, most remaining hydrogen, nitrogen and oxygen atoms are removed. This causes the carbon network to become interconnected. Above 1200°C, in the annealing phase, remaining sulphur atoms and other impurities are removed. **Figure 3.6** shows weight loss measured

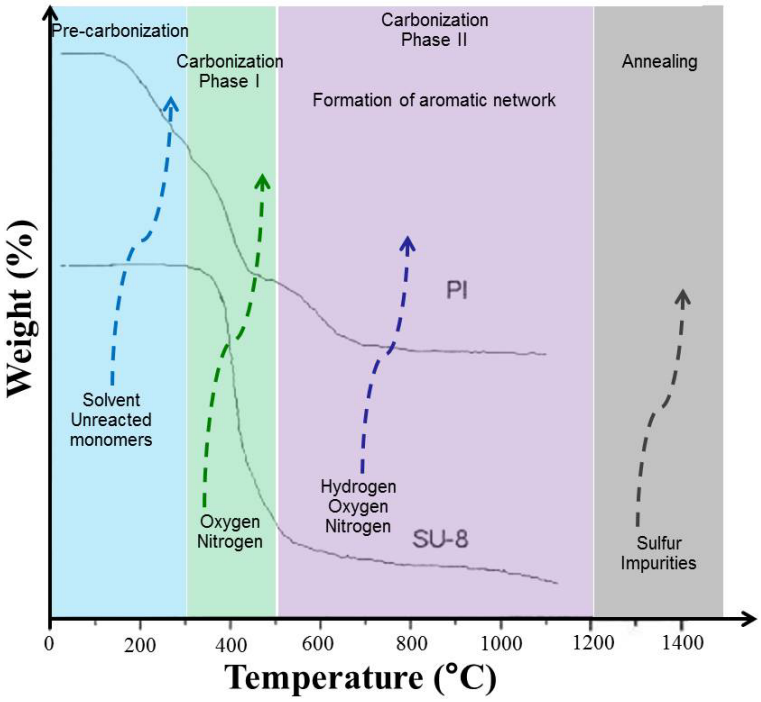

Figure 3.6: Schematic of steps involved in carbonisation overlapped with thermogravimetric analysis (TGA) of SU-8 and polyimide (PI) during pyrolysis in 5% H_2 and 95% N_2 TGA results reproduced from [178]

from thermogravimetric analysis (TGA) during pyrolysis of SU-8 and PI [178] associated with the mentioned pyrolysis steps.

3.3.2. Important parameters in pyrolysis

The parameters used in the pyrolysis process have an effect on the properties of the final carbonised structure. The final pyrolysis temperature determines the graphitic content of the obtained carbon, and thus its resistivity [178–180]. At high temperature, polymer shrinkage is also high [178] and might lead to structure collapse, especially for HAR structures. Temperature ramping is also important, because faster heating leads to faster release of gaseous products from the substrate and can lead to cracks or even the complete removal of the polymer layer from the substrate [178].

Pyrolysis needs to be done in the absence of oxygen to avoid the burning of the polymer. The furnace atmosphere is thus important. The process can be done in vacuum, inert or reducing atmosphere (nitrogen, argon or forming gas – a mixture of 95% N_2 and 5% H_2). The highest carbon content was observed for structures pyrolysed in vacuum or forming gas [181]. However, pyrolysis in vacuum can result in the formation of micro-cracks in the SU-8-based carbon due to fast removal of gaseous products released from the substrate [182]. When using inert gases for pyrolysis, the flow rate needs to be optimised, to ensure that the atmosphere remains inert inside the furnace throughout the process.

3.3.3. SU-8 and polyimide as negative photoresists

The behaviour of two negative photoresists (SU-8 and PI) during pyrolysis was investigated by Singh *et al.* on two different substrates, silicon and fused silica wafers [178]. Both precursors can lead to the formation of adherent carbon layers on both substrates when using thin resist films and a slow heating rate ($1°C \cdot min^{-1}$). Thin layers (below 3 µm) do not lead to the formation of adherent carbon layers when heated by $5°C \cdot min^{-1}$. When using thicker resist layers (8 µm), only PI on silicon survives the process at $5°C \cdot min^{-1}$. In all cases, the carbon obtained had a smooth, pore-free surface and was not crystalline [178].

The two photoresists exhibit different behaviour during pyrolysis. The weight loss and vertical shrinkage for SU-8 is much higher than for PI (**figure 3.6** and **3.7**). Also, the weight loss of SU-8 occurs quite abruptly at temperatures between 350 - 500°C, while gas evolution reactions for PI progress in a wide temperature range, between 150 and 700°C. For both polymers, film resistivities decrease considerably between 700-800°C, after which the decrease is very slow (**figure 3.7**). For pyrolysis temperatures of ~900°C, the carbon layer resistivity (regardless of precursor) is approximately 0.1 Ω·cm [178].

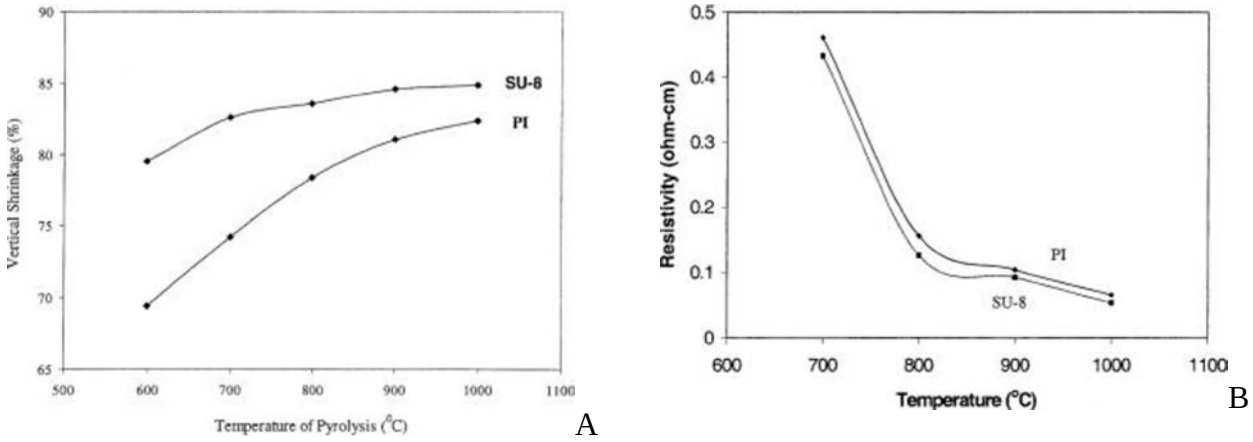

Figure 3.7: Evolution of characteristics of polyimide (PI) and SU-8 during pyrolysis as a function of temperature: vertical shrinkage (a) and resistivity (b).
Figures reproduced from [178].

3.4. Fabrication of carbon electrodes

Science is the systematic classification of experience.
George Henry Lewes

Two types of carbon electrodes were fabricated and used for the work described in this thesis: optical fibre electrodes (OFEs) and transparent electrode chips (TECs). The following subsections will motivate and describe the fabrication. The properties and applications of the electrodes will be detailed in chapter 4 and appendices I and II.

3.4.1. Optical fibre electrodes

Since the project aims at developing an optoelectrical cell carrier to be used for implantation, the use of optical fibres (OFs) was an obvious choice due to the shape, size and biocompatibility of component materials. Commercial OFs are made of plastic or fused silica. The structure of an OF is shown in **figure 3.8**. Because the fabrication process requires high temperatures during pyrolysis, the use of OFs with plastic core in this project was excluded. The core of fused silica OFs is surrounded by a cladding made of doped fused silica with slightly lower refractive index than the core material [183]. On top of the cladding, the OFs have a polymeric buffer layer which provides extra mechanical strength and prevents the silica from getting in contact with the atmosphere [184,185]. This buffer layer is suitable as carbon precursor in pyrolysis.

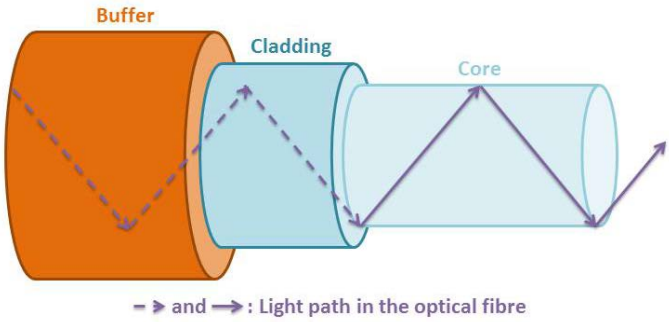

Figure 3.8: Schematic of the structure of an optical fibre and the path of light travelling through the core

Commercial fused silica OFs from Edmund Optics with polyimide buffer layer were chosen for the experiments because i) the buffer material is suitable for pyrolysis [178,186]; ii) different sizes were available for purchase; iii) the company commercialises OFs with lengths suitable for research (in the order of meters, while most producers only sell lengths suitable for industrial applications, in the order of kilometres). Three different diameters were tested and the parameters are given in table 3.1, as specified by the producer (except for the PI thickness, which was calculated as half the difference between the outer diameter and the cladding diameter).

Table 3.1: Sizes of different optical fibres tested

	OF_{100}	**OF_{200}**	**OF_{400}**
Core diameter (µm)	100 ± 2	200 ± 4	400 ± 8
Cladding diameter (µm)	110 ± 2.2	220 ± 4.4	440 ± 8.8
Outer diameter (µm)	130 ± 5	245 ± 5	480 ± 10
Polyimide thickness (µm)	10	12.5	20

3.4.1.1. OFEs fabricated using the original coating of the fibres (polyimide)

For obtaining PI-derived OFEs, the fibres were used as provided by the company, after removing residual particles from the surface (to allow cleanroom processing). 10 cm OF pieces were placed in a ceramic boat and pyrolysed using a protocol previously optimised in our group [5] and described in detail in appendix V.

Pyrolysis of OF_{100} and OF_{200} samples led to adherent carbon layers, while in the case of OF_{400} the obtained carbon layer was cracked and would easily detach upon manipulation. This is not surprising, since the polymer layer had a considerable thickness (20 µm) and was thus more prone to cracking due to gas evolution during pyrolysis [178]. For this reason, the OF_{400} pyrolysed samples were not further characterised. Pyrolysis of OF_{200} samples lead to a carbon layer with a thickness of 7.49 ± 0.06 µm (determined from SEM as described in section 4.1.8.)

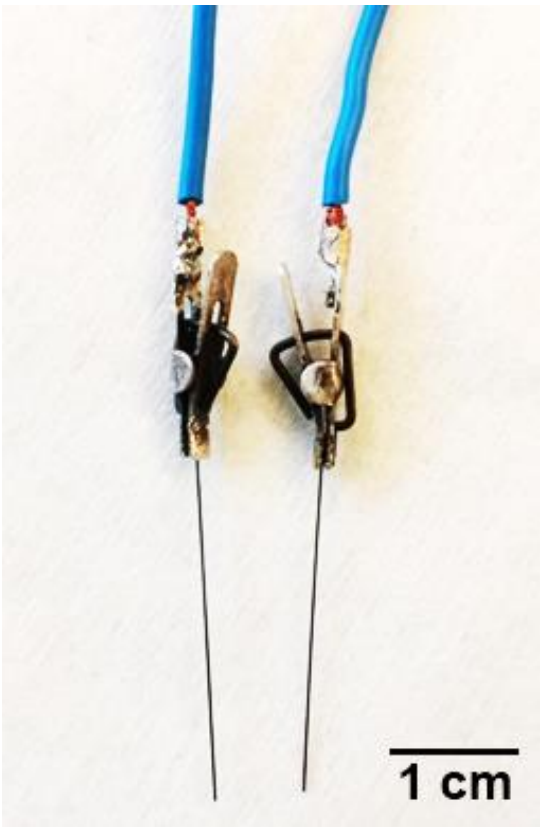

Figure 3.9: Optical fibre electrodes fabricated using optical fibres with a 200 µm core diameter, connecting crocodiles and wires

For electrochemical characterisation, the pyrolysed OFs were cut into 2.5 cm pieces and interfaced to the potentiostat using small aluminium crocodiles and copper wires, as shown in **Figure 3.9**. OF_{200} were chosen as being the most suitable for subsequent experiments, both because of the size (easier to manipulate than OF_{100}) and because of the results from electrochemical measurements.

3.4.1.2. OFEs fabricated using other carbon precursors

The original coating of the fibre (PI) proved to be a suitable carbon precursor. However, for the final goal of the work, the carbon layer needs to be "leaky". This means it should allow light to pass through the OF to reach the cells residing on the surface (**figure 3.10**). For this purpose, the precursor needs to be patterned on the surface of the OF.

Crosslinked PI is hard to manipulate, so replacing the original coating of the OFs might be necessary for patterning. Alternatively, the existing buffer layer could be patterned using laser ablation or selective etching.

Two materials were chosen as alternate carbon precursors: SU-8 photoresist and fibroin (a silk protein that can be carbonised [173,187]).

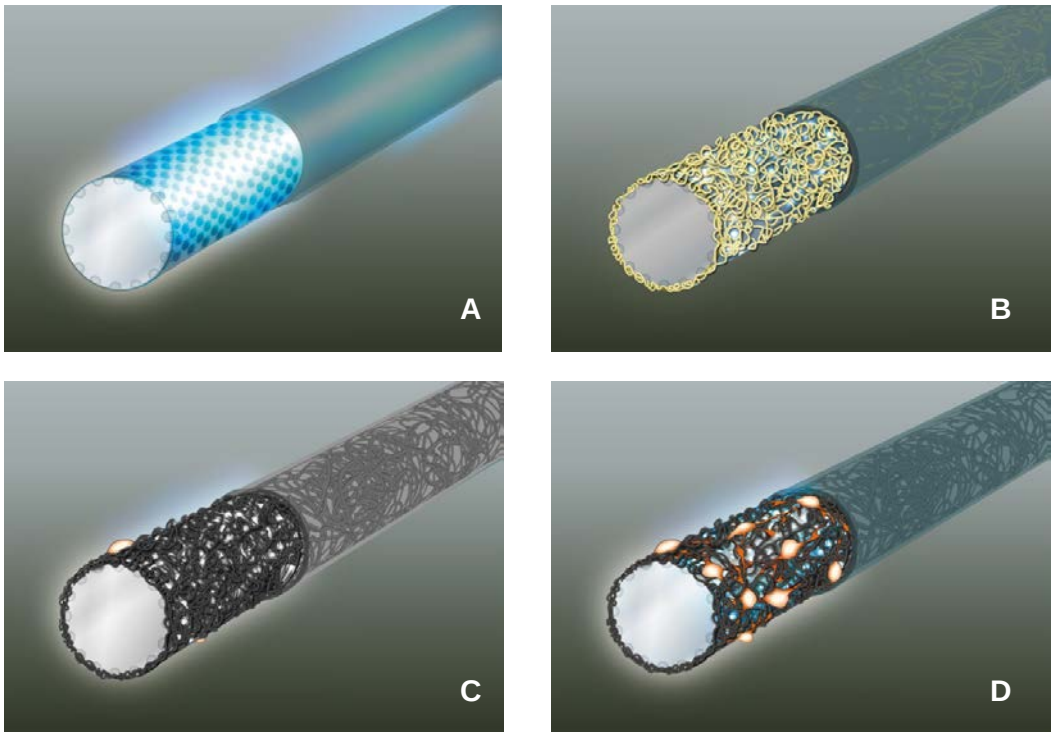

Figure 3.10: Schematic of fabrication steps necessary in the fabrication of OFEs: Leaky optical fibre (a); Polymer deposition and patterning (b); Pyrolysis (c); Cell culture on patterned carbon (d).

In order to fabricate OFEs using SU-8 and fibroin as carbon precursors, several fabrication steps were necessary (**figure 3.11**). First of all, the original coating of the fibre (PI) had to be removed. This was done by stripping with heated piranha mixture (a 3:1 mixture of H_2SO_4 and H_2O_2, used at ~60°C) for 15 min. Because the commercial PI buffer is highly crosslinked, the stripping had to be repeated 2-3 times to ensure complete removal of the polymer layer. After this step, the OF pieces became more brittle and needed careful handling. The next step involved deposition of the new carbon precursors on the unbuffered OF pieces. This was done by dip-coating using a syringe pump. The substrate (stripped fibre) was attached to the piston of the syringe pump by using adhesive tape. The substrate was then immersed in the coating solution (SU-8 2005 or 8% w/w fibroin in water) and kept there for 1 min before being pulled upwards slowly at a constant rate. After dip-coating, a soft bake step was necessary to allow solvent evaporation. The duration of the soft bake was 2h, in the case of SU-8, and 24h for fibroin. Since fibroin was used in aqueous solution, a longer time was required for solvent evaporation. Crosslinking was done by UV exposure (60 s using 365 nm, 18 $mW \cdot cm^{-2}$ source) in the case of SU-8 and by 3 min immersion in

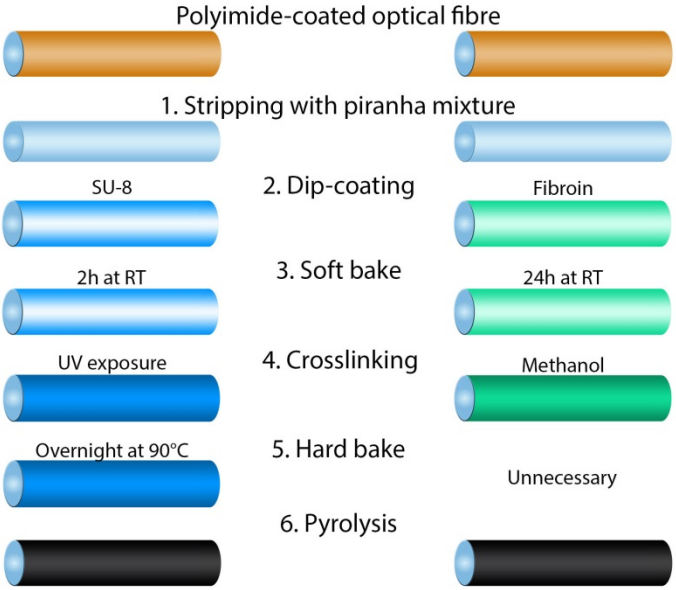

Figure 3.11: Schematic of fabrication steps necessary in the fabrication of SU-8- (left) and fibroin- (right) based OFEs.

methanol in the case of fibroin. SU-8-coated fibres were hard baked overnight at 90°C. The obtained samples were then pyrolysed as described in appendix V.

To optimise the dip-coating process, three different withdrawal rates were used: 0.25, 0.5 and 1 $cm \cdot min^{-1}$. The withdrawal rate is an important parameter influencing the thickness of the obtained layer. The dip-coating process was repeated one, two or three times (after crosslinking of each coating layer) in different experiments to try to increase the thickness of the obtained layer. SU-8 2005 was replaced with SU-8 2075 in an experiment for the same purpose.

When using SU-8 2005 and dip-coating rates of 0.25 and 0.5 $cm \cdot min^{-1}$, a continuous carbon layer was observed after pyrolysis, regardless of the number of coating layers (**figure 3.12**). At 1 $cm \cdot min^{-1}$, the carbon layer obtained after pyrolysis was brittle and the samples were unusable. The thickness of the obtained layer was investigated with SEM and proved to be of only ~100 nm. SU-8 2075 was too viscous to use as dip-coating solution. The SU-8-derived OFEs were further characterised (see section 4.3.4).

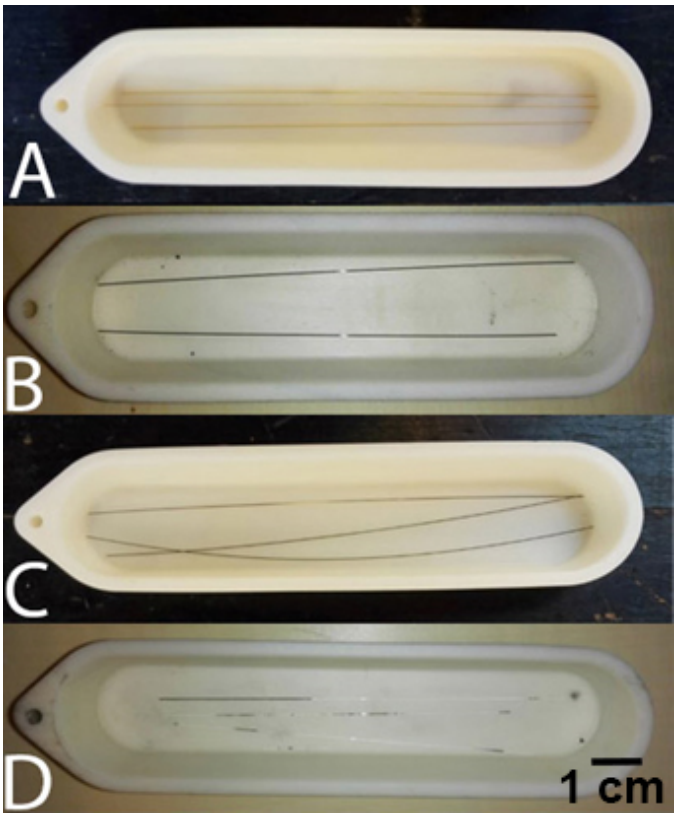

Figure 3.12: Polyimide-coated optical fibres before pyrolysis, as provided by the supplier (a). Pyrolysed samples with carbon derived from polyimide (b), SU-8 (c) and fibroin (d)

For fibroin, when using one coating layer, there was no carbon layer on the surface after pyrolysis, regardless of the coating rate. When using a dip-coating rate of 0.25 or 0.5 $cm \cdot min^{-1}$ and repeating the process two or three times, only discontinuous sections with adherent carbon were found on the surface after pyrolysis (**figure 3.12d**). This can be attributed to the low viscosity of the coating solution and the nature of the solvent (slow evaporation), which probably leads to gravitational flow of the protein coating and poor adhesion during the dip-coating process. The fibroin-derived OFEs were not further characterised.

To conclude this section, OFEs were successfully fabricated by using either PI or SU-8 as carbon precursor. Further optimisation is required when using SU-8 and fibroin as carbon precursors. For the case of SU-8, different viscosities of the polymer can be tested (such as SU-8 2025 or 2035) to increase the thickness of the carbon layer obtained after pyrolysis. For fibroin, dip-coating from an organic solution could be the solution for improving protein adhesion to the substrate. Regardless of the chosen carbon precursor, patterning is required to obtain a “leaky” section, and this will require further optimisation in future projects.

In chapter 4, the term “OFEs” refers to OFEs fabricated using OF_{200} pieces and the original polyimide coating as carbon precursor unless otherwise specified.

Preliminary experiments were performed to check that the optical fibres can still transmit light after pyrolysis. A 532 nm laser and a microscope objective were used to focus light into the optical fibres in a setup shown in **figure 3.13a**. The fibre was then bent at 90° to ensure that light seen at the terminal point was light coming through the fibre and not directly from the laser. The experiment was performed with optical fibres both before and after pyrolysis. As it can be seen in **figure 4.13b**, the optical fibres retain their ability to guide light after pyrolysis.

A

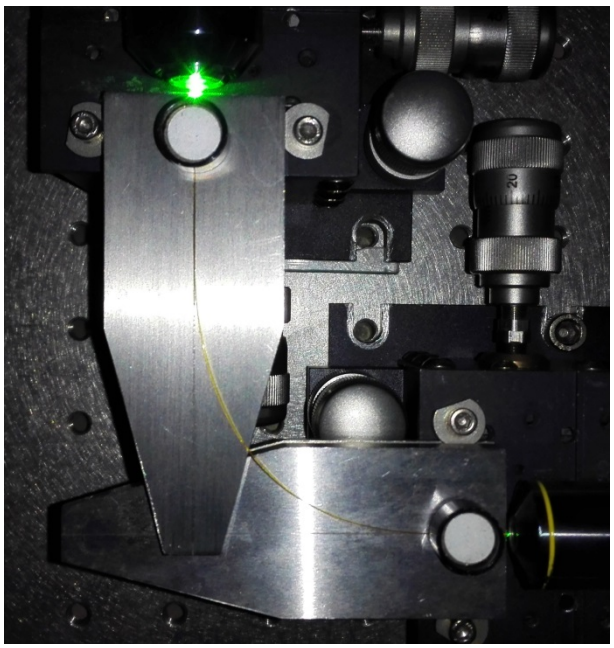

B

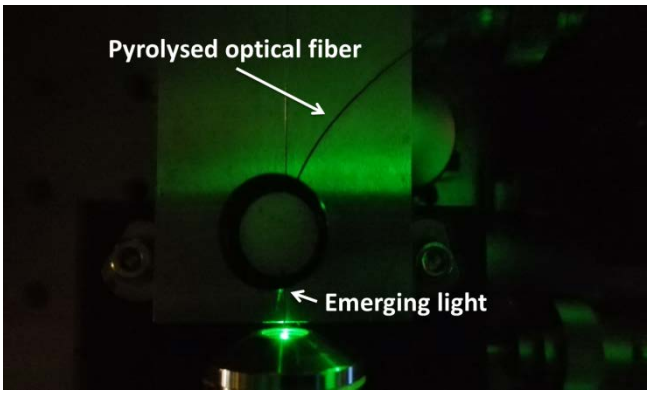

Figure 3.13: Light passing through optical fibre pieces before (a) and after pyrolysis (b). The light from a 532 nm laser was focused into the fibre using an objective. Emerging light was detected at 90°.

3.4.2. Electrode chips

OFs can be difficult to manipulate and characterise due to the availability of standard cleanroom and laboratory equipment. Also, patterning is more straight-forward on large, flat substrates. Therefore, electrode chips were fabricated for investigating different parameters relevant to our application, such as surface chemistry, conductivity and suitability as substrates for cell culture.

For the work in this project, two different polymers and two different substrates were used to fabricate electrode chips. PI was chosen for investigation because it is the initial coating material of commercial OFs, and SU-8 was chosen because it previously showed good results with stem cells [5]. When investigating material properties and cell behaviour, unpatterned carbon chips were fabricated using silicon wafers covered with SiO_2 as substrate and both SU-8 and PI were used as carbon precursors.

For the fabrication of transparent electrode chips (TECs), fused silica substrates were employed. In this case, SU-8 was used as the only carbon precursor. The available PI was not photosensitive and thus could not be directly patterned using photolithograpy. For future experiments, PI could be purchased as photoresist [178] or patterned using other techniques, such as dry-etching [188]. Unfortunately this was not possible during this PhD project due to time constraints.

3.4.2.1. Fabrication of unpatterned carbon chips

PI and SU-8 were processed using modified versions of protocols previously optimised in our department [5,188]. Si wafers with a 110 nm layer of SiO_2 were employed as substrate. The process flows and parameters can be found in appendix V.

For the fabrication of PI-derived carbon chips, the polymer was deposited from a stock of PI-2574 supplied by HD Microsystems. The PI thickness was 10.1 ± 0.4 µm. After pyrolysis, the obtained carbon layer had a thickness of 5.2 ± 0.3 µm.

In the case of SU-8 derived carbon chips, SU-8 2035 from MicroResist was chosen as it allowed us to obtain a carbon layer with a thickness of several µm. The SU-8 thickness was 16.5 ± 0.3 µm. After pyrolysis, the carbon layer obtained had a thickness of 2.9 ± 0.2 µm.

The carbon-covered wafers were then cut into 1 cm x 1 cm pieces using a dicing saw and used (as such or after surface treatment) for XPS measurements and as substrates for cell culture. Chapter 4 will expand upon this.

3.4.2.2. Fabrication of transparent electrode chips

In order to obtain electrode chips that allow light to pass through, fused silica (quartz) was chosen as substrate material. Fused silica is the material used as core and cladding for the OFs employed for fabricating OFEs. It has a wide transparency domain (from UV to near-infrared) and is resistant to high temperatures [189]. Additionally, it is hard, durable and non-porous, properties that are important for a substrate in photolithography. SU-8 2005 was used as photoresist for fabrication of the structures.

Initial fabrication attempts resulted in poorly-developed structures on the fused silica wafers. Circular lines not present on the mask used during UV exposure were visible on the samples after pyrolysis. The observed problem can be attributed to the fact that the substrate is transparent and light reflected from the wafer holder in the aligner also causes exposure of the SU-8. Further optimisation of the photolithographic process was required to obtain well-developed structures after fabrication. Different soft bake durations and different exposure doses were tested. More importantly, the holder used during UV exposure was replaced with a ring holder that only touched the edges of the wafer. The optimised protocol, the mask design and additional experimental details are included in appendix V.

Well-developed structures down to 20 µm were obtained using the optimised protocol. The fabricated chips were then diced into 22 x 22 mm pieces (**figure 3.14**) and used after oxygen PT (3

min, 50 W) for electrochemical measurements and as substrates for cell culture. The TECs were used for investigating photocurrent generation from TMs (chapter 4 and appendix II).

A

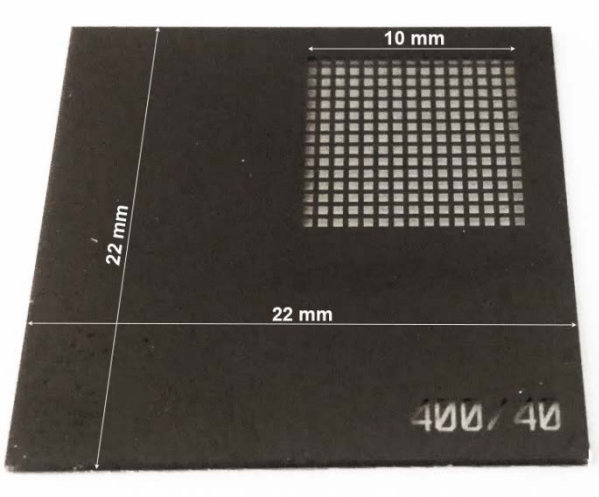

B

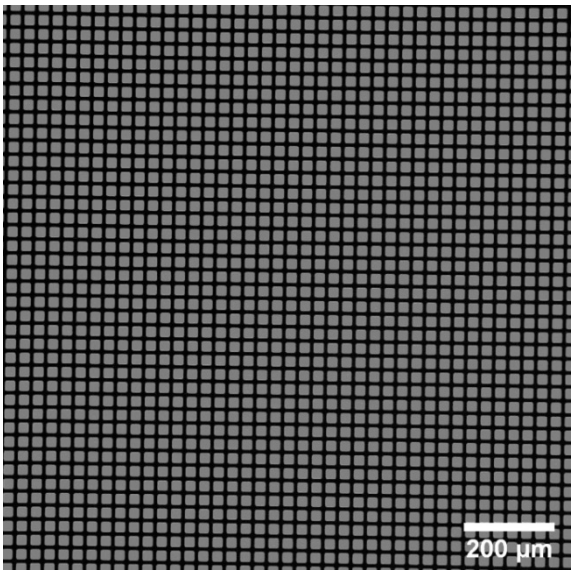

Figure 3.14: Transparent electrode chip with 400 x 400 µm holes (a). Confocal microscopy image at 5 x magnification of the patterned area of a transparent electrode chip with 20 x 20 µm holes (b).

Chapter 4: Characterisation

There's plenty of room at the bottom.
Richard Feynman

Surface, bulk and electrical properties are extremely important for electrode characterisation. They will define the electrode behaviour, sensitivity, selectivity, applicability etc. When using a material as substrate for cell culture, surface properties and physico-chemical properties are also essential, because they deeply influence the interaction between the biological components and the surface.

In this work, a combination of complementary characterisation methods was employed in order to characterise the systems of interest. Light microscopy, scanning electron microscopy (SEM) and profilometry were used to investigate surface morphology. Optical microscopy (including fluorescence and confocal) and SEM were employed also for characterising cell populations. X-ray photoelectron spectroscopy was employed to characterise surface chemistry. The electrochemical properties of the electrodes were evaluated using cyclic voltammetry. Amperometry was used for investigating reactions occurring in the tested biological systems (dopamine exocytosis from neurons and photosynthesis in thylakoid membranes).

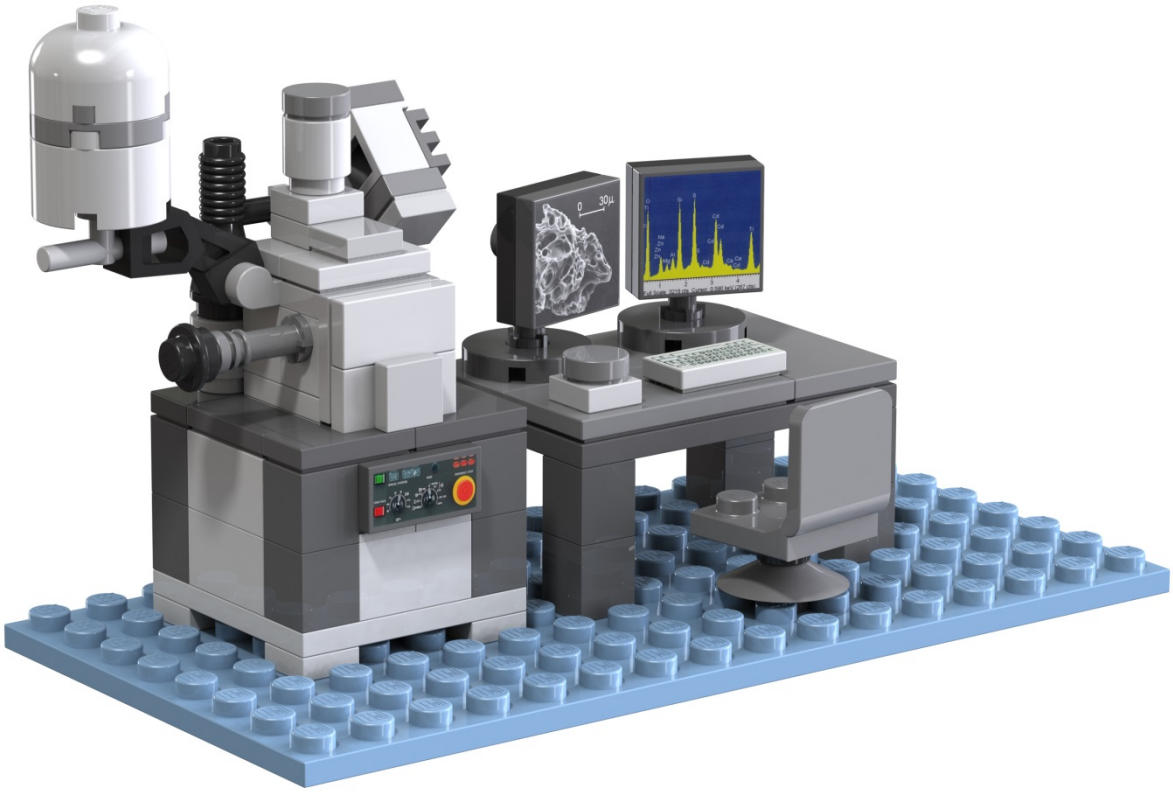

4.1. Microscopy techniques

Nothing has such power to broaden the mind as the ability to investigate systematically and truly all that comes under thy observation in life.
Marcus Aurelius

4.1.1. Light microscopy – introduction and brief history

We constantly use our senses, especially sight, to investigate and evaluate the world around us. But, as wonderful as it may be, the human eye has its limitations, one of which is the ability to see fine details. This occurs in part because of the optical properties of the cornea and crystalline lens, but also because of the cellular nature of the retina. In order for two points of an image to be separate, their projected images must fall on at least two different photoreceptor cells of the retina [190]. One other important aspect is magnification. An object appears bigger if it is moved closer to the eye, but the human eye cannot focus on objects that are closer than ~250 mm [190]. This leads to a resolution limit of the human eye of ~100 µm (**figure 4.1)**.

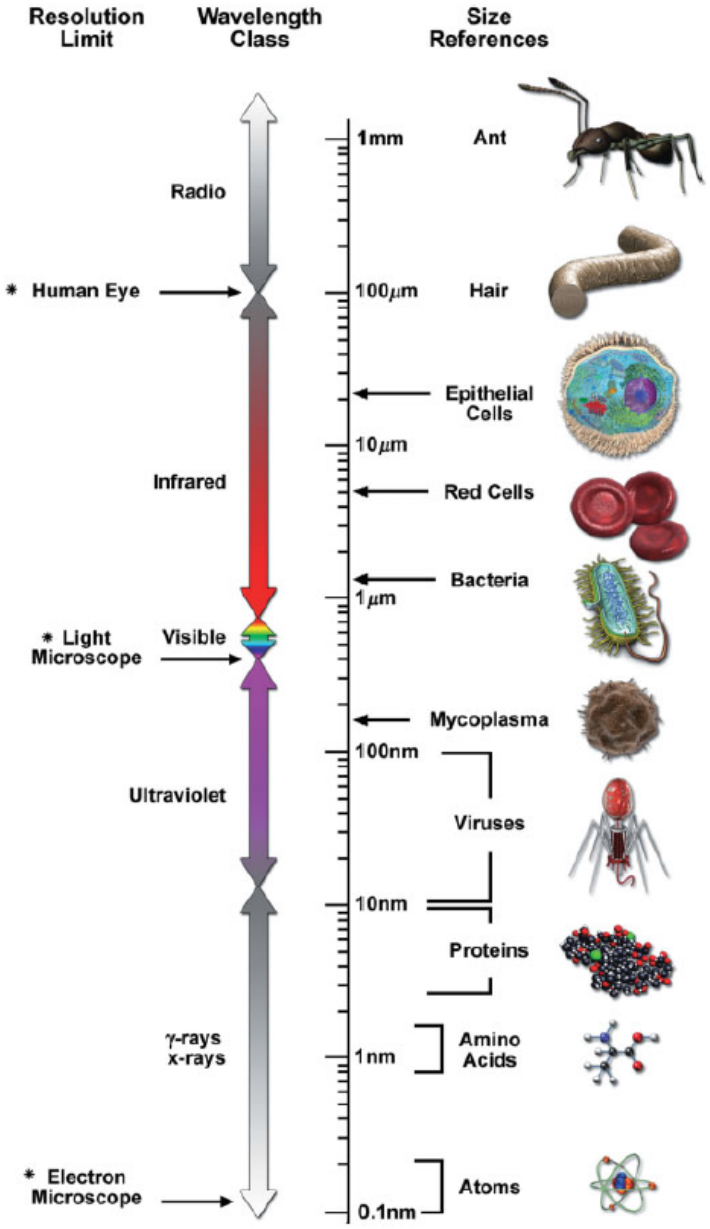

Figure 4.1: The electromagnetic spectrum (logarithmic scale from 10^{-10} to 10^{-3} m) and radiation types according to wavelength. Objects of different sizes are shown for comparison purposes (right), and the resolution limit for the human eye, light microscopes and electron microscopes is shown on the left.
Figure reproduced from [192].

Ever since antiquity, humanity has been using magnifying objects, such as burning glasses or curved mirrors [191] to overcome the limitations of the human eye. The renaissance period lead to more developments in the field. Leonardo da Vinci studied concave and convex glasses. In the 16th century, Francesco Maurolico and then Johannes Kepler enunciated some of the properties of lenses [191]. The first optical microscopes were a natural further development and consisted of a short, opaque tube, with a lens at one end and a flat glass plate at the other end, where the sample would be placed [191]. Anthony van Leeuwenhoek further

improved the simple microscopes by improving the polishing of the glasses and adding a moving stage to the microscope. Better microscopic work was afterwards accomplished with the development of the compound microscope (named so because it contains both an objective and an eyepiece). Its early history is linked with that of telescopes, and the theory behind it was first established by Galileo Galilei and Johannes Kepler, and improved by Wilibrod Snell van Royen's "sine law". The first person to mention the compound microscope was Francisco Fontana, an astronomer from Naples who claimed to have invented it in 1618 [191]. Eustachio Divini (1663) and Johannes Zahn (1685) are noteworthy early microscopists using combined microscopes with multiple lenses. Since then, the compound light microscope became the most used among scientists, and many achievements in science come (at least partly) from its use. A major improvement later on is attributed to August Köhler, who introduced a method of illumination characterised by bright and uniform illumination of the sample and proper alignment of the sets of planes involved in illumination and image formation [192]. Since then, numerous techniques have been developed in the field of light microscopy, and are still being developed nowadays. Fluorescence and confocal microscopy are now indispensable tools in science [192,193], and recent developments have shown that super resolution microscopy is a powerful tool for biological investigations [194–196].

The 2014 Nobel Prize in Chemistry was awarded to Eric Betzig, Stefan Hell and William Moerner "for the development of super-resolved fluorescence microscopy", showing that the field of microscopy can be still improved.

4.1.2. Köhler illumination and the modern light microscope

The modern light microscope is a compound optical instrument that produces a magnified image of an object by using visible light and a series of optical components [192]. There are eight focal planes involved when using Köhler illumination, distributed in two sets of conjugate planes (**figure 4.2**) [197]. One set of planes is called the aperture or illuminating set. This plane contains the lamp filament (light source), the front focal plane of the condenser, the back focal plane of the objective and the exit pupil of the eyepiece (coincident with the eye pupil) [190,192]. The field or image-forming set contains the lamp iris diaphragm, the specimen, the primary image and the retina. Having the illuminated set separate from the image set ensures uniform illumination of the sample, even when using an uneven light source (such as a tungsten filament), because the light source is not in focus in the specimen plane.

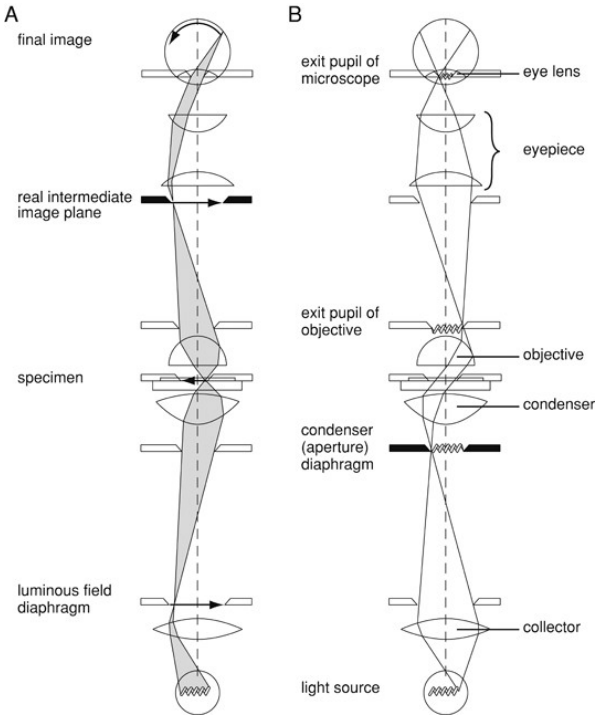

Figure 4.2: Light path in Köhler illumination. Path of the image-forming ray, with its four conjugated planes (a). Illumination path, again with four directly related or conjugated planes (b). Figure and caption reproduced from [197]

The critical element in any microscope is the objective lens. Its construction parameters determine magnification, resolution and the field of view. The quality of the objective lens influences light transmission, contract and aberrations [198]. The most common type of optics in a standard light microscope is for bright field microscopy. This is most suitable when visualising samples with inherent contrast (stained or pigmented specimens). Dark field and phase contrast optics are also relatively common. For a three dimensional effect and better depth of resolution, techniques such as differential interference contrast, Nomarski or Hoffman modulation contrast can be used.

4.1.3. Brightfield microscopy images - results

In this work, bright-field microscopy was used to monitor the cells regularly during growth and differentiation. **Figure 4.3** shows images of hVM1 Bcl-X_L cells grown on three different substrates: tissue culture polystyrene (TCPS), optical fibre electrodes (OFEs) and transparent electrode chips (TECs).

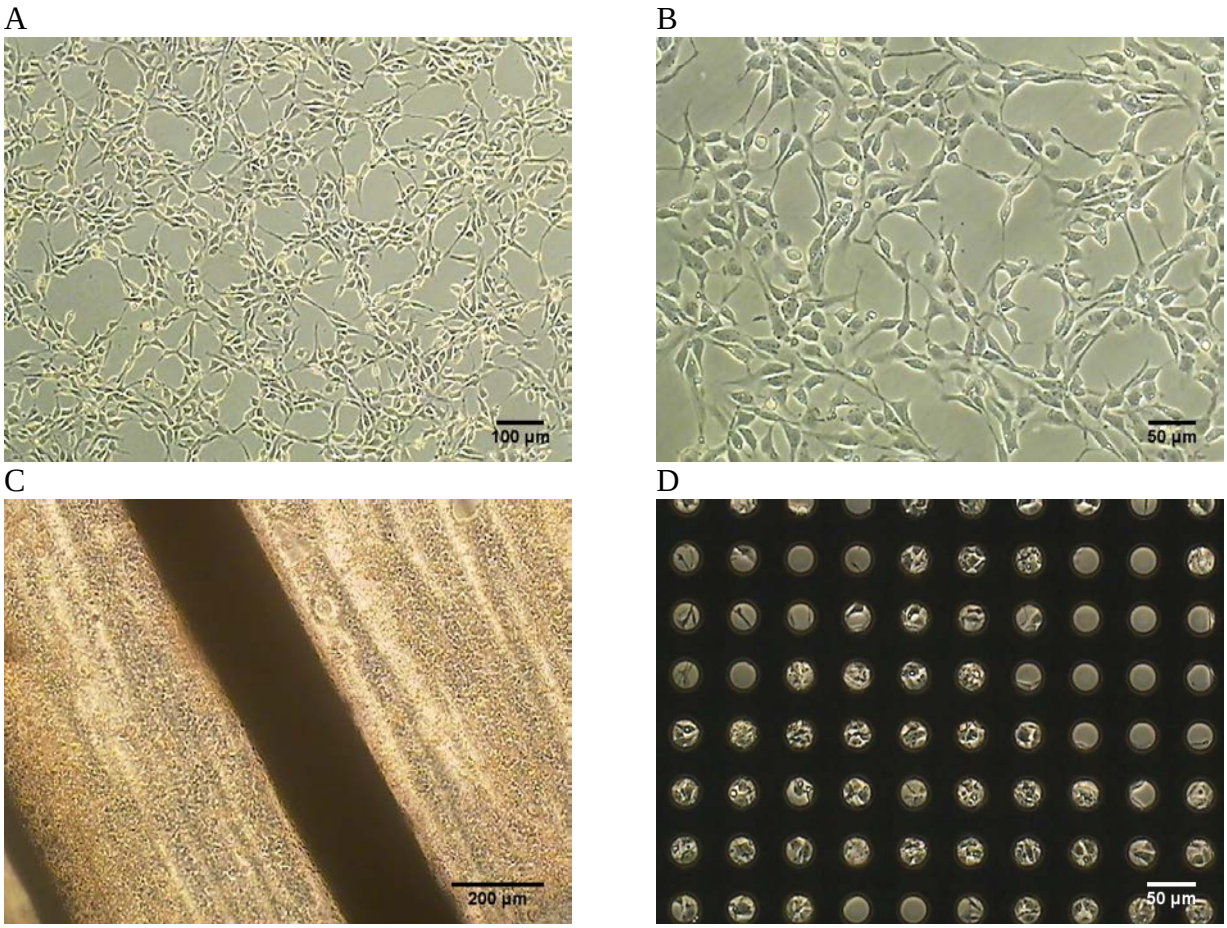

Figure 4.3: Optical microscopy images of hVM1 Bcl-X_L cells: 48 h after seeding at a density of 30000 cells/cm^2 on Geltrex-coated TCPS, 10x magnification (a) and 20 x magnification (b); 5 days after seeding at a density of 300000 cells/cm^2 on Geltrex-coated OFE, 10x magnification (c); 5 days after seeding at a density of 30000 cells/cm^2 on Geltrex-coated TCE, 20x magnification.

Since carbon is opaque, cells cannot be imaged on the carbon using transmitted light in an inverted microscope. In **figure 4.3c**, the cell population in the immediate surrounding of the OFE can be observed. In **figure 4.3d**, the cells can be seen through the transparent portions of a TEC.

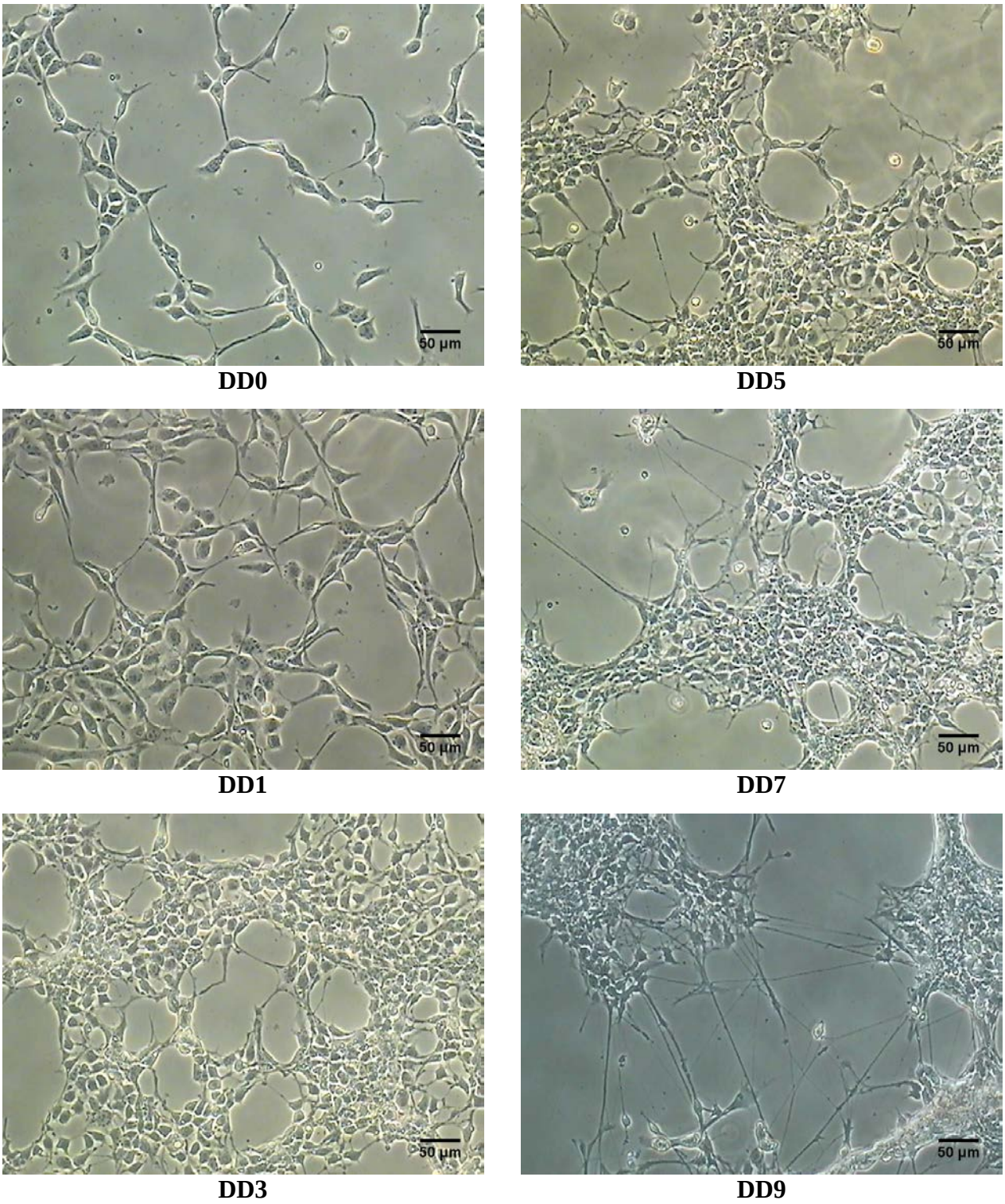

Figure 4.4: Optical microscopy images at 20x magnification of a population of hVM1 Bcl-X_L cells, passage 42, during differentiation (DDx - differentiation day x). The cells were seeded at a density of 30000 cells/cm^2 on Geltrex-coated TCPS.

Figure 4.4 shows bright-field images of hVM1 Bcl-X_L cells at different time points of the differentiation. An increase in the number of cells and changes in morphology can be observed in the image series. However, bright-field microscopy provides limited information, and thus additional microscopy methods were employed to better characterise the cell populations. These will be described in the following sections.

4.1.4. Fluorescence microscopy

Chemical species can reach an electronic excited state upon absorption of a photon. The emission of a photon from an excited species is called photoluminescence, which can be manifested as fluorescence or phosphorescence [199,200] (**figure 4.5**).

The first reported observation of fluorescence was in 1565, when Nicolás Monardes described the bluish opalescence of the water infusion from the wood of a Mexican tree. It took almost three centuries until the phenomenon started to be understood. The first person who stated that emitted light is of longer wavelength that the incident light was Edmond Becquerel in 1842. A few years later, in 1853, George Gabriel Stokes introduced the term "fluorescence" after experimenting with quinine sulfate solutions [201,202]. The first fluorometric analysis took place in 1867. A big leap forward was the synthesis of fluorescein in 1871 by Adolf von Baeyer [203]. The 20th century brought an even better understanding of the phenomenon of fluorescence, and the use of fluorescent dyes is common practice nowadays.

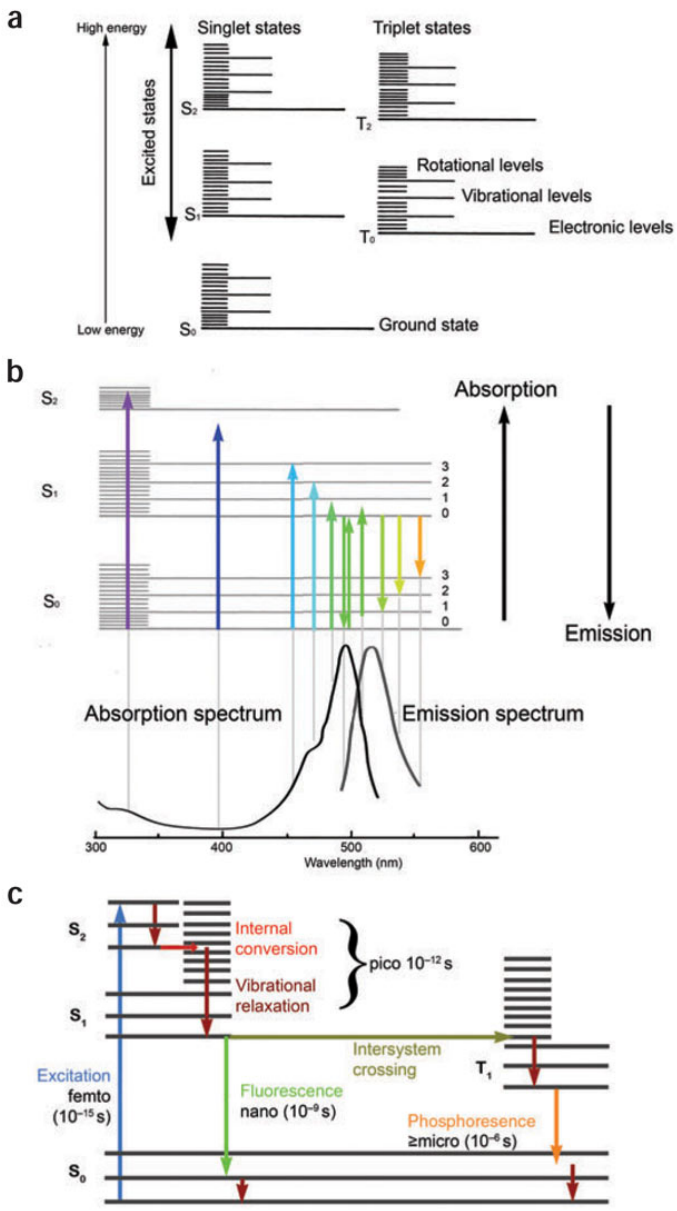

Figure 4.5: Jablonski diagram showing the possible energy states of a molecule (a); Electronic transitions correlated with the absorption and fluorescence emission spectra for the fluorophore FITC (b); Possible steps and their duration in photoluminescence excitation and emission (c).
Figure reproduced from [199].

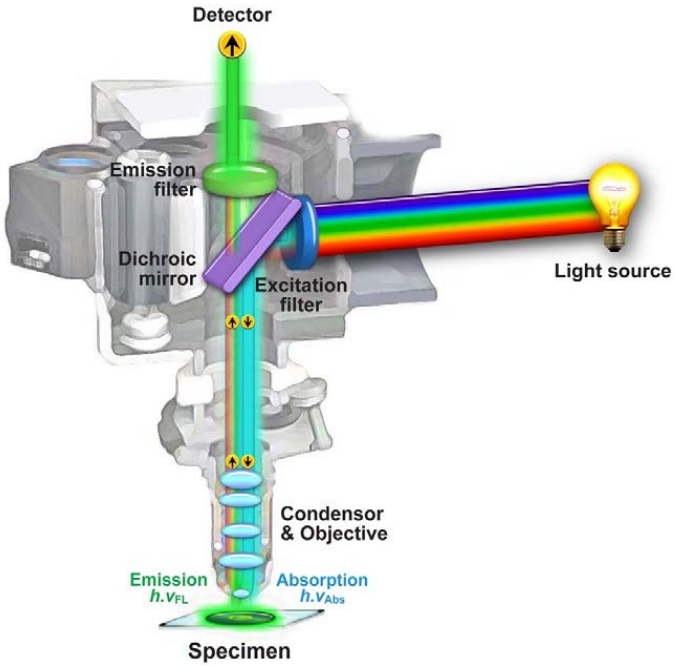

Figure 4.6: Anatomy of an epi-illumination fluorescence microscope.
Figure and caption reproduced from [238]

Fluorescence microscopes rely on the fact that light is emitted at higher wavelengths than it is absorbed (which is called the Stokes shift). Modern fluorescence microscopes use epi-illumination, where the objective also plays the role of condenser (**figure 4.6**). This ensures that the excitation light reaches the sample normally, but only a small part of the exciting light is reflected off the sample and needs to be filtered on the return path. Epi-illumination also requires the use of a dichroic beamsplitter mirror, positioned at 45° in the light path. This is designed to reflect the excitation light onto the sample, but to allow the emission to pass through on to the detector. Usually, the dichroic mirror is combined with excitation and emission filters, to obtain very specific wavelength selectivity [199].

There are several important aspects when selecting a fluorescent dye: the Stokes shift, the molar extinction coefficient (the potential of the dye to absorb photons under specified conditions), and the quantum efficiency (the fraction of absorbed photons reemitted as fluorescence). The solubility of dyes, their chemical stability and resistance to photobleaching are also important factors to consider [131]. For practical matters, the excitation and emission wavelengths should be chosen also to fit available infrastructure. For biological applications, the dyes need to be available as conjugates with the proteins of interest.

4.1.5. Confocal microscopy

The confocal microscope was invented and patented by Marvin Minski in the 1950s [204]. Compared to conventional fluorescence microscopy, it can provide high-quality images with good contrast and details by reducing noise. It becomes particularly useful when looking at thick tissue samples (especially for *in vivo* imaging) or for 3D imaging [198,205,206]. In confocal microscopy, the excitation beam is focused through the objective to a small point inside the sample (500 nm). The reflected or fluorescent light is gathered by the same objective and projected through a screen that has a pinhole. This ensures filtering of the light that is not in focus in the pinhole plane. The name “confocal” comes from the fact that the pinhole is placed in a conjugate plane to the specimen. A light detector, usually a photomultiplier, is then placed on the other side of the pinhole. The signal from the detector then goes to a computer that builds the sample image as the confocal microscope scans the sample in the x-y plane. Images can thus be obtained in several z-planes, leading to a “stack” of confocal images that can be used to reconstruct a 3D image of the sample [206,207].

4.1.6. Confocal microscopy images – results

Confocal microscopy was used in this project for imaging cells on carbon surfaces after staining with fluorescent dyes. The protocols for live staining and immunostaining can be found in appendix IV. Additionally, confocal microscopy was used for evaluating SU-8 patterning, as briefly described in section 3.4.2.2 and appendix V.

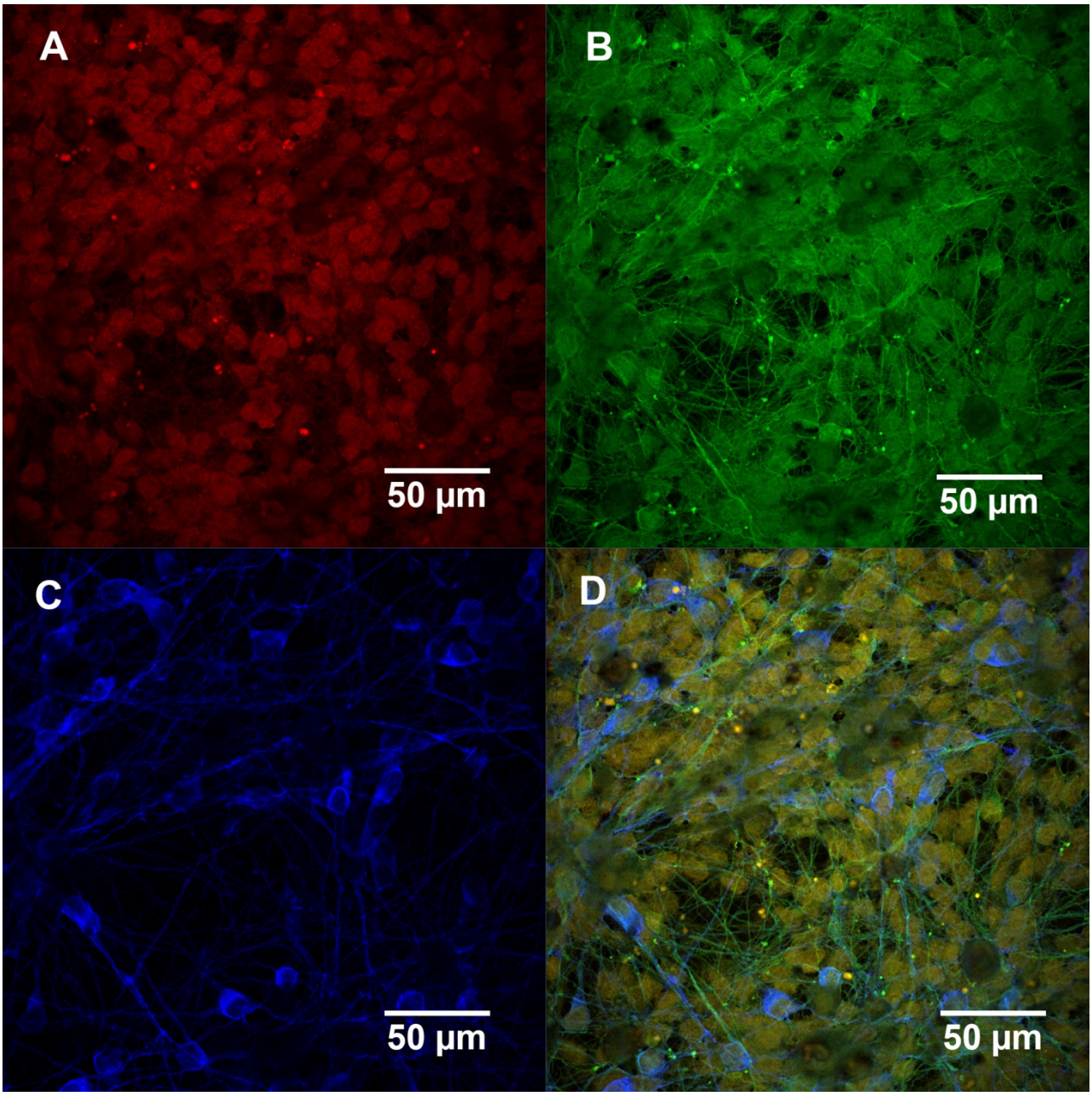

Figure 4.7: Confocal microscopy image at 50 x magnification of hVM1 Bcl-X_L cells, passage 42, after 10 day differentiation procedure. The cells were seeded at 30000 cells/cm^2 on Geltrex-coated, polyimide-derived carbon. Red channel – nuclei stained with TO-PRO3 (a); Green channel: β-tubulin stained with Alexa Fluor 568 (b); Blue channel: Tyrosine hydroxylase stained with Alexa Fluor 488 (c); Merged image (d).

The ability of cells to grow and differentiate on carbon derived from SU-8 and PI was investigated using unpatterned chips. Before seeding the cells, the chips were subjected to oxygen PT (3 min, 50 W), sterilised by autoclaving and coated with Geltrex. The cells were cultured as described in appendix IV. After the 10 days of differentiation, hVM1 Bcl-X_L cells were fixed and stained for TH, β-tubulin and nuclei and imaged using a confocal laser scanning microscope (LSM 700, Zeiss) and the ZEN software (**figure 4.7**, **4.8** and **4.9c**). TH-positive cells are shown in blue in **figure 4.7** and **4.8**. This is an indicator that the differentiation procedure leads to the generation of dopaminergic neurons. As it can be seen in **figure 4.8**, the behaviour of the cells is similar on both SU-8- and PI-derived carbon surfaces.

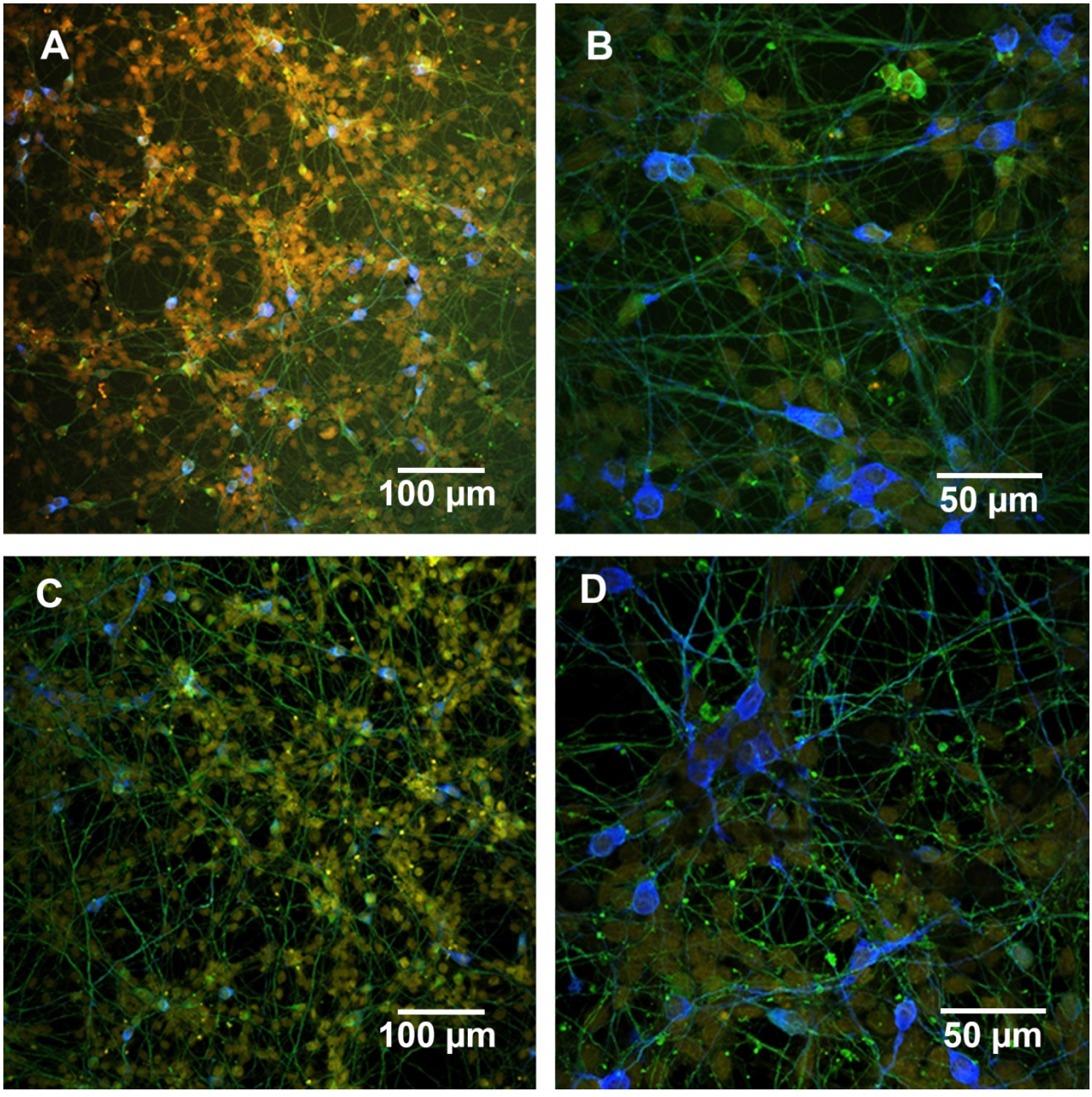

Figure 4.8: Confocal microscopy merged images of hVM1 Bcl-X_L cells stained for nuclei (red), β-tubulin (green) and TH (blue) after 10 day differentiation procedure. The cells (passage 42) were seeded at 30000 cells/cm^2 on Geltrex-coated carbon. The carbon was obtained by pyrolysing polyimide (a, b) and SU-8 (c, d).

The ability to focus in different planes and generate a Z-stack of confocal microscopy images proved to be essential for imaging cells residing on the surface of OFEs. Since OFEs are three-dimensional, focusing in a single plane does not allow obtaining a good image of the sample. **Figure 4.9** shows hVM1 Bcl-X_L cells grown and differentiated on the surface of an OFE with a diameter of 100 µm. **Figure 4.9a** and **4.9b** show images of cells growing on the OFE, and **figure 4.9c** shows an image of hVM1 Bcl-X_L cells fixed and stained for TH, β-tubulin and nuclei after 10 days of differentiation.

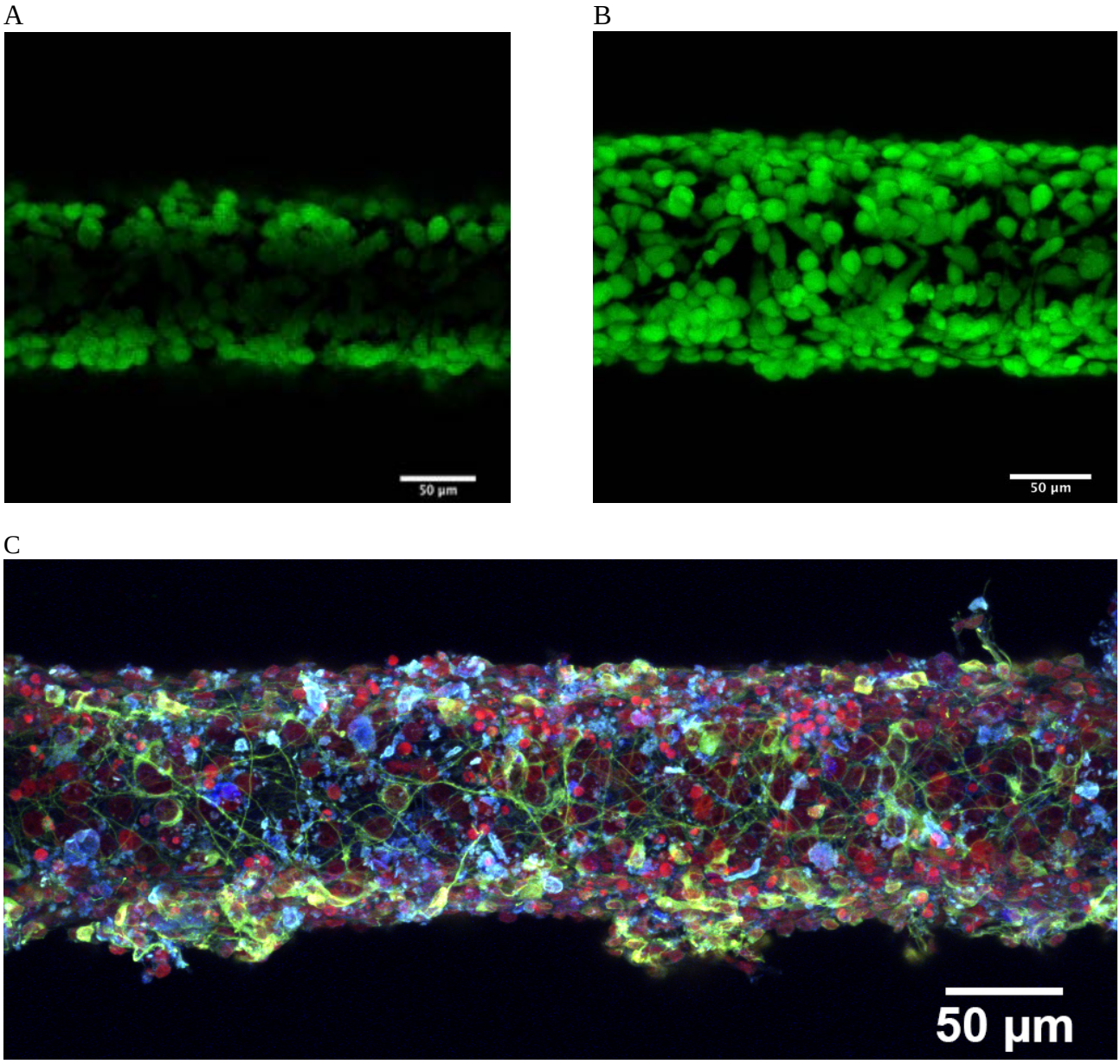

Figure 4.9: Confocal microscopy images of hVM1 Bcl-X_L cells, passage 43, grown on an OFE (100 µm diameter). and stained with calcein AM 48 h after seeding: single-plane focus (a); image reconstructed from a Z-stack of 13 slices/60 µm (b); Confocal microscopy merged image (maximum intensity projection from a Z-stack of 13 slices/60 µm) of hVM1 Bcl-X_L cells stained for nuclei (red), β-tubulin (green) and TH (blue) after 10 day differentiation procedure (c). The cells were seeded at 500000 cells/cm^2 on Geltrex-coated, polyimide-derived carbon.

4.1.7. Scanning electron microscopy (SEM)

The first scanning electron microscope was developed during World War II, at the RCA laboratories in New Jersey. After the war, SEM was further developed at Cambridge University. The first commercial model was built by the AEI company in 1958 [208]. In SEM, electrons produced by an electron source (usually a field gun, operated in vacuum) are accelerated and focused into an electron beam that will scan the sample. This is achieved with the help of electrostatic fields, the condenser lenses and the objective lens. The incident electrons interact with the sample surface, resulting in various secondary emissions, such as backscattered electrons, secondary electrons, X-rays, cathodoluminescence and Auger electrons. These secondary emissions can be detected. Usually, secondary and backscattered electrons are used in SEM, amplified and converted to a visual signal displayed on the cathode ray tube [209,210]. **Figure 4.10** shows a schematic representation of a scanning electron microscope and of possible secondary emissions.

There are several advantages of using SEM for imaging of micro- and nanofeatures. The most obvious one is the possibility of using very high magnification with good spatial resolution [208–211]. Compared to light microscopy, another advantage is the much larger depth of field, which is extremely important when investigating a specimen with large topographical variation [209,210]. However, SEM has its limitations, some related to the surface effects and others related to the necessity for fixation of biological samples [212,213].

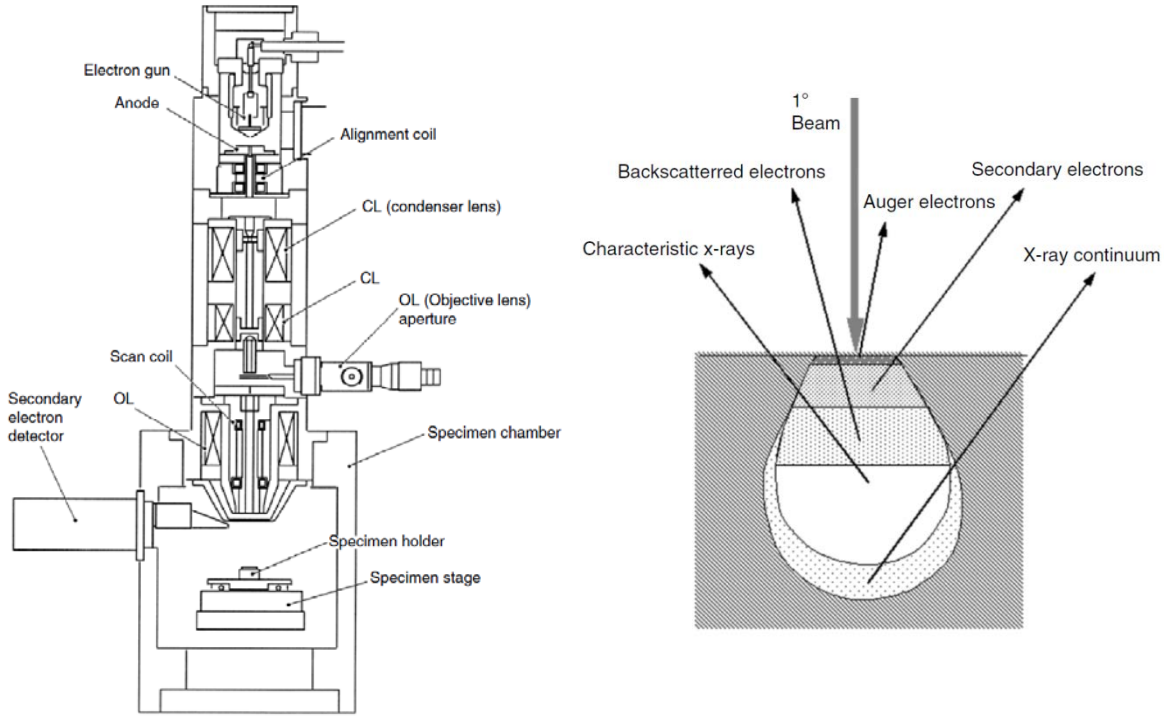

Figure 4.10: Schematic diagram of a scanning electron microscope (left) and regions within the interaction volume that generate different types of secondary radiation detected in SEM (right). Image adapted from [210].

4.1.8. Scanning electron microscopy – results

SEM was used in this project to investigate OFEs after pyrolysis and as substrate for cell culture. The carbon layer obtained through the pyrolysis of PI and SU-8 has a smooth surface with few imperfections, as it can be seen in **Figure 4.11**.

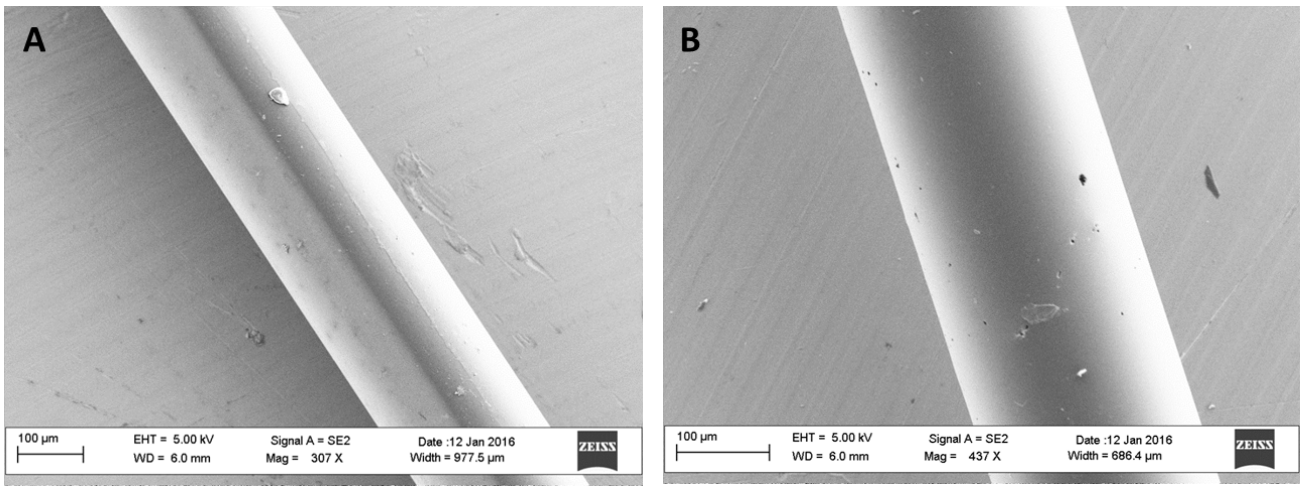

Figure 4.11: SEM of OFE with carbon coating derived from polyimide (a) and SU-8 (b).

SEM was also employed for measuring the thickness of the carbon layer obtained after the pyrolysis of OFs. A 90° holder was used for obtaining SEM images of the top of the OFEs. The contrast in SEM images between fused silica and carbon is high enough so the carbon-quartz interface is clearly visible (**figure 4.12**).

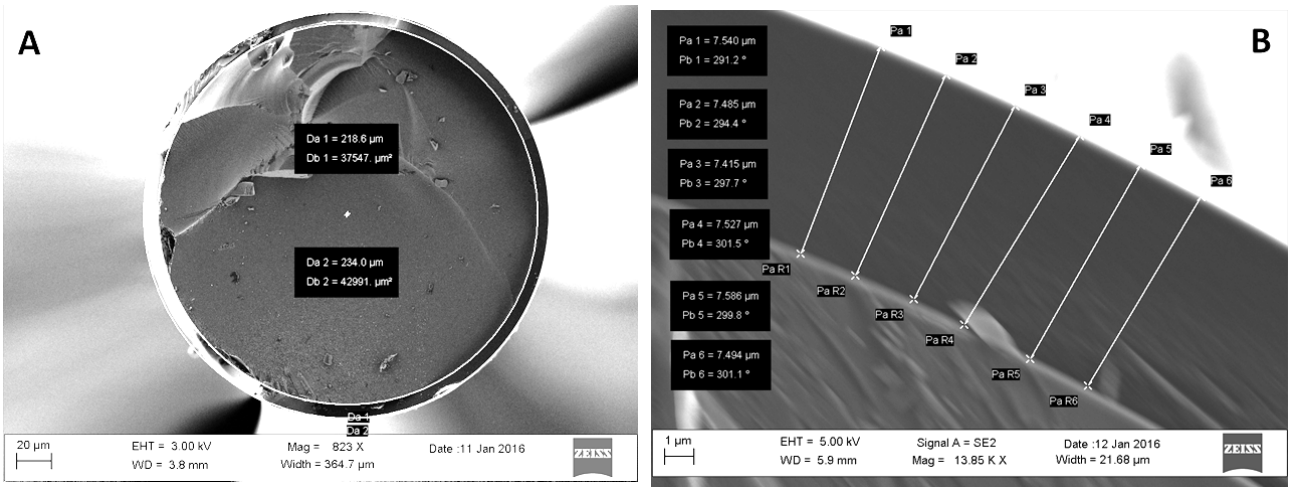

Figure 4.12: SEM imaging for measuring the thickness of the polyimide-derived carbon layer on pyrolysed OF pieces at two different magnifications.

In **figure 4.12a**, two concentric circles can be identified. The inner circle has a diameter of ~ 218.6 µm and represents the fused silica part of the OFE. The measured diameter corresponds to the cladding diameter specified by the producer of the OFs, which is 220 ± 4.4 µm. The outer circle has

a diameter of ~ 234 µm. This means that the carbon layer has a thickness of ~ 7.7 µm. It can be seen from the SEM image that carbon layer is quite uniform. At higher magnification, the thickness of the carbon layer can be measured at specific points of the OFEs (**figure 4.12b**).

SEM images of hVM1 Bcl-X_L cells differentiated on OFEs (**figure 4.13**) show that the cells attach to the surface of the OFEs. Alternating areas with and without cells can be seen. This is most likely due to the cylindrical shape of the OFEs – during seeding, the cells can easily roll off the OFEs.

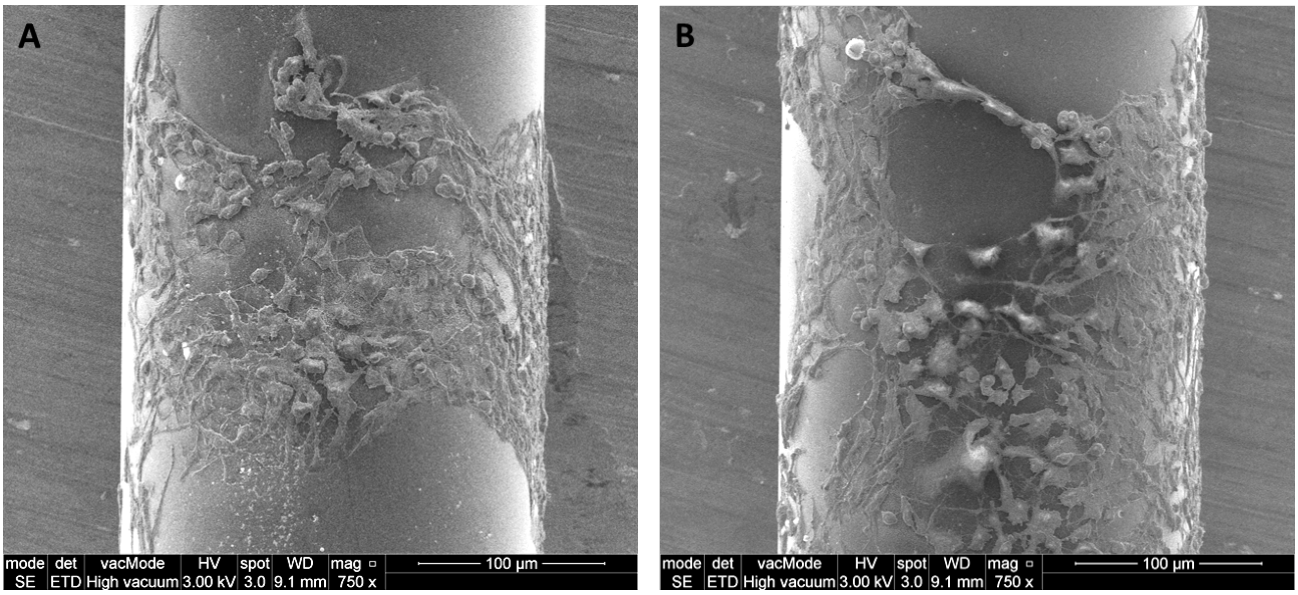

Figure 4.13: SEM images of differentiated hVM1 Bcl-X_L cells on two different OFEs.

4.2. X-ray photoelectron spectroscopy

There are no such things as applied sciences, only applications of science.
Louis Pasteur

4.2.1. Brief history

X-ray photoelectron spectroscopy (XPS) relies on the photoelectric effect, which was first observed in 1887 by Heinrich Hertz [214] and explained by Albert Einstein in 1905 [215], who later received the Nobel Prize (1921) "for his services to Theoretical Physics, and especially for his discovery of the law of the photoelectric effect". Another important discovery from the late 19th century that made the development of XPS possible was the one of X-rays (also named Röntgen radiation), credited to Wilhelm Conrad Röntgen. The German physicist was the first to systematically study X-rays, and he was awarded the Nobel Prize in 1901 "in recognition of the extraordinary services he has rendered by the discovery of the remarkable rays subsequently named after him".
In 1907, P. D. Innes recorded the first XPS spectra on photographic plates by using a Röntgen tube coupled with Helmholtz coils [216]. After World War I, Robinson continued doing research in the field [217]. Afterwards, X-ray spectroscopy had a stagnation period up until the 1950s, when R. G. Steinhardt developed it as a technique for surface chemical analysis [218]. In 1954, Kai Siegbahn built a high resolution photoelectron spectrometer and continued developing XPS as an important research and analysis tool [219]. In 1981, Siegbahn received the Nobel Prize for “his contribution to the development of high-resolution electron spectroscopy”. Nowadays, XPS is a popular analytical tool in materials science, with applications in fields such as metallurgy, corrosion, microelectronic devices, polymers and adhesion [220].

4.2.2. Principle

Electron spectroscopy usually studies the emission and energy of electrons in the range 20-2000 eV [220] (**figure 4.14**). Two main types of electron spectroscopy are widely used, XPS and Auger electron spectroscopy (AES). XPS can provide information about the surface chemistry of a sample: presence of elements, chemical states and their ratio, uniformity of the chemical composition and spatial distribution of the chemical species is on the surface. XPS is also known as electron spectroscopy for chemical analysis (ESCA).
The electron spectrometer consists of a source of primary radiation (which is an X-ray source, in the case of XPS) and an electron energy analyser. The measurements take place

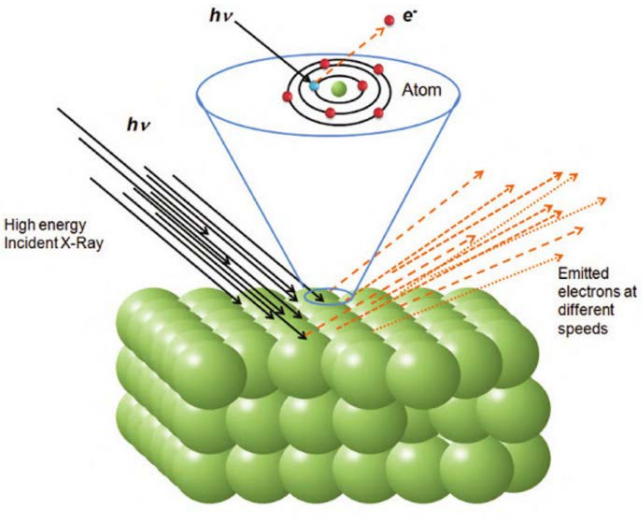

Figure 4.14: Schematic representation of the photoelectric effect and its usage in electron spectroscopy for chemical analysis (XPS/ESCA). Figure reproduced from [239]

in vacuum or ultra-high vacuum (UHV, pressure below 10^{-7} Pa) [220].
The electrons are generated from the interaction of soft X-rays (AlKα or MgKα) with the sample surface. The spectrometer measures the kinetic energy of the ejected electron. This is not an intrinsic material parameter, because it depends on the photon energy of the X-rays used to eject it. There is a simple mathematical relation between the kinetic energy and the binding energy of the electron (which is an intrinsic material parameter) (**equation 4.1** [220,221]).

$$E_B = h\nu - E_K - W \qquad \textit{Equation 4.1}$$

- *where E_B is the binding energy of the electron, hν is the photon energy, E_K is the kinetic energy of the electron and W is the spectrometer work function.*

In practice, the calculation is done by the software for data acquisition and analysis. The user can choose to directly display the data as counts vs binding energy.

4.2.3. Data acquisition and analysis

A wide energy scan (survey) provides information about the elemental composition of the surface [220]. This can be obtained by using an energy range from 0 to 1150 eV when using a MgKα source or from 0 to 1350 eV when using an AlKα source. Usually, several XPS spectra are recorded and averaged for every experiment. Characteristic peaks for almost all chemical elements (except for hydrogen and helium) appear in a survey spectrum.

The survey spectrum can be used to identify and quantify the elements present on the sample surface. The identification is done based on the binding energy, and quantification is done by integrating the experimental peaks. The integrated area of a photoelectron peak from the surface of a solid considered as homogenous is described by **equation 4.2** [220].

$$I = J \times \rho \times \sigma \times K \times \lambda \qquad \textit{Equation 4.2}$$

- *where I is the integrated area, J is the photon flux, ρ is the concentration of the atom/ion in the solid, σ is the cross-section for photoelectron production, K is an instrumental parameter and λ is the electron attenuation length.*

This equation can be used as such, but more often, an experimental sensitivity factor (F) will be determined and employed. The sensitivity factor F includes σ, K and λ from **equation 2** and additional features of the photoelectron spectrum. A set of sensitivity factors is usually incorporated in the XPS analysis software.

The atomic percentage of the elements identified on the surface can be determined by calculating the fraction normalised intensity, as described by **equation 4.3** [220].

$$[A] = \frac{I_A/F_A}{\sum(I/F)} \times 100 \qquad \textit{Equation 4.3}$$

- *where [A] is the atomic percentage of the species A, I is the peak area and F is the sensitivity factor*

For the elements of interest, higher resolution spectra can be obtained. This means that a more narrow energy range is studied, and the data acquired is an average of more XPS spectra than in the case of a survey spectrum. In this case, chemical shifts can be investigated. These chemical shifts are usually in the range of 1-3 eV, but they can be as high as 8 eV in extreme cases [220]. Chemical shifts can appear due to either initial-state or final-state effects. Initial-state effects are mostly due to the charge on the atom prior to photoemission [220]. A bond between the element of interest and an electronegative atom will cause a positive chemical shift in the XPS spectrum. For example, **figure 4.15** shows the C 1s spectrum for an epoxy monomer and the spectrum deconvolution, with individual peaks attributed to different bonds. Final-state effects occur following photoemission (core hole screening, relaxation of electron orbitals or polarisation of surrounding ions). Because of these chemical shifts, information regarding chemical bonds can be derived from XPS spectra.

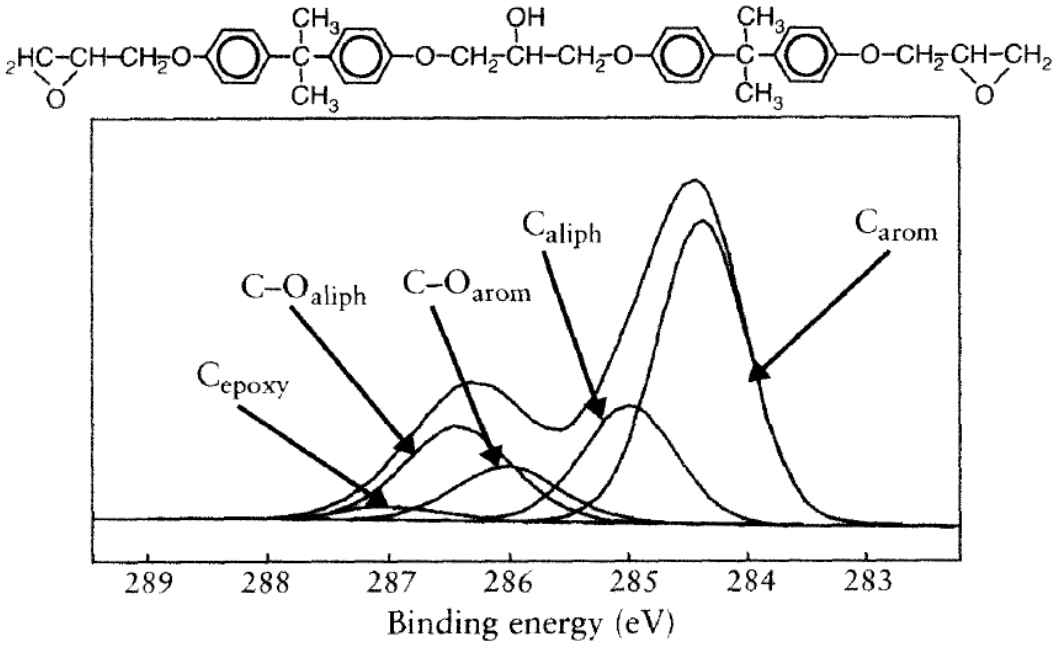

Figure 4.15: Chemical structure of the diglycidyl ether of bisphenol A, a basic building block of epoxy resins (top) and its C 1s spectrum recorded using monochromatic AlKα radiation (bottom). Figure reproduced from [220]

4.2.4. X-ray photoelectron spectroscopy – results

The unpatterned carbon chips described in section 3.4.2.1 were investigated using XPS (**figure 4.16**). The XPS survey scan shows that in the case of pyrolysed PI and SU-8 the surface consists mostly of carbon, as expected. For pyrolysed PI, traces of oxygen and nitrogen appear in the XPS spectra. Since SU-8 does not contain nitrogen, only oxygen traces remain after pyrolysis.

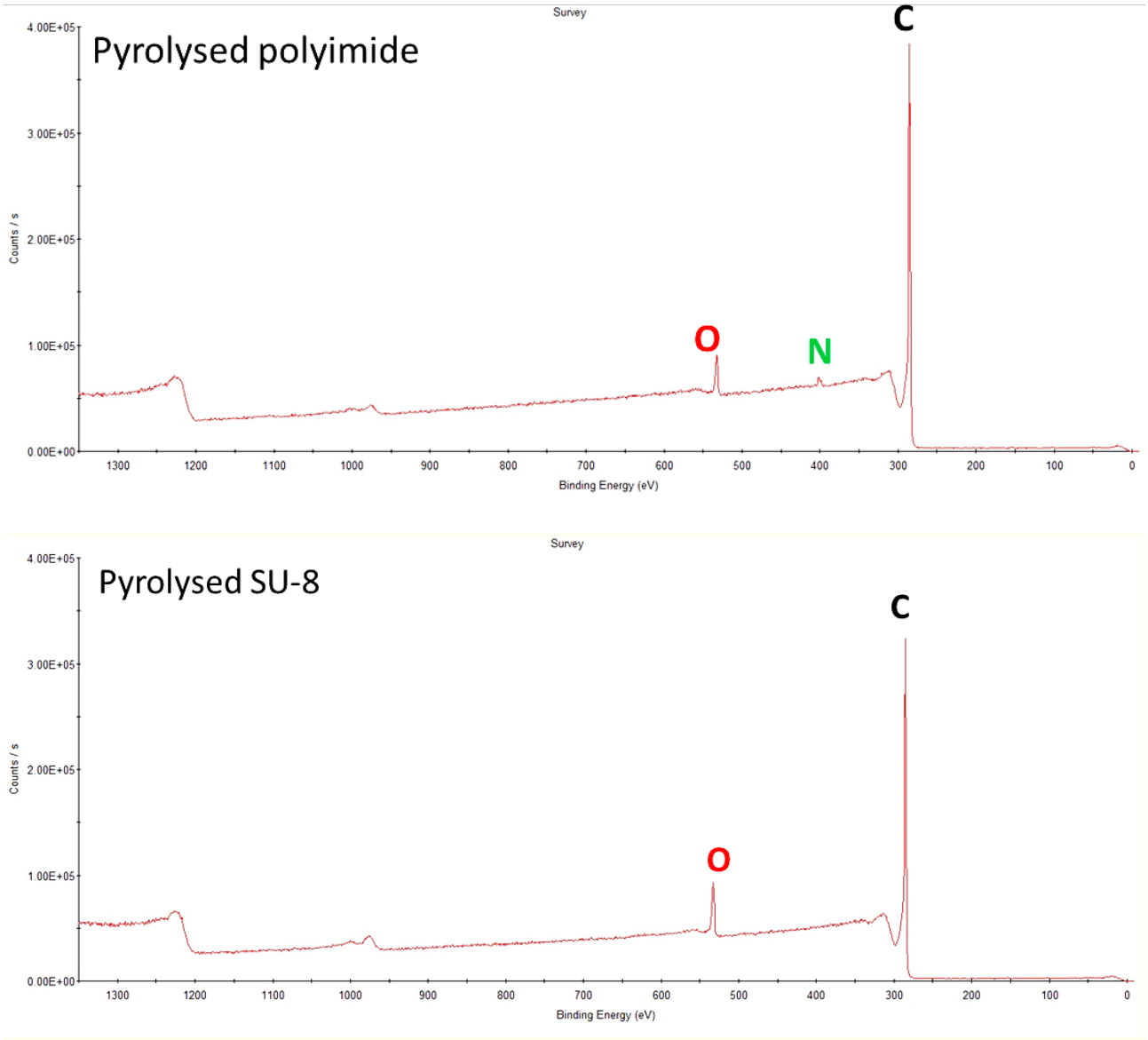

Figure 4.16: XPS survey scan for carbon obtained through the pyrolysis of PI (top) and SU-8 (bottom).

The elemental composition of surfaces obtained through the pyrolysis of PI and SU-8 is given in **table 4.1**.

Table 4.1: Elemental composition of pyrolysed PI and SU-8 surfaces

Polymer precursor	**%C**	**%O**	**%N**
Polyimide	95 ± 0.5	4 ± 0.3	1 ± 0.7
SU-8	93 ± 0.3	7 ± 0.3	-

4.3. Electrochemical techniques

Science is the acceptance of what works and the rejection of what does not. That needs more courage than we might think.
Jacob Bronowski

Electrochemical techniques are essential for characterising electrode surfaces. They are also very useful detection techniques to achieve quantification in analytical applications. For the work in this thesis, cyclic voltammetry (CV) was employed to investigate the electrochemical behaviour of the fabricated electrodes and to investigate their response to dopamine. Chronoamperometry (CA) was used to study dopamine exocytosis from cell populations and to monitor the photocurrent generated by thylakoid membranes. The following sections are meant to introduce the reader to these two electrochemical techniques, with examples from experiments which were done as part of this PhD project.

4.3.1. The electrochemical cell and redox reactions

An electrochemical cell is composed of two half cells which are separated by at least one electrolyte phase (liquid-liquid junction). The half-cell where an oxidation reaction occurs is defined as the anode, and the half-cell where a reduction reaction occurs is defined as the cathode.

If the electrochemical (redox) reaction is spontaneous, the electrochemical cell is called a galvanic cell. If an external source is used to apply a potential difference across the cell in order to induce an electrochemical reaction, the electrochemical cell is called an electrolytic cell. All experiments in this thesis are performed using electrolytic cells.

In an electrochemical cell, the reaction of interest takes place at the working electrode (WE). The potential of the working electrode is measured with respect to a reference electrode (RE). The RE must have a known potential and ideally exhibit no charge transfer across the electrode-electrolyte interface (at least for a certain potential range), which is why a counter electrode (CE) is commonly introduced. The role of the CE is to function as a complementary half-cell to the working electrode: when the WE acts as cathode, the CE will act as anode and viceversa. Thus, current will flow between the WE and CE, with minimal effect on the RE. Most measurements in modern electrochemistry are performed in a three electrode setup (employing a WE, RE and CE, **figure 4.17**).

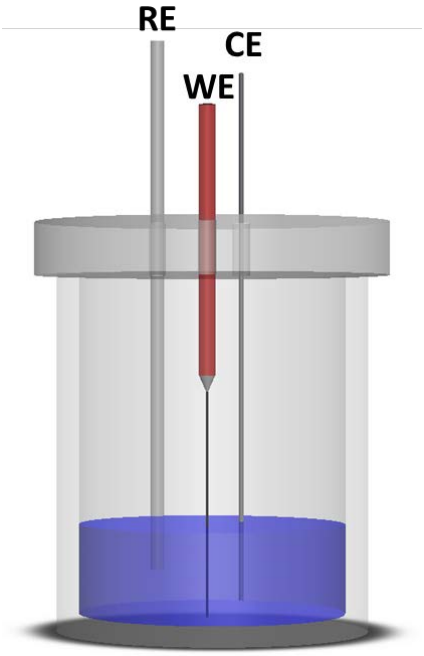

Figure 4.17: Schematic representation of the three-electrode setup used for measurements with OFEs

The conventional RE is the standard hydrogen electrode (SHE), which has by definition a potential of 0 V, regardless of temperature. However, SHE is not used, because it is a theoretical ideal RE. In this work, a Ag|AgCl|KCl (saturated in water) electrode (more commonly denoted simply Ag|AgCl) was used as RE in all measurements. The potential of the Ag|AgCl electrode is 0.197 V *vs* SHE.

It is important that the CE does not generate by-products which could interfere with the redox reaction of interest. Also, the area of the CE should be sufficiently large so as not to limit the reaction occurring at the WE. Throughout this work, a Pt wire was used as CE.

A basic redox reaction is conventionally written as a reduction reaction, as shown in **equation 4.4**:

$$Ox + ne^- \Leftrightarrow Red \qquad \textit{Equation 4.4}$$

- *where Ox is the oxidised species, Red is the reduced species and n is the number of electrons transferred between Ox and Red in the electrochemical reaction.*

The potential of the electrode can be calculated based on the standard potential of the redox reaction and the activities of the Ox and Red species, as described by the Nernst equation (**equation 4.5**):

$$E = E^{0'} + \frac{RT}{nF} ln \frac{a_{Ox}}{a_{Red}} \qquad \textit{Equation 4.5}$$

- *where E is the potential of the electrode, $E^{0'}$ is the formal potential of the electrochemical reaction, R is the universal gas constant (8.3145 $J \cdot mol^{-1} \cdot K^{-1}$), T is the absolute temperature (in K), F is Faraday's constant (96485 $C \cdot mol^{-1}$) and a_{Ox} and a_{Red} are the chemical activities for the oxidised and reduced species. For dilute solutions, the activity can be approximated to the concentration.*

The standard potential of the electrochemical reaction, E^0, is calculated conventionally vs SHE, with species present in the solution at an activity of 1, at 25°C and an atmospheric pressure of 1 atm. The E^0 values for numerous reactions can be found in literature. E^0 is also sometimes referred to as Nernstian potential. The formal potential, $E^{0'}$, is the reduction potential under a specified set of conditions (pH, ionic strength, concentrations of the involved species).

4.3.2. Charge transport in electrochemical systems

When an electrode is immersed in an electrolyte solution, an electrical double layer (EDL) is developed. This happens as a result of the spontaneous reorganisation of mobile charge carriers: electrons from the electrode material, and ions from the electrolyte solution. As suggested by the name, the EDL has two components: the inner Helmholtz plane (IHP) and the outer Helmholtz plane (OHP). The IHP is the virtual plane crossing through the centre of the layer of solvent molecules and ions adsorbed onto the electrode surface due to chemical interactions. The OHP is the virtual plane crossing through the centre of the first layer of solvent molecules and ions which interact electrostatically with the electrode. In the EDL, the potential drop is linear, while outside the EDL the potential drop is either exponential (if there is a diffusive double layer), or, if the ionic strength of the electrolyte solution is high enough, the bulk properties are the same throughout up to the OHP.

In an electrochemical system, charge is transported across an interface between two chemical phases: the electrode (electronic conductor) and the electrolyte (ionic conductor). The first step to understand the basics of electrochemistry is to understand the electron transfer (ET) process at the electrode-solution interface. ET is defined by IUPAC as "the transfer of an electron from one

molecular entity to another, or between two localised sites in the same molecular entity" [222]. There are three types of ET, depending on the state of the redox centres and their connectivity:

a) Inner-sphere ET: the electron donor and the electron acceptor are covalently linked during the ET. In the case of intramolecular ET, the event becomes permanent. In the case of intermolecular ET, there is a transient linkage followed by disconnection after the ET.
b) Outer-sphere ET: the electron donor and the electron acceptor are separate entities at all times. The electron "jumps" from the donor to the acceptor despite the facts that these two individual chemical species are not covalently linked.
c) Heterogeneous ET: the electron donor and the electron acceptor are in two different phases. This is the case for electrode reactions, which mostly involve ET between a solid electrode and species in a solution.

The concept of inner- and outer- sphere ET mechanisms can be applied to electrochemical reactions [223,224]. For example, $[Fe(CN)_6]^{3-}/[Fe(CN)_6]^{4-}$ is an outer-sphere mechanism couple, but Fe^{3+}/Fe^{2+} in sulfuric acid follows an inner-sphere mechanism [223].

A current can be generated in an electrolytic cell by applying a non-nernstian potential at the WE. This causes a perturbation of the equilibrium and drives the ET between the electrode and the electroactive species present in the solution, thus generating current. Currents generated from redox reactions happening at the electrode-solution interface are faradaic currents, governed by Faraday's law of electrolysis (**equation 4.6**). Non-faradaic (charging) currents pass through an electrochemical cell to compensate for the change in the potential of the electrode and they do not provide information on the redox reaction.

$$I = \frac{dQ}{dt} = nF\frac{dN}{dt} \qquad \textit{Equation 4.6}$$

- *where I is the faradaic current (in A), Q is the total charge (in C), t is the time (in s), n is the number of electrons transferred, F is Faraday's constant (96485 C·mol^{-1}) and N is the quantity (in moles) of species undergoing oxidation or reduction.*

There are two types of frontier orbitals in a chemical species: the lowest unoccupied molecular orbital (LUMO) and the highest occupied molecular orbital (HOMO). These are involved in ET reactions of chemical species: LUMO is the molecular orbital where an electron can be accepted, and HOMO is the molecular orbital from which an electron can be donated. In the case of metals, instead of distinct molecular orbitals, there are continuous bands of energy that electrons can occupy. A rough equivalent of HOMO in an electrode material is the Fermi level, E_F, which is defined as the energy level below which all energy states are occupied by electrons and above which all energy states are empty (which means the Fermi level is that energy value for which the probability for a state of being occupied is 50%) [225]. Applying a potential to the electrochemical system leads to changes in E_F. When a potential lower than the formal potential of the redox couple is applied, E_F shifts to higher values and electrons can flow from the electrode material to the LUMOs of species present in the electrolyte solution. This means that a reduction reaction takes place in the solution, and the generated current is cathodic. When the potential applied is higher

than the formal potential of the redox couple, E_F shifts to lower values and the electrode material can accept electrons from the HOMOs of species present in the solution. This is the case of an oxidation reaction, generating anodic current (**figure 4.18**).

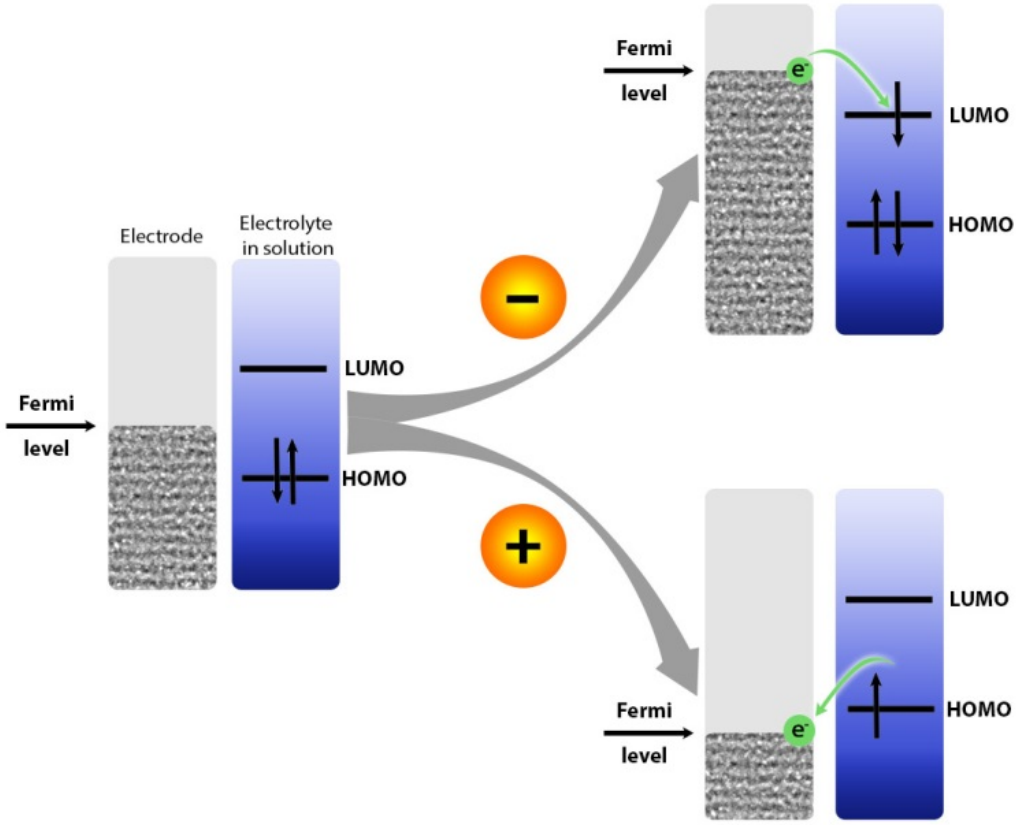

Figure 4.18: Changes in the fermi level when a non-nernstian potential is applied at the working electrode and electron transfer between the electrode and molecular orbitals from the electroactive species undergoing a reduction (top right) or oxidation (bottom right) process.

The general pathway of an electrode reaction can be considered as a set of equilibria of both physical processes and chemical reactions (**figure 4.19**). Based on this illustration, it is easy to understand why the rates of four different types of processes can govern the reaction rate at the electrode surface:

i) Mass transfer – from the bulk of the solution to the electrode surface
ii) ET at the electrode surface
iii) Chemical reactions preceding or following the ET process
iv) Other surface reactions, such as adsorption, desorption, crystallisation.

Not every electrochemical reaction involves all the aforementioned steps. The simplest reactions require only mass transfer and ET. For some of these processes (e.g. ET), the rate constants depend on the applied potential. The overall reaction rate will be determined by the slowest step of the process, which is denoted as the rate-limiting (or rate-determining) step.

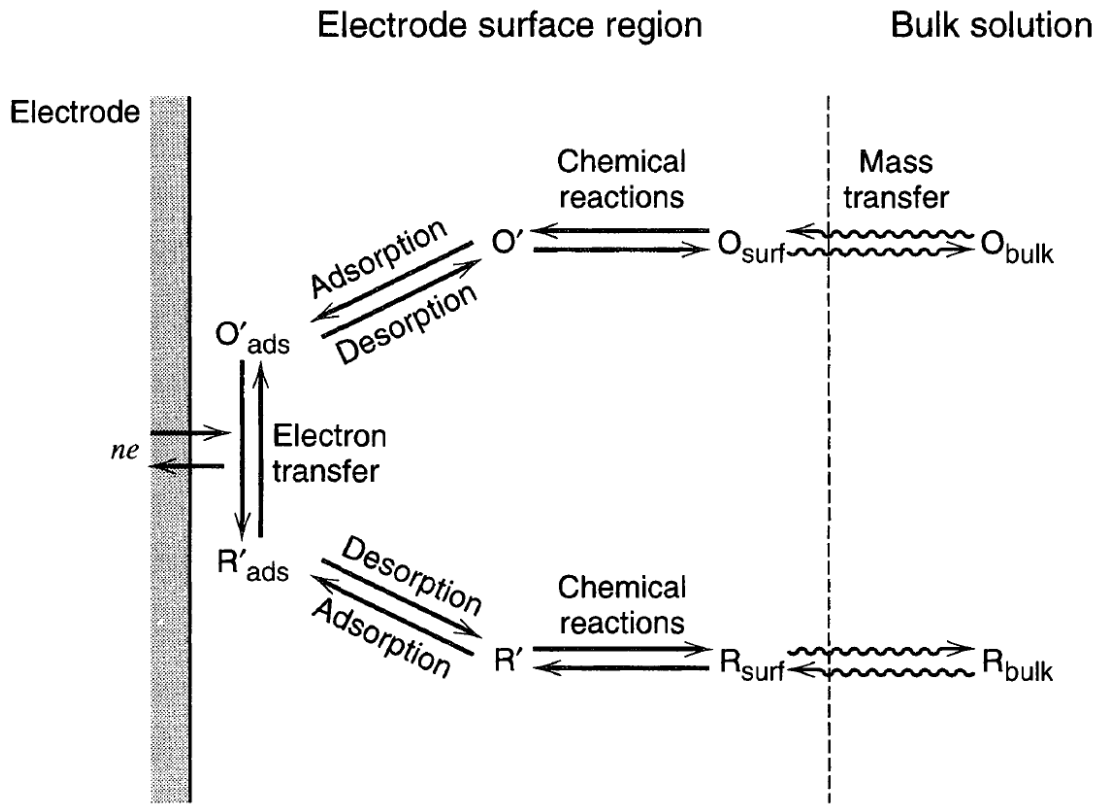

Figure 4.19: The general electrode reaction pathway. Figure reproduced from [240]

4.3.3. Cyclic Voltammetry

Cyclic voltammetry (CV) is a dynamic electrochemical technique that has been broadly investigated and used. In CV, the potential is changed linearly with time at a defined rate – which is called scan rate or sweep rate (in $V \cdot s^{-1}$) – between two potential values – the initial potential (V_1) and the switching potential (V_2), after which the scan is reversed back to V_1. The current vs potential (I vs E) trace is recorded. One cycle in CV consists of the I vs E trace recorded when the potential is changed from V_1 to V_2 and then back to V_1 (**figure 4.20**). Usually, this is repeated at least two times in an experiment – leading to multiple recorded cycles. The sweep from V_1 to V_2 and back to V_1 is usually referred to as a triangular waveform.

In the beginning, when the potential is scanned from V_1 to V_2, but the potential value is too low to drive the oxidation reaction, there is no faradaic current, and any current measured is charging current. When the potential approaches the formal potential of the redox couple, the reduced species starts being oxidised and faradaic current is generated and recorded. Due to mass transfer limitations (unstirred solution), the reduced species will be depleted in the vicinity of the electrode surface, and the current will thus start to drop. This is why there is a maximum current value, denoted in this case as peak current, i_{pa}, and its corresponding potential value, E_{pa}. The reverse scan behaves in a similar way, except that it drives the reduction reaction.

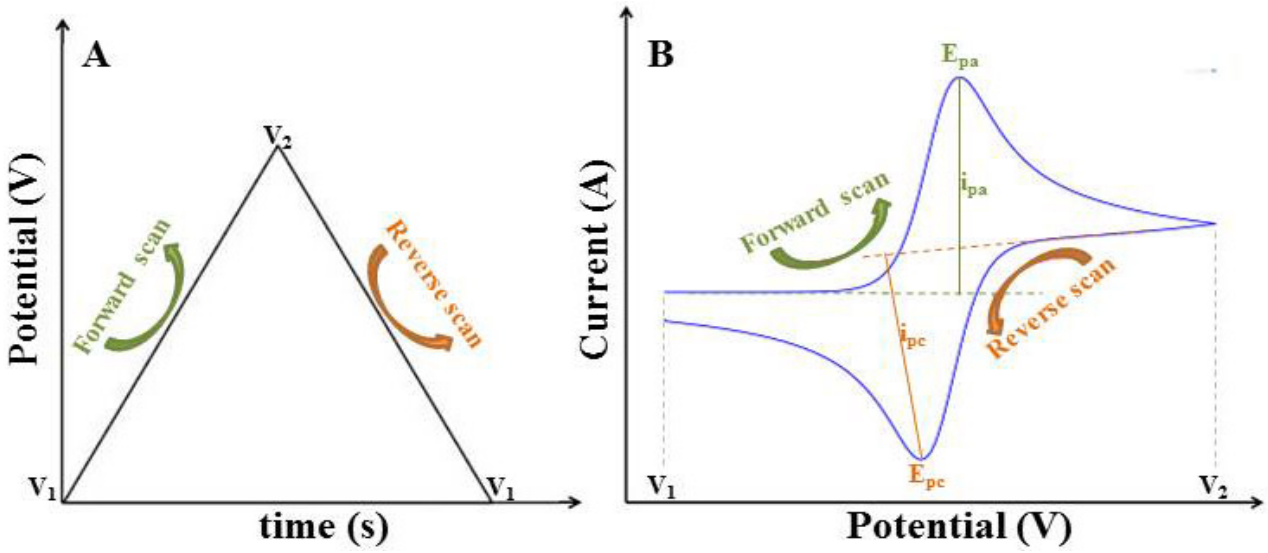

Figure 4.20: The potential triangular waveform (a) and a typical current vs potential trace in cyclic voltammetry for a reversible redox reaction (b). E_{pa} and E_{pc} represent the anodic and cathodic peak potentials, while i_{pa} and i_{pc} are the anodic and cathodic peak currents.

A reversible redox reaction has fast kinetics, and the rate-limiting step is the diffusion of the reactive species to and from the electrode surface. Peak currents and peak potentials are important parameters that can be determined experimentally and which give information about the ET process and the reversibility of the electrochemical reaction.

i) Peak potentials

The peak separation is the difference between the anodic and cathodic peak currents (**equation 4.7**).

$$\Delta E_p = E_{pa} - E_{pc} = \frac{59}{n}\, mV\ (at\ 298K) \qquad \textit{Equation 4.7}$$

- *where ΔE_p is the peak separation, E_{pa} is the potential of the anodic peak, E_{pc} is the potential of the cathodic peak and n is the number of electrons transferred in the redox reaction.*

In practice, the peak separation is usually higher than 59 mV/n (which is the value for an ideal case). Because of this, standard redox couples (such as ferrocyanide/ferricyanide) are employed to investigate electrode behaviour. The measured ΔE_p value can be used in the calculation of the heterogenous ET rate constants. For a reversible reaction, ΔE_p is independent of the scan rate. If the peak separation increases with the scan rate, the reaction is either quasireversible or irreversible.

The formal potential of a redox couple can be calculated from the experimental values of the peak potentials as the average of the anodic and cathodic peak potentials (**equation 4.8**) and it is characteristic for the redox couple tested.

$$E^{0'} = \frac{E_{pa} + E_{pc}}{2} \qquad \textit{Equation 4.8}$$

- where *$E^{0'}$ is the formal potential of the electrochemical reaction, E_{pa} is the potential of the anodic peak and E_{pc} is the potential of the cathodic peak.*

ii) Peak currents

For a reversible electrochemical reaction, the absolute values for the cathodic and anodic peak currents should be the same ($i_{pa}/i_{pc} = 1$).

In a diffusion-controlled reversible system, the peak current depends on the surface area of the electrode, on the concentration and diffusion coefficient of the analyte and also on the scan rate, according to the Randles-Sevčic equation (**equation 4.9**):

$$I_p = 0.4463 \times nFAc\sqrt{\frac{nF\nu D}{RT}} \qquad \textit{Equation 4.9}$$

- *where I_p is the peak current (in A), n is the number of electrons transferred in the electrochemical reaction, F is Faraday's constant (96485 C·mol^{-1}), A is the electrode surface area (in cm^2), c is the concentration of the analyte (in mol·cm^{-3}), v is the scan rate (in V·s^{-1}), R is the universal gas constant (8.3145 J·mol^{-1}·K^{-1}) and T is the absolute temperature (in K).*

For a temperature of 298 K (25°C) and by replacing R and F with their numerical values, the Randles-Sevčic equation can be rewritten in its simplified form (**equation 4.10**):

$$I_p = 2.69 \times 10^5 \times n^{3/2} A D^{1/2} c^{1/2} \nu^{1/2} \qquad \textit{Equation 4.10}$$

- *where all the parameters are as described above, for equation 4.10.*

This equation shows that the peak currents should increase linearly with the square root of the scan rate. Furthermore, the equation can be used to calculate the diffusion coefficient of a species in certain experimental conditions, provided that the system is reversible (I_p vs $\nu^{1/2}$ is a linear plot which passes through the origin).

4.3.4. Cyclic voltammetry for electrochemical characterisation of carbon electrodes – results

OFEs and TECs were characterised by CV in two redox couples: $[Fe(CN)]_6^{3-/4-}$ and $[Ru(NH_3)_6]^{2+/3+}$. $[Fe(CN)]_6^{3-/4-}$ is one of the most used redox couples for electrode characterisation, but it is surface sensitive, and thus not an ideal outer-sphere redox system [128,227,228]. $[Ru(NH_3)_6]^{2+/3+}$ is a reliable outer-sphere redox system widely used in the electrochemical characterisation of carbon electrodes [119,130,229,230].

The effect of plasma treatment (PT) and storage on the electrochemistry is shown in **figure 4.21a**. When using $[Fe(CN)]_6^{3-/4-}$ as redox couple, the electrochemistry is much improved after PT. The effect is long-lasting (at least 1 month). This can most likely be attributed to the fact that PT removes organic impurities from the surface, and $[Fe(CN)]_6^{3-/4-}$ is surface sensitive. For $[Ru(NH_3)_6]^{2+/3+}$, PT does not alter the electrochemistry.

Figure 4.21b shows the voltammograms obtained with 3 different OFEs with polyimide-derived carbon surface after PT and storage for 1-3 weeks. The electrodes are from different fabrication

batches. The CVs show good reproducibility. Electrochemical characterisation of TECs also shows good reproducibility (< 5% variation).

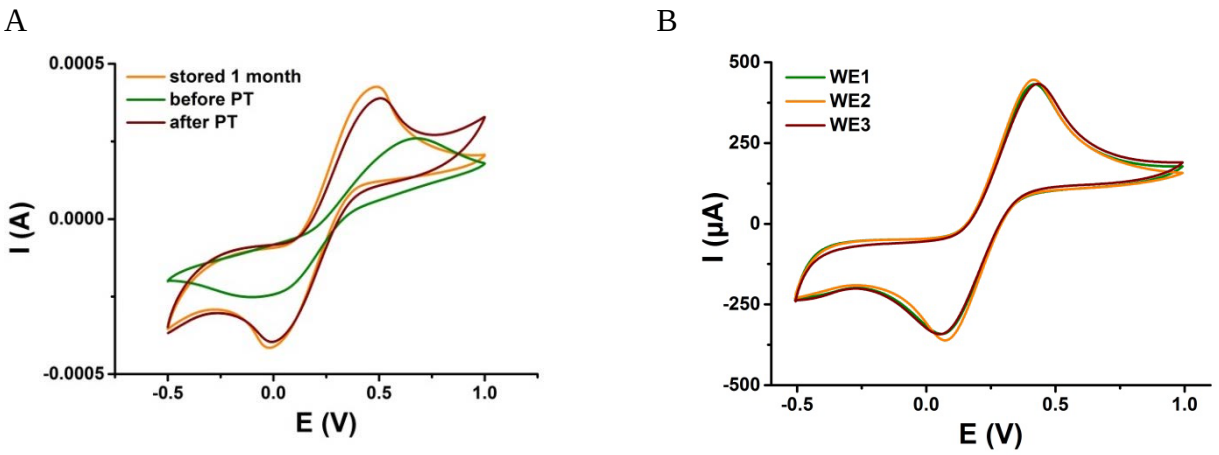

Figure 4.21: CV of OFEs in 10 mM $[Fe(CN)]_6^{3-/4-}$ at a scan rate of 50 mV/s. Effect of plasma treatment (PT) and storage on electrochemistry (a). 3 different electrodes tested in the same conditions (b). E vs Ag|AgCl.

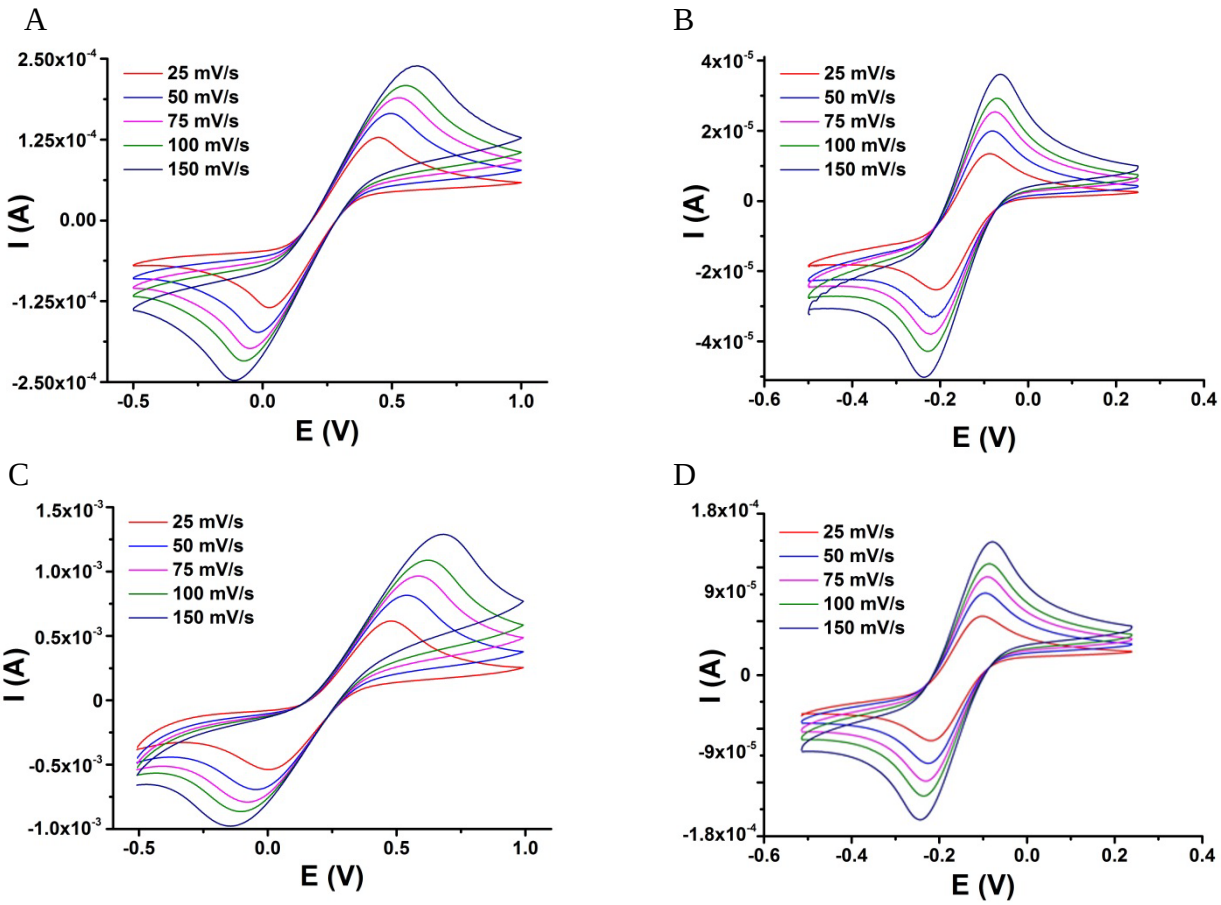

Figure 4.22: CV of polyimide-derived OFEs (a, b) and SU-8 derived TECs (c, d) in 10 mM $[Fe(CN)]_6^{3-/4-}$ (a, c) and 1 mM $[Ru(NH_3)_6]^{2+/3+}$ (b, d) at different scan rates. E vs Ag|AgCl.

Figure 4.22 shows cyclic voltammograms of OFEs and TECs with the two redox couples at scan rates between 25 and 150 $mV \cdot s^{-1}$. For $[Fe(CN)]_6^{3-/4-}$, ΔE_p is quite large and increases quickly with increasing scan rates. When using $[Ru(NH_3)_6]^{2+/3+}$, a peak separation of 71 mV is obtained with OFEs, and 73 mV with TECs at 25 $mV \cdot s^{-1}$. In this case, the increase in ΔE_p with increasing scan rates is much smaller.

OFEs fabricated using SU-8 as carbon precursor show wide peak separation (> 300 mV) in CVs with $[Ru(NH_3)_6]^{2+/3+}$ and are not reproducible (**figure 4.23**). The fabrication of SU-8-derived OFEs needs to be optimised before the electrodes can be employed for electrochemical measurements with biological systems.

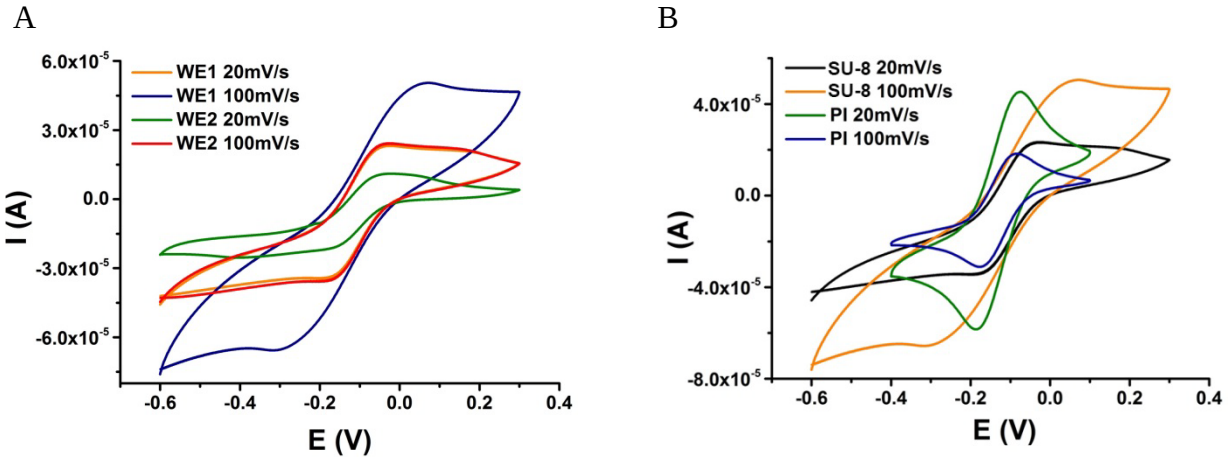

Figure 4.23: CV of two SU-8 derived OFEs in 1 mM $[Ru(NH_3)_6]^{2+/3+}$ at two different scan rates (a). Comparison between the electrochemistry of PI- and SU-8-derived OFEs (b). E vs Ag\|AgCl.

4.3.5. Chronoamperometry

In CA, a single or double potential step is applied to the system, and then the current is measured over time. CA can be performed in a static system, when the mass transfer is done by diffusion. Alternatively mass transfer can be enhanced by forced convection (for example by using magnetic stirring, a rotating disk electrode, or by the flow in flow systems).

The Cottrell equation (**equation 4.11**) is very useful in CA, when using planar electrodes, since it relates current to time. By using the Cottrell equation, the active electrode surface area can be measured accurately by using a well-defined redox couple (with known number of electrons transferred, concentration and diffusion coefficient). Similarly, if the active electrode area and the concentration are known, the number of electrons transferred or the diffusion coefficient can be determined.

$$I = \frac{nFAc_0\sqrt{D}}{\sqrt{\pi t}}$$ *Equation 4.11*

- *where I is the current (in A), n is the number of electrons transferred in the oxidation reaction, F is the Faraday constant (96485 C·mol^{-1}), A is the surface area of the planar electrode (in cm^2), c_0 is the initial concentration of the reduced species (in mol·cm^{-3}), D is the diffusion coefficient of the species (in cm^2·s^{-1}) and t is time (in s).*

When CA is employed as a tool for detecting an electroactive analyte, a baseline is recorded in the electrolyte solution in the absence of the analyte. Applying a potential step will cause a fast initial charging current, followed by a current decay that will then stabilise to a constant current level. The baseline current is to be subtracted from the measurement to make it easier to observe and quantify the reaction of interest. When the electroactive analyte is added to the system a faradaic current response related to its oxidation or reduction will be measured. In certain cases, it is important to make sure that the current generation is due to the redox conversion of the analyte and not caused by other factors (such as noise induced by pipetting or stirring). For this purpose, reference experiments are extremely important. A chronoamperogram can be seen in **Figure 4.24.** The inset shows the applied potential step.

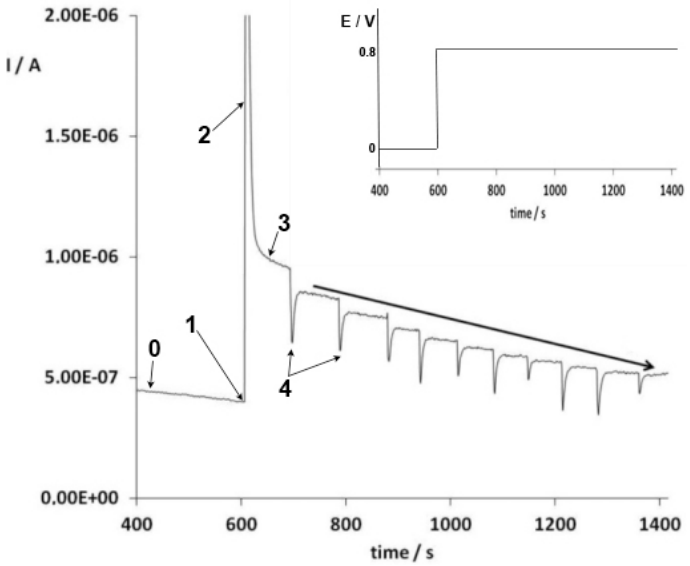

Figure 4.24: Chronoamperogram for vanadium quantification. Inset: potential step applied. 0: baseline recorded at E=0 V; 1: time point at which the potential step is applied to the system; 2: initial charging current; 3: measured current (faradaic + baseline). 4: perturbations to the system caused by analyte addition. Figure modified from [241].

4.3.6. Dopamine detection using OFEs

DA can be electrochemically oxidised to dopamine o-quinone (DQ) in a two-electron process [231] shown in **figure 4.25**. The oxidation can be studied using several electrochemistry techniques, such as CV, amperometry or differential pulse voltammetry (DPV) [128,133,228,231].

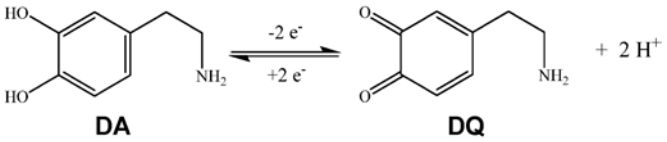

Figure 4.25: Redox reaction for the dopamine / dopamine o-quinone couple.

The suitability of OFEs for dopamine detection was tested with DA in PBS solution using CV and CA (**figure 4.26**). The anodic peak intensity (1st cycle) from CVs recorded using a scan rate of 50 mV·s^{-1} shows a linear correlation with the concentration up to 200 µM DA. In CA, the plateau intensity increases linearly with the concentration up to 75 µM DA. For CA measurements, the limit of detection is 0.17 µM, and the limit of quantification is 0.57 µM.

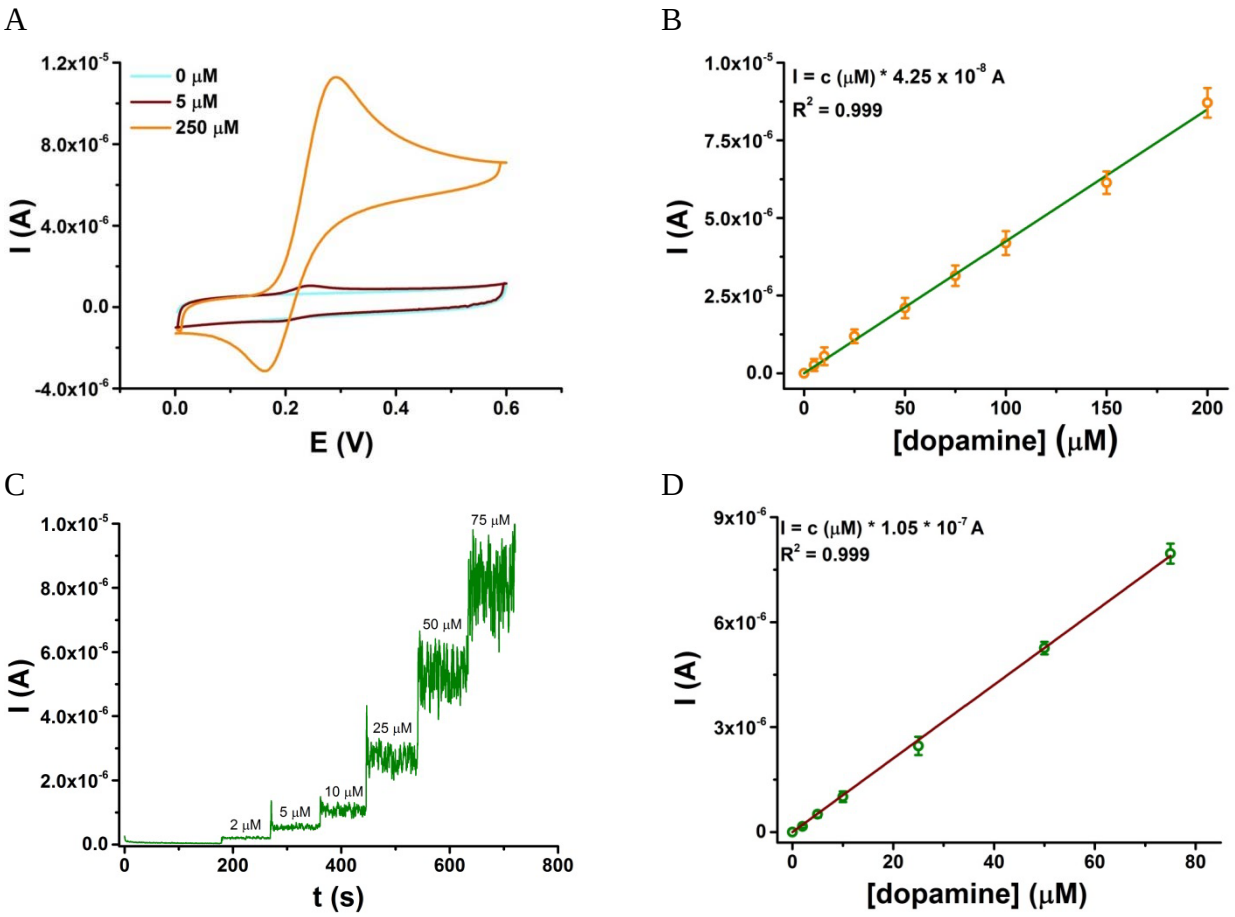

Figure 4.26: Electrochemistry using dopamine solutions and optical fibre electrodes: CV in different concentrations of dopamine (a) and calibration curve using anodic peak intensity from CV at 50 mV/s scan rate (b); Chronoamperogram with dopamine additions (c) and calibration curve using average plateau intensity from CA (d). E vs Ag|AgCl.

CA was used to monitor DA exocytosis from dopaminergic cells residing on the surface on the OFEs in real-time (**figure 4.27**). The experiment was performed under stirring. When the concentration of K^+ is elevated and dopaminergic cells are present on the OFE, a current increase is measured in CA (**figure 4.27a**). Control experiments with no cells or with cells that are not dopaminergic do not show a response to KCl.

The ability of a population of cells to release DA is expected to change during differentiation. To investigate this, CA was employed to detect DA release from cells at different time points during differentiation. The addition of K^+ was performed twice for each sample, at 15 min interval. The peaks from CA were integrated and the calculated charges for the first and second exocytosis event can be seen in **figure 4.27b**. Since the charges increase during the differentiation timeline, it can be assessed that the differentiation progresses during the 10 day procedure. Additionally, charges determined for the second exocytosis event increase, showing that the dopaminergic neurons are maturing during the differentiation.

A

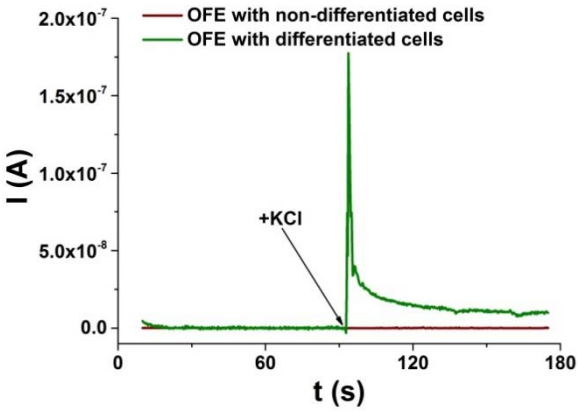

B

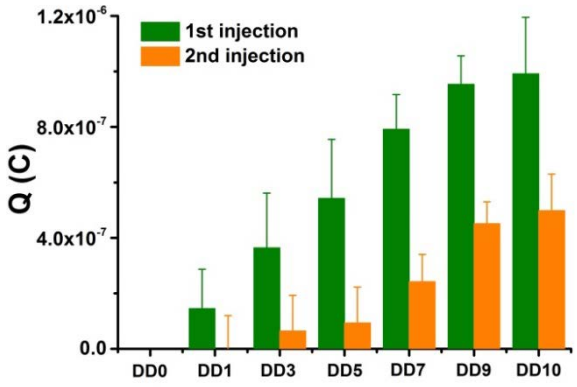

Figure 4.27: Chronoamperometric detection of dopamine released from differentiated cells upon K^+-induced stimulation: typical current-time trace recorded with an OFE from a cell population after 10 days of differentiation at E = +0.35 V vs Ag|AgCl (a). Average charges for the first and second exocytosis event at different time points in the experiment (b)

More details about the experiments performed with OFEs can be found in appendix I.

4.3.7. Photocurrent generation from thylakoid membranes – chronoamperometry results

In the presence of light, TMs perform the light-reactions of photosynthesis, as described in section 2.2.2. A redox mediator in its oxidised from can be reduced by electrons generated in the photosynthetic process and can then be re-oxidised in an electrode reaction. The oxidation of the mediator using TECs can be monitored using CA, as shown in **figure 4.28a**.

In the absence of light, there is no photocurrent generation (the current decreases from µA to nA level). TECs show good reproducibility in CA measurements of photocurrent generation from TMs (< 10% variation).

Photocurrent generation from TMs using TECs depends on multiple factors, such as the chlorophyll content of the system, the irradiance, the chip pattern and the concentration of mediator. For this work, the chlorophyll content and the concentration of mediator were optimised before investigating the influence of the chip pattern on the photocurrent collection. Small openings in the carbon layer (20 µm) and high surface coverage for the openings (60%) led to the highest measured photocurrents (details in appendix II).

The influence of irradiance on the photocurrent generation was also investigated, since it is an important parameter to consider when thinking of large-scale applications in the energy sector. By using the maximum current measured in CA and knowing that the active electrode area is 0.5 cm^2, the maximum current density was calculated. **Figure 4.28b** shows the variation of the maximum current density when using different irradiance values for electrode chips with 20 µm openings.

A B

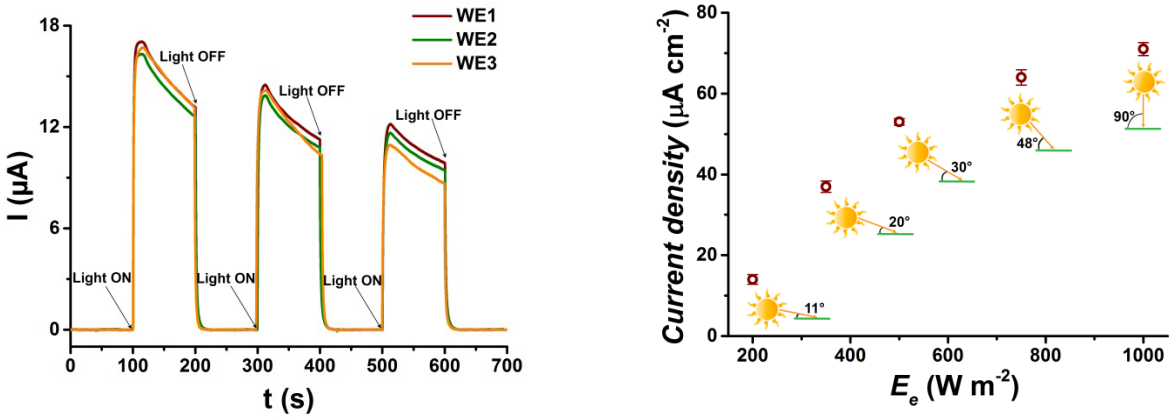

Figure 4.28: CA measurement of photocurrent generation from TMs using three TECs with the same pattern (100 µm openings) and 1 mM $[Ru(NH_3)_6]Cl_3$ as mediator for 500 W·m^2 irradiance, E = 0 V vs Ag\|AgCl (a). Maximum current density generated from TMs as a function of irradiance when using 1 mM $[Ru(NH_3)_6]Cl_3$ as mediator and TECs with 20 µm openings. Drawings show the incident angle of solar light on a clear day for the different irradiance values (b)

A more thorough description of the experiments performed with TECs can be found in the manuscript attached as Appendix II.

Chapter 5: Conclusions and outlook

A conclusion is the place where you get tired of thinking.
Arthur Block

This PhD project has focused on combining electrochemical detection and optical stimulation for biological samples, with the purpose of developing optoelectrical devices for different applications.

This chapter summarises the main findings of the work and discusses the progress in relation to the objectives and milestones stated in the introduction. The two directions (cell replacement therapy for Parkinson's disease and energy applications) are discussed separately. Future perspectives of the work are mentioned.

I. Development of an optoelectrical device for the treatment of Parkinson's disease

In the beginning of this project, the device existed only as an idea. Existing knowledge supported several aspects of the idea:

i) Optical fibres can be modified to have a leaky section [232,233].
ii) Carbon is a suitable substrate for stem cell growth and differentiation [5,157].
iii) Carbon electrodes can be employed for dopamine detection [5,128,234].
iv) Cells can be optogenetically modified to have specific responses when exposed to light with a certain wavelength [31,235,236].

The work in this project was meant to open the path for the fabrication of the device. In accordance to the milestones listed in section 1.2, optical fibres were successfully converted to carbon electrodes. The fabricated OFEs were employed as substrate for cell culture and differentiation and used for dopamine detection in solution and from cells grown on their surface.

These experiments represented the basis for writing a manuscript (appendix I, soon to be submitted) and the proof-of concept for filing a patent application (appendix III).

The idea will be further developed as part of the Training4CRM project, funded by the European Union Horizon 2020 Programme (H2020-MSCA-ITN-2016) under the Marie Skłodowska-Curie Initial Training Network and Grant Agreement No.722779. **Figure 5.1** shows the timeline of the Training4CRM project.

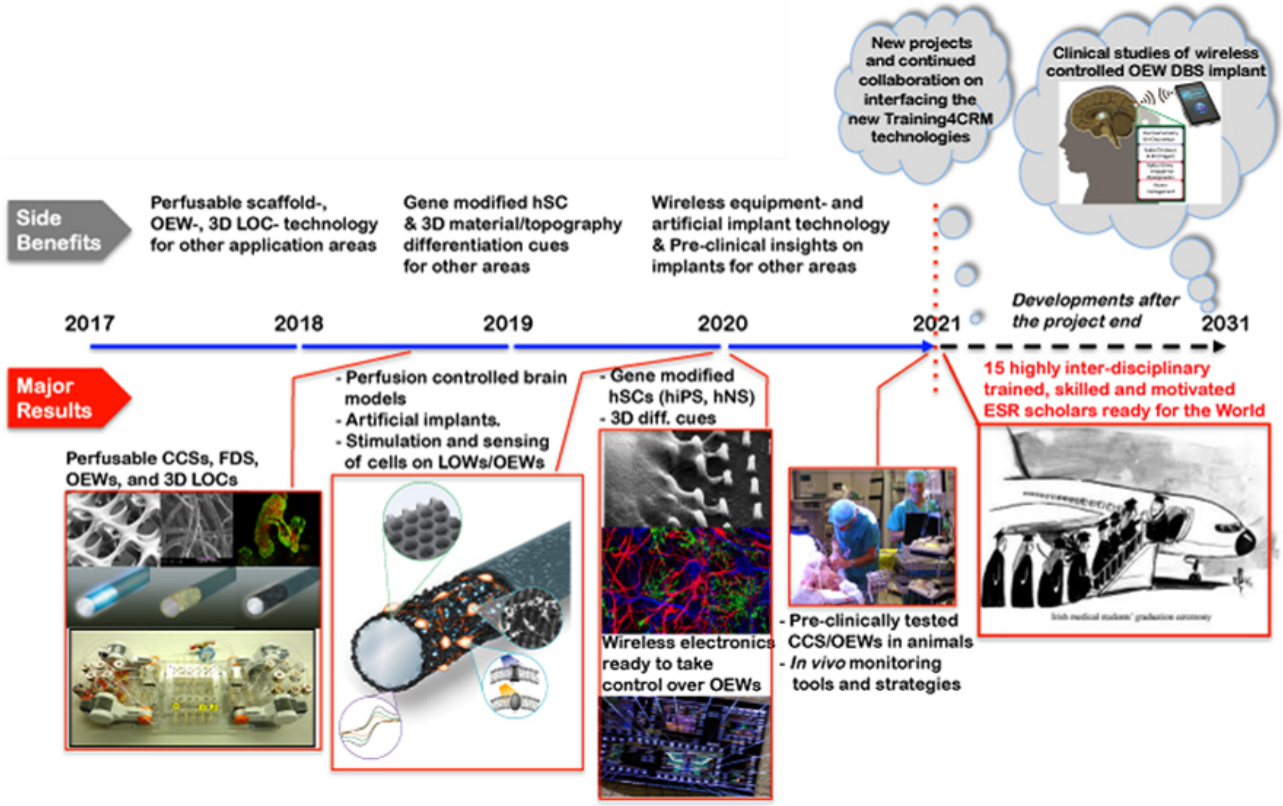

Figure 5.1: Timeline for the Training4CRM project: major outcomes during and beyond the project.

II. Development of an optoelectrical bioanode for photo-bioelectrochemical cells

Photocurrent generation from photosynthetic organisms requires a combination of optical stimulation and electrochemistry. The idea of extending the use of the envisioned optoelectrical device for Parkinson's disease treatment to energy harvesting from photosynthetic organisms became a separate direction of the work. Similar concepts can be applied for both applications, but development and optimisation needs to be done specifically for one goal.

Transparent electrode chips were designed and fabricated for this purpose. The TECs showed good electrochemical properties and transparency in the UV-visible range and were employed for harvesting energy from photosynthetic organisms. Different electrode patterns were tested in order to optimise the current generation and to elucidate the importance of different design parameters on the photocurrent generation.

The development and application of TECs for photocurrent generation from TMs was the basis for a manuscript (appendix II, soon to be submitted) and supported the claims from the patent application (appendix III).

In the future, the efficiency of photo-bioelectrochemical cells built using TEC-bioanodes needs to be investigated and maximised. The suitability of TECs for large-scale applications in the field of biophotovoltaics will depend on the efficiency of the system.

General conclusion

The idea of combining electrochemical detection and optical stimulation (e.g. carbon-on-quartz devices) can be adapted to different applications. Existing knowledge can be transferred from application to application. However, optimisation needs to be done with a specific goal in mind, since different biological systems have different requirements.

Bibliography

[1] V.P. Calabrese, E.. R. Dorsey, R.. Constantinescu, J.. P. Thompson, K.. M. Biglan, R.. G. Holloway, K.. Kieburtz, F.. J. Marshall, B.. M. Ravina, G.. Schifitto, A.. Siderowf, C.. M. Tanner, Projected Number of People with Parkinson Disease in the Most Populous Nations, 2005 through 2030, Neurology. 69 (2007) 223–224. doi:10.1212/01.wnl.0000271777.50910.73.

[2] M.L. Giroux, Parkinson disease: managing a complex, progressive disease at all stages., Cleve. Clin. J. Med. 74 (2007) 313–314. doi:10.3949/ccjm.74.5.313.

[3] F. Rossi, E. Cattaneo, Neural stem cell therapy for neurological diseases: dreams and reality, Nat. Rev. Neurosci. 3 (2002) 401–409. doi:10.1038/nrn809.

[4] T.R. Barrow, Cell replacement therapy in Parkinson's disease, Biosci. Horizons. 8 (2015) hzv002-hzv002. doi:10.1093/biohorizons/hzv002.

[5] L. Amato, A. Heiskanen, C. Caviglia, F. Shah, K. Zór, M. Skolimowski, M. Madou, L. Gammelgaard, R. Hansen, E.G. Seiz, M. Ramos, T.R. Moreno, A. Martínez-Serrano, S.S. Keller, J. Emnéus, Pyrolysed 3D-Carbon Scaffolds Induce Spontaneous Differentiation of Human Neural Stem Cells and Facilitate Real-Time Dopamine Detection, Adv. Funct. Mater. 24 (2014) 7042–7052. doi:10.1002/adfm.201400812.

[6] J.M. Savitt, Diagnosis and treatment of Parkinson disease: molecules to medicine, J. Clin. Invest. 116 (2006) 1744–1754. doi:10.1172/JCI29178.

[7] M. Parent, Substantia Nigra and Parkinson's Disease: A Brief History of Their Long and Intimate Relationship, Can. J. Neurol. Sci. 37 (2010).

[8] D. Twelves, K.S.M. Perkins, C. Counsell, Systematic review of incidence studies of Parkinson's disease, Mov. Disord. 18 (2003) 19–31. doi:10.1002/mds.10305.

[9] L. Hirsch, N. Jette, A. Frolkis, T. Steeves, T. Pringsheim, The Incidence of Parkinson's Disease: A Systematic Review and Meta-Analysis, Neuroepidemiology. 46 (2016) 292–300. doi:10.1159/000445751.

[10] J.S. Perlmutter, Assessment of Parkinson Disease Manifestations, in: Curr. Protoc. Neurosci., John Wiley & Sons, Inc., Hoboken, NJ, USA, 2009. doi:10.1002/0471142301.ns1001s49.

[11] B. V. Zlokovic, The Blood-Brain Barrier in Health and Chronic Neurodegenerative Disorders, Neuron. 57 (2008) 178–201. doi:10.1016/j.neuron.2008.01.003.

[12] K.A. Jellinger, Cerebrospinal Fluid in Clinical Practice, Eur. J. Neurol. 16 (2009) e109–e109. doi:10.1111/j.1468-1331.2009.02601.x.

[13] A. Lopez, A. Muñoz, M.. Guerra, J.. Labandeira-Garcia, Mechanisms of the effects of exogenous levodopa on the dopamine-denervated striatum, Neuroscience. 103 (2001) 639–651. doi:10.1016/S0306-4522(00)00588-1.

[14] J. Dingemanse, Issues important for rational COMT inhibition, Neurology. 55 (2000).

[15] S. Kaakkola, H. Teräväinen, S. Ahtila, M. Karlsson, T. Naukkarinen, H. Rita, A. Gordin, Entacapone in combination with standard or controlled-release levodopa/carbidopa: a clinical and pharmacokinetic study in patients with Parkinson's disease, Eur. J. Neurol. 2 (1995) 341–347. doi:10.1111/j.1468-1331.1995.tb00137.x.

[16] E. Arenas, M. Denham, J.C. Villaescusa, How to make a midbrain dopaminergic neuron, Development. 142 (2015) 1918–1936. doi:10.1242/dev.097394.

[17] H.L. Klawans, C. Goetz, P.A. Nausieda, W.J. Weiner, Levodopa-Induced dopamine receptor hypersensitivity, Ann. Neurol. 2 (1977) 125–129. doi:10.1002/ana.410020207.

[18] J.L. Cummings, Behavioral Complications of Drug Treatment of Parkinson's Disease, J. Am. Geriatr. Soc. 39 (1991) 708–716. doi:10.1111/j.1532-5415.1991.tb03627.x.

[19] E.C. Wolters, Dopamine agonists in Parkinson's disease, Neurology. 45 (1995).

[20] M. Yamamoto, A.H. Schapira, Dopamine agonists in Parkinson's disease, Expert Rev. Neurother. 8 (2008) 671–677. doi:10.1586/14737175.8.4.671.

[21] P. Riederer, G. Laux, MAO-inhibitors in Parkinson's Disease, Exp. Neurobiol. 20 (2011) 1. doi:10.5607/en.2011.20.1.1.

[22] M. Yamada, Clinical Pharmacology of MAO Inhibitors: Safety and Future, Neurotoxicology. 25 (2004) 215–221. doi:10.1016/S0161-813X(03)00097-4.

[23] H. Oshima, T. Obuchi, Y. Katayama, Neuromodulation: Deep Brain Stimulation, in: Neuroanesthesia Cerebrospinal Prot., Springer Japan, Tokyo, 2015: pp. 457–464. doi:10.1007/978-4-431-54490-6_40.

[24] A.M. Lozano, Deep brain stimulation therapy, Bmj. 344 (2012).

[25] Y. Katayama, Deep brain stimulation therapy for involuntary movements, Clin. Neurol. 41 (2001).

[26] K. Deisseroth, G. Feng, A.K. Majewska, G. Miesenböck, A. Ting, M.J. Schnitzer, Next-Generation Optical Technologies for Illuminating Genetically Targeted Brain Circuits, J. Neurosci. 26 (2006).

[27] M. Scanziani, M. Häusser, Electrophysiology in the age of light, Nature. 461 (2009) 930–939. doi:10.1038/nature08540.

[28] L. Fenno, O. Yizhar, K. Deisseroth, The Development and Application of Optogenetics, Annu. Rev. Neurosci. 34 (2011) 389–412. doi:10.1146/annurev-neuro-061010-113817.

[29] X. Han, In vivo application of optogenetics for neural circuit analysis., ACS Chem. Neurosci. 3 (2012) 577–84. doi:10.1021/cn300065j.

[30] J.A. Cardin, M. Carlén, K. Meletis, U. Knoblich, F. Zhang, K. Deisseroth, L.-H. Tsai, C.I. Moore, Targeted optogenetic stimulation and recording of neurons in vivo using cell-type-specific expression of Channelrhodopsin-2., Nat. Protoc. 5 (2010) 247–54. doi:10.1038/nprot.2009.228.

[31] O. Yizhar, L.E. Fenno, T.J. Davidson, M. Mogri, K. Deisseroth, Optogenetics in Neural Systems, Neuron. 71 (2011) 9–34. doi:10.1016/j.neuron.2011.06.004.

[32] B.Y. Chow, X. Han, A.S. Dobry, X. Qian, A.S. Chuong, M. Li, M.A. Henninger, G.M. Belfort, Y. Lin, P.E. Monahan, E.S. Boyden, High-performance genetically targetable optical neural silencing by light-driven proton pumps, Nature. 463 (2010) 98–102. doi:10.1038/nature08652.

[33] G. Schatz, My two blues, FEBS Lett. 564 (2004) 1–3. doi:10.1016/S0014-5793(04)00330-8.

[34] R.D. Airan, K.R. Thompson, L.E. Fenno, H. Bernstein, K. Deisseroth, Temporally precise in vivo control of intracellular signalling, Nature. 458 (2009) 1025–1029. doi:10.1038/nature07926.

[35] T. Kim, J.G. McCall, Y.H. Jung, X. Huang, E.R. Siuda, Y. Li, J. Song, Y.M. Song, H.A. Pao, R.-H. Kim, C. Lu, S.D. Lee, I.-S. Song, G. Shin, R. Al-Hasani, S. Kim, M.P. Tan, Y. Huang, F.G. Omenetto, J.A. Rogers, M.R. Bruchas, Injectable, Cellular-Scale Optoelectronics with Applications for Wireless Optogenetics, Science (80-.). 340 (2013).

[36] J.H. Lee, Informing brain connectivity with optogenetic functional magnetic resonance imaging, Neuroimage. 62 (2012) 2244–2249. doi:10.1016/j.neuroimage.2012.01.116.

[37] A. Barreneche, S. Fraccola, C. Jolly, M. Keenan, S. Kergroach, J. Prüß, B. Serve, B. Stevens, M. Undseth, C. Van Ooijen, An OECD Horizon Scan Of Megatrends And Technology Trends In The Context of Future Research Policy, Danish Agency for Science, Technology and Innovation, Copenhagen, 2016.

[38] A.M. Packer, B. Roska, M. Häusser, Targeting neurons and photons for optogenetics., Nat. Neurosci. 16 (2013) 805–15. doi:10.1038/nn.3427.

[39] L.U. Wahlberg, G. Lind, P.M. Almqvist, P. Kusk, J. Tornøe, B. Juliusson, M. Söderman, E. Selldén, Å. Seiger, M. Eriksdotter-Jönhagen, B. Linderoth, Targeted delivery of nerve growth factor via encapsulated cell biodelivery in Alzheimer disease: a technology platform for restorative neurosurgery, J. Neurosurg. 117 (2012) 340–347. doi:10.3171/2012.2.JNS11714.

[40] M. Al-Rubeai, M. Naciri, Stem cells and cell therapy. Volume 8, Springer Netherlands, 2014.

[41] W. Li, A.W. Flake, Stem Cell Biology, in: Renaiss. Sick. Cell Dis. Res. Genome Era, Imperial College Press, 2007: pp. 259–275. doi:10.1142/9781860947964_0016.

[42] S.J. Kelly, Studies of the developmental potential of 4- and 8-cell stage mouse blastomeres, J. Exp. Zool. 200 (1977) 365–376. doi:10.1002/jez.1402000307.

[43] M. Stadtfeld, K. Hochedlinger, Induced pluripotency: history, mechanisms, and applications, Genes Dev. 24 (2010) 2239–2263. doi:10.1101/gad.1963910.

[44] M.J. Dewey, Mosaic Mice with Teratocarcinoma-Derived Mutant Cells Deficient in Hypoxanthine Phosphoribosyltransferase, Proc. Natl. Acad. Sci. U. S. A. 74 (1977). doi:10.2307/67398.

[45] H.M. Blau, T.R. Brazelton, J.M. Weimann, The Evolving Concept of a Stem Cell, Cell. 105 (2001) 829–841. doi:10.1016/S0092-8674(01)00409-3.

[46] J.B. Gurdon, T.R. Elsdale, M. Fischberg, Sexually Mature Individuals of Xenopus laevis from the Transplantation of Single Somatic Nuclei, Nature. 182 (1958) 64–65. doi:10.1038/182064a0.

[47] K. Takahashi, S. Yamanaka, Induction of Pluripotent Stem Cells from Mouse Embryonic and Adult Fibroblast Cultures by Defined Factors, Cell. 126 (2006) 663–676. doi:10.1016/j.cell.2006.07.024.

[48] S.T. Rashid, G.J.M. Alexander, Induced pluripotent stem cells: From Nobel Prizes to clinical applications, J. Hepatol. 58 (2013) 625–629. doi:10.1016/j.jhep.2012.10.026.

[49] S. Temple, The development of neural stem cells, Nature. 414 (2001) 112–117. doi:10.1038/35102174.

[50] M. Mimeault, S.K. Batra, Recent Progress on Tissue-Resident Adult Stem Cell Biology and Their Therapeutic Implications, Stem Cell Rev. 4 (2008) 27–49. doi:10.1007/s12015-008-9008-2.

[51] A.J. Engler, S. Sen, H.L. Sweeney, D.E. Discher, Matrix elasticity directs stem cell lineage specification, Cell. 126 (2006) 677–689. doi:10.1016/j.cell.2006.06.044.

[52] D.E. Discher, D.J. Mooney, P.W. Zandstra, Growth Factors, Matrices, and Forces Combine and Control Stem Cells, Science (80-.). 324 (2009) 1673–1677. doi:10.1126/science.1171643.

[53] J. Hsieh, F.H. Gage, Epigenetic control of neural stem cell fate, Curr. Opin. Genet. Dev. 14 (2004) 461–469. doi:10.1016/j.gde.2004.07.006.

[54] C.E. Murry, G. Keller, Differentiation of Embryonic Stem Cells to Clinically Relevant Populations: Lessons from Embryonic Development, Cell. 132 (2008) 661–680. doi:10.1016/j.cell.2008.02.008.

[55] O. Lindvall, A. Björklund, Cell replacement therapy: Helping the brain to repair itself, Neurotherapeutics. 1 (2004) 379–381. doi:10.1007/BF03206624.

[56] O. Lindvall, Z. Kokaia, A. Martinez-Serrano, Stem cell therapy for human neurodegenerative disorders–how to make it work, Nat. Med. 10 (2004) S42–S50. doi:10.1038/nm1064.

[57] A. Trounson, N.D. DeWitt, Pluripotent stem cells progressing to the clinic, Nat. Rev. Mol. Cell Biol. 17 (2016) 194–200. doi:10.1038/nrm.2016.10.

[58] A. Trounson, C. McDonald, Stem Cell Therapies in Clinical Trials: Progress and Challenges, Cell Stem Cell. 17 (2015) 11–22. doi:10.1016/j.stem.2015.06.007.

[59] A. Bjo¨rklund, U. Stenevi, Reconstruction of the nigrostriatal dopamine pathway by intracerebral nigral

transplants, Brain Res. 177 (1979) 555–560. doi:10.1016/0006-8993(79)90472-4.

[60] S. Casarosa, Y. Bozzi, L. Conti, Neural stem cells: ready for therapeutic applications?, Mol. Cell. Ther. 2 (2014) 31. doi:10.1186/2052-8426-2-31.

[61] T. Yorio, A.F. Clark, M.B. Wax, Ocular therapeutics : eye on new discoveries, Academic, 2008.

[62] G.M. Cooper, R.E. Hausman, The cell : a molecular approach, ASM Press, 2004.

[63] S. Cohen, R. Levi-Montalcini, Purification and properties of a nerve growth-promoting factor isolated from mouse sarcoma 180., Cancer Res. 17 (1957) 15–20.

[64] S. Cohen, The stimulation of epidermal proliferation by a specific protein (EGF), Dev. Biol. 12 (1965) 394–407. doi:10.1016/0012-1606(65)90005-9.

[65] S. Cohen, Origins of Growth Factors: NGF and EGF, J. Biol. Chem. 283 (2008) 33793–33797. doi:10.1074/jbc.X800008200.

[66] F.M. Watt, and B.L.M. Hogan, Out of Eden: Stem Cells and Their Niches, Science (80-.). 287 (2000).

[67] E. Fuchs, T. Tumbar, G. Guasch, Socializing with the neighbors: stem cells and their niche., Cell. 116 (2004) 769–78.

[68] M.M. Nava, M.T. Raimondi, R. Pietrabissa, Controlling Self-Renewal and Differentiation of Stem Cells via Mechanical Cues, J. Biomed. Biotechnol. 2012 (2012) 1–12. doi:10.1155/2012/797410.

[69] M. Schuldiner, O. Yanuka, J. Itskovitz-Eldor, D.A. Melton, N. Benvenisty, Effects of eight growth factors on the differentiation of cells derived from human embryonic stem cells., Proc. Natl. Acad. Sci. U. S. A. 97 (2000) 11307–12. doi:10.1073/pnas.97.21.11307.

[70] K.-C. Hwang, J.Y. Kim, W. Chang, D.-S. Kim, S. Lim, S.-M. Kang, B.-W. Song, H.-Y. Ha, Y.J. Huh, I.-G. Choi, D.-Y. Hwang, H. Song, Y. Jang, N. Chung, S.-H. Kim, D.-W. Kim, Chemicals that modulate stem cell differentiation., Proc. Natl. Acad. Sci. U. S. A. 105 (2008) 7467–71. doi:10.1073/pnas.0802825105.

[71] A. Kirkeby, S. Grealish, D.A. Wolf, J. Nelander, J. Wood, M. Lundblad, O. Lindvall, M. Parmar, Generation of Regionally Specified Neural Progenitors and Functional Neurons from Human Embryonic Stem Cells under Defined Conditions, Cell Rep. 1 (2012) 703–714. doi:10.1016/j.celrep.2012.04.009.

[72] N.S. Hwang, S. Varghese, J. Elisseeff, Controlled differentiation of stem cells., Adv. Drug Deliv. Rev. 60 (2008) 199–214. doi:10.1016/j.addr.2007.08.036.

[73] C. Frantz, K.M. Stewart, V.M. Weaver, The extracellular matrix at a glance, J. Cell Sci. 123 (2010).

[74] C. Kasper, F. Witte, R. Pörtner, Tissue engineering III : cell-surface interactions for tissue culture, Springer, 2012.

[75] R. McBeath, D.M. Pirone, C.M. Nelson, K. Bhadriraju, C.S. Chen, Cell Shape, Cytoskeletal Tension, and RhoA Regulate Stem Cell Lineage Commitment, Dev. Cell. 6 (2004) 483–495. doi:10.1016/S1534-5807(04)00075-9.

[76] S. Even-Ram, V. Artym, K.M. Yamada, Matrix control of stem cell fate., Cell. 126 (2006) 645–7. doi:10.1016/j.cell.2006.08.008.

[77] F. Guilak, D.M. Cohen, B.T. Estes, J.M. Gimble, W. Liedtke, C.S. Chen, Control of Stem Cell Fate by Physical Interactions with the Extracellular Matrix, Cell Stem Cell. 5 (2009) 17–26. doi:10.1016/j.stem.2009.06.016.

[78] A. Villa, I. Liste, E.T. Courtois, E.G. Seiz, M. Ramos, M. Meyer, B. Juliusson, P. Kusk, A. Martínez-Serrano, Generation and properties of a new human ventral mesencephalic neural stem cell line, Exp. Cell Res. 315 (2009) 1860–1874. doi:10.1016/j.yexcr.2009.03.011.

[79] C. Krabbe, E. Courtois, P. Jensen, J.R. Jørgensen, J. Zimmer, A. Martínez-Serrano, M. Meyer, Enhanced dopaminergic differentiation of human neural stem cells by synergistic effect of Bcl-x_L and reduced oxygen

tension, J. Neurochem. 110 (2009) 1908–1920. doi:10.1111/j.1471-4159.2009.06281.x.

[80] E.T. Courtois, C.G. Castillo, E.G. Seiz, M. Ramos, C. Bueno, I. Liste, A. Martinez-Serrano, In Vitro and in Vivo Enhanced Generation of Human A9 Dopamine Neurons from Neural Stem Cells by Bcl-XL, J. Biol. Chem. 285 (2010) 9881–9897. doi:10.1074/jbc.M109.054312.

[81] E.G. Seiz, M. Ramos-Gómez, E.T. Courtois, J. Tønnesen, M. Kokaia, I. Liste Noya, A. Martínez-Serrano, Human midbrain precursors activate the expected developmental genetic program and differentiate long-term to functional A9 dopamine neurons in vitro. Enhancement by Bcl-XL, Exp. Cell Res. 318 (2012) 2446–2459. doi:10.1016/j.yexcr.2012.07.018.

[82] I. Dincer, Renewable energy and sustainable development: a crucial review, Renew. Sustain. Energy Rev. 4 (2000) 157–175. doi:10.1016/S1364-0321(99)00011-8.

[83] C. Koroneos, T. Spachos, N. Moussiopoulos, Exergy analysis of renewable energy sources, Renew. Energy. 28 (2003) 295–310. doi:10.1016/S0960-1481(01)00125-2.

[84] A.K. Akella, R.P. Saini, M.P. Sharma, Social, economical and environmental impacts of renewable energy systems, Renew. Energy. 34 (2009) 390–396. doi:10.1016/j.renene.2008.05.002.

[85] S. Bilgen, K. Kaygusuz, A. Sari, Renewable Energy for a Clean and Sustainable Future, Energy Sources. 26 (2004) 1119–1129. doi:10.1080/00908310490441421.

[86] N.L. Panwar, S.C. Kaushik, S. Kothari, Role of renewable energy sources in environmental protection: A review, Renew. Sustain. Energy Rev. 15 (2011) 1513–1524. doi:10.1016/j.rser.2010.11.037.

[87] M. Isaac, D.P. van Vuuren, Modeling global residential sector energy demand for heating and air conditioning in the context of climate change, Energy Policy. 37 (2009) 507–521. doi:10.1016/j.enpol.2008.09.051.

[88] R. Haas, H. Auer, P. Biermayr, The impact of consumer behavior on residential energy demand for space heating, Energy Build. 27 (1998) 195–205. doi:10.1016/S0378-7788(97)00034-0.

[89] D.O. Hall, H.E. Mynick, R.H. Williams, Cooling the greenhouse with bioenergy, Nature. 353 (1991) 11–12. doi:10.1038/353011a0.

[90] M.A. Green, Third generation photovoltaics: Ultra-high conversion efficiency at low cost, Prog. Photovoltaics Res. Appl. 9 (2001) 123–135. doi:10.1002/pip.360.

[91] M.D. Archer, M.A. Green, Clean Electricity from Photovoltaics, Imperial College Press, 2014. doi:10.1142/p798.

[92] M. Green, Third Generation Photovoltaics, Springer, Berlin Heidelberg, 2006. doi:10.1007/b137807.

[93] C.J. Brabec, Organic photovoltaics: technology and market, Sol. Energy Mater. Sol. Cells. 83 (2004) 273–292. doi:10.1016/j.solmat.2004.02.030.

[94] A.J. McCormick, P. Bombelli, R.W. Bradley, R. Thorne, T. Wenzel, C.J. Howe, R. Steuer, N. Boon, W. Blankenfeldt, D.M. Weller, L.S. Thomashow, J.L. Gibson, T.E. Hanson, C. Bobst, J.L. Torres, C. Peres, F.H. Harrison, J. Gibson, C.S. Harwood, K. Watanabe, S. Ishii, B. Logan, K.H. Nealson, J.K. Fredrickson, Biophotovoltaics: oxygenic photosynthetic organisms in the world of bioelectrochemical systems, Energy Environ. Sci. 8 (2015) 1092–1109. doi:10.1039/C4EE03875D.

[95] P.I. Gordiichuk, G.-J.A.H. Wetzelaer, D. Rimmerman, A. Gruszka, J.W. de Vries, M. Saller, D.A. Gautier, S. Catarci, D. Pesce, S. Richter, P.W.M. Blom, A. Herrmann, Solid-State Biophotovoltaic Cells Containing Photosystem I, Adv. Mater. 26 (2014) 4863–4869. doi:10.1002/adma.201401135.

[96] A. Driver, P. Bombelli, Biophotovoltaics, Catalyst. (2011).

[97] R. Mohammadpour, S. Janfaza, Efficient Nanostructured Biophotovoltaic Cell Based on Bacteriorhodopsin as Biophotosensitizer, ACS Sustain. Chem. Eng. 3 (2015) 809–813. doi:10.1021/sc500617w.

[98] M. Rasmussen, S.D. Minteer, Photobioelectrochemistry: Solar Energy Conversion and Biofuel Production with Photosynthetic Catalysts, J. Electrochem. Soc. 161 (2014) H647–H655. doi:10.1149/2.0651410jes.

[99] S. Tsujimura, A. Wadano, K. Kano, T. Ikeda, Photosynthetic bioelectrochemical cell utilizing cyanobacteria and water-generating oxidase, Enzyme Microb. Technol. 29 (2001) 225–231. doi:10.1016/S0141-0229(01)00374-X.

[100] J.O. Calkins, Y. Umasankar, H.O.' Neill, R.P. Ramasamy, High photo-electrochemical activity of thylakoid–carbon nanotube composites for photosynthetic energy conversion, Energy Environ. Sci. 6 (2013) 1891–1900. doi:10.1039/c3ee40634b.

[101] L. Xiao, E.B. Young, J.A. Berges, Z. He, Integrated Photo-Bioelectrochemical System for Contaminants Removal and Bioenergy Production, Environ. Sci. Technol. 46 (2012) 11459–11466. doi:10.1021/es303144n.

[102] G. Pankratova, D. Pankratov, K. Hasan, H.-E. Åkerlund, P.-Å. Albertsson, D. Leech, S. Shleev, L. Gorton, Supercapacitive Photo-Bioanodes and Biosolar Cells: A Novel Approach for Solar Energy Harnessing, Adv. Energy Mater. (2017) 1602285. doi:10.1002/aenm.201602285.

[103] O. Yehezkeli, R. Tel-Vered, J. Wasserman, A. Trifonov, D. Michaeli, R. Nechushtai, I. Willner, Integrated photosystem II-based photo-bioelectrochemical cells, (2012). doi:10.1038/ncomms1741.

[104] A. Efrati, C.-H. Lu, D. Michaeli, R. Nechushtai, S. Alsaoub, W. Schuhmann, I. Willner, Assembly of photo-bioelectrochemical cells using photosystem I-functionalized electrodes, Nat. Energy. 1 (2016) 15021. doi:10.1038/nenergy.2015.21.

[105] O. Yehezkeli, R. Tel-Vered, D. Michaeli, I. Willner, R. Nechushtai, Photosynthetic reaction center-functionalized electrodes for photo-bioelectrochemical cells, Photosynth. Res. 120 (2014) 71–85. doi:10.1007/s11120-013-9796-3.

[106] U.C. Vothknecht, P. Westhoff, Biogenesis and origin of thylakoid membranes, Biochim. Biophys. Acta - Mol. Cell Res. 1541 (2001) 91–101. doi:10.1016/S0167-4889(01)00153-7.

[107] M.-Y. Chen, G.-Y. Zhuo, K.-C. Chen, P.-C. Wu, T.-Y. Hsieh, T.-M. Liu, S.-W. Chu, J. Squier, Y. Huang, H. Lai, S. Chu, Multiphoton imaging to identify grana, stroma thylakoid, and starch inside an intact leaf, BMC Plant Biol. 175 (2014) 113704. doi:10.1063/1.3254021.

[108] B. Cummings, Chloroplast in a Plant Cell, Pearson Educ. Inc. (n.d.). http://biology-pictures.blogspot.dk/2011/10/chloroplast-in-plant-cell.html (accessed July 25, 2017).

[109] P.-A. Albertsson, The structure and function of the chloroplast photosynthetic membrane -a model for the domain organization, Photosynth. Res. 46 (1995) 141–149.

[110] E. Andreasson, P. Svensson, C. Weibull, P.-Å. Albertsson, Separation and characterization of stroma and grana membranes — evidence for heterogeneity in antenna size of both Photosystem I and Photosystem II, Biochim. Biophys. Acta - Bioenerg. 936 (1988) 339–350. doi:10.1016/0005-2728(88)90010-2.

[111] H. Hamidi, K. Hasan, S.C. Emek, Y. Dilgin, H.-E. Åkerlund, P.-Å. Albertsson, D. Leech, L. Gorton, Photocurrent Generation from Thylakoid Membranes on Osmium-Redox-Polymer-Modified Electrodes, ChemSusChem. 8 (2015) 990–993. doi:10.1002/cssc.201403200.

[112] R.I. Pinhassi, D. Kallmann, G. Saper, H. Dotan, A. Linkov, A. Kay, V. Liveanu, G. Schuster, N. Adir, A. Rothschild, Hybrid bio-photo-electro-chemical cells for solar water splitting, (2016). doi:10.1038/ncomms12552.

[113] L.-N. Liu, Distribution and dynamics of electron transport complexes in cyanobacterial thylakoid membranes, Biochim. Biophys. Acta - Bioenerg. 1857 (2016) 256–265. doi:10.1016/j.bbabio.2015.11.010.

[114] K. Hasan, Y. Dilgin, S.C. Emek, M. Tavahodi, H.-E. Åkerlund, P.-Å. Albertsson, L. Gorton, Photoelectrochemical Communication between Thylakoid Membranes and Gold Electrodes through Different Quinone Derivatives, ChemElectroChem. 1 (2014) 131–139. doi:10.1002/celc.201300148.

[115] Melis, Photosystem-II damage and repair cycle in chloroplasts: what modulates the rate of photodamage ?, Trends Plant Sci. 4 (1999) 130–135.

[116] I. Vass, Molecular mechanisms of photodamage in the Photosystem II complex, Biochim. Biophys. Acta - Bioenerg. 1817 (2012) 209–217. doi:10.1016/j.bbabio.2011.04.014.

[117] E.H. Falcao, F. Wudl, Carbon allotropes: beyond graphite and diamond, J. Chem. Technol. Biotechnol. 82 (2007) 524–531. doi:10.1002/jctb.1693.

[118] W. Chard, M. Conaway, D. Niesz, Petroleum Derived Carbons, American Chemical Society, Waschington, D. C., 1976. doi:10.1021/bk-1976-0021.

[119] R.L. McCreery, Advanced Carbon Electrode Materials for Molecular Electrochemistry, Chem. Rev. 108 (2008) 2646–2687. doi:10.1021/cr068076m.

[120] R.B. Heimann, S.E. Evsvukov, Y. Koga, Carbon allotropes: a suggested classification scheme based on valence orbital hybridization, Carbon N. Y. 35 (1997) 1654–1658. doi:10.1016/S0008-6223(97)82794-7.

[121] Yongjun Li, Liang Xu, Huibiao Liu, Yuliang Li, Graphdiyne and graphyne: from theoretical predictions to practical construction, Chem. Soc. Rev. 43 (2014) 2572–2586. doi:10.1039/C3CS60388A.

[122] C. Biswas, Y.H. Lee, Graphene Versus Carbon Nanotubes in Electronic Devices, Adv. Funct. Mater. 21 (2011) 3806–3826. doi:10.1002/adfm.201101241.

[123] P. Ehrenfreund, B.H. Foing, Fullerenes and Cosmic Carbon, Science (80-.). 329 (2010) 1159–1160. doi:10.1126/science.1194855.

[124] T.D. Burchell, Carbon materials for advanced technologies, Pergamon, 1999.

[125] A. Aqel, K.M.M.A. El-Nour, R.A.A. Ammar, A. Al-Warthan, Carbon nanotubes, science and technology part (I) structure, synthesis and characterisation, Arab. J. Chem. 5 (2012) 1–23. doi:10.1016/j.arabjc.2010.08.022.

[126] T.L. (Theodore L. Brown, H.E. (Harold E. LeMay, B.E. Bursten, C.J. (Catherine J. Murphy, P.M. Woodward, M. Stoltzfus, Chemistry : the central science, n.d.

[127] W.A. Harrison, Electronic Structure and the Properties of Solids : the Physics of the Chemical Bond., Dover Publications, 2012.

[128] Y. Wang, Y. Li, L. Tang, J. Lu, J. Li, Application of graphene-modified electrode for selective detection of dopamine, 2009. doi:10.1016/j.elecom.2009.02.013.

[129] Y. Shao, J. Wang, H. Wu, J. Liu, I.A. Aksay, Y. Lin, Graphene Based Electrochemical Sensors and Biosensors: A Review, Electroanalysis. 22 (2010) 1027–1036. doi:10.1002/elan.200900571.

[130] C.H. An Wong, A. Ambrosi, M. Pumera, Thermally reduced graphenes exhibiting a close relationship to amorphous carbon, Nanoscale. 4 (2012) 4972. doi:10.1039/c2nr30989k.

[131] Electrochemistry of carbon electrodes, Wiley-VCH, 2015.

[132] A.K. Geim, K.S. Novoselov, The rise of graphene, Nat. Mater. 6 (2007) 183–191. doi:10.1038/nmat1849.

[133] P. Gründler, O. Frank, L. Kavan, L. Dunsch, Carbon Nanotube Electrodes for Hot-Wire Electrochemistry, ChemPhysChem. 10 (2009) 559–563. doi:10.1002/cphc.200800659.

[134] M. Nič, J. Jirát, B. Košata, A. Jenkins, A. McNaught, eds., IUPAC Compendium of Chemical Terminology, IUPAC, Research Triagle Park, NC, 2009. doi:10.1351/goldbook.

[135] K.J. Rao, Structural chemistry of glasses, Elsevier, 2002.

[136] S. Yamada, H. Sato, Some Physical Properties of Glassy Carbon, Nature. 193 (1962) 261–262. doi:10.1038/193261b0.

[137] T. Noda, M. Inagaki, S. Yamada, Glass-like carbons, J. Non. Cryst. Solids. 1 (1969) 285–302. doi:10.1016/0022-3093(69)90026-X.

[138] W.E. Van der Linden, J.W. Dieker, Glassy carbon as electrode material in electro- analytical chemistry, Anal. Chim. Acta. 119 (1980) 1–24. doi:10.1016/S0003-2670(00)00025-8.

[139] P.J.F. Harris, Fullerene-related structure of commercial glassy carbons, Philos. Mag. 84 (2004) 3159–3167. doi:10.1080/14786430410001720363.

[140] K. Jurkiewicz, S. Duber, A. Burian, Paracrystalline Structure of Glass-Like Carbons, Int. J. Appl. Glas. Sci. 7 (2016) 355–363. doi:10.1111/ijag.12186.

[141] G.M. Jenkins, K. Kawamura, L.L. Ban, Formation and Structure of Polymeric Carbons, Proc. R. Soc. London A Math. Phys. Eng. Sci. 327 (1972).

[142] G.M. Jenkins, K. Kawamura, Polymeric carbons--carbon fibre, glass and char, Cambridge University Press, 1976.

[143] P.K. Chu, L. Li, Characterization of amorphous and nanocrystalline carbon films, Mater. Chem. Phys. 96 (2006) 253–277. doi:10.1016/J.matchemphys.2005.07.048.

[144] H.E. Zittel, F.J. Miller, A Glassy-Carbon Electrode for Voltammetry., Anal. Chem. 37 (1965) 200–203. doi:10.1021/ac60221a006.

[145] A. Dekanski, J. Stevanović, R. Stevanović, B.Ž. Nikolić, V.M. Jovanović, Glassy carbon electrodes, Carbon N. Y. 39 (2001) 1195–1205. doi:10.1016/S0008-6223(00)00228-1.

[146] W. Zhang, S. Zhu, R. Luque, S. Han, L. Hu, G. Xu, Recent development of carbon electrode materials and their bioanalytical and environmental applications, Chem. Soc. Rev. 45 (2016) 715–752. doi:10.1039/C5CS00297D.

[147] B. Uslu, S. Ozkan, Electroanalytical Application of Carbon Based Electrodes to the Pharmaceuticals, Anal. Lett. 40 (2007) 817–853. doi:10.1080/00032710701242121.

[148] C.S.S.R. Kumar, Nanomaterials for biosensors, Wiley-VCH, 2007.

[149] C.-M. Tîlmaciu, M.C. Morris, Carbon nanotube biosensors., Front. Chem. 3 (2015) 59. doi:10.3389/fchem.2015.00059.

[150] N. Yang, X. Chen, T. Ren, P. Zhang, D. Yang, Carbon nanotube based biosensors, Sensors Actuators B Chem. 207 (2015) 690–715. doi:10.1016/j.snb.2014.10.040.

[151] T. Wang, C.C. Cook, S. Serban, T. Ali, G. Drago, B. Derby, Fabrication of glucose biosensors by inkjet printing, (n.d.).

[152] L. Berisha, K. Kalcher, A. Hajrizi, T. Arbneshi, A New Biosensor for Glucose Based on Screen Printed Carbon Electrodes Modified with Tin (IV)-Oxide, Am. J. Anal. Chem. 4 (2013) 27–35. doi:10.4236/ajac.2013.46A004.

[153] H. Hui Xu, G. Guang Li, J. Jieying Wu, Y. You Wang, J. Jun Liu, A glucose oxidase sensor based on screen-printed carbon electrodes modified by polypyrrole, in: 2005 IEEE Eng. Med. Biol. 27th Annu. Conf., IEEE, 2005: pp. 1917–1920. doi:10.1109/IEMBS.2005.1616826.

[154] L.M. Moretto, K. Kalcher, Environmental analysis by electrochemical sensors and biosensors. Volume 2, Applications, n.d.

[155] G. March, T.D. Nguyen, B. Piro, Modified electrodes used for electrochemical detection of metal ions in environmental analysis., Biosensors. 5 (2015) 241–75. doi:10.3390/bios5020241.

[156] A. Thamilselvan, A.S. Nesaraj, M. Noel, Review on carbon-based electrode materials for application in capacitive deionization process, Int. J. Environ. Sci. Technol. 13 (2016) 2961–2976. doi:10.1007/s13762-016-1061-9.

[157] G.T. Teixidor, R.A. Gorkin, P.P. Tripathi, G.S. Bisht, M. Kulkarni, T.K. Maiti, T.K. Battacharyya, J.R. Subramaniam, A. Sharma, B.Y. Park, M. Madou, Carbon microelectromechanical systems as a substratum for cell growth, Biomed. Mater. 3 (2008) 34116. doi:10.1088/1748-6041/3/3/034116.

[158] R. Martinez-Duarte, P. Renaud, M.J. Madou, A novel approach to dielectrophoresis using carbon electrodes, Electrophoresis. 32 (2011) n/a-n/a. doi:10.1002/elps.201100059.

[159] P.S. Maropis, J.A. Molinari, B.N. Appel, A. Baumhammers, Comparative study of vitreous carbon, pyrolytic carbon, pyrolytic graphite/silicon-carbide, and titanium implants in rabbit mandibles., Oral Surg. Oral Med. Oral Pathol. 43 (1977) 506–12.

[160] L.F. Thompson, C.G. Willson, M.J. Bowden, Introduction to Microlithography, American Chemical Society, Washington, D. C., 1983. doi:10.1021/bk-1983-0219.

[161] H. Miyajima, M. Mehregany, High-aspect-ratio photolithography for MEMS applications, J. Microelectromechanical Syst. 4 (1995) 220–229. doi:10.1109/84.475549.

[162] I. Willner, E. Katz, Integration of Layered Redox Proteins and Conductive Supports for Bioelectronic Applications, Angew. Chemie Int. Ed. 39 (2000) 1180–1218. doi:10.1002/(SICI)1521-3773(20000403)39:7<1180::AID-ANIE1180>3.0.CO;2-E.

[163] K.Y. Lee, N. LaBianca, S.A. Rishton, Micromachining applications of a high resolution ultrathick photoresist, J. Vac. Sci. Technol. B Microelectron. Nanom. Struct. 13 (1995) 3012. doi:10.1116/1.588297.

[164] R.C. Jaeger, Introduction to microelectronic fabrication, Pearson Education South Asia, 2013.

[165] H. Sorribas, C. Padeste, L. Tiefenauer, Photolithographic generation of protein micropatterns for neuron culture applications, Biomaterials. 23 (2002) 893–900. doi:10.1016/S0142-9612(01)00199-5.

[166] S. Mitra, S. Chakraborty, Microfluidics and nanofluidics handbook, CRC Press, 2011.

[167] H. Ito, Advances in Chemical Amplification Resist Systems, Jpn. J. Appl. Phys. 31 (1992) 4273–4282. doi:10.1143/JJAP.31.4273.

[168] MEMS Materials and Processes Handbook, Springer US, 2011.

[169] B. Loechel, C.-H. Lin, G.-B. Lee, B.-W. Chang, C.-H. Ho, W. Hsu, C.-R. Yang, G.-W. Hsieh, Y.-S. Hsieh, V. Srinivasa Rao, V. Kripesh, S. Wook Yoon, C. Mo Hwang, W. Young Sim, S. Hwan Lee, T.M. Verhaar, J. Wei, P.M. Sarro, Y.-K. Yoon, M.G. Allen, H. Lorenz, M. Despont, N. Fahrni, N. LaBianca, P. Renaud, P. Vettiger, SU-8: a low-cost negative resist for MEMS, J. Micromech. Microeng. J. Micromech. Microeng. 7 (1997) 121–121.

[170] B. Loechel, V. Srinivasa Rao, V. Kripesh, S. Wook Yoon, P. Dixit, C. Wee Tan, L. Xu, C.-R. Yang, G.-W. Hsieh, Y.-S. Hsieh, V. Conédéra, B. Le Goff, N. Fabre, S. Roth, L. Dellmann, G. Racine, N.F. de Rooij, High aspect ratio UV photolithography for electroplated structures, J. Micromech. Microeng. J. Micromech. Microeng. 9 (1999) 105–105.

[171] R.E. Franklin, Crystallite Growth in Graphitizing and Non-Graphitizing Carbons, Proc. R. Soc. Lond. A. Math. Phys. Sci. 209 (1951). doi:10.2307/98890.

[172] E. Fitzer, W. Schäfer, The effect of crosslinking on the formation of glasslike carbons from thermosetting resins, Carbon N. Y. 8 (1970) 353–364. doi:10.1016/0008-6223(70)90075-8.

[173] S.Y. Cho, Y.S. Yun, S. Lee, D. Jang, K.-Y. Park, J.K. Kim, B.H. Kim, K. Kang, D.L. Kaplan, H.-J. Jin, Carbonization of a stable β-sheet-rich silk protein into a pseudographitic pyroprotein, Nat. Commun. 6 (2015) 7145. doi:10.1038/ncomms8145.

[174] Y.S. Yun, K.-Y. Park, B. Lee, S.Y. Cho, Y.-U. Park, S.J. Hong, B.H. Kim, H. Gwon, H. Kim, S. Lee, Y.W. Park, H.-J. Jin, K. Kang, Sodium-Ion Storage in Pyroprotein-Based Carbon Nanoplates, Adv. Mater. 27 (2015) 6914–6921. doi:10.1002/adma.201502303.

[175] J.W. Jeon, S.Y. Cho, Y.J. Jeong, D.S. Shin, N.R. Kim, Y.S. Yun, H.-T. Kim, S.B. Choi, W.G. Hong, H.J. Kim, H.-J. Jin, B.H. Kim, Pyroprotein-Based Electronic Textiles with High Stability, Adv. Mater. 29 (2017) 1605479. doi:10.1002/adma.201605479.

[176] H. Stenzenberger, Recent advances in thermosetting polyimides, Br. Polym. J. 20 (1988) 383–396. doi:10.1002/pi.4980200503.

[177] H.D. Stenzenberger, M. Herzog, W. Römer, R. Scheiblich, N.J. Reeves, Development of thermosetting polyimide resins, Br. Polym. J. 15 (1983) 2–12. doi:10.1002/pi.4980150103.

[178] A. Singh, J. Jayaram, M. Madou, S. Akbar, Pyrolysis of Negative Photoresists to Fabricate Carbon Structures for Microelectromechanical Systems and Electrochemical Applications, J. Electrochem. Soc. 149 (2002) E78. doi:10.1149/1.1436085.

[179] O.J.A. Schueller, S.T. Brittain, G.M. Whitesides, Fabrication of glassy carbon microstructures by pyrolysis of microfabricated polymeric precursors, Adv. Mater. 9 (1997) 477–480. doi:10.1002/adma.19970090604.

[180] A. Mardegan, R. Kamath, S. Sharma, P. Scopece, P. Ugo, M. Madou, Optimization of Carbon Electrodes Derived from Epoxy-based Photoresist, J. Electrochem. Soc. 160 (2013) 132–137. doi:10.1149/2.107308jes.

[181] S. Ranganathan, R. McCreery, S.M. Majji, M. Madou, Photoresist-Derived Carbon for Microelectromechanical Systems and Electrochemical Applications, J. Electrochem. Soc. 147 (2000) 277. doi:10.1149/1.1393188.

[182] C. Wang, G. Jia, L.H. Taherabadi, M.J. Madou, A Novel Method for the Fabrication of High-Aspect Ratio C-MEMS Structures, J. MICROELECTROMECHANICAL Syst. 14 (2005). doi:10.1109/JMEMS.2004.839312.

[183] E. Udd, W.B. Spillman, Fiber Optic Sensors: An Introduction for Engineers and Scientists, Second edition, John Wiley & Sons, Inc., Hoboken, NJ, USA, 2011. doi:10.1002/9781118014103.

[184] K. Thyagarajan, Optical Fiber, in: Fiber Opt. Essentials, John Wiley & Sons, Inc., Hoboken, NJ, USA, 2007: pp. 28–54. doi:10.1002/9780470152560.ch4.

[185] R.W. Waynant, Optical Fiber, in: Electron. Photonic Circuits Devices, IEEE, 2009. doi:10.1109/9780470544532.ch5.

[186] C.Z. Hu, J.D. Andrade, Pyrolyzed, conducting kapton polyimide: An electrically conducting material, J. Appl. Polym. Sci. 30 (1985) 4409–4415. doi:10.1002/app.1985.070301116.

[187] B. Kundu, R. Rajkhowa, S.C. Kundu, X. Wang, Silk fibroin biomaterials for tissue regenerations, Adv. Drug Deliv. Rev. 65 (2013) 457–470. doi:10.1016/j.addr.2012.09.043.

[188] A. Zulfiqar, A. Pfreundt, W.E. Svendsen, M. Dimaki, Fabrication of polyimide based microfluidic channels for biosensor devices, J. Micromechanics Microengineering. 25 (2015) 35022. doi:10.1088/0960-1317/25/3/035022.

[189] N.P. Bansal, R.H. Doremus, Handbook of glass properties, Academic Press, 1986.

[190] S. Bradbury, Microscopy Handbooks; Introduction to light microscopy, BIOS Scientific Publishers Ltd., 1998.

[191] C. Singer, Notes on the Early History of Microscopy, Proc. R. Soc. Med. 7 (1914).

[192] D.B. Murphy, M.W. (Michael W. Davidson, Fundamentals of light microscopy and electronic imaging, Wiley-Blackwell, 2013.

[193] H. Chiarini-Garcia, R.C. Melo, Light microscopy : methods and protocols, Springer, 2011.

[194] T.A. Klar, Fluorescence microscopy with diffraction resolution barrier broken by stimulated emission, Proc. Natl. Acad. Sci. U. S. A. 97 (2000).

[195] S.J. Sahl, W. Moerner, Super-resolution fluorescence imaging with single molecules, Curr. Opin. Struct. Biol. 23 (2013) 778–787. doi:10.1016/j.sbi.2013.07.010.

[196] E. Betzig, G.H. Patterson, R. Sougrat, O.W. Lindwasser, S. Olenych, J.S. Bonifacino, M.W. Davidson, J. Lippincott-Schwartz, H.F. Hess, Imaging Intracellular Fluorescent Proteins at Nanometer Resolution, Science (80-.). 313 (2006) 1642–1645. doi:10.1126/science.1127344.

[197] H. Ernst Keller, S. Watkins, Contrast Enhancement in Light Microscopy, in: Curr. Protoc. Cytom., John Wiley & Sons, Inc., Hoboken, NJ, USA, 2013. doi:10.1002/0471142956.cy0201s63.

[198] R.H. Webb, Confocal optical microscopy, Reports Prog. Phys. 59 (1996) 427–471. doi:10.1088/0034-4885/59/3/003.

[199] J.W. Lichtman, J.-A. Conchello, Fluorescence microscopy, Nat. Methods. 2 (2005) 910–919. doi:10.1038/nmeth817.

[200] B. Valeur, M.N. Berberan-Santos, Molecular Fluorescence, Wiley-VCH Verlag GmbH & Co. KGaA, Weinheim, Germany, 2012. doi:10.1002/9783527650002.

[201] G.G. Stokes, On the Change of Refrangibility of Light, Philos. Trans. R. Soc. London. 142 (1852). doi:10.2307/108550.

[202] G.G. Stokes, On the Change of Refrangibility of Light. No. II, Philos. Trans. R. Soc. London. 143 (1853) 385–396. doi:10.1098/rstl.1853.0016.

[203] A. Baeyer, Ueber eine neue Klasse von Farbstoffen, Berichte Der Dtsch. Chem. Gesellschaft. 4 (1871) 555–558. doi:10.1002/cber.18710040209.

[204] M. Minski, Microscopy apparatus, 1957.

[205] D. M. Shotton, Confocal scanning optical microscopy and its applications for biological specimens, J. Cell Sci. 94 (1989).

[206] A. Nwaneshiudu, C. Kuschal, F.H. Sakamoto, R. Rox Anderson, K. Schwarzenberger, R.C. Young, Introduction to Confocal Microscopy, J. Invest. Dermatol. 132 (2012) 1–5. doi:10.1038/jid.2012.429.

[207] A.R. Clarke, C.N. Eberhardt, A.R. Clarke, C.N. Eberhardt, 4 – 3D confocal laser scanning microscopy, in: Microsc. Tech. Mater. Sci., 2002: pp. 228–302. doi:10.1533/9781855737501.2.228.

[208] R.F. Egerton, Physical Principles of Electron Microscopy, Springer US, Boston, MA, 2005. doi:10.1007/b136495.

[209] P.J. Goodhew, F.J. Humphreys, Electron microscopy and analysis, Taylor & Francis, 1988.

[210] W. Zhou, R. Apkarian, Z.L. Wang, D. Joy, Fundamentals of Scanning Electron Microscopy (SEM), in: Scanning Microsc. Nanotechnol., Springer New York, New York, NY, 2006: pp. 1–40. doi:10.1007/978-0-387-39620-0_1.

[211] W.C. Nixon, The General Principles of Scanning Electron Microscopy, Philos. Trans. R. Soc. B Biol. Sci. 261 (1971) 45–50. doi:10.1098/rstb.1971.0035.

[212] W. Häßler-Grohne, D. Hüser, K.-P. Johnsen, C.G. Frase, H. Bosse, Current limitations of SEM and AFM metrology for the characterization of 3D nanostructures, Meas. Sci. Technol. 22 (2011) 94003. doi:10.1088/0957-0233/22/9/094003.

[213] G. Wanner, E. Schroeder-Reiter, H. Formanek, 3D Analysis of chromosome architecture: advantages and limitations with SEM, Cytogenet. Genomics Phys. Mapp. Cytogenet Genome Res. 109 (2005) 70–78. doi:10.1159/000082384.

[214] H. Hertz, Ueber einen Einfluss des ultravioletten Lichtes auf die electrische Entladung, Ann. Der Phys. Und Chemie. 267 (1887) 983–1000. doi:10.1002/andp.18872670827.

[215] A. Einstein, Über einen die Erzeugung und Verwandlung des Lichtes betreffenden heuristischen Gesichtspunkt,

Ann. Phys. 322 (1905) 132–148. doi:10.1002/andp.19053220607.

[216] P.D. Innes, On the Velocity of the Cathode Particles Emitted by Various Metals under the Influence of Röntgen Rays, and Its Bearing on the Theory of Atomic Disintegration, Proc. R. Soc. London. Ser. A, Contain. Pap. a Math. Phys. Character. 79 (1907). doi:10.2307/92660.

[217] H. Robinson, The secondary corpuscular rays produced by homogeneous X-rays, Proc. R. Soc. London Ser. A-Containing Pap. a Math. Phys. Character. 104 (1923).

[218] R.G. Steinhardt, E.J. Serfass, Surface Analysis with X-Ray Photoelectron Spectrometer, Anal. Chem. 25 (1953) 697–700. doi:10.1021/ac60077a005.

[219] K. SIEGBAHN, ELECTRON SPECTROSCOPY FOR CHEMICAL ANALYSIS (ESCA), Philos. Trans. R. Soc. London Ser. A-Mathematical Phys. Sci. 268 (1970).

[220] An introduction to surface analysis by XPS and AES, 2003.

[221] J.F. Watts, Surface analysis of polymers by XPS and static SIMS, Surf. Eng. 14 (1998) 290–290. doi:10.1179/sur.1998.14.4.290.

[222] A.D. McNaught, Compendium of Chemical Terminology, Blackwell Science, Oxford, 1997.

[223] L.M. Torres, A. Gil, L. Galicia, I. Gonzalez, Understanding the Difference between Inner- and Outer-Sphere Mechanisms: An Electrochemical Experiment, J. Chem. Educ. 73 (1996) 808–810. doi:10.1021/ed073p808.

[224] C.H. Bamford, C.F.H. (Charles F.H. Tipper, R.G. Compton, Comprehensive chemical kinetics., Elsevier Pub. Co, 1969.

[225] A. Kumar, Introduction to solid state physics., Phi Learning, 2015.

[226] Cottrell, Residual current in galvanic polarization regarded as a diffusion problem, Z Phys Chem. 42 (1903).

[227] R.L. McCreery, K.K. Cline, C.A. McDermott, M.T. McDermott, Control of reactivity at carbon electrode surfaces, Colloids Surfaces A Physicochem. Eng. Asp. 93 (1994) 211–219. doi:10.1016/0927-7757(94)02899-0.

[228] N.F. Atta, A. Galal, S.M. Ali, S.H. Hassan, Electrochemistry and detection of dopamine at a poly(3,4-ethylenedioxythiophene) electrode modified with ferrocene and cobaltocene, Ionics (Kiel). 21 (2015) 2371–2382. doi:10.1007/s11581-015-1417-z.

[229] P. Chen, M.A. Fryling, R.L. McCreery, Electron Transfer Kinetics at Modified Carbon Electrode Surfaces: The Role of Specific Surface Sites, Anal. Chem. 67 (1995) 3115–3122. doi:10.1021/ac00114a004.

[230] M.A. Guillorn, T.E. McKnight, A. Melechko, V.I. Merkulov, P.F. Britt, D.W. Austin, D.H. Lowndes, M.L. Simpson, Individually addressable vertically aligned carbon nanofiber-based electrochemical probes, J. Appl. Phys. 91 (2002) 3824–3828. doi:10.1063/1.1448671.

[231] B.J. Venton, R.M. Wightman, Psychoanalytical Electrochemistry: Dopamine and Behavior, Anal. Chem. 75 (2003) 414 A-421 A. doi:10.1021/ac031421c.

[232] T. Buss, C.L.C. Smith, M. Brokner Christiansen, R. Marie, A. Kristensen, Sub-wavelength surface gratings for light redirection in transparent substrates, Appl. Phys. Lett. 101 (2012). doi:10.1063/1.4738777.

[233] K.O. Hill, G. Meltz, Fiber Bragg grating technology fundamentals and overview, J. Light. Technol. 15 (1997) 1263–1276. doi:10.1109/50.618320.

[234] N.J. Ke, S.-S. Lu, S.-H. Cheng, A strategy for the determination of dopamine at a bare glassy carbon electrode: p-Phenylenediamine as a nucleophile, Electrochem. Commun. 8 (2006) 1514–1520. doi:10.1016/J.ELECOM.2006.07.007.

[235] K. Deisseroth, Optogenetics, Nat. Methods. 8 (2011). doi:10.1038/NMETH.F.324.

[236] A. Yakushenko, Z. Gong, V. Maybeck, B. Hofmann, E. Gu, M. Dawson, A. Offenhäusser, B. Wolfrum, On-chip optical stimulation and electrical recording from cells., J. Biomed. Opt. 18 (2013) 111402. doi:10.1117/1.JBO.18.11.111402.

[237] M. Ibrahim, L. Alexander, C. Shy, S. Farr, R. Horner, E. Director, Calculating person-time, ERIC Noteb. (2000).

[238] H.C. Ishikawa-Ankerhold, R. Ankerhold, G.P.C. Drummen, Advanced Fluorescence Microscopy Techniques—FRAP, FLIP, FLAP, FRET and FLIM, Molecules. 17 (2012) 4047–4132. doi:10.3390/molecules17044047.

[239] L. De Sio, Active plasmonic nanomaterials, in: Act. Plasmonic Nanomater., Pan Stanford Publishing Pte. Ltd., 2015.

[240] A.J. Bard, L.R. Faulkner, Electrochemical methods : fundamentals and applications, 2nd ed., Wiley, 2001.

[241] A. Alvarado-Gámez, M. Alonso-Lomillo, O. Domínguez-Renedo, M. Arcos-Martínez, A Disposable Alkaline Phosphatase-Based Biosensor for Vanadium Chronoamperometric Determination, Sensors. 14 (2014) 3756–3767. doi:10.3390/s140203756.

Summary of the publications

Paper I is a manuscript in preparation for Electrochemistry Communications. It describes the fabrication, characterisation and applications of optical fibre electrodes (OFEs). OFEs were fabricated by pyrolysing polyimide-coated optical fibres. The electrochemical properties of OFEs were characterised using cyclic voltammetry and chronoamperometry. The OFEs were then employed as substrate for the culture and differentiation of human neural stem cells into dopaminergic neurons. SEM was used to image the cells on the OFEs after differentiation. Chronoamperometry using the OFEs as working electrodes was employed in order to monitor cells residing on the surface of the OFEs during the process of differentiation. The results show that the OFEs can be used as integrated device for cell culture and sensing.

Paper II is a manuscript for Advanced Energy Materials. It describes the fabrication, characterisation and applications of transparent electrode chips (TECs). TECs were fabricated by pyrolysing SU-8 patterned on fused silica substrates using photolithography. The electrochemical properties of TECs were characterised using cyclic voltammetry. The photocurrent generation from thylakoid membranes illuminated through the TECs was recorded using chronoamperometry. Different mediators and irradiance values were tested. The influence of the TEC pattern on the current generation was investigated. Experimental data was correlated with a theoretical model. Electrons generated in the photosynthetic process need to reach the electrode surface to generate current. The TEC pattern alters the distance that a mediator carrying the electrons needs to travel before reaching the electrode surface. As a result, the amount of energy harvested from thylakoid membranes depends on the pattern of the TEC.

The patent is a PCT application. It describes the concept and fabrication method for an optoelectric scaffold holding photo-responsive biological components. The application refers to i) an implantable device for the monitoring, delivery and release of neurotransmitters in a patient suffering from a neurodegenerative disorder (such as Parkinson’s disease or epilepsy); and ii) an anode containing biological components able to convert solar light into electrical energy.

Acknowledgements

There are so many people I would like to thank for the past three years: co-workers, friends, family… Everyone around me contributed, in a certain amount, to my life during my PhD, and, in a way, also to who I am now…

I will start with my supervisors, since "they are the ones who made this possible" (very cliché, sorry, very appropriate though) ☺ You are all so different, but somehow it worked out very well, and I always had someone to go to for advice or brainstorming sessions.

Thank you, Jenny, for your constant optimism and creativity! You are always up for exploring new research topics and, as exhausting as it may be to follow, this is how good ideas develop ☺ Also, thank you for being so open, honest and friendly – you have been more than just a supervisor to me during these past three years.

Niels, thank you for your ability to give useful advice on so many different things! I have always been amazed at how much you know about science and at how involved you still are in experiments…

Stephan, thank you for proving that you can have both a good career and a nice family at such a young age. Your knowledge of fabrication has been so useful to me, and your companionship at conferences was always fun ☺

I would like to thank professor Lo Gorton for welcoming me to Lund University for my external stay. Lo, it was a pleasure to discuss science with you – you made me believe that my results are amazing!

Arto, you were a constant presence during my PhD, and having you around has made my research life more enjoyable, especially on the late evenings spent at DTU. Having someone to talk to (about research, science, driving and whatever else) made "coffee" breaks both useful and entertaining, and you were always ready to help me when needed.

I would like to thank past and present members of the Bioanalytics group (especially Claudia, Janko and Karin). Our lunches together were very-much-needed work breaks sometime and our breakfast meetings were both enjoyable and productive ☺ Oh, and let's not forget the awesome teambuilding!

Thanks to all the lab technicians from 423 and Danchip, and the administration people from Nanotech – you have made a lot of things easier for me, and for all those working with you. A special thanks to Lotte here, for always being extra-helpful, and to Jesper, for his help with taking pretty pictures ☺

Abhay, Miranda, Suhith – thanks for a great year of bartending ☺ Even though things didn't usually work out as planned, we always made it work somehow, and we had some awesome parties

together! Also, thanks to everyone else who stopped by the Friday bar (while I was “on duty” or not), I met so many interesting people because of this ☺

Rujing, you have been the best friend that I could possibly hope for. You are always there for me; it doesn’t matter if I need help with work, travel/dinner/shopping company, or maybe just someone to complain to… You have helped me so much, and you are so caring and understanding.

Vida, thanks for all the time we spent together, and for your ability to cheer me up ☺ I don’t think anyone ever made me laugh as much as you did! You were the only girly presence in my life during this time, and it is much appreciated ☺ I miss you!

Ramona, we only spent time together towards the end of my PhD, but that time is much appreciated. You started as a helpful scientist and ended up being a good friend. Mulţumesc! ☺

Thanks to the Thursday teokem gaming sessions and to all the people joining there – this allowed me to enjoy one of my hobbies – boardgames – in Scandinavia ☺

Tati – iti multumesc ca ai sprijinit decizia mea de a imi face doctoratul in strainatate, desi nu a fost niciodata in planurile noastre. Am putut invata mult mai multe asa, si am putut sa imi dezvolt reteaua profesionala in cu totul alt mod.

Multumesc familiilor (Bunea si Cristea, in varianta extinsa) – m-ati facut sa simt ca va e dor de mine de cand m-am mutat “peste hotare”. Desi mami, Stelu si Doru nu mai sunt aici, as vrea sa stie si ei (oriunde ar fi acum) ca au ramas in gandurile mele si au contribuit la cine sunt eu acum…

Last, but definitely not least… Octav, I need to thank you for being able to put up with me during the past 11+ years. You have been the most supporting and understanding person in the world, especially during my PhD. I am sure that the main reason for not freaking out completely towards the end of my PhD was having you around… Thank you so much for everything and good luck putting up with me in the following years! Oh… I meant to say “Good luck with your PhD!” ☺

Appendix I: Paper I

Single step fabrication of optical fiber-based carbon electrodes for dopamine detection from cells

Ada-Ioana Bunea, Ramona Valentina Mateiu, Alberto Martinez Serrano, Arto Heiskanen, Stephan Sylvest Keller, Niels Bent Larsen and Jenny Emnéus

Graphical abstract:

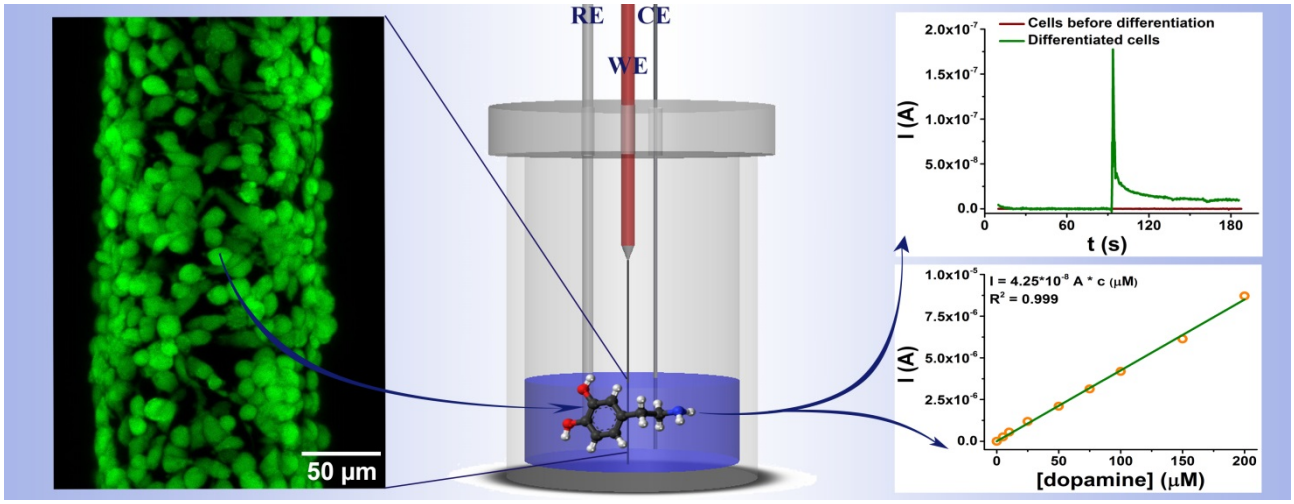

Single step fabrication of optical fiber-based carbon electrodes for dopamine detection from cells

Ada-Ioana Bunea[1], Ramona Valentina Mateiu[2], Alberto Martinez Serrano[3], Arto Heiskanen[1], Stephan Sylvest Keller[1], Niels Bent Larsen[1] and Jenny Emnéus[1]

1 – Department of Micro- and Nanotechnology, Technical University of Denmark, Ørsted Plads, Kongens Lyngby, Denmark
2 – DTU KT CoaST, Technical University of Denmark, Søltofts Plads 229, Kongens Lyngby, Denmark
3 – Centro de Biologia Molecular Severo Ochoa, Universidad Autonoma de Madrid, Consejo Superior de Investigaciones Científicas, Campus Cantoblanco, Madrid, Spain

Abstract

Optical fibers usually have a buffer coating made of polymeric material. Pyrolysis can be used to turn the buffer into conductive carbon with good electrode properties. In this work, commercially-available optical fibers with polyimide coating were pyrolysed in order to fabricate working electrodes suitable for electrochemical detection of dopamine. Furthermore, the carbon electrodes were successfully employed as cell culture substrate during stem cell differentiation into dopaminergic neurons, and subsequently used *in situ* to monitor dopamine exocytosis from the differentiated cells.

1. Introduction

Parkinson's disease is characterized by neural degeneration in the midbrain, in *Substantia nigra* [1]. This leads to insufficient dopamine production and a disruption in the nigrostriatal pathway [2]. Current pharmacological treatment options aim at increasing the neurotransmitter concentration in target areas in the brain. Since dopamine cannot pass the blood-brain barrier, alternative chemicals are used as medication [3–6] and deep brain stimulation is employed in severe cases [7].

Cell replacement therapy is a developing area of biomedicine which might change the future of treatments for neurodegenerative disorders, such as Parkinson's disease, amyotrophic lateral sclerosis or Huntington's disease [8–12]. By replacing damaged neurons with healthy cells, the neurotransmitter could be replenished in target areas of the brain, and exocytosis could be triggered using optogenetic tools. Improvements in damaged nigrostriatal dopamine pathways by using a transplant of embryonic *substantia nigra* in rats were reported as early as 1979 [13]. Since then, research in this field has been done in both rodent and primate models. Cell therapies have reached the point of clinical trials, including the use of human neural stem cells for Parkinson's disease treatment [10,11,14]. For preclinical testing, using adherent stem cells ensures better access to growth factors and better monitoring compared to cells in suspension or neurospheres [14,15].

Carbon is a biocompatible electrode material which enhances stem cell differentiation into dopaminergic neurons and facilitates dopamine detection [16]. Other advantages of carbon as electrode material are its abundance, low cost and high versatility for fabrication, relatively inert chemistry, wide potential window, and good electrocatalytic activity [17].

Optical fibers usually consist in a core, made of fused silica, a cladding made of doped fused silica, and a polymeric buffer material which ensures extra mechanical protection and does not allow contact of the silica with the atmosphere [18,19]. Most commercial OFs are coated with polyimide, which can be pyrolysed in order to obtain conductive carbon material with good mechanical strength, especially when supported on quartz [20].

In this work we show that pyrolysis can be employed to fabricate optical fiber electrodes (OFEs) from commercial optical fibers in a single-step process. Due to their shape and size, OFEs are suitable for implantation as such, or after encapsulation [21], making them interesting candidates for the future of cell-replacement therapy. OFEs can function as cell culture substrate during stem cell differentiation into dopaminergic neurons. Furthermore, the ability to release dopamine of cells grown on OFEs can be monitored using electrochemical techniques directly on the OFE.

2. Materials and methods

2.1. Optical fiber treatment

Optical fibers with fused silica cladding and core, buffered with polyimide, were purchased from Edmund Optics (UK). The pyrolysis process was performed as previously described [22] using a PEO-601 furnace from ATV Technologie (Vaterstetten, Germany) under inert atmosphere (nitrogen flow, 20 L/min). The thickness of the carbon layer after pyrolysis was 7.49 ± 0.06 µm (SI). The fibers were cut into 2.5 cm pieces and employed as working electrodes and cell culture substrates. To ensure removal of potential organic contaminants and improve surface wettability, OFEs were subjected to oxygen plasma treatment (3 min, 50 W) using a 13.56 MHz RF generator-equipped Atto Plasma System (Diener Electronic, GmbH, Ebhausen, Germany).

2.2. Standard redox probe measurements using optical fiber electrodes

All reagents were purchased from Sigma Aldrich: potassium hexacyanoferrate (II) trihydrate (≥99.5%), potassium hexacyanoferrate (III) (≥99.0%), hexaammineruthenium (II) chloride (≥99.9%), hexaammineruthenium (III) chloride (≥98%) and Dulbecco's phosphate buffered saline (PBS).

Electrochemical measurements were performed using a CHI 1030 potentiostat (CH Instruments, Austin TX, USA) and a three electrode setup, with OFE as working electrode (WE), a 3 cm long Pt wire with 500 µm diameter (Advent Research Materials Ltd, Oxford, England) as counter electrode (CE) and a DRIREF-L Ag|$AgCl_{sat}$ (WPI, Sarasaota FL, USA) as reference electrode (RE).

The OFEs were characterized using cyclic voltammetry (CV) with two standard redox couples: potassium hexacyanoferrate (II/III) 10 mM in PBS (E scan from -0.5 to +1.0 V vs Ag|AgCl, scan rates between 25 and 150 mV/s) and hexaammineruthenium (II/III) chloride 1 mM in degassed PBS (E scan from -0.5 to +0.25 V vs Ag|$AgCl_{sat}$, scan rates between 25 and 2000 mV/s).

2.3. Electrochemical dopamine measurements using optical fiber electrodes

Dopamine hydrochloride was purchased from Sigma Aldrich. Solutions were prepared in degassed PBS and used within 1 h, to avoid uncontrolled dopamine oxidation due to O_2.

Cyclic voltammetry measurements (E scan from 0 to +0.6 V *vs* $Ag|AgCl_{sat}$) were performed using concentrations between 5 and 200 µM dopamine, and scan rates between 25 and 150 mV/s, in the same setup as the standard redox probes. Chronoampetrometry measurements were performed at a potential of +0.35V *vs* $Ag|AgCl_{sat}$, using dopamine concentrations between 2 and 75 µM.

2.4. Stem cell culture and differentiation on optical fiber electrodes

Cells from the immortalized human ventral mesencephalic cell line overexpressing Bcl-xL (hVM1-Bcl-xL) were cultured as previously described [23,24] (details in SI).

For differentiation of the stem cells on the OFEs, a holder was designed to fit 6 well-plates (details in SI). The OFEs, holders and adhesive tape were sterilized by using 20 min exposure to UV-C irradiation (254 nm, UC sterilization cabinet, Cleaver Scientific Ltd, UK) in a laminar flow bench. The fibers were glued onto the holders using adhesive tape, to avoid rotational movements that could prevent the cells from attaching, and placed into 6 well-plates. Prior to cell seeding, OFEs were coated with Geltrex (ThermoFisher) diluted 100 times in sterile PBS by 1 h incubation at 37°C. The cells were seeded at 250000 cells/cm^2 and cultured under differentiation conditions as previously described [23,24].

A stock solution of 1 mg/mL Calcein AM (Sigma Aldrich) (Sigma Aldrich) was prepared in DMSO and diluted to 2 µg/mL in PBS prior to use. Staining was done by 1 h incubation at 37°C. Imaging was done using a confocal laser scanning microscope (LSM 700, Zeiss) and the ZEN software. Excitation was done by laser at a wavelength of 488 nm and emission was monitored at 516 nm.

2.5. Exocytosis measurements from dopaminergic cells using optical fiber electrodes

Preparation of baseline and stimulation buffers is presented in SI. The procedure consisted in chronoamperometry measurements using the same parameters as for dopamine detection in PBS. Each OFE with differentiated cells was immersed in 9 mL baseline buffer and a current-time trace was recording until the signal became stable. Then, 1 mL stimulation buffer was added to the system (under stirring), so the K^+ concentration was elevated to 100 mM, triggering exocytosis. After 15 min, a second injection of stimulation buffer was performed. As references, OFEs without cells and OFEs with non-differentiated cells were subjected to the same measurements. Dopamine exocytosis is an end-point measurement in the current setup, because it requires the cells to be taken out of the sterile environment.

2.6 Scanning electron microscopy

Scanning electron microscopy (SEM) was used to investigate the optical fibers after pyrolysis with a Zeiss Supra 40 VP (Carl Zeiss AG, Germany) and to visualize the cell coverage of OFEs with a FEI Quanta 200F FEG ESEM (ThermoFisher). SEM was performed in high vacuum, by monitoring the secondary electrons produced by a beam of electrons at spot 3 accelerated to 3 keV for

investigating cells, and 5 keV for investigating the carbon layer. Sample pretreatment for OFEs with cells is described in SI.

3. Results and discussion

$[Fe(CN)]_6^{3-/4-}$ is probably the most widely used redox couple for electrode characterization. However, it is surface-sensitive, and thus is it not an ideal outer-sphere redox system[17,25,26]. A reliable outer-sphere redox system is $[Ru(NH_3)_6]^{2+/3+}$ [17,26], which has been widely used for the characterization of carbon electrodes[17,26–28]. Characterization using both aforementioned redox systems showed good electrochemical behavior of the OFEs, with peak separations as low as 71 mV for $[Ru(NH_3)_6]^{2+/3+}$. The shapes of the CVs indicate a reversible, diffusion-controlled reaction happening at the electrode surface [29], as it is to be expected (**figure 1a** and **1b**). A linear dependency between the peak separation and the square root of the scan rate is observed up to 900 mV/s (**figure 1c**). Plotting the peak current versus the square root of the scan rate shows that the process is diffusion-controlled up to 200 mV/s (**figure 1d**). CVs in buffer solution show no redox peaks (SI).

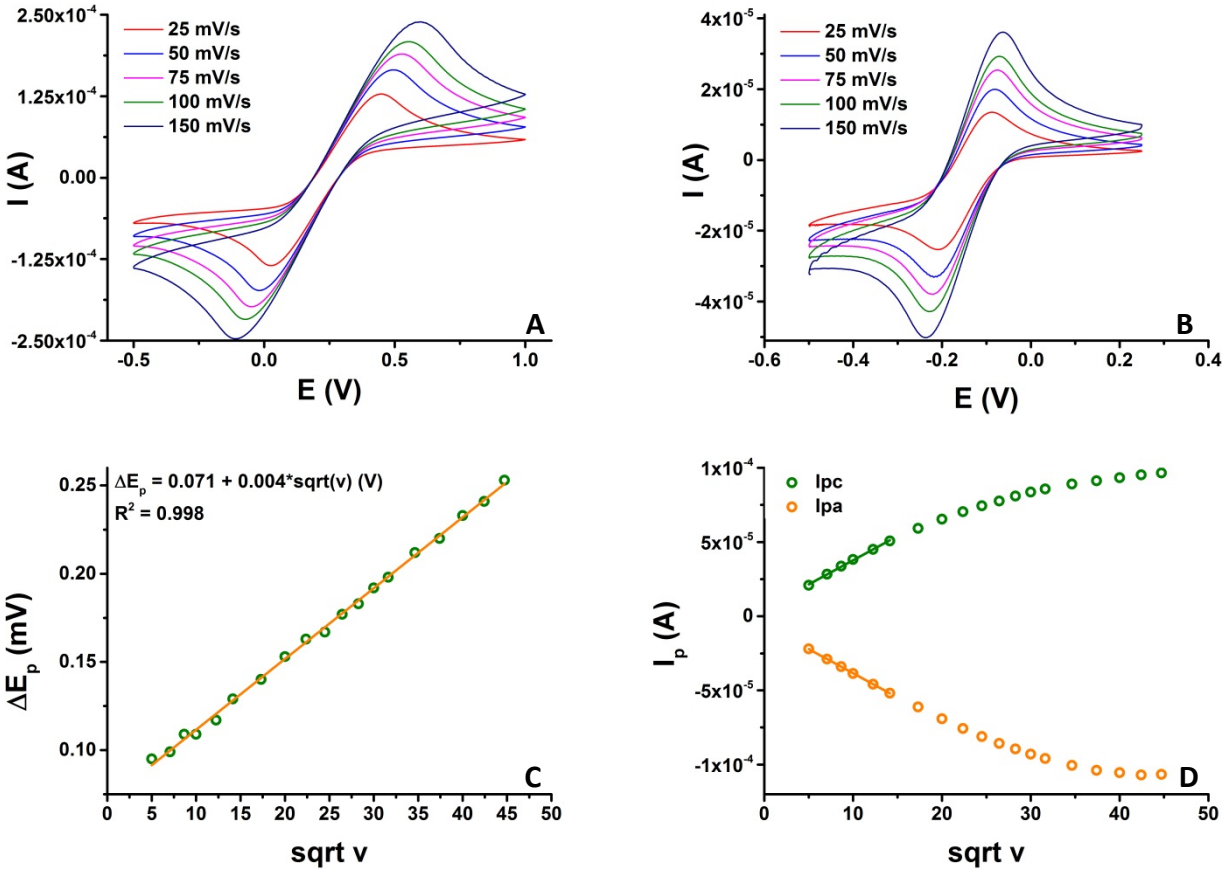

Fig. 1: Electrochemistry results using standard redox probes: CV in 10mM $[Fe(CN)]_6^{3-/4-}$ at different scan rates (A); CV in $[Ru(NH_3)_6]^{2+/3+}$ at different scan rates (B); Peak separation (C) and peak intensity (D) vs square root of scan rate for $[Ru(NH_3)_6]^{2+/3+}$. E vs Ag|AgCl.

Dopamine is an electroactive compound, which can be oxidized to dopamine-o-quinone in a 2-electron process [30]. The oxidation can be studied using several electrochemistry techniques, such as CV, amperometry or differential pulse voltammetry [30–33]. Using CV with OFEs, characteristic shapes are obtained (**figure 2a** and **2b**) and a linear dependency between anodic peak currents and dopamine concentrations is observed in the 0 – 200 µM range (**figure 2c**). Using chronoamperometry with OFEs, a linear dependency between average plateau currents and concentration is observed up to 75 µM dopamine (**figure 2d**). In chronoamperometry, the limit of detection is 0.17 µM, and the limit of quantification is 0.57 µM.

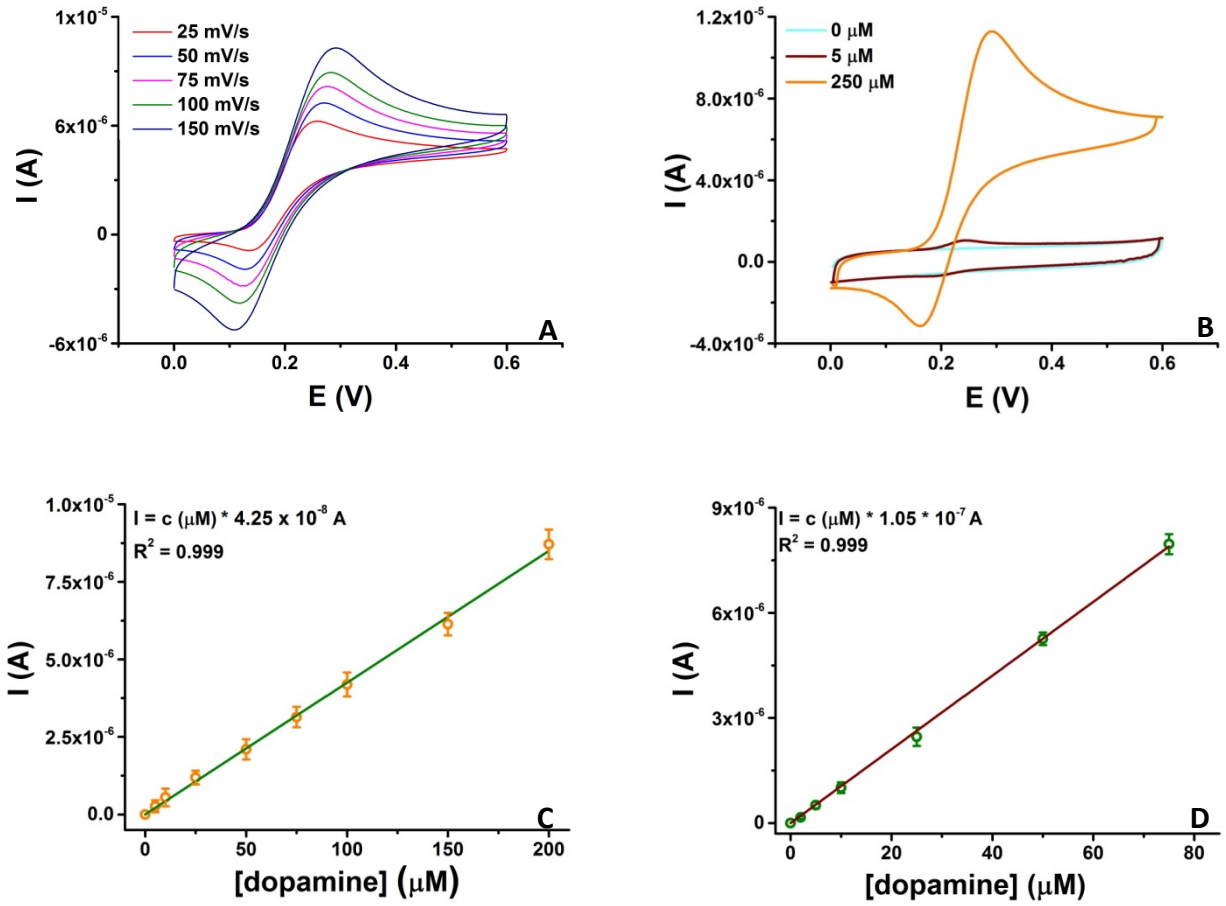

Fig. 2: Electrochemistry results using dopamine: CV in 250 µM dopamine at different scan rates (A); CV in buffer and different dopamine concentrations (B); Calibration curve using anodic peak intensity at 50 mV/s scan rate (C); Calibration curve using average plateau intensity from chronoamperometry (D). E vs Ag|AgCl.

Figure 3a shows a confocal microscopy image of stem cells stained with calcein attached to an OFE 24 h after seeding. **Figure 3b** shows an SEM image of cells differentiated on an OFE for 10 days. The two images confirm that stem cells attach to the OFEs.

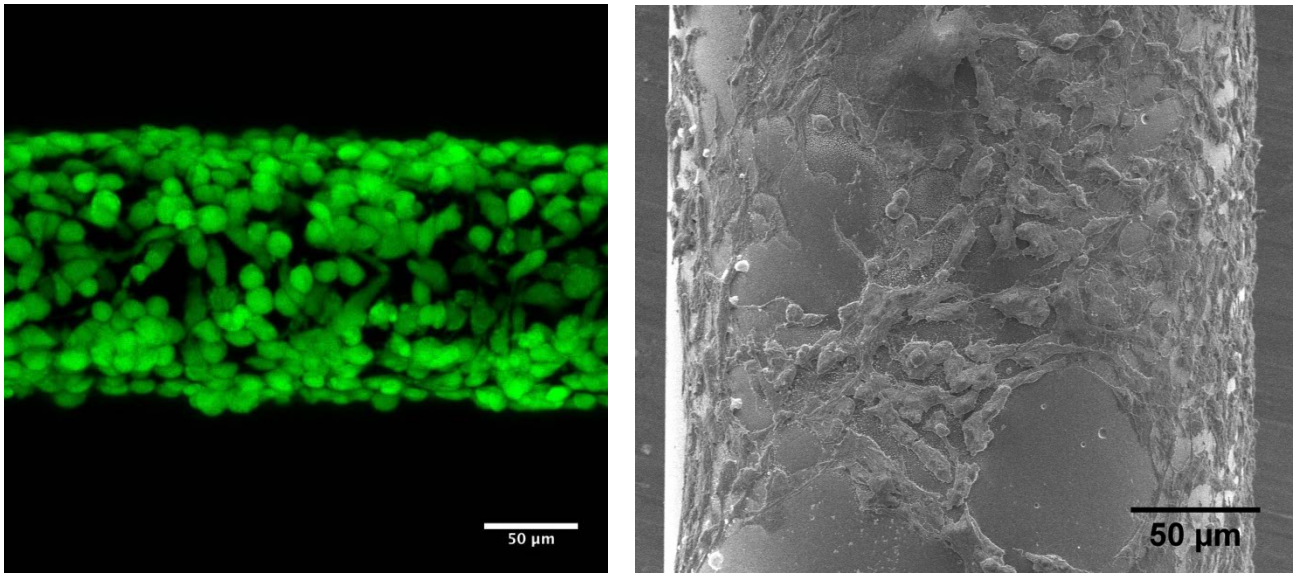

Fig. 3: Cells on optical fiber electrodes: confocal microscopy image of calcein-stained cells 24 h after seeding (A); SEM image of fixed cells after 10 days of differentiation (B).

Chronoamperometry measurements from differentiated cells show a current peak immediately after the injection of KCl (**figure 4a)**. The measured current is attributed to dopamine oxidation because: i) a reference system where the cells are not differentiated does not show a current peak after KCl injection and ii) hVM1-Bcl-xL cells do not differentiate into cells that can release other electroactive compounds [24,34].

To monitor the evolution of the dopaminergic population and their ability to release dopamine, OFEs with cells were employed in chronoamperometry at different time points of the differentiation process. **Figure 4b** shows the determined charges for the first and second exocytosis events. 24 h after seeding (differentiation day 0, DD0), no current is measured upon addition of KCl. Starting with DD1, current is measured and the corresponding charges increase up to DD10. In 15 min, the cells are able to partly replenish the dopamine pool and a second exocytosis event can be detected with chronoamperometry. In the early stage of differentiation (DD1 - DD5), the charge is ~4 times lower for the second exocytosis event. However, in DD9 and DD10, the charge for the second exocytosis event is only 2 times lower than for the first. This is an indicator that cells are maturing during the differentiation process.

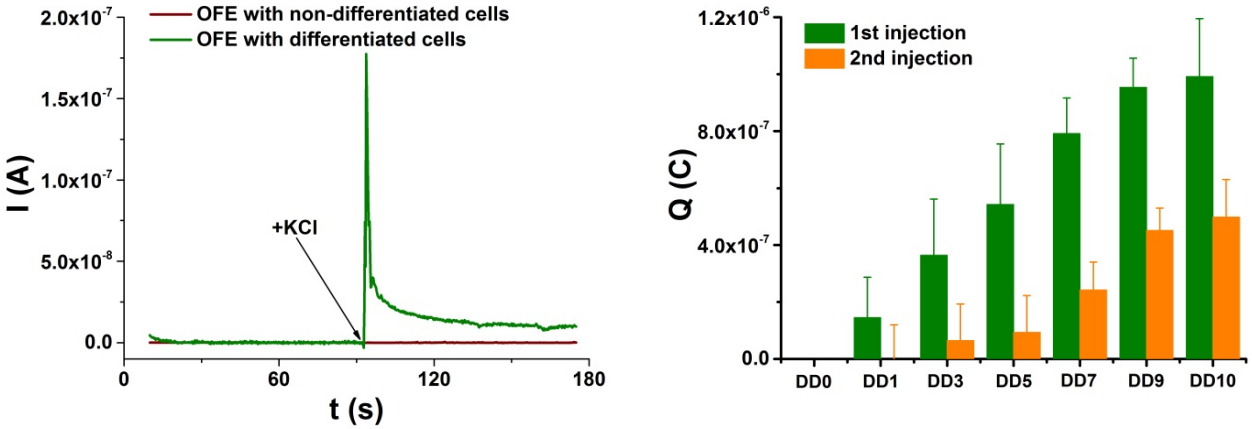

Fig. 4: Chronoamperometric detection of dopamine released from differentiated cells upon K^+-induced exocytosis: typical current-time trace recorded with an OFE from a cell population after 10 days of differentiation (A) and average charges for the first and second exocytosis events at different time points in the experiment (B)

4. Conclusions

OFEs show good electrochemical behavior with standard redox probes and dopamine. The carbon surface is biocompatible and can be used as substrate for cell growth and differentiation. Dopaminergic neurons generated on the OFEs can be stimulated using KCl to locally release dopamine, which can then be immediately detected with chronoamperometry. The OFEs could be developed in the future as implants for cell replacement therapy.

Acknowledgements

Bibliography

[1] M. Parent, Substantia Nigra and Parkinson's Disease: A Brief History of Their Long and Intimate Relationship, Can. J. Neurol. Sci. 37 (2010).

[2] M.L. Giroux, Parkinson disease: managing a complex, progressive disease at all stages., Cleve. Clin. J. Med. 74 (2007) 313–314. doi:10.3949/ccjm.74.5.313.

[3] B. V. Zlokovic, The Blood-Brain Barrier in Health and Chronic Neurodegenerative Disorders, Neuron. 57 (2008) 178–201. doi:10.1016/j.neuron.2008.01.003.

[4] K.A. Jellinger, Cerebrospinal Fluid in Clinical Practice, Eur. J. Neurol. 16 (2009) e109–e109. doi:10.1111/j.1468-1331.2009.02601.x.

[5] A. Lopez, A. Muñoz, M.. Guerra, J.. Labandeira-Garcia, Mechanisms of the effects of exogenous levodopa on the dopamine-denervated striatum, Neuroscience. 103 (2001) 639–651. doi:10.1016/S0306-4522(00)00588-1.

[6] J. Dingemanse, Issues important for rational COMT inhibition, Neurology. 55 (2000).

[7] F.M. Weaver, Bilateral Deep Brain Stimulation vs Best Medical Therapy for Patients With Advanced Parkinson Disease<subtitle>A Randomized Controlled Trial</subtitle>, JAMA. 301 (2009) 63. doi:10.1001/jama.2008.929.

[8] O. Lindvall, Z. Kokaia, A. Martinez-Serrano, Stem cell therapy for human neurodegenerative disorders–how to make it work, Nat. Med. 10 (2004) S42–S50. doi:10.1038/nm1064.

[9] O. Lindvall, A. Björklund, Cell replacement therapy: Helping the brain to repair itself, Neurotherapeutics. 1 (2004) 379–381. doi:10.1007/BF03206624.

[10] A. Trounson, C. McDonald, Stem Cell Therapies in Clinical Trials: Progress and Challenges, Cell Stem Cell. 17 (2015) 11–22. doi:10.1016/j.stem.2015.06.007.

[11] A. Trounson, N.D. DeWitt, Pluripotent stem cells progressing to the clinic, Nat. Rev. Mol. Cell Biol. 17 (2016) 194–200. doi:10.1038/nrm.2016.10.

[12] T.R. Barrow, Cell replacement therapy in Parkinson's disease, Biosci. Horizons. 8 (2015) hzv002-hzv002. doi:10.1093/biohorizons/hzv002.

[13] A. Bjo¨rklund, U. Stenevi, Reconstruction of the nigrostriatal dopamine pathway by intracerebral nigral transplants, Brain Res. 177 (1979) 555–560. doi:10.1016/0006-8993(79)90472-4.

[14] S. Casarosa, Y. Bozzi, L. Conti, Neural stem cells: ready for therapeutic applications?, Mol. Cell. Ther. 2 (2014) 31. doi:10.1186/2052-8426-2-31.

[15] S.M. Pollard, L. Conti, A. Smith, Exploitation of adherent neural stem cells in basic and applied neurobiology, Regen. Med. 1 (2006) 111–118. doi:10.2217/17460751.1.1.111.

[16] L. Amato, A. Heiskanen, C. Caviglia, F. Shah, K. Zór, M. Skolimowski, M. Madou, L. Gammelgaard, R. Hansen, E.G. Seiz, M. Ramos, T.R. Moreno, A. Martínez-Serrano, S.S. Keller, J. Emnéus, Pyrolysed 3D-Carbon Scaffolds Induce Spontaneous Differentiation of Human Neural Stem Cells and Facilitate Real-Time Dopamine Detection, Adv. Funct. Mater.

24 (2014) 7042–7052. doi:10.1002/adfm.201400812.

[17] R.L. McCreery, Advanced Carbon Electrode Materials for Molecular Electrochemistry, Chem. Rev. 108 (2008) 2646–2687. doi:10.1021/cr068076m.

[18] K. Thyagarajan, Optical Fiber, in: Fiber Opt. Essentials, John Wiley & Sons, Inc., Hoboken, NJ, USA, 2007: pp. 28–54. doi:10.1002/9780470152560.ch4.

[19] R.W. Waynant, Optical Fiber, in: Electron. Photonic Circuits Devices, IEEE, 2009. doi:10.1109/9780470544532.ch5.

[20] C.Z. Hu, J.D. Andrade, Pyrolyzed, conducting kapton polyimide: An electrically conducting material, J. Appl. Polym. Sci. 30 (1985) 4409–4415. doi:10.1002/app.1985.070301116.

[21] L.U. Wahlberg, G. Lind, P.M. Almqvist, P. Kusk, J. Tornøe, B. Juliusson, M. Söderman, E. Selldén, Å. Seiger, M. Eriksdotter-Jönhagen, B. Linderoth, Targeted delivery of nerve growth factor via encapsulated cell biodelivery in Alzheimer disease: a technology platform for restorative neurosurgery, J. Neurosurg. 117 (2012) 340–347. doi:10.3171/2012.2.JNS11714.

[22] L. Amato, A. Heiskanen, C. Caviglia, F. Shah, K. Zór, M. Skolimowski, M. Madou, L. Gammelgaard, R. Hansen, E.G. Seiz, M. Ramos, T.R. Moreno, A. Martínez-Serrano, S.S. Keller, J. Emnéus, Pyrolysed 3D-Carbon Scaffolds Induce Spontaneous Differentiation of Human Neural Stem Cells and Facilitate Real-Time Dopamine Detection, Adv. Funct. Mater. (2014) n/a-n/a. doi:10.1002/adfm.201400812.

[23] E.T. Courtois, C.G. Castillo, E.G. Seiz, M. Ramos, C. Bueno, I. Liste, A. Martinez-Serrano, In Vitro and in Vivo Enhanced Generation of Human A9 Dopamine Neurons from Neural Stem Cells by Bcl-XL, J. Biol. Chem. 285 (2010) 9881–9897. doi:10.1074/jbc.M109.054312.

[24] C. Krabbe, E. Courtois, P. Jensen, J.R. Jørgensen, J. Zimmer, A. Martínez-Serrano, M. Meyer, Enhanced dopaminergic differentiation of human neural stem cells by synergistic effect of Bcl-x_L and reduced oxygen tension, J. Neurochem. 110 (2009) 1908–1920. doi:10.1111/j.1471-4159.2009.06281.x.

[25] R.L. McCreery, K.K. Cline, C.A. McDermott, M.T. McDermott, Control of reactivity at carbon electrode surfaces, Colloids Surfaces A Physicochem. Eng. Asp. 93 (1994) 211–219. doi:10.1016/0927-7757(94)02899-0.

[26] P. Chen, M.A. Fryling, R.L. McCreery, Electron Transfer Kinetics at Modified Carbon Electrode Surfaces: The Role of Specific Surface Sites, Anal. Chem. 67 (1995) 3115–3122. doi:10.1021/ac00114a004.

[27] M.A. Guillorn, T.E. McKnight, A. Melechko, V.I. Merkulov, P.F. Britt, D.W. Austin, D.H. Lowndes, M.L. Simpson, Individually addressable vertically aligned carbon nanofiber-based electrochemical probes, J. Appl. Phys. 91 (2002) 3824–3828. doi:10.1063/1.1448671.

[28] C.H. An Wong, A. Ambrosi, M. Pumera, Thermally reduced graphenes exhibiting a close relationship to amorphous carbon, Nanoscale. 4 (2012) 4972. doi:10.1039/c2nr30989k.

[29] J.F. Rusling, S.L. Suib, Characterizing Materials with Cyclic Voltammetry, Adv. Mater. 6

(1994) 922–930. doi:10.1002/adma.19940061204.

[30] B.J. Venton, R.M. Wightman, Psychoanalytical Electrochemistry: Dopamine and Behavior, Anal. Chem. 75 (2003) 414 A-421 A. doi:10.1021/ac031421c.

[31] P. Gründler, O. Frank, L. Kavan, L. Dunsch, Carbon Nanotube Electrodes for Hot-Wire Electrochemistry, ChemPhysChem. 10 (2009) 559–563. doi:10.1002/cphc.200800659.

[32] N.F. Atta, A. Galal, S.M. Ali, S.H. Hassan, Electrochemistry and detection of dopamine at a poly(3,4-ethylenedioxythiophene) electrode modified with ferrocene and cobaltocene, Ionics (Kiel). 21 (2015) 2371–2382. doi:10.1007/s11581-015-1417-z.

[33] Y. Wang, Y. Li, L. Tang, J. Lu, J. Li, Application of graphene-modified electrode for selective detection of dopamine, 2009. doi:10.1016/j.elecom.2009.02.013.

[34] A. Villa, I. Liste, E.T. Courtois, E.G. Seiz, M. Ramos, M. Meyer, B. Juliusson, P. Kusk, A. Martínez-Serrano, Generation and properties of a new human ventral mesencephalic neural stem cell line, Exp. Cell Res. 315 (2009) 1860–1874. doi:10.1016/j.yexcr.2009.03.011.

Single step fabrication of optical fiber-based carbon electrodes for dopamine detection from cells

Ada-Ioana Bunea[1], Ramona Valentina Mateiu[2], Alberto Martinez Serrano[3], Arto Heiskanen[1], Stephan Sylvest Keller[1], Niels Bent Larsen[1] and Jenny Emnéus[1]

Supplementary information

S1. Preparation of cell samples for SEM

Fixation buffer was purchased from ThermoFisher. Osmium tetroxide was purchased from Agar Scientific Ltd. Ethanol and acetone were purchased from Sigma Aldrich.

The cells were fixed by 15 min incubation in fixation buffer. After fixation, the samples were stained by 60 min incubation in 1% osmium tetroxide in Millipore water. Next, the samples were dried in ethanol/water series (50%, 70%, 90% and 100%), followed by acetone/ethanol series (50%, 70%, 90% and 100%) and critical point drying in a Leica CPD 300. The samples were mounted onto a square piece of silicon, and electrically grounded with aluminum tape.

S2. Investigation of the carbon layer using SEM

The carbon surface was investigated after the pyrolysis of polyimide-coated optical fibers using SEM. From **figure S1a**, it can be seen that the surface of the carbon layer is uniform and non-porous. The high contrast in SEM between the fused silica core and cladding, and the carbon layer, of the optical fiber electrodes (OFEs), allowed measurement of the thickness of the carbon layer, as shown in **figure S1b**. Before pyrolysis, the polyimide buffer of the optical fibers had a thickness of 12.5 ± 5 µm, as specified by the producer. The polyimide-derived carbon layer had a thickness of 7.49 ± 0.06 µm, as determined from SEM.

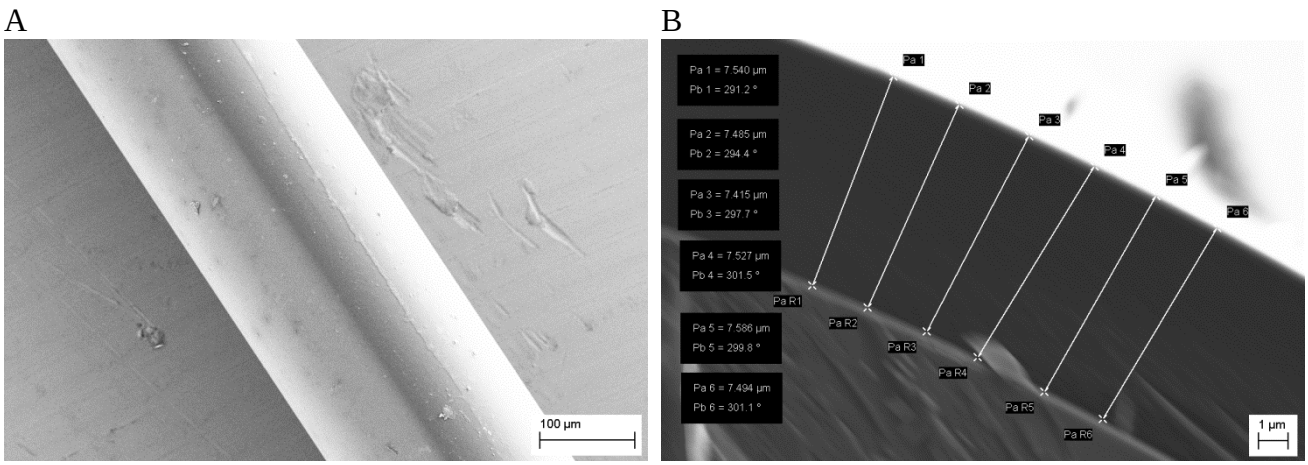

Figure S1: SEM of optical fiber electrodes at different magnifications: uniform carbon surface (a) and carbon layer on fused silica core and cladding, including measurement lines (b).

S3. Preparation of baseline and stimulation buffers for exocytosis measurements

All reagents were purchased from Sigma Aldrich: HEPES (1M), glucose (≥99.5%), $MgCl_2$, $CaCl_2$ (≥96%), NaCl (≥99%) and KCl (≥99%). Millipore water (18.2 MΩ resistivity) was used for preparing the solutions. Two buffers were prepared: a baseline buffer (10mM HEPES, 5 mM glucose, 1.2 mM $MgCl_2$, 2 mM $CaCl_2$, 150 mM NaCl and 5mM KCl) and a stimulation buffer (10mM HEPES, 5 mM glucose, 1.2 mM $MgCl_2$, 2 mM $CaCl_2$, 5 mM NaCl and 950 mM KCl). The buffers were filter sterilized (0.22 µm) before performing the measurements.

S4. Setup for electrochemical measurements

Electrochemical measurements were performed in a 3 electrode setup in 25 mL Berzelius beakers (**Figure S2**). A lid with inserts for the electrodes was fabricated from 5 mm poly(methyl methacrylate) (Röchling Technische Teile KG, Mainburg, Germany) using a laser cutter (Epilog Laser Mini 18 from Epilog Laser, Golden CO, USA) to ensure reproducible alignment in the system. The measurement setup defines an active geometrical area of 7.2 mm^2 for OFEs.

A cylindrical magnetic stirring bar (VWR, Radnor PA, USA) and a IKA® RH basic 2 magnetic stirrer (IKA®-Werke GmbH, Staufen, Germany) were used for chronoamperometry experiments.

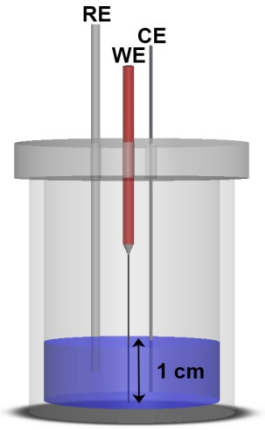

Figure S2: Setup for electrochemical measurements

S5. Cyclic voltammetry – additional investigations

The electrochemical behavior of OFEs was investigated immediately after oxygen plasma treatment and after storage in a dry cupboard. It is clear from **figure S3** that storage for a period of 20 days does not lead to significant changes in the voltammograms recorded with OFEs.

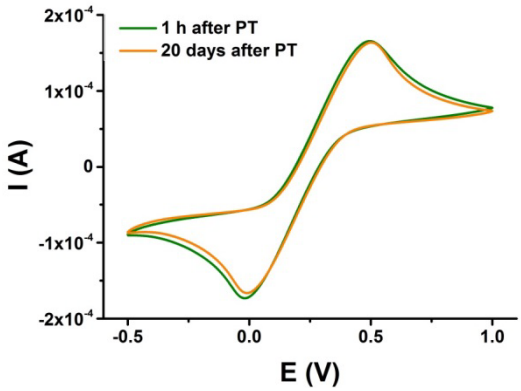

Figure S3: Cyclic voltammograms recorded at a scan rate of 50 mV/s with one optical fiber electrode 1h and 20 days after plasma treatment, respectively. E vs $Ag|AgCl_{sat}$.

From **figure S4** it can be seen that the electrode-to-electrode variability is low for cyclic voltammetry measurements (< 5% for both peak current and peak separation).

A B

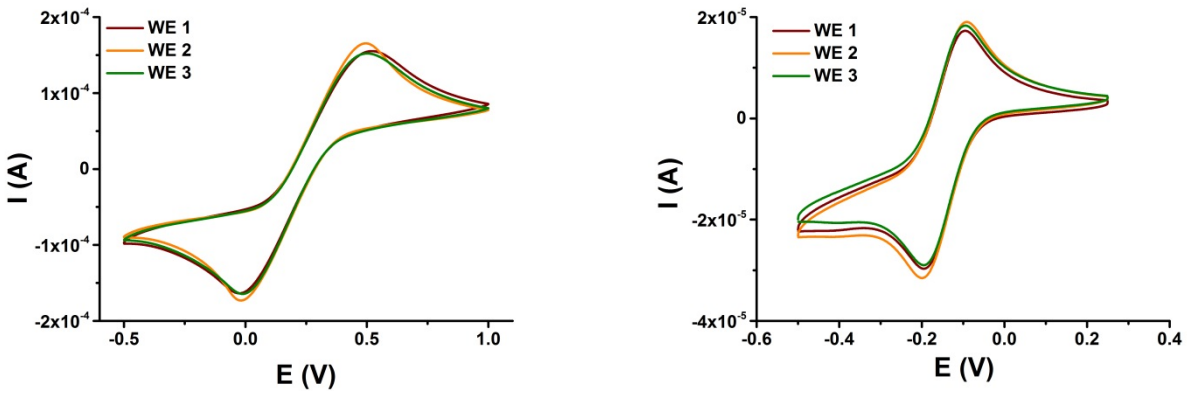

Figure S4: Cyclic voltammograms recorded at a scan rate of 50 mV/s with three different optical fiber electrodes in 10 mM $[Fe(CN)]_6^{3-/4-}$ (a) and 1 mM $[Ru(NH_3)_6]^{2+/3+}$ (b). E vs $Ag|AgCl_{sat}$.

The effect of Geltrex coating on the electrochemical behaviour of OFEs was investigated using cyclic voltammetry (**figure S5**). As it can be seen in **figure S5b**, the sensitivity of the OFEs decreases by 30% after Geltrex coating. However, the correlation between anodic peak currents and concentration remains linear up to 200 µM dopamine.

A B

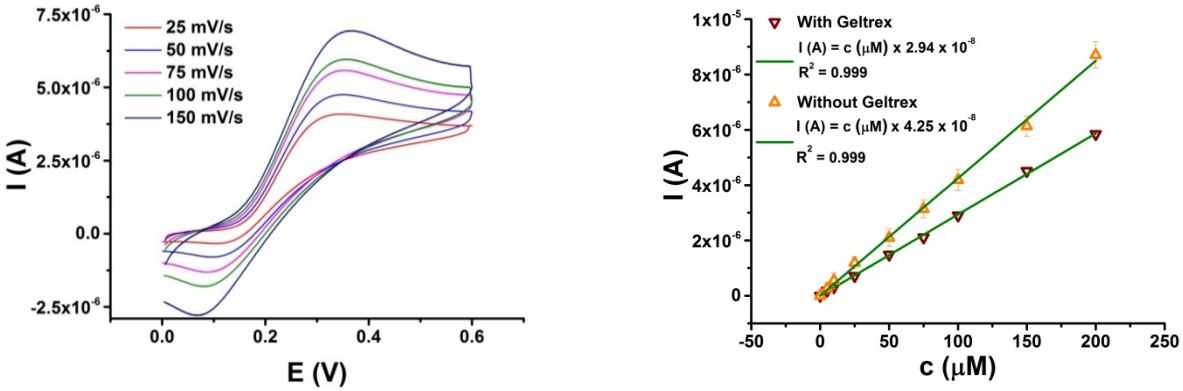

Figure S5: Electrochemistry results using dopamine: CV in 250 µM dopamine at different scan rates on Geltrex-coated optical fiber electrode (A); Calibration curve using anodic peak intensity at 50 mV/s scan rate for optical fiber electrodes before and after Geltrex coating (B). E vs $Ag|AgCl_{sat}$.

S6. Setup for cell culture and imaging

Silicone isolators (0.5 mm thick) were purchased from Sigma Aldrich. VistaVision™ soda-lime glass microscope slides were purchased from VWR (VWR, Radnor PA, USA). A scalpel was used to cut the silicone rubber to fit 6 well-plates and to make channels in the silicone for supporting the OFEs. The glass microscope slides were cut using a Pro Glass Cutter (Carl Kammerling International Ltd, Pwllheli, UK). The OFEs were glued to the silicone pieces using blue adhesive poly(vinylchloride) film. The individual components and the system were sterilized by using i)

ethanol and ii) 20 min exposure to UV-C irradiation (254 nm, UC sterilization cabinet, Cleaver Scientific Ltd, UK) in a laminar flow bench.

A top view and side view of the OFEs in the holder for cell culture and confocal microscopy imaging are shown in **figure S6**. For the OFEs used in electrochemical measurements, the segment of the OFE in contact with the liquid, representing the active electrode area, is 1 cm in length. When placing the OFEs in the holder, a terminal segment of ~1.2 cm was kept free of adhesive tape. The holder ensured i) that the OFEs would not rotate after cell seeding, which would prevent cells from attaching; ii) that the OFEs would not rotate during imaging, which would cause difficulties for generating a clear image; iii) that the cells on the OFEs are ~ 500 µm above the cells attached to the holder, which minimized the background signal.

A B

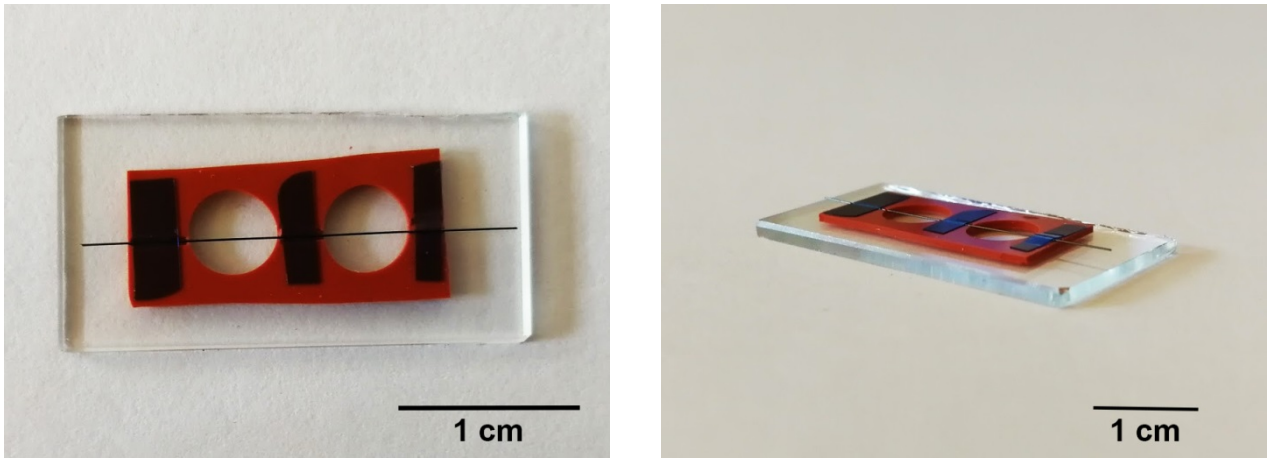

Figure S6: Holder for cell culture and confocal microscopy imaging: top view (A) and side view (B). The optical fiber electrode is suspended by ~ 500 µm by the silicone rubber piece.

S7. Protocols for cell culture and differentiation

DMEM/F12 with GlutaMAX, AlbuMAX I, HEPES, N-2 supplement and Geltrex were purchased from ThermoFisher Scientific. L-alanine, L-asparagine monohydrate, L-aspartic acid, L-glutamic acid and L-proline were purchased from MerckMillipore. Glucose (Bioreagent, ≥ 99.5%), N^6,2′-O-Dibutyryladenosine 3′,5′-cyclic monophosphate sodium salt and cell-tested water were purchased from Sigma Aldrich. Human recombinant epidermal growth factor (EGF) and human recombinant fibroblast growth factor (FGF) were purchased from R&D Systems. Glial derived neutrophic factor (GDNF) was purchased from PeproTech.

Growth medium was prepared by using DMEM/F12 (1:1) with GlutaMAX as basis. Additionally, the medium contained glucose (6 g/L), HEPES (5 mM), AlbuMAX (0.5% m/m), L-alanine, L-asparagine monohydrate, L-aspartic acid, L-glutamic acid and L-proline (40 µM of each aminoacid), N-2 supplement (diluted 100x), penicillin/streptomycin mix, EGF (20 ng/mL) and NGF (20 ng/mL).

Differentiation medium was prepared by using DMEM/F12 (1:1) with GlutaMAX as basis. Additionally, the medium contained glucose (6 g/L), HEPES (5 mM), AlbuMAX (0.5% m/m), L-alanine, L-asparagine monohydrate, L-aspartic acid, L-glutamic acid and L-proline (40 µM of each aminoacid), N-2 supplement (diluted 100x), penicillin/streptomycin mix, dibutyryladenosine 3′,5′-cyclic monophosphate sodium salt (1 mM) and GDNF (2 ng/mL).

hVM1 Bcl-X_L cells cultured from at least two passages after thawing were seeded on Geltrex-coated OFEs in growth medium. 24 h after seeding, growth medium was replaced with differentiation medium. This was denoted as differentiation day 0 (DD0). 24 h after, the differentiation medium was replaced fresh differentiation medium (DD1). Every 48 h, in DD3, DD5, DD7 and DD9, 2/3 of the differentiation medium was replaced with fresh differentiation medium. The end-point of the experiment is DD10.

All experiments in this work were performed with hVM1 Bcl-X_L cells from passage 38 to 43.

Appendix II: Paper II

Transparent, Carbon-based Electrode Chips for Enhanced Photocurrent Generation from Thylakoid Membranes

Ada-Ioana Bunea, Arto Heiskanen, Galina Pankratova, Giulio Tesei, Mikael Lund, Hans-Erik Åkerlund, Dónal Leech, Niels Bent Larsen, Stephan Sylvest Keller, Lo Gorton and Jenny Emnéus

Graphical abstract

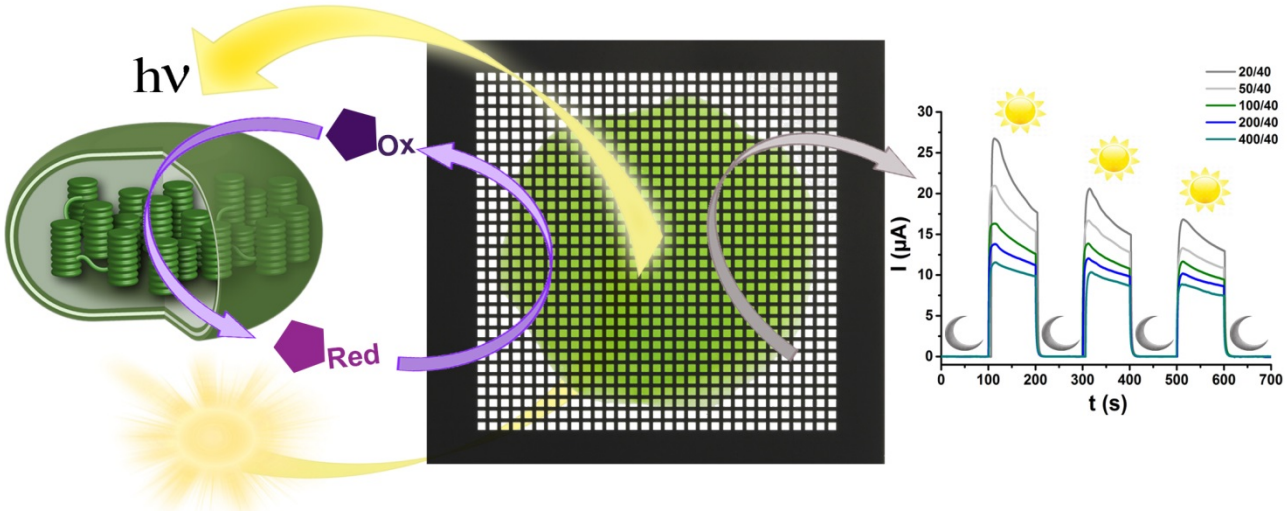

DOI: 10.1002/ ((please add manuscript number))
Full paper

Transparent, Carbon-based Electrode Chips for Enhanced Photocurrent Generation from Thylakoid Membranes

Ada-Ioana Bunea, Arto Heiskanen, Galina Pankratova, Giulio Tesei, Mikael Lund, Hans-Erik Åkerlund, Dónal Leech, Niels Bent Larsen, Stephan Sylvest Keller, Lo Gorton and Jenny Emnéus[*]

A.-I. Bunea, Dr. A. Heiskanen, Dr. S. Sylvest Keller, Prof. N. Bent Larsen, Prof. J. Emnéus
Department of Micro- and Nanotechnology, Technical University of Denmark, 2800 Kongens Lyngby, Denmark,
E-mail: jenny.emneus@nanotech.dtu.dk
G. Pankratova, Giulio Tesei, Dr. Mikael Lund, Prof. H.-E. Åkerlund, Prof. L. Gorton
Department of Biochemistry and Structural Biology, Lund University, 22362 Lund, Sweden
Prof. D. Leech
School of Chemistry & Ryan Institute, National University of Ireland, H91 CF50 Galway, Ireland

Keywords: carbon, bioanode, thylakoid membrane, photosynthesis

Harvesting the energy generated by photosynthetic organisms through light-reactions is a significant step towards a sustainable future. Thylakoid membranes are the site of photosynthesis, and thus particularly suited for developing photo-bioelectrochemical cells. For commercial applications, electrodes with large surface areas are needed. One affordable and scalable option for fabrication is photolithographic patterning of a conductive material on a transparent substrate. This allows backside illumination, protecting the system from the environment and vice versa. Electrode chips made of patterned carbon supported on quartz were designed and fabricated and the influence of patterning on photocurrent generation is reported. The patterned electrode area is 1 cm^2, and the measurement chamber footprint is 0.5 cm^2, one order of magnitude larger than previously-tested electrodes for thylakoid membrane immobilization. Different mediators, monomeric ($[Ru(NH_3)_6]Cl_3$) and polymeric ($[Os(2,2\text{-bipyridine})_2\text{-poly(N-vinylimidazole)}_{10}Cl]^{+/2+}$) are used for evaluating current generation from

thylakoid membranes. Current densities up to 71 μA cm^{-2} are measured upon illumination through the transparent electrode chip with solar simulated irradiance (1000 W m^{-2}).

1. Introduction

As the population of Earth grows, so does the demand for energy. Ever since the energy crisis of the 1970s, the energy demand has been investigated at both global and consumer level.[1–3] In the context of climate change, it is important not only to produce sufficient energy for our ever-growing needs, but also to move towards clean, renewable energy sources as a step towards a sustainable future.[4–6] In 2010, renewable sources accounted for 16.6% of the energy consumed worldwide, and there is a projected increase to almost 50% by 2040.[6] One of the main renewable energy sources is the Sun; therefore there is considerable focus on the development of methods for harvesting solar energy. Solar energy is the primary energy source for organisms capable of photosynthesis, such as algae, green plants and cyanobacteria. For these organisms, photosynthesis takes place inside thylakoid membranes (TMs), which for algae and plants are found within chloroplasts.[7,8] The natural photosynthetic system is complex and involves numerous processes after photoexcitation, with two coupled proteins, photosystems I and II (PS I and PS II) being the key components in the light-reactions of photosynthesis.[9–11] A variety of photosynthetic components have been studied for harnessing sunlight in photo-bioelectrochemical cells (PBECs), e.g. isolated PS I and PS II,[10–12] TMs, [13] cyanobacteria [14] and algae.[15] However, in order to commercially explore PBECs, their efficiency needs to be substantially improved by increasing the rate of the extracellular electron transfer and the viability of these systems. This suggests the need for improvement of the electrochemical interactions between photosynthetic components and electrode materials,[16] which can be achieved at several levels, e.g. i) development of new, transparent electrodes which maximize the surface area while minimizing the geometrical surface and diffusion distances and enhancing the total light

absorbing region and distribution to the photosynthetic components; and ii) engineering of photosynthetic systems.[17] The ultimate goal is to develop mediator-less devices, but so far these show very low efficiency.[18] This is why most approaches use different soluble redox species and osmium redox polymers as mediators between TMs and electrodes.[19,20]

Photovoltaic systems make use of transparent electrode materials as an integral part of the device structure,[21] and transparent conducting oxides (TCOs) are the most commonly-used because of their good conductivity and transparency. Several options are available, from well-known indium-based materials, such as ITO (indium tin oxide), to doped ZnO, TiO_2 and SnO_2 materials.[21,22] One TCO, fluorinated-tin oxide (FTO), was used as electrode material for a recently-developed PBEC,[23] but illumination was done from the top, without taking advantage of the transparency of FTO. An ITO bio super capacitor was recently reported.[18] However, due to price and stability issues, researchers are interested in alternatives to TCOs,[24–27] with graphene, carbon nanotubes and metal nanowire electrodes showing the most promising results.

Carbon, with its different allotropes, is one of the most widely used electrode materials, especially for fuel cell applications,[28–30] because of its numerous advantages: abundance, low fabrication costs, wide potential window, relatively inert chemistry, biocompatibility and good electrocatalytic activity.[31] Photolithography can be used to deposit and pattern a photoresist onto the substrate of choice in a simple process, easy to upscale. By pyrolysing the polymer precursor, glass-like carbon is obtained and the pattern defined in the precursor is preserved.[32] Fused silica is transparent in the UV-Vis domain, hard, durable and thermally resistant up to 1600 °C.[33] These properties make it an excellent choice as substrate for developing large-area transparent electrode chips.

Here we report the fabrication and application of patterned carbon electrode chips on fused silica substrates to investigate the influence of two parameters on photocurrent generation: i) the carbon surface area versus light-exposed area; ii) the size of the light-exposed openings in

the carbon. TMs were used as model light-harnessing systems, since they are easier to extract and purify than PS I and PS II, and at the same time more stable, because all the protein complexes retain their native environment. Photocurrent generation from TMs was tested with one soluble mediator, $[Ru(NH_3)_6]Cl_3$, and one redox polymer mediator, $[Os(2,2'\text{-bipyridine})_2\text{-poly}(N\text{-vinylimidazole})_{10}Cl]^{+/2+}$.[20] Experimental data was analyzed through diffusion models, which provide additional insight into the processes taking place in the system.

2. Results and discussion

2.1. Electrode chips and measurement system

The electrode chips consist of carbon electrodes on a transparent carrier substrate. The fused silica substrate is transparent in the visible range, but it does not conduct electrons.[33] The carbon electrodes are opaque, but excellent electron conductors.[34,35] Since photocurrent generation requires light and photocurrent collection requires conductivity, there is a trade-off between the degree of exposed fused silica and carbon areas of the chip.

For the purpose of optimizing photocurrent collection from TMs using transparent electrode chips, two series with a total of nine different designs were fabricated (**figure 1**). Each chip design was labelled as xx/yy, where xx is the lateral size of the openings (in µm) and yy was the transparent surface area percentage of the patterned area (for example, the label 100/40 means that the size of the openings is 100 µm and 40 % of the patterned area is transparent). There are two particular cases, 0 % transparency, which is denoted as “full C”, and 100 % transparency, which is denoted as “full opening”. In the “100/yy” series, the dimension of the openings was kept constant at 100 µm, but the percentage of the transparent area was varied (**figure 1c**). In this way, the trade-off between light reaching the sample and the electrode surface area was investigated. For the “xx/40” series, the openings accounted for 40% of the patterned area, and the size of the openings was varied between 20 and 400 µm (**figure 1d**). This allowed investigation of the influence of the size of the openings on the photocurrent

collection. 20 µm was chosen as the smallest size for design because lowering the dimensions even further can cause issues in fabrication.

The measurement holder (**figure 1b** and supporting information, SI) defines the electrode footprint in the middle of the patterned electrode area and it ensures that i) light from the source can reach the sample in a reproducible manner and ii) the path that the electrons need to travel outside the patterned area is the same regardless of the design. The same holder was used for all the experiments described in this paper.

2.2. Photocurrent collection using thylakoid membranes

TMs were immobilized on the differently-patterned electrode chips and tested for photocurrent collection using both the monomeric (**figure 2a** and **2c**) and the redox polymer (**figure 2b** and **2d**) mediators. Arrows in the figures indicate where the lamp was turned *on* and *off*. As seen for all cases, no photocurrent was generated in the absence of light, i.e. when the lamp was *off*. When the lamp was turned *on*, the current increased instantly, after which it slowly declined while the sample was illuminated. This current decline was previously reported to be due to photo-induced damage of PS II.[20,36]

Chronoamperometry measurements with TMs show no photocurrent in the absence of light. In the presence of light, the current increases abruptly and then slowly decreases while the sample is illuminated (**figure 2**). This is due to photo-induced damage,[36] and its study is beyond the scope of this paper, since TMs are used here as a model system.

It can be clearly seen in **figure 2** that both the density and the size of the openings influence the generated photocurrent. Since TMs need light to generate energy, an increase in photocurrent collection can be expected when the area exposed to light increases. This is verified by data in figure 2a, 2b, 2f and **Table 1**, showing how an increased density of the

openings from 20 to 60% for a constant 100 µm opening size, led to increasing photocurrent densities from 29.3 ± 0.4 µA cm^{-2} to 39.4 ± 0.8 µA cm^{-2} for the ruthenium complex mediator, and from 15.5 ± 0.4 to 31.1 ± 0.6 for the osmium redox polymer, respectively.

In figure 2c, 2d, 2f and Table 1, we can observe that varying the size of the openings for a constant transparency of 40% has a remarkable influence on the generated photocurrent, i.e., when decreasing the size of the openings from 400 µm to 20 µm, the current density increases by a factor of two for the ruthenium complex mediator, from 23.1 ± 0.4 µA cm^{-2} to 53.2 ± 0.8 µA cm^{-2}, and by a factor of four for the osmium redox polymer, from 11.6 ± 1 to 42.8 ± 0.6 respectively.

Figure 2e shows a schematic representation of how light passes through the transparent fused silica substrate and further through the openings in the carbon layer in order to reach the TMs. The inset of figure 2e shows a schematic representation of the reactions of interest that occur when TMs are illuminated: the mediator, in its oxidized form, is reduced by electrons generated in the water-splitting reaction performed by the TMs; the reduced mediator is then oxidized at the electrode surface, completing a redox cycle and generating current. In the case of soluble mediator, the ruthenium complex diffuses between TMs and the electrode surface. In the case of Os-redox polymer, charge is transferred through an electron-hopping mechanism.

Figure 3a shows the theoretically calculated and experimentally obtained maximum current densities for chips with a constant transparency of 40 % as a function of the size of the openings. The diffusion model assumes that electrons are initially homogeneously distributed on a square surface corresponding to an opening. Through isotropic two-dimensional diffusion, electrons carried by the mediator reach the carbon electrode. The exit probability for an electron to hit the boundary of the square after a time interval is considered to be

proportional to the current intensity peak. The theoretical model is in excellent agreement with the experimental data for both mediators. **Figure 3b** shows the exit probability as a function of the initial position of the electron for openings of increasing size. The two time intervals used were chosen based on the maximum current intensities from chronoamperometry (5 s for Ru-complex and 25 s for Os-RP as mediators). The color-maps clearly indicate that electrons generated near the edge of the opening have higher probability to reach the electrode surface within the time interval. For openings larger than 50 µm, electrons generated in the central region of the opening do not reach the electrode quickly enough to significantly contribute to the current signal. Based on the experimental results and the model, we can infer that 20 µm openings are optimal for photocurrent generation in the described setup.

The fit of the experimental current intensities to the theoretical model yields estimates of the effective two-dimensional diffusion coefficients, D. For the ruthenium complex, D = 17 ± 1 $\mu m^2 s^{-1}$, one order of magnitude smaller than the diffusion coefficient of $[Ru(NH_3)_6]Cl_3$ in 0.1 M phosphate buffer at pH 7.0.[37] The large discrepancy can be ascribed to the high viscosity of the thylakoid dispersion, as well as to the fact that the model neglects out-of-plane displacement.

The electron transport through the Os-RP occurs by an electron-hopping mechanism and can be treated as a diffusive process.[38] The effective in-plane diffusion coefficient was estimated to be D = 5 ± 1 $\mu m^2 s^{-1}$, in good agreement with experimental values reported in literature.[39]

For large-scale applications in the energy sector, it is important to know how the electrode chips behave in different irradiance conditions. The value at which solar cells are tested is of 1000 W m^{-2}, which is also denoted as 1 sun.[40] This value corresponds to normal illumination (when the sun is at zenith and its rays fall perpendicular to the ground). However, effective

daytime irradiance has lower values, due to as geometrical factors, terrain and atmospheric attenuation.[41] **Figure 4** shows the maximum current density generated with the 20/40 chips and soluble mediator in different illumination conditions. For the tested interval, 200 – 1000 W m^{-2}, the maximum current density increases with increasing irradiance, as expected, up to 71 µA cm^{-2}.

3. Conclusion

Patterning a conductive material on a transparent substrate allows taking advantage of both properties. Carbon-on-quartz transparent electrode chips were fabricated and successfully employed for photocurrent generation from thylakoid membranes using back-side illumination with solar-simulated irradiance.

The pattern design influences photocurrent generation, with small openings generating the highest currents. This can be explained by a diffusion model where electrons transported by the mediators are modeled as non-interacting particles freely propagating in two dimensions. Increasing the transparency to at least 60% of the total surface area also leads to enhanced photocurrent due to an increase in the surface area where photosynthesis is taking place. Electrode chips with large surface areas can be fabricated in a scalable process, which makes them interesting for future development in energy applications.

4. Experimental Section

Fabrication of electrode chips:

The electrode chips were fabricated using UV photolithograpy and pyrolysis. 500 µm thick fused silica wafers were employed as substrate and SU-8 2005 was used as carbon precursor. The process flow was as follows: overnight dehydration bake of the wafers at 250°C, spin coating of SU-8 2005: 30 s, acceleration of 2000 rpm·min^{-1} (RCD8 T spinner from Süss MicroTec, Germany), 3h solvent evaporation at room temperature, proximity exposure, 12 µm gap, through chromium mask and a dose of 100 mJ·cm^{-1} (MA6 contact aligner from Süss

MicroTec, Germany), 1h bake at 50°C, development: PGMEA, 2 x 5 min, followed by isopropanol washing and N_2 blow-drying, 16h hard bake at 90°C, pyrolysis (PEO-601 furnace from ATV Technologie GmbH, Germany). The pyrolysis process was performed as previously reported.[42] The resist thickness was 5.9 ± 0.2 µm before pyrolysis and the obtained carbon layer had a thickness of 790 ± 30 nm, as measured with a DektakXT Stylus profilometer (Bruker, Billerica, MA, USA). A dicing saw (DAD 321 DISCO automatic, Japan) was used to dice the wafers. Each electrode chip has a footprint of 22 x 22 mm and a patterned area of 10 x 10 mm with the same positioning on all the different chip designs. In the patterned area, square openings permeating the carbon layer were designed in order to expose the transparent substrate material (figure 1) and thus to allow light to reach the TMs. Nine different chip designs were fabricated and tested. All chips were oxygen-plasma treated for 3 min using a power of 50 W with a 13.56 MHz RF generator-equipped Atto Plasma System (Diener Electronic, GmbH, Ebhausen, Germany) before performing the electrochemical measurements.

Photosynthetic process

The thylakoid membranes (TMs) were extracted from *Spinacia oleracea* as described elsewhere.[43] The chlorophyll content of the extracts was measured in accordance with literature.[44] The thylakoid membrane solution had a chlorophyll content of 3.2 mg mL^{-1} and it was preserved as deep-frozen aliquots (-80 °C) and thawed before performing the experiments.

A 150W 220 V fiber optic illuminator (Titan Tool Supply, Inc. Buffalo, NY, USA) providing white visible light was used to induce photosynthesis in the TMs. The irradiance was calibrated using a light intensity meter (Techtum Lab AB, Umeå, Sweden) and adjusted to 500 W m^{-2} unless otherwise specified. The TMs were illuminated through the transparent electrode chips (back-side illumination) for all experiments unless otherwise specified.

Electrochemical measurements

$MgCl_2$ was purchased from Scharlau Chemie S.A. NaCl (433209, ≥ 99 %), Hexaammineruthenium (II) chloride (303690, ≥ 99.9 %) and hexaammineruthenium (III) chloride (262005, ≥ 98 %) were purchased from Sigma Aldrich. [Os(2,2′-bipyridine)$_2$-poly(*N*-vinylimidazole)$_{10}$Cl]$^{+/2+}$ was synthesized as previously reported.[45] Millipore water (18.2 MΩ resistivity) was used for preparing all solutions.

Cyclic voltammetry (CV) and chronoamperometry (CA) measurements were performed using a PalmSens potentiostat (EmStat2, Utrecht, The Netherlands) and the PSTrace software in a conventional three-electrode setup. DRIREF-L, a Ag|$AgCl_{sat}$ electrode from WPI (UK) was employed as reference electrode (RE). A Pt wire (500 µm diameter, from Advent research materials, UK) was used as counter electrode (CE). The different electrode chips were interfaced to the potentiostat using copper wires and used as working electrodes (WEs) in a setup designed for these experiments and described in the SI and figure 1. The measurement chamber defines the active electrode footprint area to be 0.5 cm^2. The electrolyte is 10 mM phosphate buffer with 10 mM NaCl and 5 mM $MgCl_2$ (PBS). The electrolyte solution was degassed by purging with nitrogen for at least 10 min before experiments. 1 mM $[Ru(NH_3)_6]Cl_2$/$[Ru(NH_3)_6]Cl_3$ in PBS was used to characterize electrode behavior (SI, **figure S2** and **S3**).

For experiments with TMs and soluble mediator, 3.6 µL TM extract (optimized value, corresponding to 11.5 µg chlorophyll) was first dropcast on the patterned area of the electrode chip (11.5 µg cm^{-2}). After 5 minutes, a dialysis membrane (Spectrum Laboratories Inc., USA, MWCO: 6-8 kDa) presoaked in buffer was added and the chip was immediately assembled in the designed holder. CA was then performed at 0.0 V vs Ag|AgCl in 1 mM $[Ru(NH_3)_6]Cl_3$ in PBS.

For experiments with TMs and osmium-redox-polymer (Os-RP) as mediator, a solution of 10 mg mL^{-1} [Os(2,2′-bipyridine)$_2$-poly(*N*-vinylimidazole)$_{10}$Cl]$^{+/2+}$ (redox potential 220 mV vs Ag|$AgCl_{sat}$) in milli-Q water was first prepared. 15 µL Os-RP solution was deposited onto the

patterned area and allowed to dry at room temperature for 1 h (optimized values for volume and drying time). After that, TMs and dialysis membrane were added in the same way as for experiments with soluble mediator. CA was then performed at 0.22 V vs $Ag|AgCl_{sat}$ in electrolyte solution.

All data presented is based on three independent experiments and the standard deviation is less than 10 %. Baseline correction was used for all chronoamperometric measurements, as described in the SI and shown in **figure S5**. Control experiments without TMs (SI, **figure S6**) were used to ensure the currents reported in this paper are due to the photosynthetic process. Results obtained with full carbon chips in top illumination are shown in the SI (**figure S7**). Maximum current densities are calculated by using the current measured 5 s after the first illumination pulse when using $[Ru(NH_3)_6]Cl_3$ as mediator or 25 s after the first illumination pulse when using Os-RP as mediator.

Calculations

Electrons are generated through photosynthetic reactions on the square surfaces representing the openings in the carbon layer. Thus, at the start of the illumination pulse, the electrons are considered to be uniformly distributed on the openings in the carbon layer.

Electrons transported by the mediators were modeled as non-interacting particles freely diffusing in two dimensions. The probability for an electron to escape the irradiated region where it is generated, during an interval of time, was calculated.

An electron is transferred to the electrode as soon as the mediator transports it to the carbon surface, meaning that it diffuses outside the irradiated region. The current intensity is hence related to the average probability for an electron to reach the boundary during the time interval between the illumination pulse and the measurement of the current intensity peak.

As detailed in the SI, the time-dependent exit probability of a particle in a square surface with absorbing boundaries was used,[46,47] and this parameter was averaged over all starting positions on the square. The average electron exit probability is a function of the size of the

opening, the time interval, and the effective diffusion coefficient of the mediator transporting the electron. Experimental current intensities were fitted to the average electron exit probability.

Supporting Information
Supporting Information is available from the Wiley Online Library or from the author.

Acknowledgements
Nanna Bild is acknowledged for help with graphical design.

Received: ((will be filled in by the editorial staff))
Revised: ((will be filled in by the editorial staff))
Published online: ((will be filled in by the editorial staff))

References

[1] D. R. Bohi, M. B. Zimmerman, *Annu. Rev. Energy* **1984**, *9*, 105.
[2] R. Haas, H. Auer, P. Biermayr, *Energy Build.* **1998**, *27*, 195.
[3] M. Isaac, D. P. van Vuuren, *Energy Policy* **2009**, *37*, 507.
[4] I. Dincer, *Renew. Sustain. Energy Rev.* **2000**, *4*, 157.
[5] S. Bilgen, K. Kaygusuz, A. Sari, *Energy Sources* **2004**, *26*, 1119.
[6] N. L. Panwar, S. C. Kaushik, S. Kothari, *Renew. Sustain. Energy Rev.* **2011**, *15*, 1513.
[7] P.-A. Albertsson, *Photosynth. Res.* **1995**, *46*, 141.
[8] M.-Y. Chen, G.-Y. Zhuo, K.-C. Chen, P.-C. Wu, T.-Y. Hsieh, T.-M. Liu, S.-W. Chu, J. Squier, Y. Huang, H. Lai, S. Chu, *BMC Plant Biol.* **2014**, *175*, 113704.
[9] R. Tel-Vered, I. Willner, *ChemElectroChem* **2014**, *1*, 1778.
[10] O. Yehezkeli, R. Tel-Vered, J. Wasserman, A. Trifonov, D. Michaeli, R. Nechushtai, I. Willner, **2012**, DOI 10.1038/ncomms1741.
[11] A. Efrati, C.-H. Lu, D. Michaeli, R. Nechushtai, S. Alsaoub, W. Schuhmann, I. Willner, *Nat. Energy* **2016**, *1*, 15021.
[12] O. Yehezkeli, R. Tel-Vered, D. Michaeli, I. Willner, R. Nechushtai, *Photosynth. Res.* **2014**, *120*, 71.
[13] G. Pankratova, D. Pankratov, K. Hasan, H.-E. Åkerlund, P.-Å. Albertsson, D. Leech, S. Shleev, L. Gorton, *Adv. Energy Mater.* **2017**, 1602285.
[14] S. Tsujimura, A. Wadano, K. Kano, T. Ikeda, *Enzyme Microb. Technol.* **2001**, *29*, 225.
[15] L. Xiao, E. B. Young, J. A. Berges, Z. He, *Environ. Sci. Technol.* **2012**, *46*, 11459.
[16] P. Bombelli, M. Zarrouati, R. J. Thorne, K. Schneider, S. J. L. Rowden, A. Ali, K. Yunus, P. J. Cameron, A. C. Fisher, D. Ian Wilson, C. J. Howe, A. J. McCormick, *Phys. Chem. Chem. Phys.* **2012**, *14*, 12221.
[17] A. J. McCormick, P. Bombelli, R. W. Bradley, R. Thorne, T. Wenzel, C. J. Howe, *Energy Environ. Sci.* **2015**, *8*, 1092.
[18] E. González-Arribas, O. Aleksejeva, T. Bobrowski, M. D. Toscano, L. Gorton, W. Schuhmann, S. Shleev, *Electrochem. commun.* **2017**, *74*, 9.
[19] K. Hasan, Y. Dilgin, S. C. Emek, M. Tavahodi, H.-E. Åkerlund, P.-Å. Albertsson, L. Gorton, *ChemElectroChem* **2014**, *1*, 131.
[20] H. Hamidi, K. Hasan, S. C. Emek, Y. Dilgin, H.-E. Åkerlund, P.-Å. Albertsson, D.

Leech, L. Gorton, *ChemSusChem* **2015**, *8*, 990.
[21] D. C. Fortunato, Elvira; Ginley, David; Hosono, Hideo; Paine, *MRS Bull.* **2007**, *32*, 242.
[22] K. Ellmer, *Nat. Photonics* **2012**, *6*, 809.
[23] R. I. Pinhassi, D. Kallmann, G. Saper, H. Dotan, A. Linkov, A. Kay, V. Liveanu, G. Schuster, N. Adir, A. Rothschild, *Nat. Commun.* **2016**, DOI 10.1038/ncomms12552.
[24] A. Kumar, C. Zhou, *ACS Nano* **2010**, *4*, 11.
[25] S. Pang, Y. Hernandez, X. Feng, K. Müllen, *Adv. Mater.* **2011**, *23*, 2779.
[26] H. Wu, D. Kong, Z. Ruan, P.-C. Hsu, S. Wang, Z. Yu, T. J. Carney, L. Hu, S. Fan, Y. Cui, *Nat. Nanotechnol.* **2013**, *8*, 421.
[27] X. Wang, L. Zhi, K. Mu, **n.d.**, DOI 10.1021/nl072838r.
[28] G. Wang, L. Zhang, J. Zhang, *Chem. Soc. Rev. Chem. Soc. Rev* **2012**, *41*, 797.
[29] M. Zhou, M. Chi, J. Luo, H. He, T. Jin, *J. Power Sources* **2011**, *196*, 4427.
[30] P. Y. You, S. K. Kamarudin, *Chem. Eng. J.* **2017**, *309*, 489.
[31] R. L. McCreery, *Chem. Rev.* **2008**, *108*, 2646.
[32] A. Singh, J. Jayaram, M. Madou, S. Akbar, *J. Electrochem. Soc.* **2002**, *149*, E78.
[33] N. P. Bansal, R. H. Doremus, *Handbook of Glass Properties*, Academic Press, **1986**.
[34] S. Yamada, H. Sato, *Nature* **1962**, *193*, 261.
[35] L. A. Pesin, *J. Mater. Sci.* **2002**, *37*, 1.
[36] Melis, *Trends Plant Sci.* **1999**, *4*, 130.
[37] J. E. Baur, R. M. Wightman, *J. Electroanal. Chem. Interfacial Electrochem.* **1991**, *305*, 73.
[38] P. G. Pickup, R. W. Murray, *J. Am. Chem. SOC. J. Phys. Chem. J. Electroanal. Chem* **1983**, *105*, 4510.
[39] N. A. Surridge, C. S. Sosnoff, R. Schmehl, J. S. Facci, R. W. Murray, *J. Phys. Chem.* **1994**, *98*, 917.
[40] M. A. Green, K. Emery, Y. Hishikawa, W. Warta, E. D. Dunlop, *Prog. Photovoltaics Res. Appl.* **2015**, *23*, 1.
[41] M. Suri, J. Hofierka, *Trans. GIS* **2004**, *8*, 175.
[42] L. Amato, A. Heiskanen, C. Caviglia, F. Shah, K. Zór, M. Skolimowski, M. Madou, L. Gammelgaard, R. Hansen, E. G. Seiz, M. Ramos, T. R. Moreno, A. Martínez-Serrano, S. S. Keller, J. Emnéus, *Adv. Funct. Mater.* **2014**, *24*, 7042.
[43] E. Andreasson, P. Svensson, C. Weibull, P.-Å. Albertsson, *Biochim. Biophys. Acta - Bioenerg.* **1988**, *936*, 339.
[44] R. J. Porra, W. A. Thompson, P. E. Kriedemann, *Biochim. Biophys. Acta Modem Methods Plant Anal.* **1989**, *975*, 384.
[45] F. Barrière, Y. Ferry, D. Rochefort, D. Leech, *Electrochem. commun.* **2004**, *6*, 237.
[46] R. A. Siegel, R. Langert, *J. Colloid Interface Sci.* **1986**, *109*, 426.
[47] S. Redner, *A Guide to First-Passage Processes*, Cambridge University Press, **2001**.

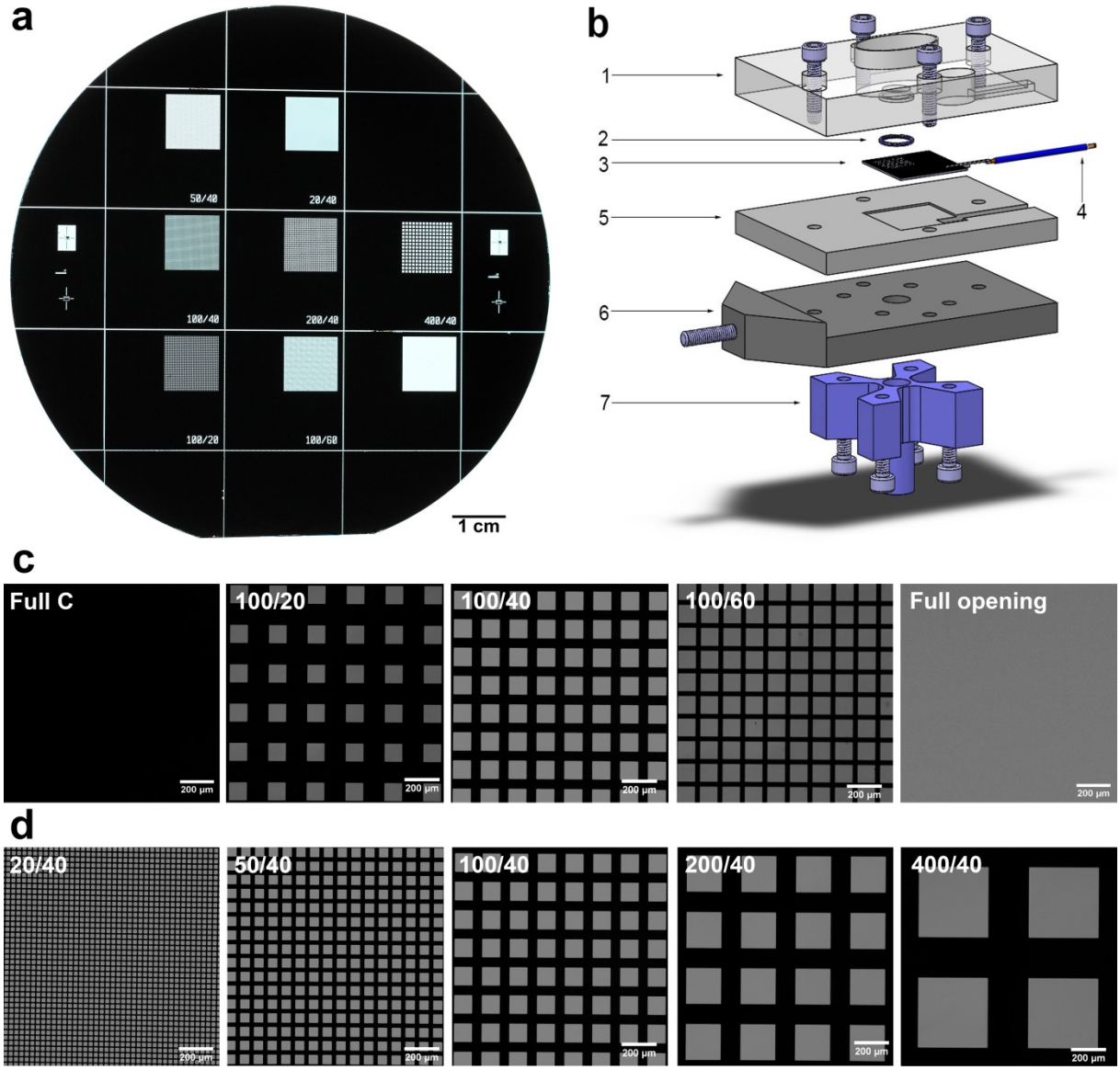

Figure 1: Fused silica wafer with 9 different chip patterns after pyrolysis (a); Holder designed for electrochemistry measurements: 1 – top part, which contains the measurement chamber, space for the connections and the top screws; 2 – o-ring, which ensures the sealing of the measurement chamber; 3 – electrode chip, which serves as working electrode; 4 – wire ensuring electrical connection to the potentiostat; 5 – middle part, containing a pocket for the electrode chip and space for the connections and screws; 6 – metal bottom part, containing holes for screws and for the light source and a lateral connector which allows it to be mounted on a stand; 7 – connector for the light source and its corresponding screws (b); Microscopy images at 5x magnification of 100 µm openings at different densities (c) and of openings of different sizes for a constant transparency of 40 % (d).

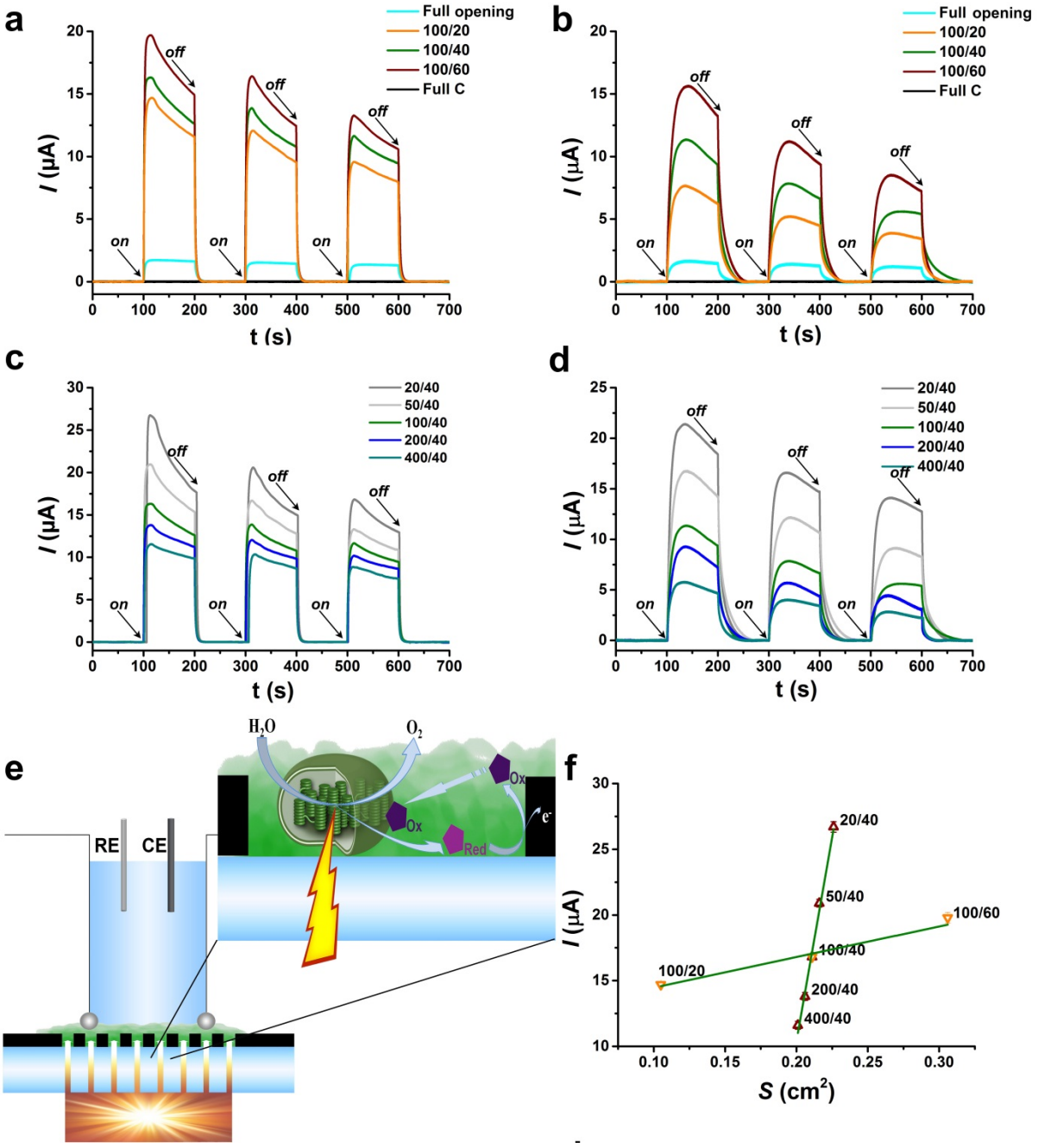

Figure 2: Current-time trace (vs Ag|AgCl) for photocurrent collection from thylakoid membranes using different electrode chip patterns and as mediator 1 mM $[Ru(NH_3)_6]Cl_3$ in PBS (a, c) or Os-redox polymer (b, d). The light source was turned *on* and *off* every 100 s after the first 100 s, as indicated by the arrows; Schematic representation of measurement system and inset showing a schematic of the reactions of interest triggered by illumination of the thylakoid membranes (e); Maximum measured current plotted *vs* the transparent surface area for photocurrent collection from thylakoid membranes using different electrode chip patterns and as mediator 1 mM $[Ru(NH_3)_6]Cl_3$ in PBS (f).

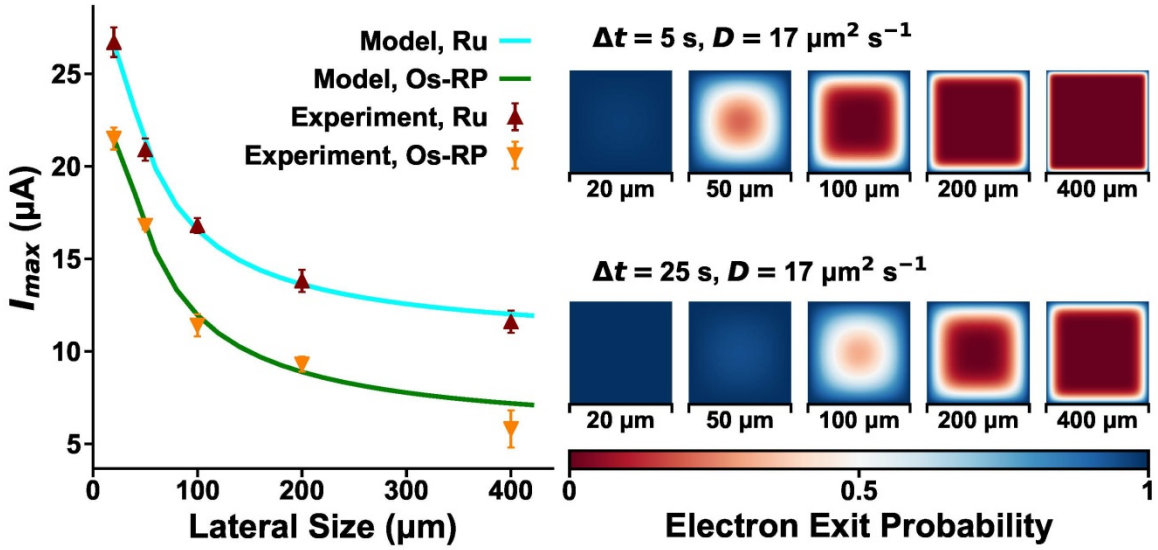

Figure 3: Experimental maximum currents measured with the xx40 series (▲- using $[Ru(NH_3)_6]Cl_3$ as mediator and ▼ – using Os-RP as mediator) and corresponding curves obtained from the model (a); Probability distribution on the surface of an opening for an electron generated in a certain position to reach the carbon electrode (and thus generate current) for two different time intervals, 5 s and 25 s. The diffusion coefficient D = 17 μm s^{-1} was calculated from the diffusion model (b).

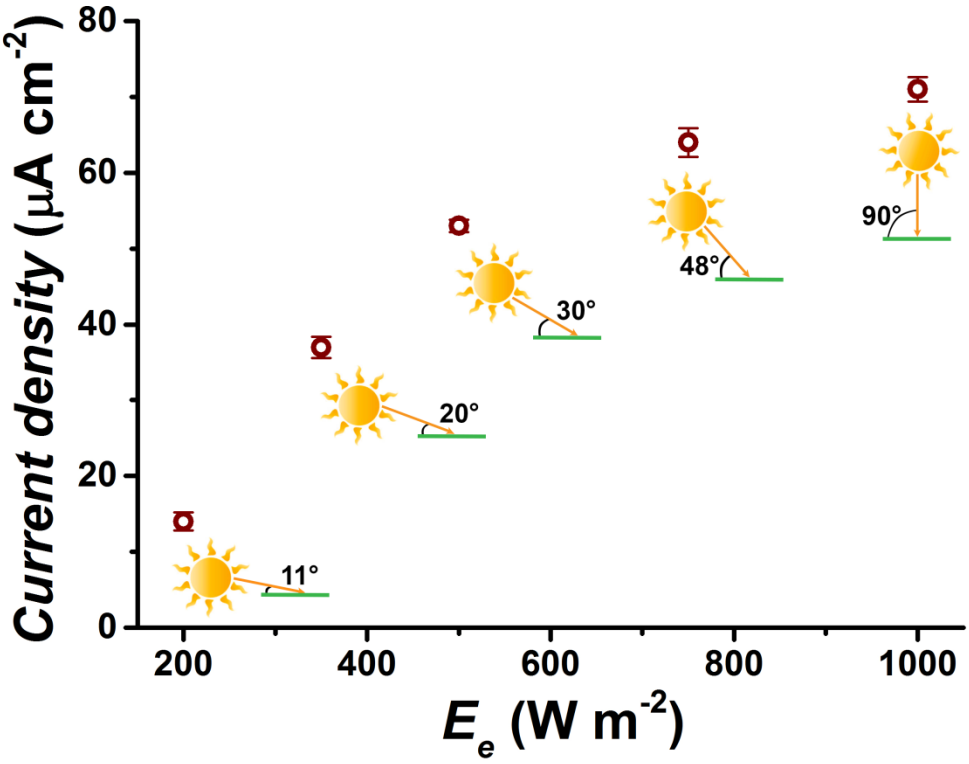

Figure 4: Maximum current density generated from thylakoid membranes as a function of irradiance when using $[Ru(NH_3)_6]Cl_3$ as mediator. Sun drawings show the corresponding incident angle of solar light on a clear day for different irradiance values.

Table 1: Experimental values for maximum currents and current densities measured with the differently-patterned chips. The carbon surface area used for the measurement is specified for every pattern.

Pattern	C area (cm^2)[a)]	I (µA) with TMs + Ru^{3+}	Current density (µA cm^{-2}) with TMs + Ru	I (µA) with TMs + Os-RP	Current density (µA cm^{-2}) with TMs + Os-RP
Full opening	0	1.8 ± 0.2	3.6 ± 0.4	1.6 ± 0.3	3.2 ± 0.6
Full C	0.502	0 ± 0	0 ± 0	0 ± 0	0 ± 0
20/40	0.276	26.7 ± 0.4	53.2 ± 0.8	21.5 ± 0.3	42.8 ± 0.6
50/40	0.286	20.9 ± 0.3	41.6 ± 0.6	16.8 ± 0.1	33.5 ± 0.2
100/40	0.291	16.8 ± 0.2	33.5 ± 0.4	11.4 ± 0.3	22.7 ± 0.6
200/40	0.296	13.8 ± 0.3	27.5 ± 0.6	9.3 ± 0.2	18.5 ± 0.4
400/40	0.301	11.6 ± 0.3	23.1 ± 0.4	5.8 ± 0.5	11.6 ± 1
100/20	0.397	14.7 ± 0.2	29.3 ± 0.4	7.8 ± 0.2	15.5 ± 0.4
100/60	0.196	19.8 ± 0.4	39.4 ± 0.8	15.6 ± 0.3	31.1 ± 0.6

a) The total surface area in contact with the electrolyte is constant, with a value of 0.5 cm^2.

Transparent electrode chips made of patterned carbon on quartz are employed for photocurrent generation from thylakoid membranes using back-side illumination. A maximum current density of 71 µA cm^{-2} is reported. The electrode chips are robust and easy to fabricate in a scalable process. The electrode chips can be employed as large-surface bioanodes, which represents a significant step towards energy conversion applications.

Photocurrent

A.-I. Bunea, A. Heiskanen, G. Pankratova, G. Tesei, M. Lund, H.-. Åkerlund, D. Leech, S. Sylvest Keller, N. Bent Larsen, L. Gorton and J. Emnéus*

Transparent, Carbon-based Electrode Chips for Enhanced Photocurrent Generation from Thylakoid Membranes

ToC ffigure:

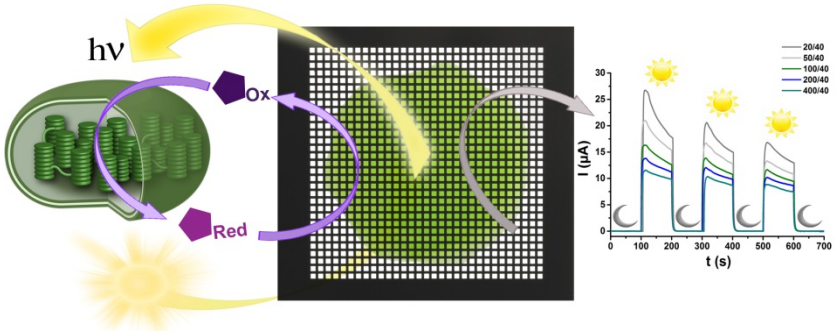

Supporting Information

Transparent, Carbon-based Electrode Chips for Enhanced Photocurrent Generation from Thylakoid Membranes

Ada-Ioana Bunea, Arto Heiskanen, Galina Pankratova, Giulio Tesei, Mikael Lund, Hans-Erik Åkerlund, Dónal Leech, Niels Bent Larsen, Stephan Sylvest Keller, Lo Gorton and Jenny Emnéus*

S1. Fabrication of the measurement holder

The components of the electrochemical measurement setup shown in **figure S1** were machined using a computer-numerically-controlled (CNC) Mini-Mill/3Pro micromilling system (Minitech Machinery Corporation, Norcross, GA, USA) by executing G-code generated by EZ-CAM17 Express software (EZCAM Solutions, Inc., New York, NY, USA) based on Autocad drawings (Autocad 2016 from Autodesk Inc., San Rafael, CA, USA). The following materials were used for fabrication of the components: 15 mm polycarbonate (Bayer MaterialScience AG, Leverkusen, Germany) for the top part (1) containing the oval measurement chamber (major/minor radius: 12.5/7.5 mm; opening to the electrode chip: Ø 8 mm; height of the oval chamber: 11.7 mm); 5 mm poly(methyl methacrylate) (Röchling Technische Teile KG, Mainburg, Germany) for the middle part (5) containing the pocket for the electrode chip; 10 mm aluminum for the metal bottom (6) supporting the assembly of the of the electrochemical cell; 31 mm Teflon® (supplied by Linatex A/S, Herlev, Denmark) for the connector of the light source (7). The O-ring (inner/outer Ø 8/10 mm) for sealing the measurement chamber was cut from 1 mm thick transparent RCT®SH-40 silicon sheet (Reichelt Chemietechnik GmbH, Heidelberg, Germany) using an Epilog Mini CO_2 laser system (Epilog Laser, Golden, CO, USA).

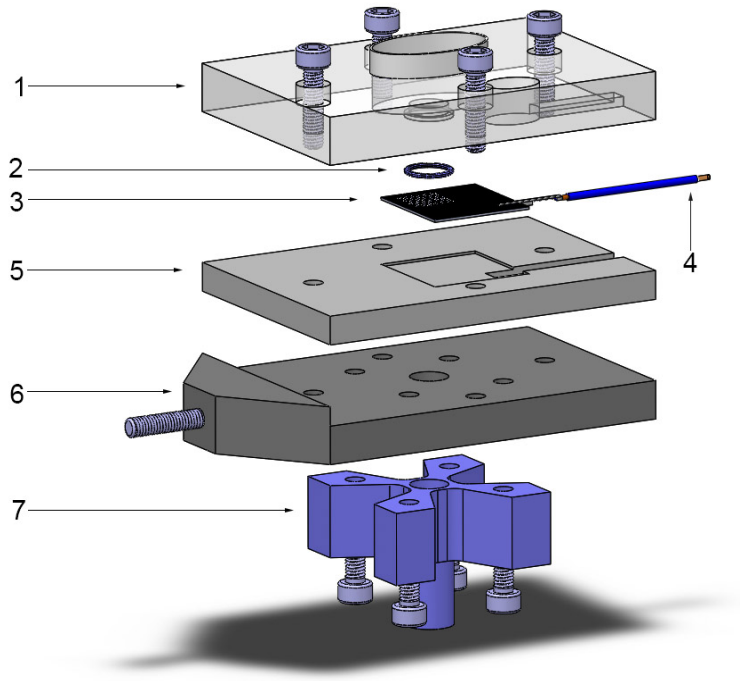

Figure S1: Exploded view of the holder used in the electrochemical measurements.

S2. Characterization of electrode chips using cyclic voltammetry

The electrode chips were characterized using cyclic voltammetry in $[Ru(NH_3)_6]^{2+/3+}$, a reliable outer-sphere redox system[2] widely used for the characterization of carbon electrodes[3]. **Figure S2 a** shows voltammograms recorded using different electrode chip patterns at a scan rate of 10 mV s^{-1}. The anodic peak intensity varies by less than 20 % between different chip patterns and by less than 10 % for 3 chips of the same pattern.

Figure S2 b shows voltammograms recorded using a 20/40 chip and scan rates between 10 and 150 mV s^{-1}. At a scan rate of 10 mV s^{-1}, ΔE_p (the separation between the anodic and cathodic peak) is 93 mV. ΔE_p increases with increasing scan rates.

[2] R. L. McCreery, *Chem. Rev.* **2008**, *108*, 2646' P. Chen, M. A. Fryling, R. L. McCreery, *Anal. Chem.* **1995**, *67*, 3115.

[3] M. A. Guillorn, T. E. McKnight, A. Melechko, V. I. Merkulov, P. F. Britt, D. W. Austin, D. H. Lowndes, M. L. Simpson, *J. Appl. Phys.* **2002**, *91*, 3824; C. H. An Wong, A. Ambrosi, M. Pumera, *Nanoscale* **2012**, *4*, 4972.

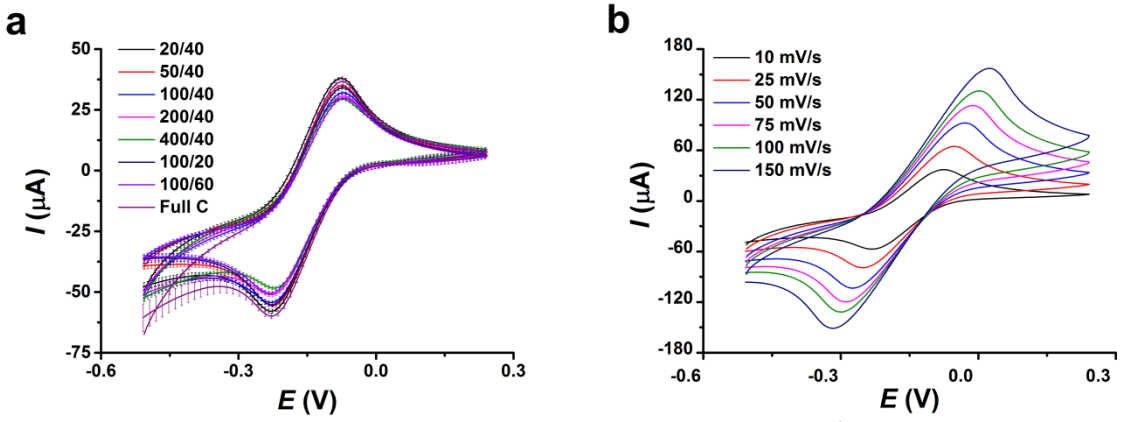

Figure S2: Average results from cyclic voltammetry using different chip patterns in 1 mM $[Ru(NH_3)_6]^{2+/3+}$ at a scan rate of 10 mV s^{-1} (a); Voltammograms obtained with a 20/40 electrode chip in 1 mM $[Ru(NH_3)_6]^{2+/3+}$ at scan rates between 10 and 150 mV s^{-1} (b). E vs Ag|AgCl.

The influence of the presence of the thylakoid dispersion on the electrode was investigated using cyclic voltammetry. It is clear from **Figure S3** that the thylakoid membrane dispersion functions as a passivation layer on the electrode surface, leading to a faradaic current decrease. The anodic peak intensity decreases from 44.5 ± 0.1 µA (in the absence of TMs) to 31.3 ± 0.4 µA (in the presence of TMs).

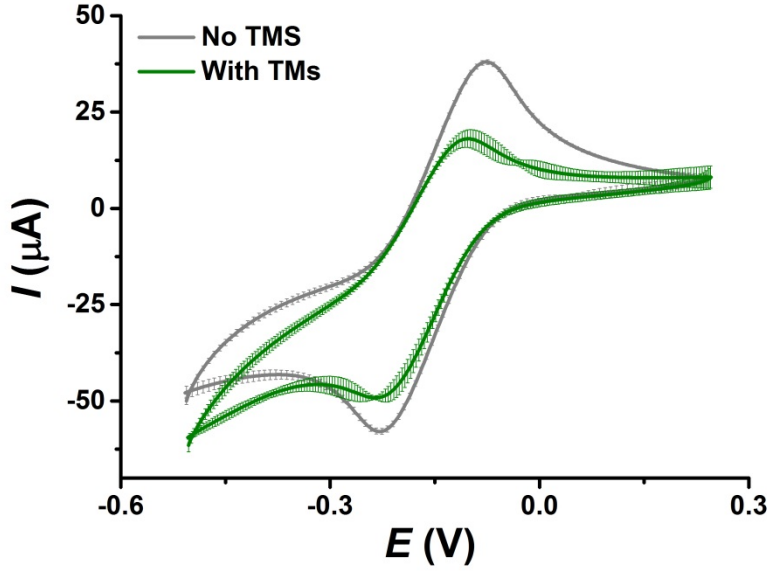

Figure S3: Average results from cyclic voltammetry using 2/40 electrode chips in 1 mM $[Ru(NH_3)_6]^{2+/3+}$ at a scan rate of 10 mV s^{-1} with and without thylakoid membranes on the electrode. The system was protected from light during the measurements. E vs Ag|AgCl.

S3. Irradiance measurements

The irradiance of the lamp was measured in air, through the holder and through chips with different patterns. The lamp was set to supply 500 W m^{-2} (measured through the holder), corresponding to 505 W m^{-2} measured in air (1 % dampening). **Figure S4** shows the correlation between the measured irradiance and the transparent surface area percentages of different chips. As expected, the light passing through the chips is directly proportional to the transparent surface area. The slope of the linear regression shows an average loss in irradiance of less than 3% from the initial set value of 500 W m^{-2}.

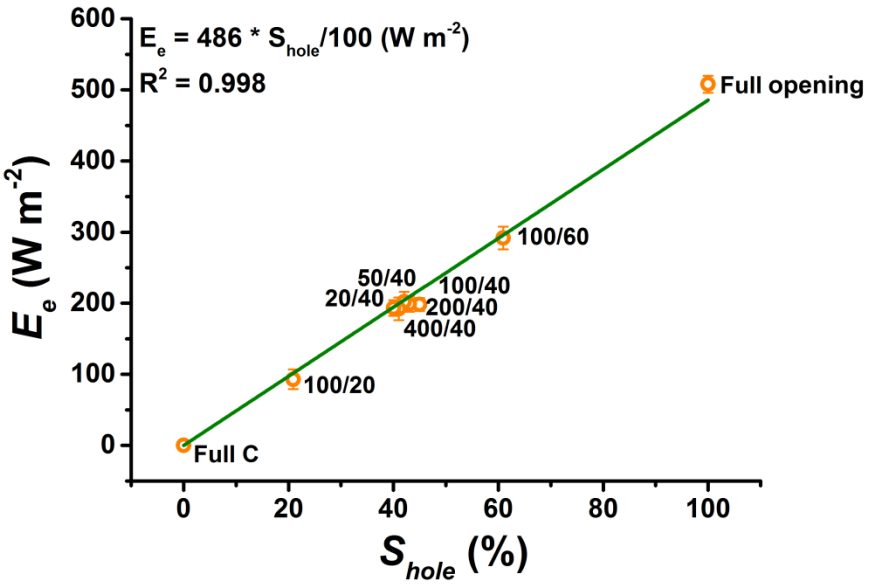

Figure S4: Irradiance measured in the experimental setup through chips with different patterns *vs* the transparent surface area percentage.

S4. Baseline correction

All chronoamperometric measurements were baseline-corrected using the OriginPro 9 software (OriginLab Corporation). The baseline was manually defined by selecting raw data values obtained in the absence of light (while the lamp was turned *off*). The baseline was then subtracted from the raw data. **Figure S5** shows the raw data, the baseline and the data after baseline correction for one chronoamperometric measurement using a 20/40 electrode chip.

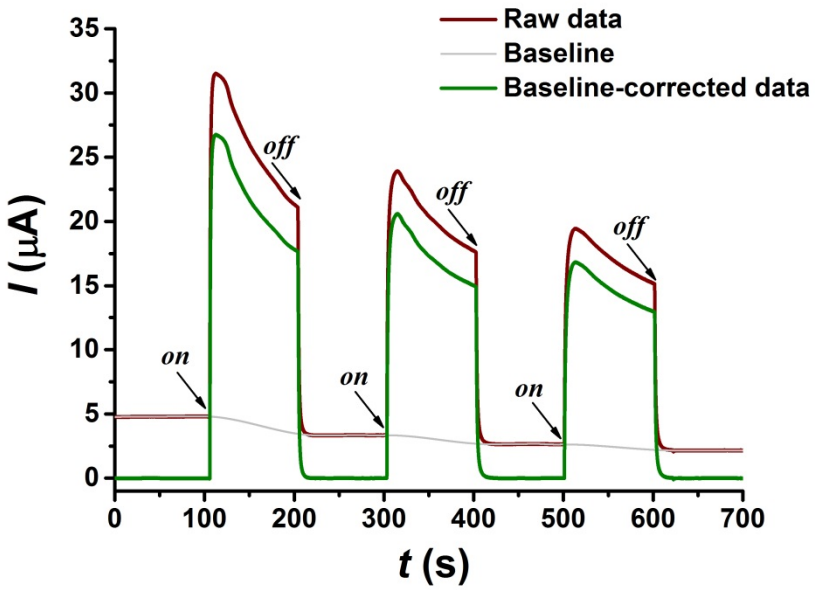

Figure S5: Current-time trace (vs Ag|AgCl) for photocurrent collection from thylakoid membranes using a 20/40 electrode chip and as mediator 1 mM $[Ru(NH_3)_6]Cl_3$ in PBS. Raw data, the baseline and baseline-corrected data is shown. The light source was turned *on* and *off* every 100 s after the first 100 s, as indicated by the arrows.

S5. Control experiments without thylakoid membranes

Control chronoamperometry experiments without thylakoid membranes (TMs) were performed. As shown in **figure S6**, a negative current peak (< 0.5 µA) is measured when the light source is turned *on* in the absence of TMs. This could be attributed to a slight change of temperature in the system upon illumination.

Since control experiments do not show a current increase in the presence of light, the positive current peak from measurements with TMs can be attributed to photocurrent collection.

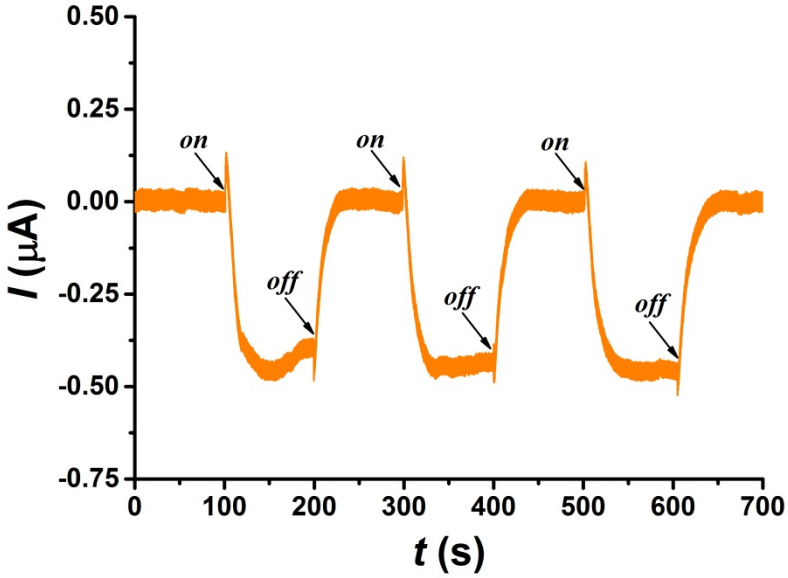

Figure S6: Current-time trace (vs Ag|AgCl) for photocurrent collection in the absence thylakoid membranes (control experiment) using a 20/40 electrode chip and as mediator 1 mM $[Ru(NH_3)_6]Cl_3$ in PBS. The light source was turned *on* and *off* every 100 s after the first 100 s, as indicated by the arrows.

S6. Experiments with top-side illumination

Photocurrent generation from TMs was recorded using 20/40 chips in top-side illumination mode using $[Ru(NH_3)_6]Cl_3$ in PBS as mediator (**figure S7**). The light source was positioned to illuminate the top of the chip, and the measurement setup was otherwise unaltered. A maximum current of 45.2 ± 0.5 µA was measured, ~ 1.7 times higher than in back-side illumination mode. However, since the chip is only 40% transparent, top-side illumination leads to an increase of 2.5 times in the surface area exposed to light. The discrepancy could be connected to the diffusion of the soluble mediator through the viscous TM layer.

It can also be implied from figure S5 that the photo-induced damage is more severe when the chip is illuminated from the top (the current decreases faster).

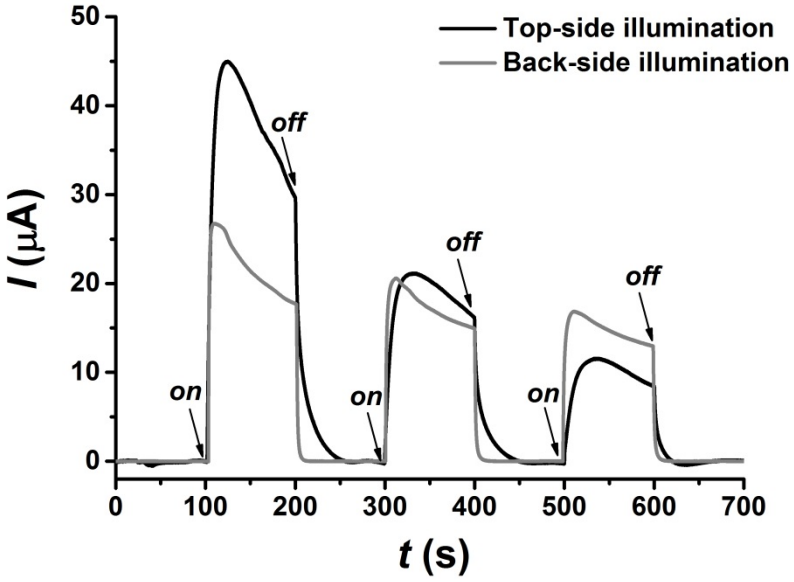

Figure S7: Current-time trace (vs Ag|AgCl) for photocurrent collection from thylakoid membranes in top-side and back-side illumination mode, using a 20/40 electrode chip and as mediator 1 mM $[Ru(NH_3)_6]Cl_3$ in PBS. The light source was turned *on* and *off* every 100 s after the first 100 s, as indicated by the arrows.

S7. Calculations – the diffusion model

At t = 0 we assume the generated electrons to be uniformly distributed within a square surface of area $A = L^2$. We calculate the probability that during a time interval Δt an electron has reached the sides of the square, given that it is absorbed the first time it hits the boundary of the region. We use the analytical expression of the exit probability for freely diffusing particles within a square with absorbing boundaries.[4] For a particle located at (x_0, y_0) at t = 0, the exit probability at $t = \Delta t$ is given by equation S1.

[4] R. A. Siegel, R. Langert, *J. Colloid Interface Sci.* **1986**, *109*, 426.

$$P\left(x_0, y_{0,}\, L, \Delta t, D\right) =$$

$$= \frac{16}{\pi^2} \times \left[\sum_{n=0}^{n=\infty} \frac{(-1)^n}{2n+1} exp\left(-(2n+1)^2\pi^2 \frac{\Delta t D}{L^2}\right) \cos\left(\frac{(2n+1)\pi x_0}{L}\right)\right]$$

$$\times \left[\sum_{n=0}^{n=\infty} \frac{(-1)^n}{2n+1} exp\left(-(2n+1)^2\pi^2 \frac{\Delta t D}{L^2}\right) \cos\left(\frac{(2n+1)\pi x y_0}{L}\right)\right]$$

Equation S1.

P (x_0, y_0, L, Δt, D) is integrated over the uniform electron distribution of the electrons generated at t = 0 to obtain the average exit probability (equation S2).

$$\bar{P}(L, \Delta t, D) = \frac{1}{L^2} \int_{x_0=-L/2}^{x_0=L/2} dx_0 \times \int_{x_0=-L/2}^{x_0=L/2} dy_0 \times P(x_0, y_0, L, \Delta t, D)$$

Equation S2.

The maximum current measured using the chip, I_{max} (L), is related to the average exit probability as shown in equation S3:

$$I_{max}(L, \Delta t, D, m, n) = m \times \bar{P}(L, \Delta t, D) + q$$

Equation S3

Where $\Delta t \times D$, *m*, and *q* are fitting parameters. The experimental current values for the devices with the two mediators (Ru complex and Os redox polymer) are fitted to I_{max} (L, Δt, D, m, n). We obtain m ≈ 16 μA and Δt × D ≈ 100 μm^2 for both data sets, whereas *q* is 10.3 ± 0.5 μA for the Ru complex and 5 ± 1 μA for the Os redox polymer.

The fact that *m* has approximately the same value for both mediators suggests that *m* could be related to Ne/Δt, where N is the number of electrons transported in the system, and e ≈ 1.602 × 10^{-19} C is the elementary charge. The time-independent parameter *q* largely differs between the Os redox polymer and $[Ru(NH_3)_6]Cl_3$, indicating that its value is affected by the efficiency of transfer from the thylakoid membrane to the mediator, or from the mediator to the electrode.

A Jupyter Notebook (to reproduce calculations and Figure 3) is available as SI in native as well as HTML format.

Appendix III: Patent application

Pyrolysed optical waveguides as optoelectrical scaffolds for cell replacement therapy and energy applications

Jenny Emnéus, Ada-Ioana Bunea, Stephan Sylvest Keller, Anders Kristensen and Arto Heiskanen

Optoelectric Scaffold for Photo-Responsive Biological Components

FIELD

An optoelectric scaffold holding photo-responsive biological components and a method of producing the optoelectric scaffold are provided.

BACKGROUND

Recent developments in the field of carbon electrode technologies in the microscale have shown that microscale conductive carbon electrodes are particularly useful as scaffolds for cultivating biological cells thereon and at the same time perform electrochemical experiments on the cells, e.g. for detecting and monitoring biological activity. For example, recent studies show that microscale patterned conductive carbon electrodes made of pyrolysed SU-8 photoresist can be used to promote differentiation of human neural stem cells towards dopaminergic cells and monitor the stimulated release of dopamine, see e.g. Amato et al. (2014) “Pyrolysed 3D-Carbon Scaffolds Induce Spontaneous Differentiation of Human Neural Stem Cells and Facilitate Real-Time Dopamine Detection”, Adv. Funct. Mater., 24: 7042–7052.

SUMMARY

It is an important merit of the optoelectric scaffold disclosed below that recent achievements in the field of microscale conductive electrodes have been developed further for use in combination with photo-responsive biological components in order to synergistically facilitate the practical application of photo-responsive biological components.

Indeed, numerous efforts have been made to harness photo-responsive biological components for a large range of applications spanning as wide as from medical applications to energy applications.

However, one challenge in this context is providing a viable concept for the infrastructure combining in one device a viable support for immobilising or cultivating the biological components to be harnessed as well as optical access and good electrical contact to the immobilised or cultivated biological components.

Therefore, it is an object of the present invention to provide a viable concept that may easily be adapted to provide the necessary infrastructure for the practical application of photo-responsive biological components within fields of application as different from each other as medical applications and energy applications.

According to a first aspect, the object is fulfilled by an optoelectric scaffold for accommodating photo-responsive biological components, wherein the scaffold comprises an optical waveguide configured for confining light propagating in a longitudinal direction thereof. The optical waveguide comprises at least one leaky section configured for enhanced emission of light in a direction transverse or lateral to the longitudinal direction of the optical waveguide. The optical waveguide further comprises an electrically conductive layer arranged on an outer surface of the optical waveguide. The electrically conductive layer has a support surface for accommodating the photo-responsive biological components and transparent regions at least partially overlapping the at least one leaky section for transmission of light to biological components when accommodated at the support surface.

The electrically conductive layer should be made of a material that provides a biocompatible support surface. Biocompatibility is here to be understood as compatibility with respect to the photo-responsive biological components for which the optical scaffold is designed. The term ‘biocompatible’ thus refers to the quality of not having toxic or injurious effects on the biological elements/components/systems in question.

Within the context of the present application, the terms “optical” and “light”, without any further specification, relate to electromagnetic radiation including the UV, visible and infrared regions, in particular near infrared. The terms “optical” and “light” may thus refer to wavelengths in the range above 100 nm, above 200 nm, above 300 nm and up to 1 µm, up to 2 µm or up to 3 µm, wherein the visible range of the spectrum in agreement with common definitions is considered to range from about 400 nm to about 700 nm. The term “photo” denotes phenomena related to the conversion of light with a certain spectral specificity, i.e. occurring within a relevant spectral range as determined by the respective phenomenon.

Throughout the present disclosure, the term “biological component” denotes one or more biological cells of one or more types of biological cells; or, one or more parts of biological cells.

Biological cells include single celled or multicellular living organisms, such as microorganisms, mammalian cells, e.g. mesenchymal stem cells, or neural stem cells, or other cells capable of, possibly having been modified to be capable of, producing and releasing a substance beneficial for the treatment of a disease, etc.

Parts of biological cells include enzymes, proteins, membranes, such as thylakoid membranes, etc., organelles, such as chloroplasts, etc., etc.

A photo-responsive biological component is a biological component that provides a response to light incident upon it.

A scaffold for accommodating photo-responsive biological components is hereby provided that yields both optical and electrical access to the biological components. In particular, an optoelectrical configuration is provided, where photo-responsive biological components accommodated at the support surface of the scaffold, can be illuminated from the side facing the optical waveguide, and at the same time can be contacted electrically via the conductive layer making up the support. Simultaneously, the biological components accommodated at the support surface can be exposed to a predefined environment, e.g. in an electrochemical set-up, if desired.

Regarding the term “enhanced”, the emission of light in a direction transverse or lateral to the longitudinal direction within each of the at least one leaky section, in the following denoted “leaky emission”, is enhanced as compared e.g. to remaining “non-leaky” sections of the optical waveguide. Alternatively or in addition thereto, the leaky emission from the optical waveguide may be enhanced within a given spectral region for leaky emission (one or more leaky bands) as compared to the transverse or lateral loss of light for waveguide modes in spectral ranges outside the given spectral region for leaky emission. The electrically conductive layer comprises one or more transparent regions at least partially overlapping the at least one leaky

section both spatially and spectrally, thereby allowing for the transmission of light that is coupled into the optical waveguide for propagation in the longitudinal direction, that is leaked at the at least one leaky section in transverse or lateral directions through the one or more transparent regions to photo-responsive biological components accommodated at the support surface.

Advantageously according to some embodiments, the electrically conductive layer may be a conductive carbon layer, e.g. a layer made by pyrolysing a layer of polymer resulting in a layer of pyrolytic carbon; a layer of a conducting polymer; a layer of a polymer made conductive by inclusion of conductive nanoparticles, such as carbon nanoparticles, etc.; a layer including graphene, etc.; As further detailed below, a conductive carbon layer has advantages with respect to its generally good biocompatibility, and with respect to producing micro-structured regions that at the same time provide a support surface for the biological components, optical access through the layer for illuminating the biological components “from behind”, and an efficient collection of any photo-induced electrical response.

Advantageously according to some embodiments the leaky emission of light in transverse or lateral directions of the optical waveguide is achieved e.g. by so-called “leaky modes” which have an enhanced emission in transverse or lateral directions as compared to guided or confined modes. Alternatively, or additionally, leaky emission in the at least one leaky section may be provided by partial or complete removal of the cladding, internal modification of the waveguide properties, roughening of the waveguide surface, e.g. by etching, etc., etc. Furthermore, the at least one leaky section provides enhanced emission in transverse or lateral directions at least within a first spectral band. Accordingly, the transparent region of the electrically conductive layer must be transparent at least for sub-bands within the one or more spectral bands with leaky emission in order to allow for transfer of light to the support surface and further to any photo-responsive biological components thereon. Furthermore, the spectral characteristics of the delivered light needs to allow for stimulating the desired photo-response of the photo-responsive biological components. Preferably, the spectral characteristics of the at least one leaky section and the spectral characteristics of the transparency of the transparent regions of the electrically conductive layer and the spectral characteristics of the

photo-response of the biological components are matched such that respective sub-bands of enhanced leakage, transparency, and photo-response at least overlap. Preferably, these spectral characteristics are matched to optimize the photo-response with respect to the light input. Optimizing criteria may depend on the respective application and can be derived accordingly. For example, in a power conversion application intended for converting input light power into electrical energy an optimizing criterion may be derived as maximizing the electrical energy output with respect to the light input power by maximizing the integrated spectral overlap of the leaked light power, of the transmission through the electrically conductive layer, and of the release of electrons from a given photo-responsive biological component for photoelectric conversion. To give another non-limiting example, optimization criteria may be set up for adapting the spectral characteristics of a light signal delivered at the support surface to maximize its overlap with spectral characteristics for the photo-responsive release by the cultivated biological component of a substance beneficial for the treatment of a disease.

Light is coupled into the optical waveguide at one end and propagates along the optical waveguide to a leaky section of the at least one leaky section. In each leaky section of the at least one leaky section, light is emitted in directions transverse or lateral to the longitudinal direction of the waveguide and reaches the electrically conductive layer. The electrically conductive layer is arranged on the outside of the waveguide, at least partially covering the at least one leaky section. The electrically conductive layer has an inwardly facing interface with the optical waveguide oriented towards the waveguide, and an exposed surface facing away towards the surroundings. The exposed surface is adapted to accommodate the biological components and for example act as immobilisation or growth support surface for the biological components. The electrically conductive layer comprises transparent regions overlapping one or more or all leaky sections of the at least one leaky section. The electrically conductive layer may in itself be transparent to light at least within one or more relevant spectral sub-bands of the light. Alternatively or in addition thereto, the transparent regions may be formed by a thinning of the electrically conductive layer, by a perforation of the electrically conductive layer and or by a nano- and/or microscale structuring of the electrically conductive layer. The term “transparent” should be interpreted as allowing a substantial portion of light

within a given wavelength band entering the leaky section to propagate through a transparent region of the transparent regions from the leaky section in question in a direction lateral or transversal to the direction of propagation of the light at entry to the leaky section in question.

At least 5%, at least 10%, at least 20%, at least 30%, at least 40%, at least 50%, at least 60%, at least 70%, at least 80%, or at least 90%, of light in the wavelength band entering the at least one leaky section is transmitted through the transparent regions of the electrically conductive layer from the at least one leaky section in a direction lateral or transversal to the direction of propagation of the light at entry to the leaky section in question. The light emitted from the one or more or all leaky sections of the at least one leaky section and transmitted through the transparent regions of the electrically conductive layer can then finally couple to photo-responsive biological components accommodated, e.g. immobilised or cultivated, at the exposed surface of the electrically conductive layer.

The exposed surface delimits the electrically conductive layer material and thereby defines an interface of the electrically conductive layer opposite to the interface of the electrically conductive layer with the optical waveguide. The exposed surface may have any suitable form. To provide some non-limiting examples, the exposed surface may be smooth, it may define a uniform layer thickness of the electrically conductive layer with respect to the interface with the optical waveguide, it may be patterned with a two-dimensional nano- and/or microscale pattern, it may be porous, it may comprise quasi three-dimensional structures, e.g. pillars projecting outwardly with respect to the optical waveguide, it may be formed by a truly three dimensional microscale structure including multiple levels, it may be a microscale foam-like structure, e.g. of the open cell type, or it may be a suitable combination thereof.

A quasi three-dimensional micro-structuring of the support surface can be advantageous e.g. for an improved cultivation of cells and/or an improved electrical interaction of the biological components, and/or any substance released therefrom, with the electrically conductive layer for collecting electrical signal and/or power. A particularly improved enhancement of these effects is conceived for truly three-dimensional microstructures including vertical structures that are laterally

interconnected at different levels, thereby defining truly three-dimensional multi-level structures. In a cylindrical geometry of e.g. an optical fibre, vertical can be mapped to radial coordinates, whereas lateral directions can be mapped to angular and circumferential and axial directions, wherein axial directions are parallel to the longitudinal axis of the optical fibre. In a planar geometry waveguide, a vertical direction is to be understood as perpendicular to a plane defined by the waveguide, whereas lateral directions are to be understood as perpendicular to the vertical direction, i.e. parallel to said waveguide plane. A three-dimensional micro-structuring may also be useful for a differentiation into specific cell types, such as cells adapted for the release of a particular neurotransmitter, such as dopamine. A two- or three-dimensional micro-structuring and/or patterning may also be conceived for improving the optical coupling and transfer of light from the optical waveguide to biological components accommodated, e.g. immobilised or grown, on the exposed surface of the electrically conductive layer.

The optical configuration allows for delivering and coupling light through the optical waveguide to the photo-responsive biological component; the electrical configuration allows for collecting electrical signals and/or electrical power from the biological components provided in response to light, and allows for electrical stimulation of the biological components, e.g. for stimulation of growth and/or cell differentiation; and the configuration of the support surface as an exposed surface allows for bringing biological components, e.g. immobilised or cultivated thereon, in contact with a desired biochemical and/or electrochemical environment.

Further according to one embodiment of the optoelectric scaffold, the electrically conductive layer is a conductive carbon layer in the form of a pyrolysed polymer film. Thereby, a conductive carbon layer can be fabricated in a reliable and cost-effective manner, which in addition is particularly useful and advantageous for growing cells thereon, for performing electrochemical measurements and/or for using the optoelectric scaffold as part of an electrode in an electrochemical system.

Furthermore it has surprisingly turned out that optical fibres coated with a conductive carbon layer made of a pyrolysed polymer film remain surprisingly flexible without damaging the integrity of the electrically conductive layer and apparently without

affecting the favourable conductive properties of the electrically conductive carbon layer obtained by pyrolysing the polymer film.

The polymer may be a natural or a synthetic polymer, and advantageously, the polymer is a radiation-sensitive resist, such as a SU-8-based resist.

Further advantageously, the polymer film, e.g. a photoresist, may be patterned prior to pyrolysis so as to define a microscale structuring and/or texturing of the electrically conductive layer. Most preferably, the radiation sensitive resist is adapted for patterning by optical pattern transfer techniques, such as photolithography or mask-less optical pattern transfer techniques.

Further advantageously, the microscale structuring may be a three-dimensional structure enhancing and/or favouring the cultivation and/or differentiation of stem cells. Thereby an improved specific adaption of the photo-responsive biological component to a specific application, such as tailoring the photo-response of the biological component towards the (enhanced) release of a specific substance, may be achieved. Furthermore, an enhanced collection of electrical signals for monitoring cell activity, such as monitoring dopamine release may be achieved.

Further according to one embodiment of the optoelectric scaffold the electrically conductive layer may have a thickness ranging from 200 nm to 10 µm. An increased thickness of the electrically conductive layer may improve the conductivity of the electrically conductive layer, while a reduced thickness may facilitate formation of the transparent regions. Accordingly, the skilled person is instructed to strike a balance of transparency and conductivity when selecting the thickness of the conductive electrically conductive layer, wherein the above cited lower and upper limits of the electrically conductive layer thickness are conceived to provide an advantageous or at least useful regime.

Advantageously according to some embodiments a compromise of transparency and conductivity may be obtained by selectively thinning the electrically conductive layer only within leaky sections of the waveguide. Alternatively or in addition thereto, transparency may be enhanced by a microscale structuring of the electrically

conductive layer comprising openings (or thinned regions) arranged in a pattern that favours electrical conduction in an axial direction parallel to the longitudinal axis of the optical waveguide, and/or a nanoscale patterning that provides for an enhanced transmission of light in transverse or lateral directions while otherwise maintaining a material thickness sufficient for the required electrical conductivity. Also here, such microscale and/or nanoscale patterning may be restrained to the leaky sections of the optical waveguide and to favour electrical conductivity of the electrically conductive layer in the remaining regions.

The optical waveguide may comprise photonic crystals. Thereby, an increased flexibility of design is achieved for adapting the optical waveguide to particular applications. In particular, the leaky sections may be tailored and engineered more flexibly with respect to their optical characteristics, such as with respect to their spectral characteristics.

The optical waveguide may be a photonic crystal waveguide.

The optical waveguide may be an optical fibre. Optical fibres allow for a relatively cheap and easy fabrication of the waveguide. Optical fibres are particularly useful e.g. for applications where only a very narrow access channel is available and/or where large mechanical flexibility is required for both the optical and electrical access path. As further detailed below, embodiments using an optical fibre as optical waveguide are therefore conceived as particularly useful as part of an implantable device. As mentioned above, an optoelectrical scaffold that is surprisingly robust with respect to bending is obtained by the combination of an optical fibre coated with a pyrolysed polymer film forming the electrically conductive carbon layer.

However, embodiments of the optoelectric scaffold using an optical fibre may also be particularly useful and advantageous for other applications, such as power conversion applications, since a bundled arrangement of many optical fibre-based optoelectrical scaffolds in parallel can provide large interfacial areas for instance for cultivating microbial cultures of photo-sensitive microorganisms, for illuminating these microbial cultures from one side and yet provide a large interfacial area for

contacting an environment, such as an electrochemical environment of a bio-photovoltaic fuel cell. Embodiments of the optoelectric scaffold based on optical fibres as optical waveguide are therefore also highly scalable.

The optical waveguide may be a photonic crystal fibre.

According to a second aspect, the object of the invention is fulfilled by an optoelectric device comprising an optoelectric scaffold according to any of the above embodiments, the device further comprising photo-responsive biological components accommodated, e.g. immobilised or cultivated, at the support surface, wherein the photo-responsive biological components are in electrical contact with the electrically conductive layer, and wherein the photo-responsive biological components are arranged to receive light from the optical waveguide at the at least one leaky section, through the transparent regions of the electrically conductive layer material.

According to some embodiments of an optoelectric device for bio-photonic applications, the optoelectric scaffold carries biological components at the support surface, wherein the biological components are in optical communication with the leaky section of the optical fibre as described above, and wherein the biological components are in electrical communication with the electrically conductive layer as also described above.

A non-limiting example of photo-responsive biological components are biological components that are responsive to light, such as opto-genetically modified dopaminergic human neural stem cells that are adapted to release dopamine upon illumination with light, wherein the exocytosis of dopamine can be monitored as an electrochemical signal using the electrically conductive layer as an electrode.

Another non-limiting example of photo-responsive biological components are biological components that are responsive to light, e.g. for converting light into electrical energy, such as photo-synthetically active microorganisms like cyanobacteria or algae, or components of these such as thylakoid membranes or chloroplasts from plant cells.

In any case, as also mentioned above, the spectral characteristics of light having propagated through the optical waveguide and transparent regions of the electrically conductive layer is preferably adapted or matched to the spectral response of the photo-sensitive biological components in order to maximize their response.

Further according to one embodiment of the optoelectric device, the photo-responsive biological components are adapted for the photo-stimulated release of a substance beneficial for the treatment of a disease. Thereby a device is provided that is useful for performing an optically controlled release of the beneficial substance from the biological component for therapeutic applications. Accordingly, the release of the beneficial substance can be stimulated by light coupled into the optical waveguide.

Further according to one embodiment of the optoelectric device the photo-responsive biological components are stem cells, such as human stem cells, such as human mesenchymal stem cells, human neural stem cells, etc. Stem cells may be differentiated and adapted for the release of certain beneficial substances.

The stem cells may be obtained from any suitable source. In the case of human stem cells it should be noted, that the use of human embryonic stem cells may equivalently be substituted by the use of stem cells derived from other sources of precursor cells, i.e. by any appropriate alternative means known in the art. For example, Ernest Arenas et al. (Development, 2015, 142, 1918-1936 doi:10.1242/dev.097394) as well as Andrzej Swistowski et al. (Stem Cells 2010;28:1893–1904) describe ways to obtain midbrain dopaminergic neurons by differentiating cells that are not embryonic stem cells.

According to some embodiments, the differentiation can be induced e.g. by means of a surface structuring of the support surface or by electrical stimuli using the conductive properties of the optoelectric device. Thereby a specific device, such as an implantable device for the optically controlled release of a specific substance that is beneficial for treating a specific disease may be provided.

Further according to one embodiment of the optoelectric device the beneficial substance is a neurotransmitter, such as dopamine. Thereby, a device is provided that is useful for the treatment of neurological disorders that can be linked to a neurotransmitter deficiency, such as Parkinson's disease or epilepsy.

The optoelectric device may be an implantable device, and the optoelectric device may be particularly useful as an implantable device for the production, release, and delivery of therapeutic substances in a user. An implantable device with functional cells placed on a transparent carbon-based electrode applied to the outside of a leaky section of an optical fibre allows for directly stimulating the release of the beneficial substance from a cell culture by illumination through transparent regions of the conductive support surface, wherein the support surface simultaneously can be used for in-situ monitoring the release by electrochemical detection or measurement. In particular, an implantable device for the controlled release of neurotransmitters can be provided.

The implantable device may be adapted for cell replacement therapy in the brain of a mammal, such as a human being.

The photo-responsive biological components may be photosynthetic microorganisms, such as cyanobacteria, or algae. The optoelectric device with photosynthetic microorganisms arranged at the support surface is e.g. useful as an anode for a microbial photovoltaic system. Advantageous examples of photosynthetic microorganisms are cyanobacteria or algae. However, any biological component susceptible to the photosynthetic conversion of light input power, such as solar light, to electrical energy may be conceived for this function.

According to a third aspect, the object of the invention is achieved by a method of fabricating an optoelectric device as defined in the following, with the analogue advantages and effects as described above.

According to some embodiments, the method comprises the steps of: providing an optical waveguide configured for confining light propagating in a longitudinal direction thereof; providing a leaky section of the optical waveguide, wherein the

leaky section is configured for enhanced emission of light in a direction transverse or lateral to the longitudinal direction of the optical waveguide; coating the optical waveguide with an electrically conductive layer having a support surface for accommodating photo-responsive biological components and having transparent regions at least partially overlapping the leaky section for transmission of light to the photo-responsive biological components when accommodated at the support surface.

The step of coating may comprise pyrolysing a polymer layer to obtain an electrically conductive carbon layer with a surface adapted to act as the support surface, e.g. an immobilisation or growth support surface, configured to support photo-responsive components thereon, wherein the electrically conductive layer is at least partially transparent so as to allow for light from the leaky section of the optical waveguide to reach the support surface of the electrically conductive layer. The leaky section allows for an enhanced emission of light in a direction transverse or lateral to the longitudinal direction of the optical waveguide at least within one or more spectral bands, which may be referred to as one or more leaky bands.

Further according to one embodiment, the method further comprises the step of: patterning the polymer coating with a microscale pattern, prior to pyrolysing the polymer coating. The pattern may be applied e.g. using state of the art microscale pattern transfer techniques. Alternatively or in addition thereto, according to some embodiments, the method comprises steps of patterning the polymer coating with a nano-scale pattern, prior to pyrolysing the polymer coating.

Further according to one embodiment of the method the optical waveguide is an optical fibre.

Further according to one embodiment the method further comprises the step of: immobilising or cultivating a biological component of photo-responsive biological components on the surface. Preferably said photo-responsive biological components are responsive at least to radiation within the one or more leaky bands.

BRIEF DESCRIPTION OF THE DRAWINGS

Preferred embodiments of the invention will be described in more detail in connection with the appended drawings, which show in

Fig. 1A-D schematically steps of fabricating an optoelectric scaffold and an optoelectric device according to some embodiments of the invention, wherein Figs.1C and 1D show schematically embodiments of an optoelectric scaffold and an optoelectric device, respectively;

Fig. 2 schematically, a personalized treatment system comprising an implantable device according to one embodiment of the invention;

Fig. 3 schematically, an anode assembly for use in a bio-photovoltaic system;

Fig. 4 schematically, a bio-photovoltaic system with an anode assembly comprising optoelectrical devices according to some embodiments;

Fig. 5 a graph with cyclic voltammograms using an optical fibre with an electrically conductive carbon layer of pyrolysed polymer film;

Fig. 6 a graph with current traces generated when illuminating photo-responsive biological elements through a micro-structured electrically conductive carbon layer carrying the biological elements; and in

Fig. 7 a further graph with current traces generated when illuminating photo-responsive biological elements through a micro-structured electrically conductive carbon layer carrying the biological elements.

DETAILED DESCRIPTION

Referring to Figs.1A-D, steps of fabricating an optoelectric scaffold and an optoelectric device according to some embodiments of the invention are illustrated. In Fig.1A an optical waveguide 101 is provided in the form of an optical fibre. The optical fibre is configured for confining light for propagation in an axial direction Z

along a longitudinal direction of the fibre as indicated by the broken line. The optical waveguide 101 is further provided with a leaky section 102 allowing for an enhanced emission of light through a peripheral surface of the optical waveguide 101, in directions transverse or lateral of the optical waveguide 101, i.e. here in directions comprising a radial component perpendicular to the axial direction Z. The emission, or loss, of light from the leaky section 102 of the optical waveguide 101 is enhanced as e.g. compared to non-leaky sections 103 of the optical waveguide 101. In Fig.1B, at least the leaky section 102 of the optical waveguide 101 is coated with an organic polymer layer 104, e.g. a photosensitive resist as commonly used in microfabrication, such as an SU-8 based resist. The polymer layer 104 may optionally be provided with a nano- or microscale structure, and may further optionally be processed to form a three-dimensional structure (not shown). Techniques of micro-fabricating three-dimensional structures for subsequent pyrolysis in order to form immobilisation or growth support for biological components made of conductive carbon are e.g. disclosed in the co-pending European patent application EP 15186066. Fig.1C shows an embodiment of an optoelectric scaffold 100 with an electrically conductive carbon layer 105 arranged to at least overlap the leaky section 102 of the optical waveguide 101. The electrically conductive carbon layer 105 is here formed as a pyrolysed polymer layer, which is obtained after pyrolysis of the polymer coating 104 on the optical fibre 101. Fig.1D shows an embodiment of an optoelectric device 110, which has been obtained by cultivating a microbial culture of photo-responsive biological component 111 on an exposed surface of the electrically conductive carbon layer 105 acting as a growth support surface for the microorganisms 111. Light may be coupled into the optical waveguide 101 at a distal end thereof (not seen in Fig.1D), may then be guided along the longitudinal direction Z to the leaky section 102 of the optical waveguide with the electrically conductive carbon layer 105 thereon. The electrically conductive carbon layer 105 is at least partially transparent so as to allow for light from the leaky section 102 of the optical fibre to reach the growth support surface of the electrically conductive carbon layer 105, which carries the photo-sensitive biological components 111. In this way, a large amount of photo-sensitive biological components distributed over a relatively large surface area as compared to a cross-sectional footprint of the optoelectric device 110, or as compared to the device volume required, may thus be stimulated by a light input provided and controlled

remotely from the biological component. Also, multiple optoelectric devices 110 may easily be bundled without compromising the optical access to the microorganisms 111. At the same time, the electrically conductive carbon layer 105 can be used for monitoring the electrochemical environment and/or any activity of the biological components 111, such as monitoring optically stimulated exocytosis of certain substances. Monitoring may be performed by e.g. electrochemical measurements, such as voltammetry, using the optoelectric device 110 as an electrode of the monitoring set-up.

Fig. 2 illustrates schematically a personalized treatment system including an optoelectric device 200 configured for implantation in a user 99. The implantable device 200 comprises an optoelectric scaffold 100 with an optical fibre 101 having a leaky section 102. The leaky section 102 may comprise a microscale structuring providing an enhanced emission in transverse or lateral directions in a particular spectral range, such as a photonic band-gap structure as indicated in inset “A” in Fig.2. the leaky section 102 is at least partially covered by a conductive carbon electrode 105 made of a pyrolysed polymer film, which may e.g. comprise a three-dimensional microscale structuring, as indicated in inset “C” of Fig.2, acting as a functionalised scaffold for growing photo-responsive microorganisms 111 thereon, such as human neural stem cells. The three-dimensional structuring may improve cultivation, interconnectivity and/or electrical interaction between the biological component and the electrically conductive carbon layer. The micro-scale structuring may further be designed to promote differentiation of stem cells cultivated thereon. The photo-responsive biological components 111 may be adapted to produce a certain neurotransmitter, such as dopamine, and may be photo-responsive by promoting exocytosis of the neurotransmitter upon stimulation with a photonic signal as illustrated by the inset “B” in Fig.2. The photonic stimulation may be controlled by a control unit 201 of the personalized treatment system communicating with the implantable device 200, e.g. via a cabled or wire-less communication link 202. The control unit 201 may comprise a user interface displaying measurement results indicative of a disposition or condition of the user 99, and the personalized treatment of such condition may be in response to user input and/or controlled by programmed routines or algorithms for the automated or semi-automated treatment according to personalized parameters. Furthermore, the personalized treatment may be in

response to the measurement results indicative of a disposition or condition of the user 99 input to or received by the control unit 201. According to some embodiments, the implantable device 200 of the personalized treatment system may include measurement means adapted for providing measurements of indicative of a disposition or condition of the user 99, wherein the measurements may be provided as monitoring data in a regular or periodic manner and/or upon an external request, e.g. in reply to a user 99 initiated request and/or a programmed request from the control unit 201.

Figs. 3 and 4 show an alternative use of the optoelectric scaffold according to some embodiments of the invention in a bio-photovoltaic application. Fig. 3 shows schematically an anode arrangement 300, which is configured for use in a bio-photovoltaic system, such as the one illustrated in Fig.4. The anode 300 has a multitude of optoelectric devices 310 arranged in a bundle with a distal end arranged for receiving solar energy. Each of the optoelectric devices comprises an optoelectric scaffold made of an optical fibre with a long leaky section covered by a transparent electrically conductive carbon layer, preferably made of a pyrolysed polymer. The electrically conductive carbon layer carries on exposed surfaces thereof a culture of photo-synthetically active microorganisms, such as cyanobacteria or algae, as the photo-responsive microorganisms. The microorganisms are in electrical contact with the electrically conductive carbon layer, which in turn is electrically connectable to an external circuit to provide electrons to an electrical load (indicated as 330; not shown). The optoelectric anode 300 can thus collect light ($h\nu$) and guide that light to the inside of the anode, where it is gradually transferred in radial directions via leaky sections of the optical fibres to the photo-responsive microorganisms on the surface of the transparent conductive carbon coating. At the same time, the optoelectric anode 300 can, via the electrically conductive carbon layer, provide harvested electrons to a contact lead connectable to an external electric load 330.

Fig. 4 illustrates schematically a bio-photovoltaic system 400 useful for the conversion of light $h\nu$ into electrical power (e-) by means of photo-synthetically driven hydrolysis. The system comprises an anode 410 and a cathode 420

immersed in an aquatic medium, and electrically connected externally via an electric load 430.

The anode 410 is advantageously configured as the anode 300 described above with reference to Fig.3. Light ($h\nu$), typically sunlight, is coupled into an optical input end of the anode 410 and transferred to photo-synthetically active microorganisms 411 on growth surfaces of the electrically conductive carbon layers of the optoelectric scaffolds, here indicated as cyanobacteria (CYAN). In response to the light power received via the optical waveguide, the microorganisms 411 perform photosynthesis, inducing oxygen along with excess electrons. The excess electrons are collected by the anode 410, via external electrical circuitry the electrons are provided to the electric load 430, and further to the cathode 420, which donates electrons to reverse the hydrolysis reaction in an oxidation-reduction reaction with oxygen as the electron acceptor. The cathode reaction is typically catalysed by means of a metal such as platinum, either the cathode being a metal electrode itself or a metal deposited on the cathode. Alternatively, or additionally, enzymes are placed on the surface of the cathode to act as catalysts. Advantageously in the later case, the cathode 420 has a conductive carbon surface carrying an enzyme that catalyses an oxidation-reduction reaction, such as laccase (LAC as shown in Fig.4)) or bilirubin oxidase (BOx not shown in the figure). The conductive carbon substrate material of the cathode may be made of e.g. pyrolysed polymer, which further advantageously may be micro-structured to increase surface area and enhance electrical connectivity and external electron exchange between the enzyme and the conductive carbon substrate material.

Fig. 5 shows cyclic traces as obtained by voltammetry in ruthenium hexamine II/III using an optical fibre coated with a pyrolysed polymer film as an anode with sweep rates of 25 mV/s, 50 mV/s, and 100 mV/s, respectively.

Figs. 6 and 7 show by way of example different graphs with current traces obtained by illuminating photo-responsive biological elements accommodated on an electrically conductive layer and measuring the electrical response in a potentiostat set-up using the electrically conductive layer with the biological components thereon as a working electrode. In the present example, the photo-sensitive biological

components are thylakoid membranes, and the electrically conductive layer is a micro-structrured electrically conductive carbon layer. In the present example, the carbon layer has been produced by pyrolysing a micro-structured template of a precursor polymer layer carried on the front-side of a transparent quartz glass substrate. Here, the obtained pyrolysed carbon material is essentially opaque, but is made at least partially transparent by microscale openings produced by means of conventional photolithographic patterning of the precursor template prior to pyrolisation. A thylakoid membrane extract is distributed on the patterned surface of the pyrolysed carbon layer, allowed to gelify (by drying for 5 min), and then the carbon layer is electrically connected to the potentiostat to form the working electrode. The photo-responsive biological components are then illuminated “from behind”, i.e. through the electrically conductive layer accommodating the biological components by guiding light to the back side of the quartz substrate in the region of the patterned surface. The light will thus reach the photo-responsive systems on the supporting surface of the electrically conductive layer. In the present example, a soluble mediator, ruthenium III hexamine chloride, has been used to shuttle electrons between the thylakoids and the electrode surface.

The graphs shown in Figs. 6 and 7 show a clearly photo-induced current of the photo-responsive biological components in response to illumination through the conductive carrier layer accommodating the biological components.

The illuminating light was switched ON and OFF every 100 seconds. There is a clear current response when the light is turned on. When the light is turned off, the system stops producing current. The actual intensity of the response somewhat depends on the pattern coverage as indicated by the different traces 601-605 in Fig.6 and 701-705 in Fig.7. In all cases of the present example, the microscale patterning is a uniformly distributed arrangement of holes separated from each other by continuous lines of the conductive material. The holes provide optical access through the electrically conductive layer for illuminating the photo-responsive biological components thereon, and the continuous lines of the conductive material form a network of electrical leads for the collection of electrical current generated in response to the illumination.

Note that the pyrolysed carbon material forming the electrically conductive layer of the present example is actually opaque, but has successfully been made sufficiently transparent by providing a microscale pattern of openings, yet ensuring an efficient current collection. The example of Figs. 6 and 7 thus also illustrates that the invention can even be exercised using an otherwise opaque electrically conductive layer as a support for accommodating the photo-responsive biological components, as long as the opaque layer comprises transparent regions, e.g. provided in the form of a pattern with microscale openings.

Table 1 summarizes the particular geometry parameters of the patterns used for producing the traces 601-605 in Fig.6. and Table 2 summarizes the corresponding geometry parameters for traces 701-705 in Fig.7. The holes are square shaped and hole sizes are given as the side length of the squares in micrometres. Hole-coverage is the fraction in percent of the patterned area covered by holes. Carbon coverage is the complementary fraction in percent of the patterned area covered by the electrically conductive material made of SU8-derived pyrolysed carbon. The electrochemical measurements were performed on samples with an active patterned area of about 8mm in diameter as delimited by an O-ring.

Table 1

Trace	hole size / µm	hole coverage / %	carbon coverage / %
601	20	40	60
602	50	40	60
603	100	40	60
604	200	40	60
605	400	40	60

Table 2

Trace	hole size / µm	hole coverage / %	carbon coverage / %
701	Full hole	100	0
702	100	20	80
703	100	40	60
704	100	60	40
705	Full C	0	100

Generally speaking, microscale openings in an otherwise opaque conductive layer can advantageously be used as one means of providing sufficient transparency for illuminating the photo-responsive biological elements from behind, i.e. through the conductive layer acting as a support.

While the actual shape of the openings is subordinate, the scale of the microstructure plays a role. For a given fraction of uncovered area (40% in Fig.6), a microstructure with smaller dimensions of the openings is apparently better for an efficient current collection. Also, as evident from Fig.7, for given hole dimensions (100µm square holes in Fig.7) an increased fraction of opening apparently increases the photo-induced response as more and more light reaches the photo-responsive biological components as long as an efficient current collection can be performed. An upper limit is illustrated in the limit of “full hole coverage” in trace 701, i.e. where no material of the electrically conductive material remains in the patterned area for collecting current. The remaining photo-response is here carried through the photo-responsive biological components, i.e. here through the applied layer of gelified thylakoid membrane extract. The reference measurement (trace 705) with full coverage of the electrically conductive material shows that the material used here, i.e. the pyrolysed carbon layer, is apparently opaque. No significant photo-response is detected in this case (trace 705).

Advantageously the openings have a cross-sectional dimension of less than and up to 500µm, less than and up to 200µm, less than and up to 100µm, less than or up to 50µm, or less than and up to 20µm. Further advantageously, the hole coverage is at least 10%, at least 20%, at least 40%, or at least 60%. Further advantageously, the hole coverage is less than and up to 90%, or less than and up to 80%.

CLAIMS

1. Optoelectric scaffold for accommodating photo-responsive biological components, the scaffold comprising an optical waveguide configured for confining light propagating in a longitudinal direction thereof, the optical waveguide comprising:

   at least one leaky section configured for supporting leaky modes with an enhanced emission of light in a direction transverse or lateral to the longitudinal direction of the optical waveguide as compared to guided or confined modes;

   and

   a biocompatible electrically conductive layer arranged on an outer surface of the optical waveguide, the electrically conductive layer having

   - a support surface configured for accommodating photo-responsive biological components, and
   - transparent regions at least partially overlapping the at least one leaky section for transmission of light to photo-responsive biological components when accommodated at the support surface.

2. Optoelectric scaffold according to claim 1, wherein the electrically conductive layer comprises an electrically conductive carbon layer.

3. Optoelectric scaffold according to any of the preceding claims, wherein the electrically conductive layer is a pyrolysed polymer film.

4. Optoelectric scaffold according to any of the preceding claims, wherein the optical waveguide is an optical fibre.

5. Optoelectric scaffold according to any of the preceding claims, wherein the optical waveguide comprises photonic crystals.

6. Optoelectric device comprising an optoelectric scaffold according to any of the preceding claims, the device further comprising photo-responsive biological components accommodated at the support surface, wherein the photo-

responsive biological components are in electrical contact with the electrically conductive layer, and wherein the photo-responsive biological components are arranged to receive light from the optical waveguide at the at least one leaky section, through the transparent regions of the electrically conductive material.

7. Optoelectric device according to claim 6, wherein the photo-responsive biological components are adapted for the photo-stimulated release of a substance beneficial for the treatment of a disease.

8. Optoelectric device according to any one of claims 6-7, wherein the photo-responsive biological components comprise stem cells.

9. Optoelectric device according to claim 8, wherein the stem cells are not human embryonic stem cells.

10. Optoelectric device according to any one of claims 7-9, wherein the beneficial substance comprises a neurotransmitter, or therapeutic factors, for neuromodulation, neuroprotection and/or neuroregeneration.

11. Optoelectric device according to any one of claims 7-10, wherein the beneficial substance comprises dopamine.

12. Optoelectric device according to claim 6, wherein the photo-responsive biological components comprise photosynthetic microorganisms.

13. Optoelectric device according to any one of claim 6 or claim 12, wherein the photo-responsive biological components comprise cyanobacteria or algae, or photo responsive components or organelles of microorganisms.

14. Optoelectric device according to any one of claim 6, claim 12, or claim 13, wherein the photo-responsive biological components comprise proteins, bacteriorhodopsin, thylakoid membranes, or chloroplasts.

15. Optoelectric device according to any one of claims 6-14, wherein the optoelectric device is an implantable device.

16. A personalized treatment system comprising an optoelectric device according to claim 15, and a control unit adapted to communicate with the optoelectric device.

17. Method of fabricating an optoelectric device, the method comprising the steps of

- providing an optical waveguide configured for confining light propagating in a longitudinal direction thereof,
- providing a leaky section of the optical waveguide, wherein the leaky section is configured for supporting leaky modes with an enhanced emission of light in a direction lateral to the longitudinal direction of the optical waveguide as compared to guided or confined modes;
- coating the optical waveguide with a biocompatible electrically conductive layer, the electrically conductive layer having a support surface for accommodating photo-responsive biological components and having transparent regions at least partially overlapping the leaky section for transmission of light to photo-responsive biological components when accommodated at the support surface.

18. Method according to claim 17, wherein the electrically conductive layer comprises an electrically conductive carbon layer.

19. Method according to claim 18, wherein the step of coating comprises

- pyrolysing a polymer layer to obtain the electrically conductive carbon layer with a surface adapted to act as the support surface.

20. Method according to claim 19, further comprising the step of

- patterning the polymer layer with a microscale pattern, prior to pyrolysing the polymer layer.

21. Method according to any one of claims 17-20, further comprising the step of
    - immobilising or cultivating photo-responsive biological components at the support surface.

22. Method according to claim 21, wherein the photo-responsive biological components are adapted for the photo-stimulated release of a substance beneficial for the treatment of a disease.

23. Method according to any one of claims 21-22, wherein the photo-responsive biological components comprise stem cells.

24. Method according to claim 23, wherein the stem cells are not human embryonic stem cells.

25. Method according to any one of claims 22-24, wherein the beneficial substance comprises a neurotransmitter, or therapeutic factors, for neuromodulation, neuroprotection and/or neuroregeneration.

26. Method according to any one of claims 22-25, wherein the beneficial substance comprises dopamine.

27. Method according to claim 21, wherein the photo-responsive biological components comprise photosynthetic microorganisms.

28. Method according to any one of claim 21 or claim 27, wherein the photo-responsive biological components comprise cyanobacteria or algae.

29. Method according to any one of claim 21, claim 27, or claim 28, wherein the photo-responsive biological components comprise cyanobacteria or algae, or photo responsive components or organelles of microorganisms.

30. Method according to any one of claim 21, claim 27, claim 28, or claim 29, wherein the photo-responsive biological components comprise proteins, bacteriorhodopsin, thylakoid membranes, or chloroplasts.

ABSTRACT

According to one aspect, an optoelectric scaffold for accommodating photo-responsive biological components is provided. The scaffold comprises an optical waveguide configured for confining light propagating in a longitudinal direction thereof. The optical waveguide comprises at least one leaky section with enhanced emission of light in a direction transverse or lateral to the longitudinal direction. The scaffold further comprises an electrically conductive layer arranged on an outer surface of the optical waveguide, wherein the electrically conductive layer has an immobilisation or growth support surface for the immobilisation or cultivation of photo-responsive biological components thereon. The electrically conductive layer comprises transparent regions at least partially overlapping the leaky section. The transparent region is configured so as to transmit light from the leaky section of the waveguide to the immobilisation and/or growth support surface. According to a further aspect, an optoelectric device comprises an optoelectric scaffold and a photo-responsive biological component arranged on the immobilisation/growth support surface. The growth support surface is arranged so as to transmit light received from the leaky section of the optical waveguide to the biological component placed thereon.

Fig.1

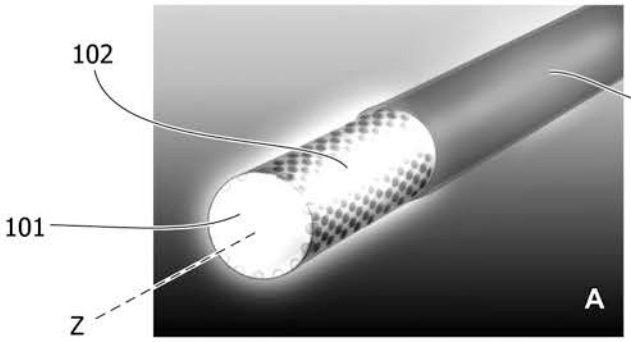

Fig. 1A

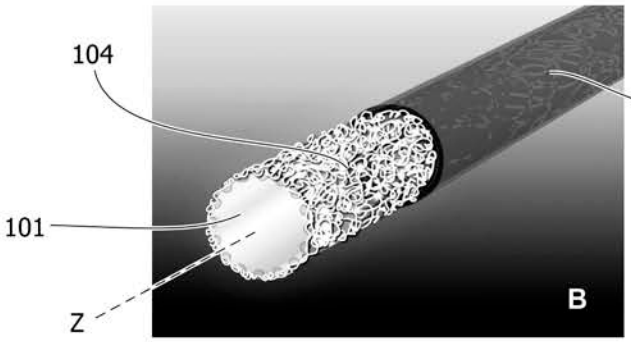

Fig. 1B

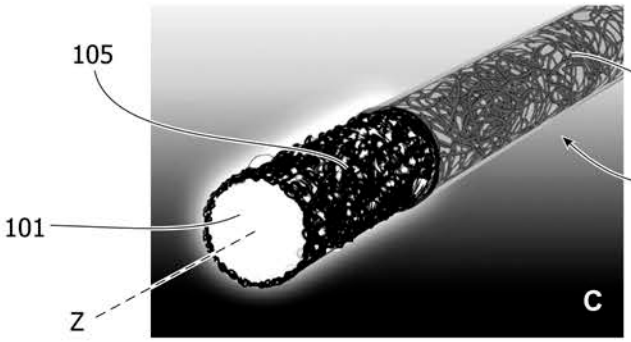

Fig. 1C

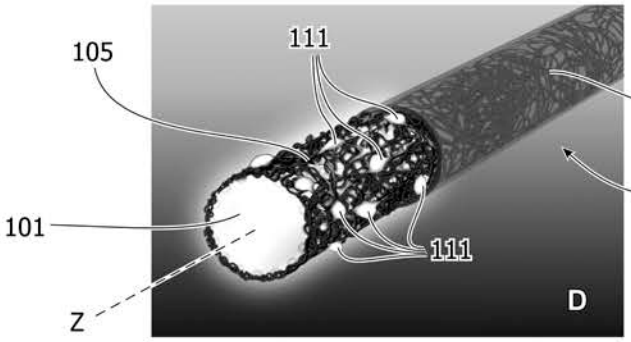

Fig. 1D

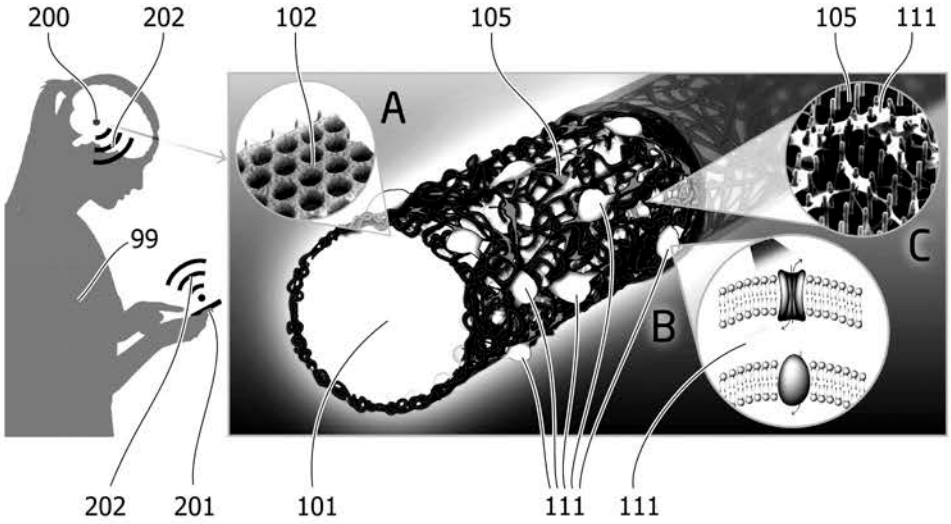
200
202
102
105
105
111
A
99
B
C
202
201
101
111
111

Fig. 2

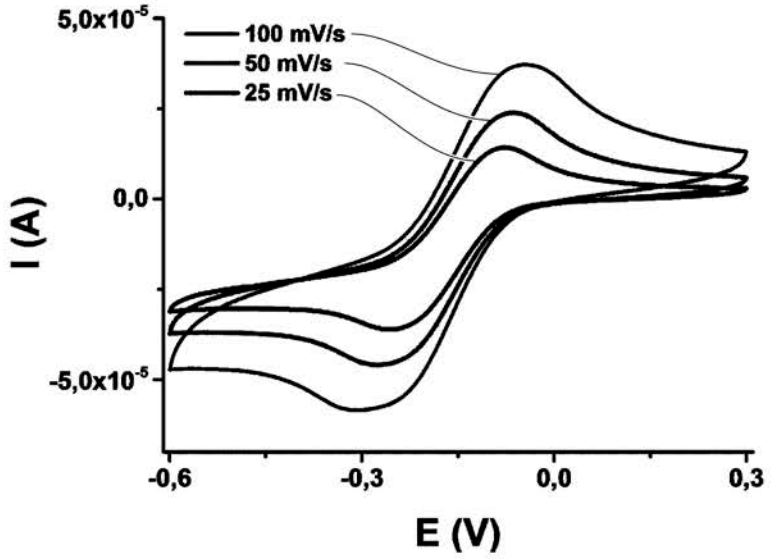
5,0x10-5
100 mV/s
50 mV/s
25 mV/s
0,0
I (A)
-5,0x10-5
-0,6
-0,3
0,0
0,3
E (V)

Fig. 5

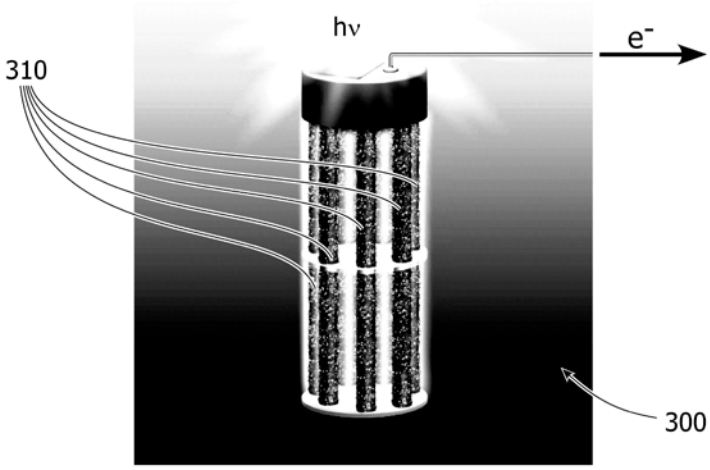
hν
e-
310
300

Fig. 3

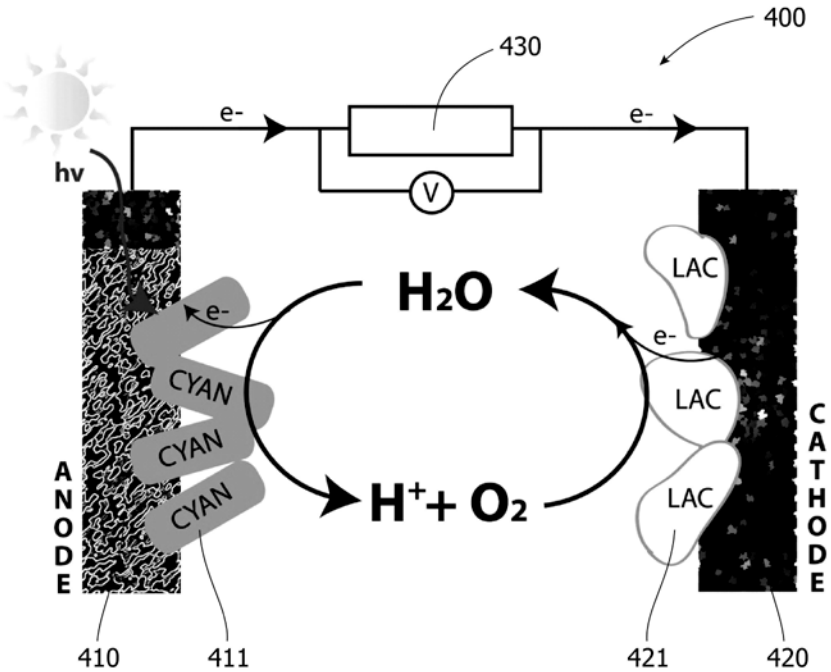
400
430
e-
e-
hν
V
LAC
H2O
e-
e-
CYAN
CYAN
CYAN
LAC
LAC
H+ + O2
ANODE
CATHODE
410
411
421
420

Fig. 4

Fig. 6

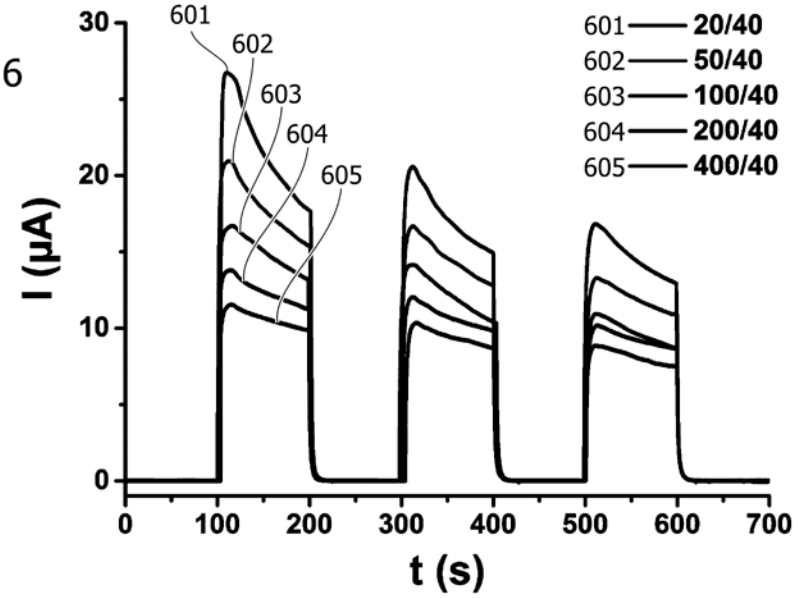
601
602
603
604
605
601 — 20/40
602 — 50/40
603 — 100/40
604 — 200/40
605 — 400/40
I (µA)
t (s)
0
10
20
30
0
100
200
300
400
500
600
700

Fig. 7

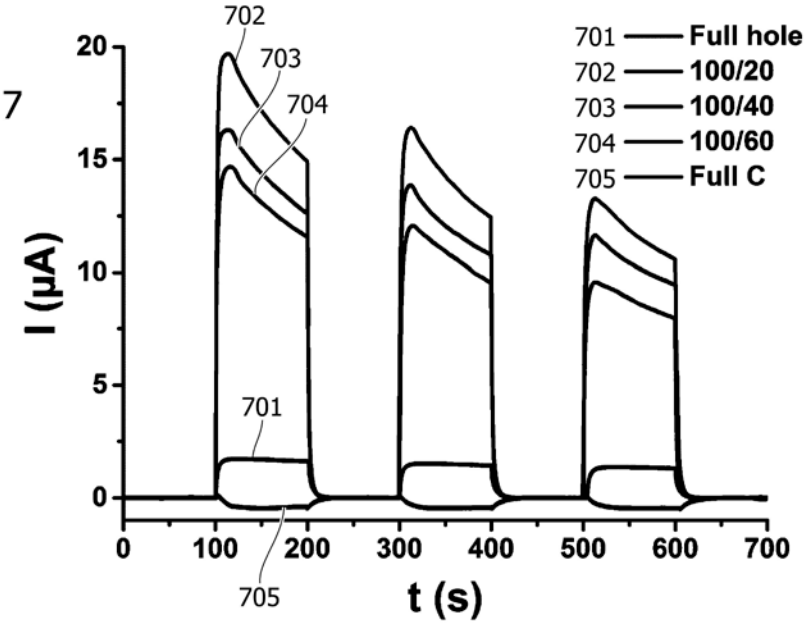
702
703
704
701
705
701 — Full hole
702 — 100/20
703 — 100/40
704 — 100/60
705 — Full C
I (µA)
t (s)
0
5
10
15
20
0
100
200
300
400
500
600
700

Appendix IV: Protocols related to cell culture

Contents

1) Reagents for cell culture and differentiation for hVM1 Bcl-X_L cells

DMEM/F12 with GlutaMAX:

Order from ThermoFisher Scientific, product number 31331028.
Store in refrigerator at 2-8°C for up to 12 months.

Glucose:

Use BioReagent quality from Sigma Aldrich, product number G7021.

AlbuMAX I:

Order from ThermoFisher Scientific, product number 11020039.
Store in refrigerator at 2-8°C.

HEPES:

Order from ThermoFisher Scientific, product number 15630056.
Store in refrigerator at 2-8°C for up to 24 months.

Non-essential aminoacid mix (NEAA mix):

Purchase from MerckMillipore: L-alanine (product number 101007); L-asparagine monohydrate (product number 101565); L-aspartic acid (product number 100126); L-glutamic acid (product number 100291) and L-proline (product number 107434).
Warm up cell-tested water (product number W3500-500ML from Sigma Aldrich) to 55°C. Weigh the aminoacids and add them to the warm water under stirring (see table 1 for quantities). Allow ~15 min for the aminoacids to dissolve. Filter sterilise and aliquot at 500 µL. Store in freezer (-20°C) for up to 6 months. The mix has a concentration of 40 mM for each aminoacid.

Table 1: Recipe for preparing 25 or 100 mL NEAA mix

Aminoacid	For 25 mL NEAA mix (g)	For 100 mL NEAA mix (g)
L-alanine	0.089	0.356
L-asparagine·H_2O	0.150	0.600
L-aspartic acid	0.133	0.532
L-glutamic acid	0.147	0.588
L-proline	0.115	0.460

N-2 supplement:

Purchase 5 mL from ThermoFisher Scientific, product number 17502048.
Aliquot at 500 µL and store in the freezer (-5 to -30°C) for up to 3 months.

EGF:

Purchase 200 µg from R&D Systems, product number 236-EG-200.
Reconstitute in sterile conditions in 400 µL sterile PBS. Transfer to a 2 or 5 mL Eppendorf tube and dilute to 2 mL (concentration is 100 µg/mL). Aliquot at 10 µL. Store in freezer (-20 to -70°C) for up to 3 months.

FGF:

Purchase 25 µg from R&D Systems, product number 233-FB-025.
Prepare 5 mL PBS containing at least 0.1% BSA. Filter sterilize.
Reconstitute FGF in 200 µL sterile PBS containing >0.1% BSA. Transfer to a 2 mL Eppendorf tube and dilute to 1.25 mL with sterile PBS containing >0.1% BSA (concentration is 20 µg/mL). Aliquot at 50 µL. Store in freezer (-20 to -70°C) for up to 3 months.

GDNF:

Purchase 2 µg from PeproTech, product number 450-10.
Reconstitute in 1 mL cell-tested water (product number W3500-500ML from Sigma Aldrich). Aliquot at 10 µL and store in freezer (-20 to -70°C) for up to 6 months.

db-cAMP:

Purchase 250 mg from Sigma Aldrich, product number D0627-250MG
Solubilise in 5 mL cell-tested water (product number W3500-500ML from Sigma Aldrich). Filter sterilise. Aliquot at 500 µL. Store in freezer (-20°C) for up to 6 months.

Geltrex (for coating):

Purchase 1 mL from ThermoFisher Scientific, product number A1413301.
Thaw overnight at 5°C. Aliquot at 100 µL in 15 mL Eppendorf tubes in sterile conditions in laminar flow (LAF) bench. The aliquoting needs to be done quickly, to avoid gelification. Store aliquots in the freezer (-20 to -80°C) for up to 18 months.
Before using: thaw aliquot overnight at 5°C. Dilute in 10 mL sterile PBS in LAF bench (100 x).

Antibiotics mix (P/S):

100x mix available in the cell lab.

Trypsine:

Available in the cell lab.

DMSO:

Available in the cell lab.

2) Media preparation for hVM1 Bcl-X_L cells

Basic medium (BM) – 500 mL

To 1 flask (500 mL) DMEM/F12 with GlutaMAX add:

- 3 g glucose;
- 2.5 g AlbuMAX I;
- 2.5 mL HEPES;

Mix well and filter sterilise. Store in the refrigerator (2-8°C) and use within 1 month.
BM is used for centrifugation (when thawing or passing cells).

Growth medium (GM) – 50 mL

To 48.5 mL BM add:

- 500 µL P/S 100x;
- 500 µL N-2 supplement;
- 500 µL NEAA mix;
- 10 µL EGF;
- 50 µL FGF;

GM is used for routine culture and expansion of the cells.

Differentiation medium (DM) – 50 mL

To 48 mL BM add:

- 500 µL P/S 100x;
- 500 µL N-2 supplement;
- 500 µL NEAA mix;
- 500 µL db-cAMP;
- 10 µL GDNF;

DM is used for differentiation into dopaminergic neurons.

Freezing medium (FM)

Prepare GM and add 10% DMSO (available in the cell lab).

3) Step-by-step cell culture procedure for hVM1 Bcl-X_L cells

Coating of flasks / wells / devices

Add a sufficient quantity of diluted Geltrex to the culture flask / well / device to cover the surface (for example: 100 µL for 24 well plate; 1 mL for T25 flasks; 3 mL for T75 flasks). Spread the liquid well to cover the entire surface. Incubate for at least 1 h prior to cell seeding.

Thawing and seeding cells

Have all reagents (BM, GM) pre-warmed (30 min in 37°C water bath) and a coated T25 flask ready. Take frozen cell vial from -130°C freezer and thaw in 37°C water bath until almost the entire content is liquid. Add 5 mL warm BM to 15 mL Eppendorf tube and then transfer the cell suspension into the same tube. Centrifuge for 5 min at 900 rpm.
While centrifuging, prepare flask for seeding: remove coating solution and add warm GM to the flask (5 mL for a T25 flask).
When the cell suspension is centrifuged, carefully remove the supernatant, resuspend the cells in 1 mL warm GM (pipette several times to ensure uniform dispersion of the cells in the medium) and transfer cell suspension to the flask. Gently mix by tilting the flask. Label the flask (name, date, cell line and passage number from the frozen vial) and place in the incubator (37°C and 5% CO_2).
The cells become adherent after at least 1 h. Do not manipulate flask during this period.

Growing cells

Check every day the aspect of the cells and how confluent they are (what percentage of the surface is covered by cells). hVM1 Bcl-X_L cells should be kept in culture until they are ~ 80% confluent, after which they need to be passed to new flasks. It is recommended to culture cells after thawing for at least 2 passages before starting an experiment.
The GM needs to be replaced every second day for cells kept in culture. When replacing medium, first pre-warm GM in 37°C water bath. Remove old medium and add fresh and warm GM.

Passing cells

When the cells are 80% confluent, they need to be passed to a new flask / well / device, where they have space to grow.
Coat the surface to be used as substrate for cell growth (flask / well / device) as described above. Pre-warm PBS, trypsine, BM and GM (30 min in 37°C water bath).

Remove medium from culture flask. Add warm PBS (on the side of the flask, in order to not perturb the cells) and thoroughly rinse the entire surface that has been in contact with GM. Remove PBS. Add trypsine in a quantity that covers the entire surface (for example: 100 µL for 24 well plate; 1 mL for T25 flasks; 3 mL for T75 flasks). Wait 1-5 min for cells to detach. Add BM to inactivate the trypsine (add a volume equal or higher to the trypsine volume used). Centrifuge for 5 min at 900 rpm. While centrifuging, prepare flask / well / device for seeding: remove coating solution and add

warm GM to the flask / well / device (for example, 5 mL for a T25 flask or 12 mL for a T75 flask). When the cell suspension is centrifuged, carefully remove the supernatant and resuspend the cells in 1 mL warm GM (pipette several times to ensure uniform dispersion of the cells in the medium). Count the cells in the cell suspension and seed at the desired cell density in the new flask / well / device (often 30 000 cells/cm^2). Gently mix by tilting. Label with name, date, cell line and passage number (increase passage number by 1 every time when passing the cells) and place in the incubator (37°C and 5% CO_2).
The cells become adherent after at least 1 h. Do not manipulate flask / well / device during this period.

Differentiating cells

Pass cells normally onto the desired surface and at the desired density. After 24 h, remove all GM and add warm DM. This is denoted as differentiation day 0 (DD0). After 24 h, replace all DM with fresh DM (DD1). In DD3, DD5, DD7 and DD9, remove 2/3 of the DM and add the same quantity of fresh and warm DM. The end-point of the experiment is DD10. See table 2 for clarifications.

Table 2: Experimental procedure for differentiation

Time point	**DD**	**Activity**
Seeding	-	Seed cells in GM on the surface at the desired cell density
24 h after seeding	**DD0**	Replace all the GM with DM
48 h after seeding	**DD1**	Replace all the DM with fresh DM
4 days after seeding	**DD3**	Replace 2/3 of DM with fresh DM
6 days after seeding	**DD5**	Replace 2/3 of DM with fresh DM
8 days after seeding	**DD7**	Replace 2/3 of DM with fresh DM
10 days after seeding	**DD9**	Replace 2/3 of DM with fresh DM
11 days after seeding	**DD10**	End-point of the experiment

Freezing cells

Cells can be stored as deep-frozen aliquots. The initial step is to harvest the cells in culture and prepare a cell suspension. This is done the same way as when passing the cells (see above). After centrifugation, the supernatant is removed and cells are resuspended in FM and aliquoted at 1 mL in freezing vials. The cell suspension should be prepared so that 1 vial can be thawed and seeded in a T25 flask (~ 1 million cells / vial). After aliquoting, the freezing vials should be placed in an isopropanol container in the -80°C freezer for 4 h and then transferred to -130°C freezer.

Live staining of hVM1 Bcl-X_L cells

Calcein AM can be purchased from Sigma Aldrich (product number 56496). A stock solution of 1 mg/mL in DMSO (product number D2650 from Sigma Aldrich) stored in the refrigerator (2-8°C) for up to 1 month. For staining, the stock solution should be diluted to 2 µg/mL calcein in PBS or cell culture medium. Cells can be stained by 1 h incubation in 2 µg/mL calcein solution. For imaging of stained live cells, excitation can be done using a wavelength of 488 nm and emission should be monitored at 516 nm.

4) Reagents for immunostaining of hVM1 Bcl-X_L cells

Fixation buffer

Order from ThermoFisher Scientific, product number FB001, and store in refrigerator (2-8°C).

Goat serum

Order from Sigma Aldrich, product number G9023.
Should be stored in freezer (-20°C).

Triton X-100

Order from Sigma Aldrich, product number T9284-100ML, and store at room temperature.

Anti-TH (mouse)

Order 200 µL from Sigma Aldrich, product number T2928-.2ML.
Aliquot at 10 µL and store in freezer (-20°C).

Anti-β tubulin III (rabbit)

Order 200 µL from Sigma Aldrich, product number T2200-200UL.
Aliquot at 10 µL and store in freezer (-20°C).

Anti-mouse Alexa Fluor 488

Order 500 µL from ThermoFisher Scientific, product number A-11029.
Aliquot at 15 µL and store in refrigerator (2-8°C), protected from light.

Anti-rabbit Alexa Fluor 568

Order 500 µL from ThermoFisher Scientific, product number A-11011.
Aliquot at 15 µL and store in refrigerator (2-8°C), protected from light.

TO-PRO 3

Order 1 mL from ThermoFisher Scientific, product number T3605.
Aliquot at 20 µL and store in freezer (-5 to -30°C), protected from light.

VECTASHIELD Mounting medium

Order from Vectorlabs, product number H-1400, and store in refrigerator (2-8°C).

5) Step-by-step procedure for immunostaining of hVM1 Bcl-X_L cells

Reagent preparation

Add 125 µL Triton X-100 (cut the pipette tip, Triton is viscous) to 50 mL PBS (=> 0.25% Triton solution). Mix gently to avoid foaming.
To 30 mL of the solution add 304 µL goat serum (=> 1% goat serum and 0.25% Triton).
To 5 mL of the 0.25% Triton X solution add 550 µL goat serum (=> 1% goat serum and 0.25% Triton).

Fixing the cells

Wash (5 min) with warm PBS.
Incubate for 15 min with fixation buffer at room temperature, then wash (3 x 5 min) with PBS.

Permeabilization

1 h incubation at room temperature on a shaker-plate in PBS with 1% goat serum and 0.25% Triton.

Incubation with primary antibodies

Use one aliquot of anti-TH (mouse) and one of anti-β tubulin III (rabbit). Mix them and dilute them in a total volume of 10 mL PBS with 1% goat serum and 0.25% Triton (diluted 1000 x).
Incubate on a shaker plate either for 4 h at room temperature or overnight in the fridge (2-8°C).
Wash (10 min each) with:

- PBS with 1% goat serum and 0.25% Triton
- PBS with 0.25% Triton
- PBS

Incubation with secondary antibodies

Use one aliquot of anti-mouse Alexa Fluor 488 and one of anti-rabbit Alexa Fluor 568. Mix them and dilute them in a total volume of 3 mL PBS (diluted 200x).
Incubate on a shaker plate protected from light for 30 min at room temperature.
Wash twice (10 min each) with PBS.

Nuclei staining

Use one aliquot of TO-PRO 3 and dilute it in 10 mL PBS (diluted 500 x).
Incubate on a shaker plate protected from light for 10 min at room temperature.
Wash three times (10 min each) with PBS and once with Millipore water (to remove salt residues).
Stained samples can be kept 2-3 days in refrigerator before imaging or can be mounted using VECTASHIELD and stored in refrigerator for longer periods of time.

Appendix 5: Protocols related to the cleanroom fabrication of transparent electrode chips (TECs)

Contents

1) Cleanroom equipment used for steps involved in UV lithography

Wafer pretreatment (dehydration)

Oven 250°C.

Spin coating

SU-8 processing: RCD8 T (Süss Micro-Tec, Garching bei München Germany), using manual dispensing of photoresist.
Polyimide processing: WS-650 (Laurell Technologies Corporation, North Wales, PA, USA).

UV Exposure

MA6 contact aligner (Süss Micro-Tec, Garching bei München, Germany). The aligner is equipped with a 350 W mercury lamp and a long pass filter (SU-8 filter) adjusted to a constant intensity of 7 mW/cm^2 at 365 nm.

Baking

Hotplate for SU-8 baking (Harry Gestigkeit GmbH, Düsseldorf, Germany).
Benchtop hotplate Präzitherm PZ 28-2 (Harry Gestigkeit GmbH, Düsseldorf, Germany) – used for polyimide samples.

Development

SU-8 Developer bench using PGMEA (supplied in the cleanroom as mr-Dev 600) and isopropanol for rinsing.

Profilometry

Dektak XTA stylus profiler (Bruker, Billerica, MA, USA) equipped with 5 µm, 45^o cone tip.

Dicing

DAD 321 DISCO automatic dicing saw (Japan) using pyrex (B1A86) blade.

2) Experimental details regarding the pyrolysis process

For all experiments presented in this thesis, pyrolysis was performed using a PEO-601 furnace from ATV Technologie GmbH (Vaterstetten, Germany) available in the cleanroom at DTU Danchip under the name “Resist pyrolysis furnace”.
The samples were kept under inert atmosphere for the entire duration of the pyrolysis process. This was done by introducing a continuous flow of N_2 in the furnace at a rate of 24 L/min.
The pyrolysis process can be split into 5 individual steps:

i) Temperature ramping from room temperature to 200°C at a rate of 2°C/min.
ii) 30 min dwelling time at 200°C – to allow removal of residual oxygen in the furnace.
iii) Temperature ramping from 200°C to 900°C at a rate of 2°C/min.
iv) 1 h dwelling time at 900°C – to allow carbonisation of the polymer.
v) Cooling down from 900°C to room temperature at a rate of 2°C/min.

Figure 1 shows the temperature ramping over time for the pyrolysis process. The total duration of the process is 16.1 h.

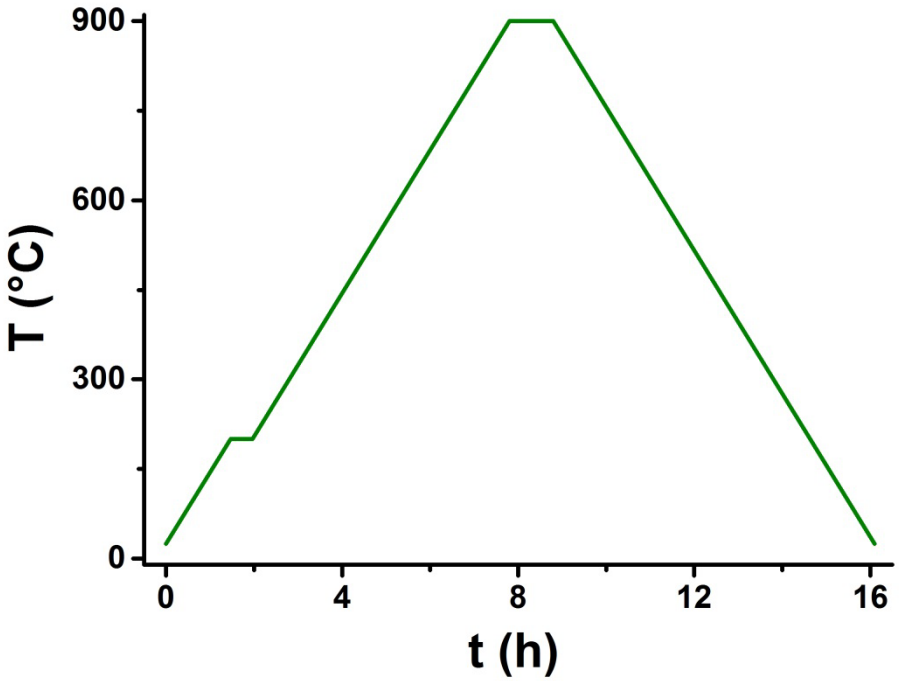

Figure 1: Temperature vs time plot for the pyrolysis process.

I have performed pyrolysis several times in an ESTF 11 furnace from Entech (Angelholm, Sweden). This furnace is available in the DTU Chemical Engineering (DTU Kemiteknik) Department. The experiments in DTU Chemical Engineering served as preliminary assessment of the behaviour of optical fibers and polyimide during pyrolysis before transferring the process to the cleanroom.

3) Process flow for the fabrication of unpatterned carbon chips

SU-8-derived carbon chips

Step Nº	Description	Equipment	Program/Parameters
1	**Wafer pretreatment**		
1.1	Stock out		4" silicon wafers, 500 µm thick, with 110 nm SiO2
1.2	Dehydration bake		250ºC, overnight
2	**SU-8 spin-coating**		
2.1	Spin-coating of SU-8 2035	RCD8	1) 1000 rpm for 10 s using an acceleration of 200 rpm/s 2) 5000 rpm for 120 s using an acceleration of 1000 rpm/s Recipe: YMSU2035
2.2	Solvent evaporation	Hotplate	15 min at 50ºC
3	**SU-8 photolithography**		
3.1	SU-8 exposure	KS Aligner	2 x 250 mJ/cm2 (30 s waiting time), Flood Exposure
3.2	Post-exposure bake	Hotplate	1 h, 50ºC, 2ºC/min
3.3	SU-8 development	Developer	5 min FIRST, 5 min FINAL, PGMEA
3.4	Hard bake	Hotplate	16 h, 90°C, 2ºC/min
3.5	Rinse	Developer	Isopropanol, Air
3.6	Thickness measurement	Dektak	
4	**Pyrolysis**		
4.1	Pyrolysis	Resist Pyrolysis Furnace	Ramp to 200ºC, 30 min dwell at 200ºC, ramp to 900ºC, 1 h dwell at 900ºC, then cool to room temperature. Ramp: 2ºC/min. Max N2 flow. (recipe: adabu900)
4.2	Thickness measurement	Dektak	
5	**Dicing**		
5.1	Dicing	Disco saw	Si blade (27HEEF), blade height 0.2 mm, 20 mm/s

Polyimide-derived carbon chips

Step Nº	Description	Equipment	Program/Parameters
1	**Wafer pretreatment**		
1.1	Stock out		4" silicon wafers, 500 µm thick, with 110 nm SiO2
1.2	Dehydration bake		250ºC, overnight
2	**Polyimide spin-coating**		
2.1	Spin-coating of polyimide	Manual all resist	2400 rpm for 30 s using an acceleration of 100 rpm/s
2.2	Solvent evaporation	Hotplate	5 min at 120ºC
3	**Crosslinking**		
3.1	Crosslinking	Resist Pyrolysis Furnace	Ramp to 300ºC, 1 h dwell at 300ºC, then cool to room temperature. Ramp: 2ºC/min. Max N2 flow.
3.6	Thickness measurement	Dektak	
4	**Pyrolysis**		
4.1	Pyrolysis	Resist Pyrolysis Furnace	Ramp to 200ºC, 30 min dwell at 200ºC, ramp to 900ºC, 1 h dwell at 900ºC, then cool to room temperature. Ramp: 2ºC/min. Max N2 flow. (recipe: adabu900)
4.2	Thickness measurement	Dektak	
5	**Dicing**		
5.1	Dicing	Disco saw	Si blade (27HEEF), blade height 0.2 mm, 20 mm/s

4) Optimized process flow for the fabrication of TECs

Step Nº	Description	Equipment	Program/Parameters
1	**Wafer pretreatment**		
1.1	Stock out		4" fused silica wafers, 500 µm thick, IF525
1.2	Dehydration bake		250ºC, overnight
2	**SU-8 spin-coating**		
2.1	Spin-coating of SU-8 2005	RCD8	100 rpm for 30 s. Recipe: YMSU2005
2.2	Solvent evaporation		3 h at room temperature
3	**SU-8 photolithography**		
3.1	SU-8 exposure	KS Aligner	100 mJ/cm2, Proximity Exposure with 12 µm gap (14.3 s)
3.2	Post-exposure bake	Hotplate	1 h, 50ºC, 2ºC/min
3.3	SU-8 development	Developer	5 min FIRST, 5 min FINAL, PGMEA
3.4	Hard bake	Hotplate	16 h, 90°C, 2ºC/min
3.5	Rinse	Developer	Isopropanol, Air
3.6	Thickness measurement	Dektak	
4	**Pyrolysis**		
4.1	Pyrolysis	Resist Pyrolysis Furnace	Ramp to 200ºC, 30 min dwell at 200ºC, ramp to 900ºC, 1 h dwell at 900ºC, then cool to room temperature. Ramp: 2ºC/min. Max N2 flow. (recipe: adabu900)
4.2	Thickness measurement	Dektak	
5	**Dicing**		
5.1	Dicing	Disco saw	Pyrex blade (B1A86), blade height 0.1 mm, 10 mm/s

5) Photomask used for the fabrication of TECs

The photomask for UV lithography was designed in the L-EDIT software and fabricated on demand by Delta Mask (Enschede, Netherlands).
It is a 5” chrome mask on soda-lime glass. Since SU-8 is a negative photoresist, the mask contains a negative of the pattern desired on the wafer.
The mask (**figure 2**) contains: pattern for transparent electrode chips (1), separation lines between chips (cut lines, 2) and alignment marks (which are reference structures that can also be used for estimating resolution, 3).

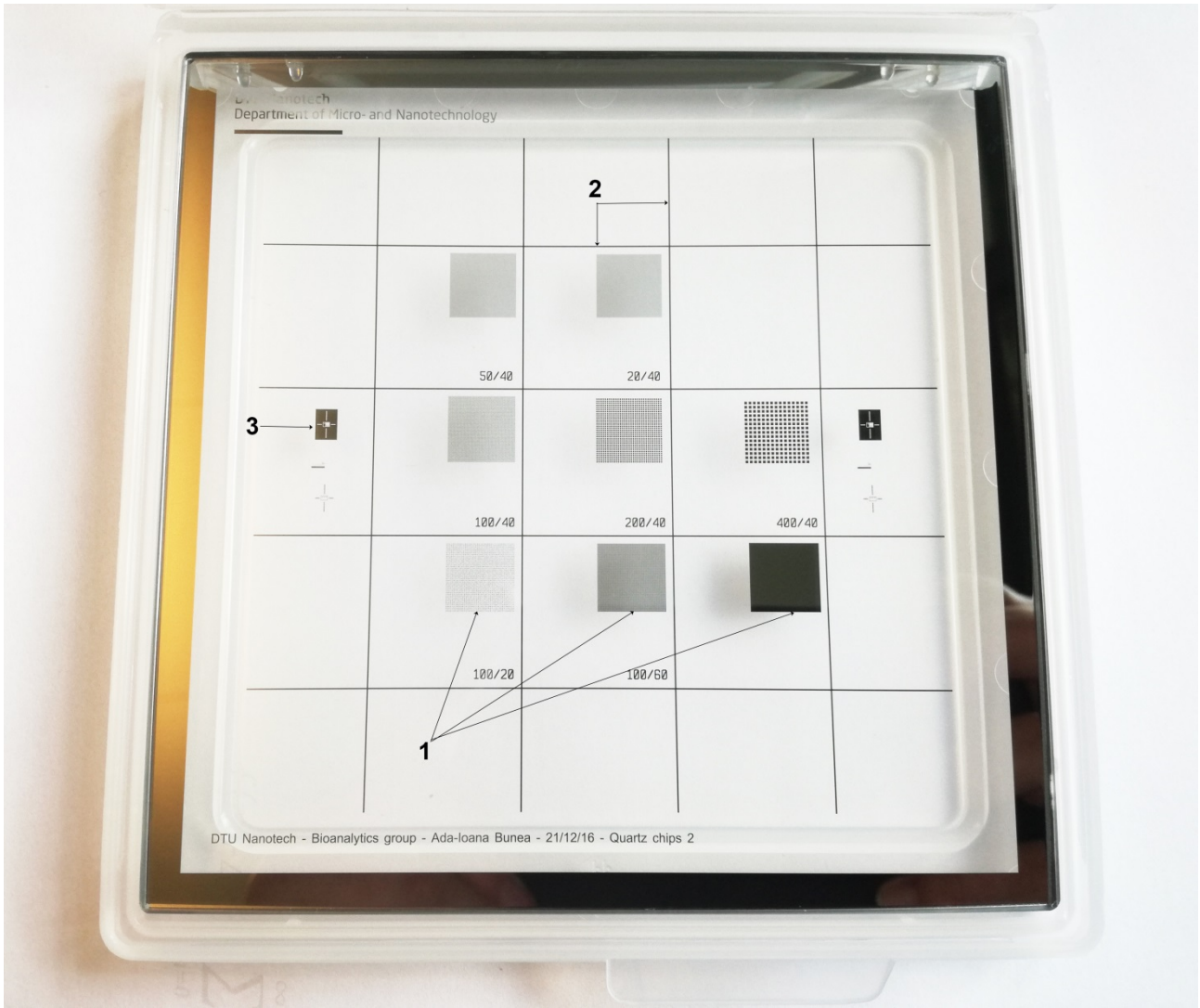

Figure 2: Photo of the mask used in the fabrication of transparent electrode chips. 1: pattern for transparent electrode chip active area; 2: separation lines between chips, used for dicing; 3: alignment marks.

6) Challenges encountered during the fabrication of TECs

The process flow for photolithographic patterning of SU-8 on silicon wafers has been previously optimised in our group for the DTU Danchip machines. However, the process needed to be adapted when using fused silica as substrate. The first attempts at fabrication showed two interconnected issues: improper development of structures and detachment of the SU-8 derived carbon after dicing.
Figure 3a and **3b** show two photos of failed fabrication attempts, after the process of pyrolysis. Since fused silica and SU-8 are both transparent, it is sometimes hard to assess the quality of the photolithographic process before pyrolysing the sample. When the polymer is carbonized, the imperfections become obvious.
Figure 3a shows the patterned area on a TEC. Instead of obtaining a square array of holes in the carbon layer, circular stripes with developed holes alternating with non-developed areas can be observed. Additionally, the dicing lines are not well-developed for the whole wafer (in the photo it can be seen how they "disappear"). Figure 3b shows a diced wafer with TECs. The pattern cannot be seen and the carbon is detached from the substrate around the cut lines.
Both issues were solved by optimising the UV exposure process. The circular lines seen in figure 3a are present on the wafer holder in the aligner used for UV exposure. Fused silica is transparent, so the holder can reflect the light and cause re-exposure of the photoresist. Replacing the regular wafer holder with a ring holder that only touches the wafer edges solved the issue of re-exposure.
The exposure dose had to be optimised for the fused silica wafers. This was done using a "pie-slicer" additional mask during the UV exposure. The "pie-slicer" allowed testing 6 different exposure doses on the same wafer, saving time and materials. The exposure doses tested were: 50, 75, 100, 125, 150 and 200 mJ/cm^2. After baking and development, the outcome was evaluated by using confocal microscopy and the autofluorescence of SU-8 [1, 2] . This was done by checking if the developed holes went all the way through the photoresist layer.
Detachment of the carbon layer during dicing can be partly attributed to the fact that the dicing lines were not well-developed. Dicing is done under strong water flow. If the dicing lines are not well-developed, the blade can cause micro-cracks in the carbon layer. Water can creep in these micro-cracks and cause the layer to detach, as seen in figure 3b. It can be observed that the carbon layer is more damaged around the cut lines, and in the direction of the water flow. Optimisation of the exposure and proper development of the cut lines solved the problem of detaching carbon layers.
Figure 3c and **3d** show two photos of TECs fabricated using optimized parameters. In figure 3c, one can see that the patterned area of the electrode is an array of well-developed holes. Figure 3d shows a whole wafer fabricated using optimised parameters after dicing, with no detachment of the carbon layer.

---

[1] R. Marie, S. Schmid, A. Johansson, L. Ejsing, M. Nordström, D. Häfliger, C.B. Christensen, A. Boisen, M. Dufva, Immobilisation of DNA to polymerised SU-8 photoresist., Biosens. Bioelectron. 21 (2006) 1327–32. doi:10.1016/j.bios.2005.03.004.

[2] R. Walczak, P. Śniadek, J.A. Dziuban, SU-8 photoresist as material of optical passive components integrated with analytical microsystems for real-time polymerase chain reaction, Opt. Appl. XLI (2011).

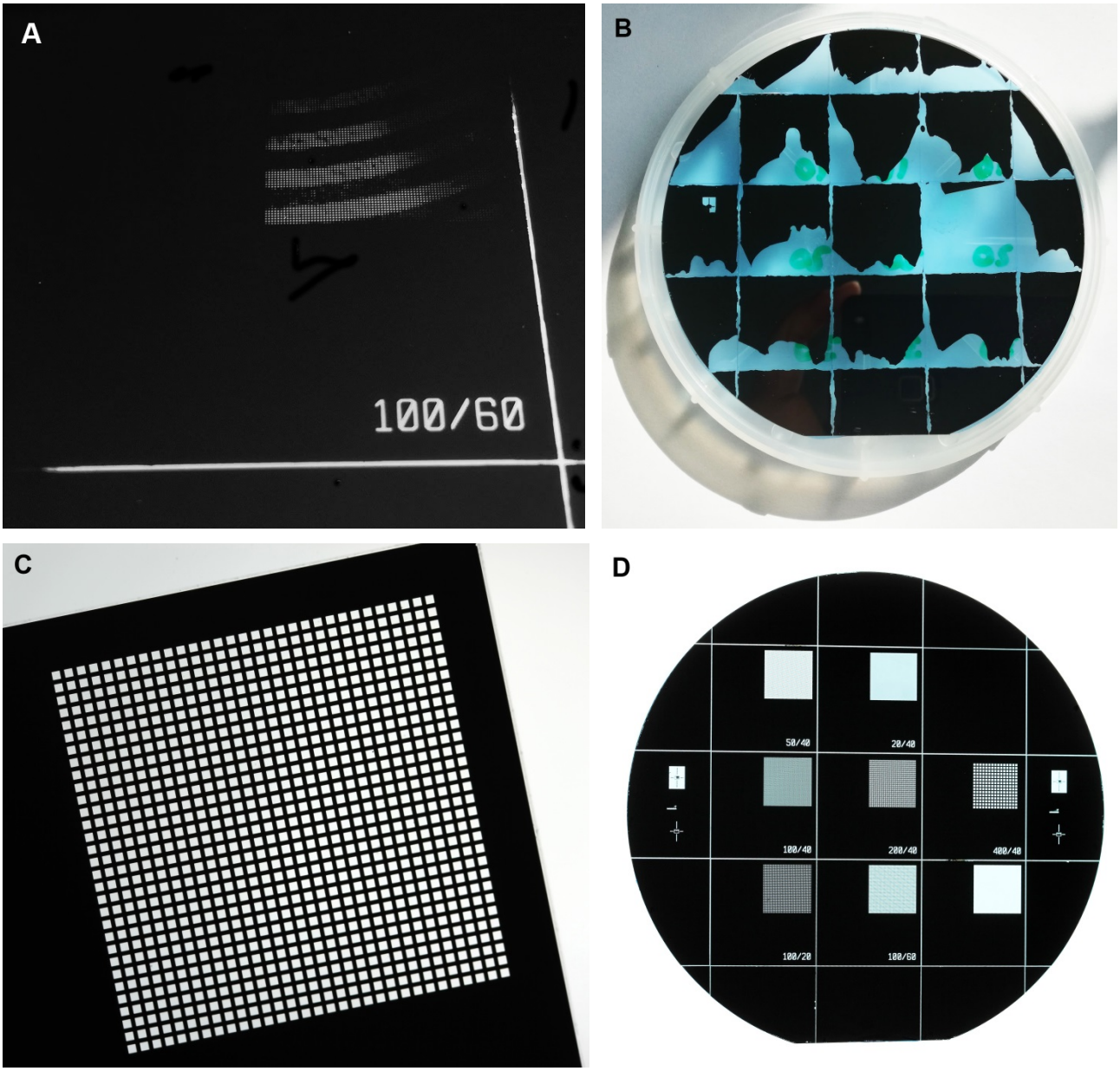

Figure 3: Top: Issues encountered during fabrication of TECs: Circular lines and improper development of the holes and dicing lines (a); Detachment of the carbon layer after dicing (b); Bottom: TECs fabricated using optimised parameters: Array of holes (c); Wafer after dicing (d).

Appendix 6: Attended conferences

The scope of each conference is described, as well as my personal contribution to the conference. The conferences are listed in chronological order.

XXIII International Symposium on Bioelectrochemistry and Bioenergetics

14-18 June 2015, Malmö, Sweden

The symposium featured aspects of the highly interdisciplinary areas of bioelectrochemistry and bioenergetics on the following themes: biosensors, biomolecular recognition, bioelectroanalysis, biological fuel cells, photobioelectrochemistry, electroporation – new biotechnological and clinical applications, new advanced nanomaterials for bioelectrochemistry.

I participated as student helper for the organization of the conference and I presented a poster titled **"Interdigitated carbon electrodes for stem cell differentiation and dopamine detection"**.

PhD Symposium on Bioelectrochemistry and Bioanalysis

26-27 November 2015, Luckenwalde, Germany

The yearly symposium addresses aspects of bioelectrochemistry and bioanalysis. It mostly focuses on recent developments in the field of biosensors and lab-on-a-chip devices. It is meant as an opportunity for PhD students to develop, network and brainstorm in an encouraging environment.

I participated with an oral presentation titled "**Polymer-derived carbon surfaces for enhancing stem cell differentiation"** and I chaired one of the sessions.

Sustain DTU Conference

17 December 2015, Kongens Lyngby, Denmark

Sustain DTU is a yearly conference that, as the title suggests, focuses on sustainability. On-going research activities from DTU and Danish companies were presented here. It was also a good place to look for collaborators and it had a talk dedicated to obtaining funding (with examples from Horizon 2020 or Forsk 2020 projects). The different topics related to sustainability in science were divided into 18 different sessions and workshops.

I participated with an oral presentation titled "**Carbon nanopillars for stem cell differentiation and dopamine detection"** in the section "Quality of Life".

Biosensors 2016

25-27 May 2016, Gothenburg, Sweden

This is the largest biosensors congress in the world, and it takes place every second year. Its parallel sessions and poster sessions covered: biological fuel cells, biocomputing, commercial biosensors, manufacturing and markets, aptasensors, DNA chips and nucleic acid sensors, electronic noses, enzyme biosensors, immunosensors, lab-on-a-chip, microfluidics and μTAS, mobile diagnostics and tele-computing, nanomaterials and nanoanalytical systems, natural and synthetic receptors, organism- and whole cell-based biosensors, printed biosensors and organic electronics, single-cell detection/analysis, infectious disease detection and personal health monitoring.

I participated to the congress with a poster presentation titled "**Carbon nanopillars for enhanced stem cell differentiation and dopamine detection"**.

229th ECS Meeting

29 May – 2 June 2016, San Diego, CA, USA

This meeting of the Electrochemical Society focused on carbon nanostructures and devices. Various aspects were addressed in parallel sessions, from fabrication and characterization to applications.

I participated with an oral presentation titled **"Polymer-derived carbon surfaces for enhancing stem cell differentiation"** in the symposium "Carbon Nanostructures in Medicine and Biology".

Sustain-ATV DTU Conference

30 November 2016, Kongens Lyngby, Denmark

In the 2016 edition of the DTU Sustain conference, I participated with an oral presentation titled **"Pyrolytic carbon electrode for dopamine detection from cells"** in the session "The future of healthcare".

First European / 10th German BioSensor Symposium

20-23 March 2017, Potsdam, Germany

The symposium covered different topics of biosensor research, distributed in two parallel sessions. The focus was on: technologies for innovative formats, bioengineered and biomimetic recognition elements, nanotechnology, surface engineering and bioelectronics, cell biosensors, advances in applications (in areas such as diagnostics, medicine, food and environment) and software development: theory and mathematics.

I participated with an oral presentation titled **"Carbon-coated optical fibre for dopamine detection from cells"** in the session: "Cell biosensors: Diagnostics".

XIX Euroanalysis 2017

28 August – 1 September 2017, Stockholm, Sweden

The conference had a broad program within the field of analytical chemistry, including topics such as: separation methods, mass spectrometry, electroanalysis, imaging, environmental analysis and toxicology, sample preparation, microfluidics, sensors and biosensors.

I participated with an oral presentation titled **"Optoelectrical scaffolds for cell-replacement therapy and energy applications"** in the session "Microfluidics and nanotechnology".

Published by:
DTU Nanotech
Department of Micro- and Nanotechnology
Technical University of Denmark
Ørsteds Plads, building 345C
DK-2800 Kgs. Lyngby